UNIVERSITY OF ZAGREB
FACULTY OF MECHANICAL ENGINEERING AND NAVAL ARCHITECTURE

MASTER'S THESIS

Ljudevit Putarek

Zagreb, 2019

UNIVERSITY OF ZAGREB
FACULTY OF MECHANICAL ENGINEERING AND NAVAL ARCHITECTURE

MASTER'S THESIS

Mentor:

Asst. Prof. Darko Kozarac, PhD

Student:

Ljudevit Putarek

Zagreb, 2019

Izjavljujem da sam ovaj rad izradio samostalno koristeći znanja stečena tijekom studija i navedenu literaturu.

I declare that I have completed this thesis using the knowledge and skills gained during my university studies and using specified literature.

Ljudevit Putarek

Acknowledgments

I would like to express gratitude to AVL-AST d.o.o. from Zagreb and AVL List GmbH from Graz for all technical support during this study.

First, I want to thanks to *MPhil Nikola Naranča* from AVL-AST d.o.o. for giving me opportunity and providing dynamic environment with good engineering support.

Secondly, I want to give special thanks to *DI Bernhard Thonhauser* and *DI Dr. Heinz- Georg Flesh* from AVL List GmbH for giving me constant guidance and for their dedication throughout this thesis study.

Specially, I want to give thanks to *Msc. Damjan Ule* for support and giving me advices during thesis study. I also thank all my colleagues from AVL-AST d.o.o. who, with their advice and critical thinking, helped me during the thesis.

I would like to express gratitude to my mentor, *prof. dr.sc. Darko Kozarac* for his support and advices during this thesis study.

My special thanks go to my parents, *Zlata* and *Ivan*, to my sister *Vanja* and gradmother *Marija*. You have been there for me my entire life, helping and guiding me and always wishing me all the happiness in the world.

Also, big thanks to all friends for being my support during my studies and writing of this thesis.

Thank you!
Ljudevit Putarek

SVEUČILIŠTE U ZAGREBU
FAKULTET STROJARSTVA I BRODOGRADNJE
Središnje povjerenstvo za završne i diplomske ispite
Povjerenstvo za diplomske ispite studija strojarstva za smjerove:
procesno-energetski, konstrukcijski, brodostrojarski i inženjersko modeliranje i računalne simulacije

Sveučilište u Zagrebu Fakultet strojarstva i brodogradnje	
Datum	Prilog
Klasa:	
Ur. broj:	

DIPLOMSKI ZADATAK

Student: **Ljudevit Putarek** Mat. br.: 0035195422

Naslov rada na hrvatskom jeziku: **Numerička simulacija dinamike klipa i klipnih prstena**

Naslov rada na engleskom jeziku: **Simulation of piston and piston ring dynamics**

Opis zadatka:

Piston group is the main contributor in friction of the internal combustion engines, with an amount of 40%-50%. In order to increase the performance, the market is looking for efficient friction reduction methods without drawbacks in durability and NVH. With this perspective, the efficient parameter studies and optimization processes performed by multibody dynamics simulations are gaining more importance. The objective of the simulation tasks is to support the concept investigations, failure mode analysis and definition of optimization potential of the piston group. The advantages of simulations are short response times for different variants, view 'beyond the edge' and low cost compared to hardware testing.
Based on the above, in this study it is necessary to:

1. Study literature and publications for steel piston development in diesel passenger car engines. This should cover friction related topics, e.g. piston to liner warm clearance, pros & cons for steel and aluminum pistons and current developments in low friction ring packs.
2. Setup the new Excite Power Unit model for piston to liner interaction (including EHD contact) and Excite Piston & Rings model for piston rings investigation that represents the FRISC (FRIction Single Cylinder) engine of the AVL diesel development project, based on full engine models.
3. Compare the simulation results (EPU, EPR) between simplified and advanced modelling approaches. Define guidelines and recommendations for an efficient modelling.
4. Compare the simulation results with FRISC measurements (friction force, LOC and blow by) for two ring pack applications with the steel piston.
5. Study the tuning parameters for model parametrization and show the sensitivity of the tuning parameters and perform parametric studies for further friction improvements without drawbacks in function (blow by / LOC / ring motion).

During thesis preparation one must comply with the rules for preparation of the Master thesis.
It is necessary to list all literature used and received assistance.

Zadatak zadan:	Datum predaje rada:	Predviđeni datum obrane:
7. ožujka 2019.	9. svibnja 2019.	15., 16. i 17. svibnja 2019.

Zadatak zadao: Predsjednica Povjerenstva:

izv. prof. dr. sc. Darko Kozarac Prof. dr. sc. Tanja Jurčević Lulić

CONTENT

LIST OF FIGURES

LIST OF TABLES

LIST OF SYMBOLS

Symbol	Unit	Description
a	m^3	Piston acceleration
A	m^2	Nominal piston surface area
BDC	m	Cylinder bottom dead center
BMEP	bar	Brake mean effective pressure
c_v	J/(kg K)	Specific heat at constant volume
D	m	Cylinder diameter
F	N	Combined forces acting upon the piston
FMEP	bar	Friction mean effective pressure
F_g	N	Gas forces
F_{GC}	N	Gas forces from crankcase
F_{NS}	N	Sealring normal force
F_{R}	N	Friction force
F_{RS}	N	Sealring friction force
F_{S}	N	Spring force
F_{in}	N	Inertia force
F_{t}	N	Tangential force
F_{y}	N	Side force
h	mm	Axial ring width
H	m	Cylinder stroke
IMEP	bar	Indicated mean effective pressure
l	m	Conrod length
m_{osc}	kg	Oscillating mass
m_p	kg	Piston mass
m_{rot}	kg	Rotating mass
n	rpm	Engine speed in rpm
p	Pa	Contact pressure
p_c	Pa	Cylinder pressure
R	J/(kg K)	Specific gas constant
r	m	Crankshaft radius
T_c	K	Cylinder temperature

T_l	K	Liner temperature
T_p	K	Piston temperature
T_s	K	Standard temperature
TDC	m	Cylinder top dead center
V	m^3	Cylinder volume
V_H	m^3	Cylinder displacement
v	-	Piston speed
W_i	J	Indicated work
W_m	J	Mechanical or friction work
z	-	Number of cylinders
α	rad	Crank angle
α_w	$W/(m^2 K)$	Heat transfer coefficient
κ	-	Specific heat ratio
λ	-	Lambda coefficient, equivalence ratio
ω	rad/s	Engine speed

LIST OF ABBREVIATIONS

Abbrevation	Description
ATS	Anti-Thrust Side
BL	Boundary Lubrication
BMEP	Break Mean Effective Pressure
BSFC	Break Specific Fuel Consumption
DOF	Degree Of Freedom
EHD2	Elasto-Hydro-Dynamic
EHL	Elasto-Hydrodynamic Lubrication
EPIL	Elastic Piton-Liner Contact
FE	Finite Element
FMEP	Friction Mean Effective Pressure
FPL	Friction Power Loss
FRISC	FRIction Single Cylinder
FTAB	Table Force/ Moment Jonit
FTDC	Firing Top Dead Center
HL	Hydrodynamic Lubrication
ICE	Internal Combustion Engine
IMEP	Indicated Mean Effective Pressure
LOC	Lube Oil Consumption
ML	Mixed Lubrication
NVH	Noise Vibration Harshness
REVO	Revolute Joint
TDC	Top Dead Center
TS	Thrust Side

SAŽETAK

Trenje izazvano radom klipnog mehanizama doprinosi 40% do 50% ukupnom trenju motora s unutarnjim izgaranjem. Proizvođači automobila traže učinkovite metode u smanjenju trenja bez nedostataka u izdržljivosti, buci i vibracijama. S obzirom na to, efikasno ispitivanje parametara i optimizacije simulacijskih modela dobiva sve više na važnosti. Cilj rada istražiti je razlike u rezultatima između simulacije i mjerenja provedenih na motoru AVL FRISC.

AVL FRISC je jednocilindarski motor s unutarnjim izgaranjem konstruiran za proučavanje rezultata dinamike klipa i klipnih prstena s naglaskom na rezultate sile trenja, bočne sile klipa, srednjeg tlaka trenja, potrošnje ulja klipnog mehanizma i prestrujavanja zraka u donji dio kućišta motora (*blow-by*). Simulacijski modeli izrađeni su u programima *AVL EXCITE™ Piston&Ring* i *AVL EXCITE™ Power Unit*. U programu *AVL EXCITE™ Piston&Ring* izrađena su dva modela koji se razlikuju s obzirom na korišteni paket klipnih prstena, osnovni paket klipnih prstena i paket klipnih prstena sa smanjenim trenjem. Također, izrađeni su modeli koji se razlikuju u pristupu rješavanja simulacijskog modela: pojednostavljeni pristup ili 2D te napredniji pristup ili 3D. Rezultati potrošnje ulja klipnog mehanizma, prestujavanja zraka, dinamike klipnih prstena i gubitaka trenja klipnih prstena dobiveni su simulacijom u programu *AVL EXCITE™ Piston&Ring*. Proučavanje ukupnih gubitaka tlaka trenja klipnog mehanizma, sile trenja i bočne sile na klip provedeno je u programu *AVL EXCITE™ Power Unit* s osnovnim paketom klipnih prstena i paketom klipnih prstena sa smanjenim trenjem. Simulacijski modeli izrađeni su na pojednostavljen i napredan način. Pojednostavljeni model koristi REVO spoj, dok napredan model koristi EHD spoj. Prikazani su rezultati dinamike klipa, gubitci trenja klipa, sile trenja i bočne sile na klipu. Dostupna su mjerenja potrošnje ulja, prestrujavanja zraka, sile trenja, bočne sile na klipu i srednjeg tlaka trenja, kao i njihova usporedba sa simulacijskim rezultatima. Na kraju je prikazan utjecaj parametara na usklađivanje simulacijskog modela i mjerenja.

Ključne riječi: *trenje klipnog mehanizma, mjerenja AVL FRISC, AVL EXCITE™ Piston&Ring, AVL EXCITE™ Power Unit, srednji tlak gubitaka, potrošnja ulja, prestrujavanje zraka, sila trenja, bočna sila na klipu, tangencijalna sila klipnog prstena, 2D i 3D pristup, REVO, EHD, utjecaj parametara***.**

SUMMARY

Piston group is the main contributor to friction with an amount of 40%-50% of the total IC engine friction. The market is looking for efficient friction reduction methods without drawbacks in durability and NVH. In light of this, efficient parameter studies and optimization processes in multibody dynamics simulation are becoming increasingly important and must be setup. The aim of this thesis is to investigate the differences in the results of simulation and measurement on the AVL FRISC engine.

The AVL FRISC (FRIction Single Cylinder) engine is a research IC engine designed for the investigation of piston and piston ring dynamics in view of measuring friction force side force, friction mean effective pressure (FMEP), lube oil consumption (LOC) and blow-by values. Simulation models are built in the AVL EXCITE™ Piston&Ring and AVL EXCITE™ Power Unit software's. In EXCITE™ Piston&Ring, models with two different piston ring packages (basic and low friction package) are created for different simulation solvers: simplified (2D) and advanced (3D) solver. The differences between the basic and low friction ring package is in the tangential force. The results of LOC, blow-by, piston ring dynamics and piston ring friction losses are given by the AVL EXCITE™ Piston&Ring software. To investigate the total FMEP values of piston group, friction force and side force, AVL EXCITE™ Power Unit models are created for a basic and low friction package. Simulation models are also created with a simplified and advanced approach. Revolute Joints (REVO) are used in the simplified approach, whereas Elasto-Hydrodynamic journal sliding bearing (EHD2) is used in the advanced approach. The results of piston dynamics, piston friction losses, friction and side force are presented. For the simulated AVL FRISC engine, the measurements of LOC, blow-by, FMEP, friction and side forces are available and simulation results are compared with the available measurements. Finally, a study on tuning parameters for results correlation and sensitivity of tuning parameters is presented.

Key words: *piston group friction, AVL FRISC measurement, AVL EXCITE™ Piston&Ring, AVL EXCITE™ Power Unit, FMEP, LOC, blow-by, friction force, side force, tangential force on piston ring, 2D and 3D simulation solver, REVO, EHD, tuning parameters*

PROŠIRENI SAŽETAK

Ovaj diplomski rad je izrađen u suradnji sa tvrtkom AVL - AST d.o.o. iz Zagreba i AVL List GmbH iz Graza s ciljem da se usporede rezultati simulacije i mjerenja dinamike klipa i klipnih prstena. Simulacijski modeli izrađeni su u 2 programska alata: *AVL EXCITE™ Piston&Ring* i *AVL EXCITE™ Power Unit*. U programu *AVL EXCITE™ Piston&Ring* proučava se dinamika klipnih prstena i potrošnja ulja klipnog mehanizma, dok se u programu *AVL EXCITE™ Power Unit* proučava dinamika klipa.

Ovaj rad je strukturiran u 4 poglavlja te je na kraju dan zaključak i predložene su preporuke za daljnji rad. U prilogu se nalaze dodatni rezultati simulacijskih modela i usporedbe simulacija i mjerenja. Sam rad je baziran na stranim doktorskim radovima, znanstvenim člancima i dokumentaciji korištenih programa.

U 1. poglavlju je dan motivacija u kojoj je opisana važnost simulacija u odnosu na testiranja i prikazan je utjecaj trenja klipnog mehanizma na sveukupni iznos trenja u automobilskim sustavima. Nadalje, opisana je funkcija i značajke klipa, predočena je podjela klipova s obzirom na materijal (čelični, čelični lijev, aluminijski) te su prikazani različiti tipovi čeličnih klipova u automobilima pogonjeni dizelskim gorivom. Osim navedenog, prikazana je usporedba čeličnog i aluminijskog klipa. Na Slici 1., prikazana je konstrukcijska usporedba čeličnog i aluminijskog klipa.

Slika 1. Konstrukcijske razlike između čeličnog i aluminijskog klipa. [8]

Iz slike je vidljivo da čelični klip ima manju kompresijsku visinu i visinu plamenog pojasa. Smanjenjem kompresijske visine za istu konstrukciju motora možemo ugraditi dulju klipnjaču a da ne mijenjamo kompresijski volumen. Time smanjujemo iznos bočne sile na klipu a samim time i trenje uzrokovano klipom u košuljici cilindra. Glavni uzrok korištenja čeličnih

u odnosu na aluminijske klipove je veća zamorna čvrstoća Čelični klipovi time ispunjaju zahtjeve čvrstoće za moderne automobile pogonjene dizelskim gorivom gdje vršne vrijednosti tlaka u cilindru iznose čak 250 bar. Osim klipova, u uvodnom dijelu opisana je svrha klipnih prstena, njihova podjela i današnje prevlake za smanjenje trenja uzrokovane klipnim prstena. Također, prikazani su modeli trenja s obzirom na podmazivanje te su prikazani uzroci potrošnje ulja u klipnom mehanizmu.

U 2. poglavlju opisan je rad i konstrukcija AVL FRISC motora. AVL FRISC motor je jednocilindarski razvojni motor na kojem se izvode ispitivanja klipnog mehanizma s naglaskom na mjerenje iznosa sile trenja a samim time i odrezivanja srednjeg tlaka trenja. Princip rada zasniva se na sistemu „plutajuće košuljice cilindra“ (*floating liner*) kod kojeg je cilindar oslonjen na četiri senzora sile koji mjere dinamiku sile uzrokovanu uslijed gibanja klip u cilindru od gornje do donje mrtve točke. Shematski prikaz AVL FRISC motora prikazan je na Slici 2.

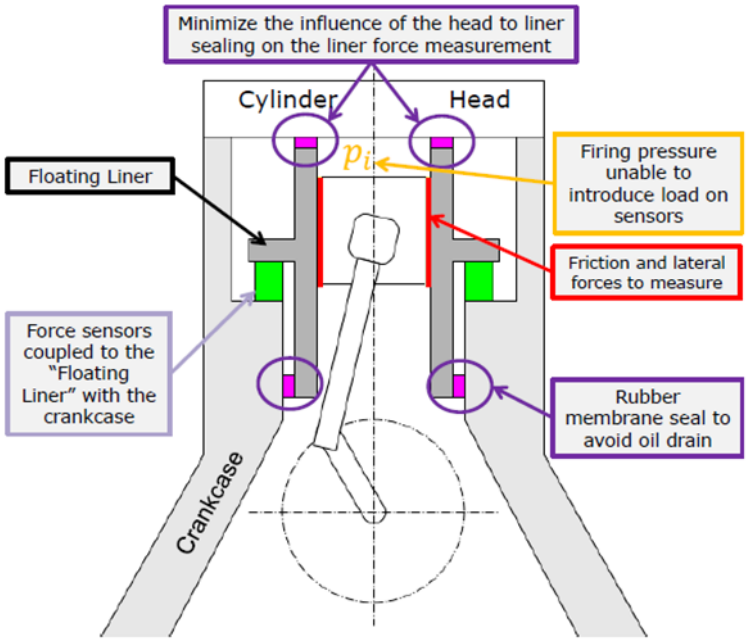

Slika 2. Shematski prikaz AVL FRISC motora. [2]

Osim plutajuće košuljice cilindra, jedan od osnovnih dijelova je i brtveni prsten koji se nalazi između plutajuće košuljice cilindra i glave motora. Uslijed kontakta brtvenog prstena i košuljice cilindra te djelovanja tlaka u cilindru na prsten, generira se sila u aksijalnom smjeru (z os) koja utječe na iznos trenja i stvara „Stick-slip“ efekt. Mjerenja, a kasnije i simulacije, provodna su za dva slučaja paketa klipnih prstena, osnovni i paket sa smanjenim trenjem. Razlika između paketa je vidljiva u iznosu tangencijalne sile prvog i drugog kompresijskog klipnog prstena.

U trećem poglavlju su prikazani simulacijski modeli te su opisani osnovni ulazni podaci. Od ulaznih podataka, prikazane su krivulje opterećenja, profili košuljice cilindra, klipa, klipnih prstena i karakteristike površinske hrapavosti. U programu *AVL EXCITE™ Piston&Ring* uspoređeni su rezultati dinamike klipnih prstena za osnovni sklop klipnih prstena i sklop klipnih prstena sa smanjenim trenjem. Uz to, prikazane su razlike između rješavanja između korištenja 2D i 3D simulacijskog *solvera*. Na Slici 3. je prikazan simulacijski model izrađen u *AVL EXCITE™ Piston&Ring* programu.

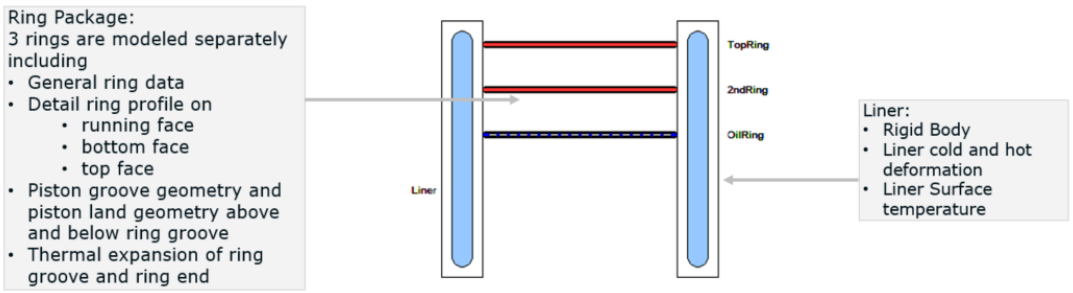

Slika 3. EXCITE™ Piston&Rings model.

Osima navedenog simulacijskog modela, u ovom poglavlju su prikazani rezultati dobiveni programom *AVL EXCITE™ Power Unit.* U tom programu uspoređeni su rezultati dinamike klipa za osnovni sklop klipnih prstena i sklop klipnih prstena sa smanjenim trenjem. Uz to, prikazane su razlike između korištenja *REVO* i *EHD* spojeva u modelu. . Na Slici 4. je prikazan simulacijski model izrađen u *AVL EXCITE™ Power Unit* programu.

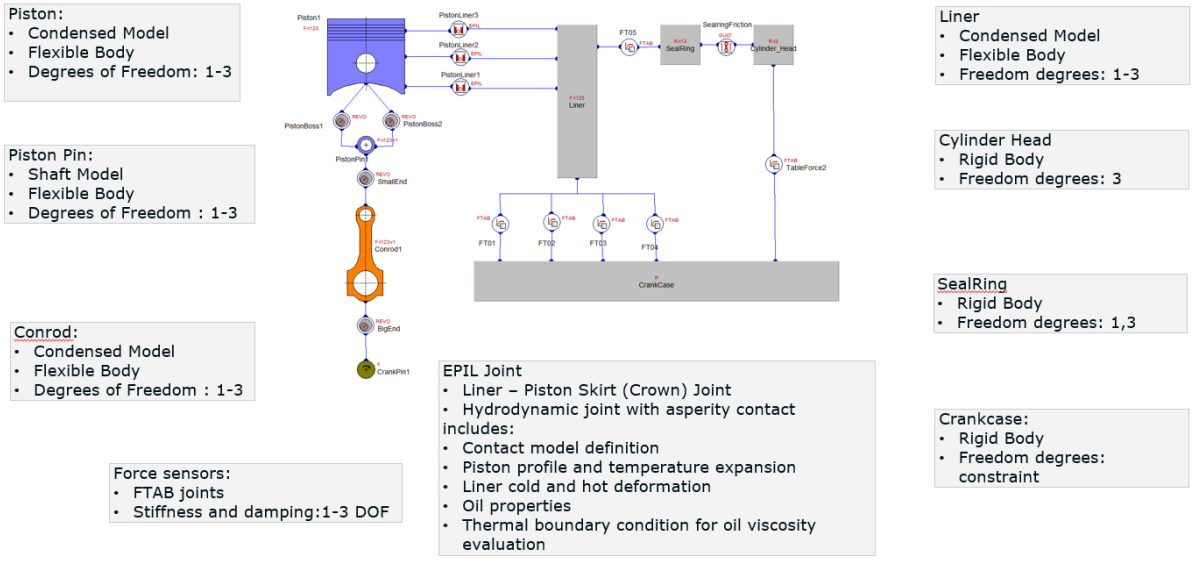

Slika 4. EXCITE™ Power Unit REVO FRISC model.

U 4. poglavlju je prikazana usporedba rezultat između mjerenja i simulacija. Uspoređeni su profili sile trenja i bocne sile na klipu, srednjeg tlaka trenja, potrošnje ulja klipnog mehanizma i prestrujavanja zraka. Također, prikazana je raspodjela srednjeg tlaka trenja klipnog mehanizma i ispitan je utjecaj mijenjanja različitih parametara trenja na rezultate srednjeg tlaka trenja.

U 5. poglavlju istaknuti su zaključci provedenog istraživanja i preporuke za daljnji rad. Male razlike su vidljive u rezultatima prestrujavanja zraka u kućište motora između rezultata simulacija osnovnog paketa i paketa smanjenog trenja klipnih prstena, te su vidljive značajnije razlike u prestrujavanju između mjerenja i rezultata modela sa smanjenim trenjem. Također, vrijednosti prestrujavanja izračunati sa 3D *solverom* imaju vise vrijednosti u odnosu na rezultate sa 2D *solverom*. Postignuta je sličnost u obliku krivulja sile trenja i bocne sile izračunate simulacijom i dobivene mjerenjem. Između naprednijeg modela (EHD) i jednostavnijeg modela (REVO) nije vidljiva razlika u krivuljama sile trenja. Na slici 5. je prikazana usporedba sile trenja između simulacija i mjerenja.

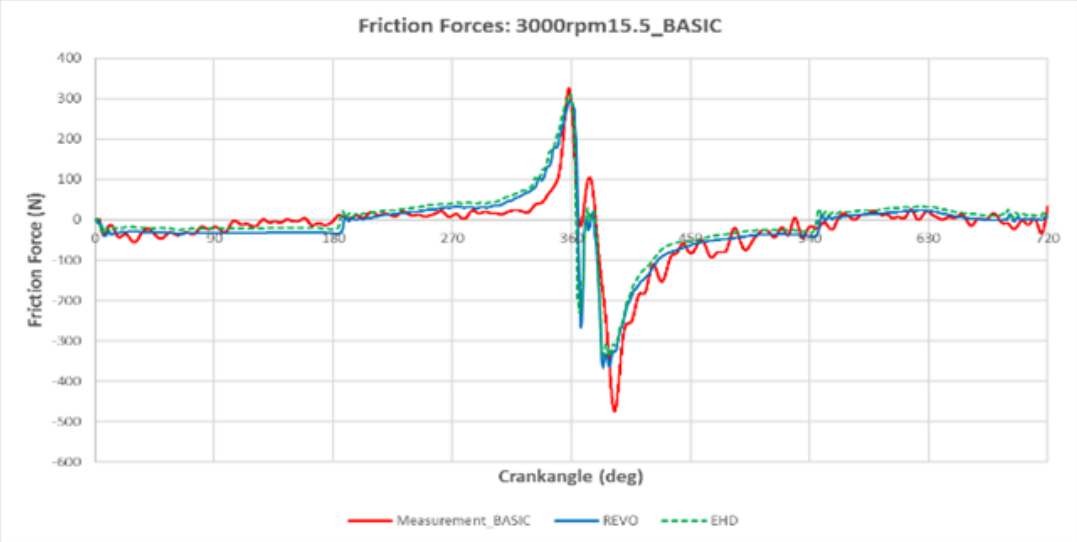

Slika 5. Usporedba rezultata sile trenja.

Simulacijski rezultati srednjeg tlaka trenja izračunati paketom klipnih prstena sa smanjenim trenjem ukazuju nize vrijednosti u odnosu na rezultate osnovnog paketa klipnih prstena dok rezultati mjerenja ukazuju na vise vrijednosti srednjeg tlaka trenja kod paketa sa smanjenim trenjem. Klipni prsteni najviše doprinose srednjem tlaku trenja u ukupnom iznosu srednjeg tlaka trenja klipnog mehanizma, a najveći doprinos dolazi od uljnog klipnog prstena. Povećanjem opterećenja, doprinos srednjoj vrijednost tlaka od glave motora se povećava, a srednja vrijednost tlaka generirana dodirom klipa i košuljice cilindra se smanjuje

1. INTRODUCTION

This thesis is done in cooperation with AVL – AST d.o.o. from Zagreb and AVL List GmbH from Graz with the purpose of simulating a FRISC (FRIction Single Cylinder) engine of the AVL diesel development project, based on full engine models.

1.1. Motivation

The automotive industry is one of the largest industries in the world. As such, every part of it is brought almost to perfection in regard to cost efficiency and sustainability. ICEs are still the power source of the majority of the automotive powertrains. Although hybrid and electric vehicles are lately coming into fashion, the ICE is still ruling the market, at least for the time being Internal combustion. Fired hardware test are essential for the engine development process but is very time and cost intensities. Therefor it has to be planed carefully and the tested set up has to be selected in a prober way. To reduce the hardware variants on the testbed the efficient parameter studies and optimization processes performed by simulation (multibody dynamics simulation) are gaining more importance. The advantages of simulations are short response times for different variants, lower cost compared to testbed and view “beyond the edge”.

Internal combustion engines are a major fossil fuel consumer as well as a main source of air pollution. Engine friction and oil consumption are the major contributors to the oil and fuel economy. The engine durability, emission and fuel economy are the main targets, which characterize the development of a modern internal combustion engine [1].

A significant contribution of the total power losses in ICEs is due to the piston ring-pack friction. Diesel engines are inefficient with only approximately 40% of the total energy produced by combustion being used as work. Friction accounts for approximately 10% of the total loss and, of that, 50% can be attributed to the piston, connecting rod, and rings with the rings being the cause of the majority. The rest is lost to heat, friction, or auxiliaries such as oil pumps, water pumps, etc. [2].

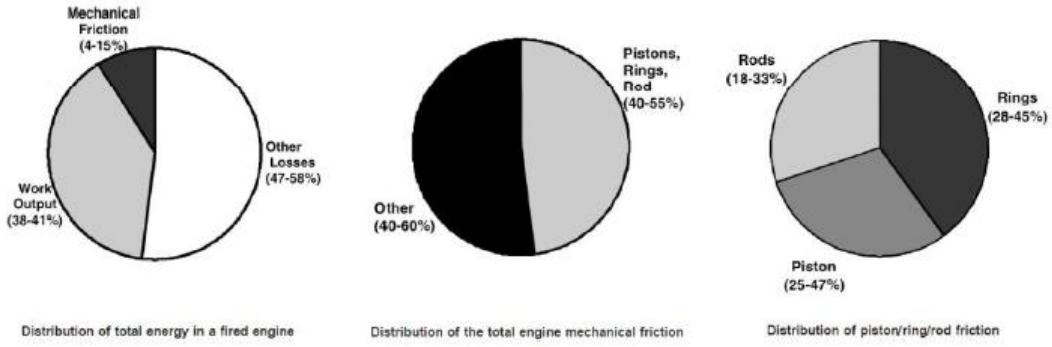

Figure 1. Distribution of engine losses and friction [3].

A common term used to describe engine friction loss is the friction mean effective pressure (FMEP). To calculate fired engine FMEP, the indicated mean effective pressure (IMEP) and the brake mean effective pressure (BMEP) are measured with FMEP being the difference between the two. Indicated mean effective pressure is calculated from the cylinder pressure and represents power produced by combustion pressure. Brake mean effective pressure is calculated from the output torque and represents engine output after losses.

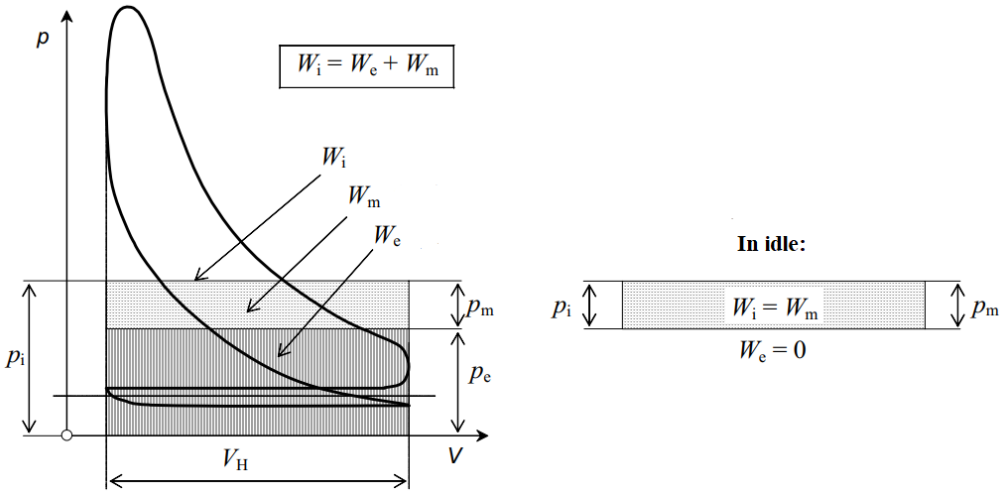

Figure 2. Engine working cycle [3].

1.2. PISTON

The piston is one of the most important parts of internal combustion engines. In the cylinder of an engine, the energy bound up in the fuel is rapidly converted into heat and pressure during the combustion cycle. The heat and pressure values have a strong increase within a very short time period. The piston, as the moving part of the combustion chamber, has the main function of converting this released energy into mechanical work.

The basic structure of the piston is a hollow cylinder, closed on one side, with the segments piston crown, top land, second land, third land, top compression ring groove, second compression ring groove, oil ring groove, skirt and pin boss.

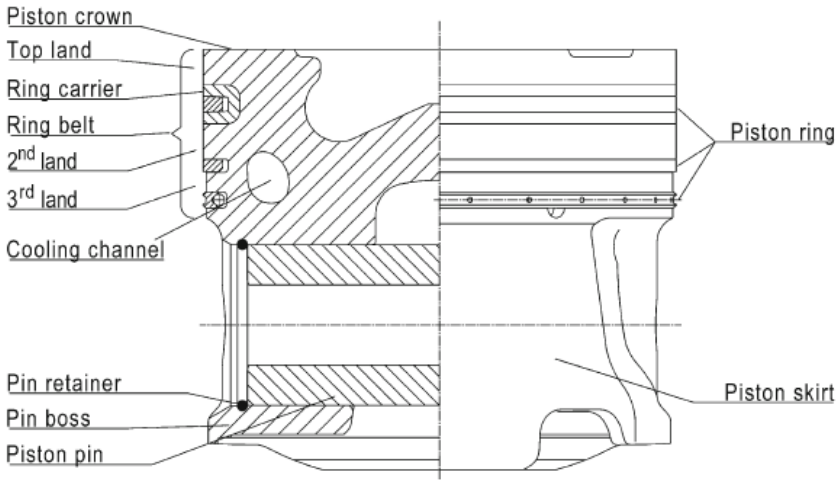

Figure 3. Piston structure [2].

At Figure 4. the most important piston dimensions are shown.

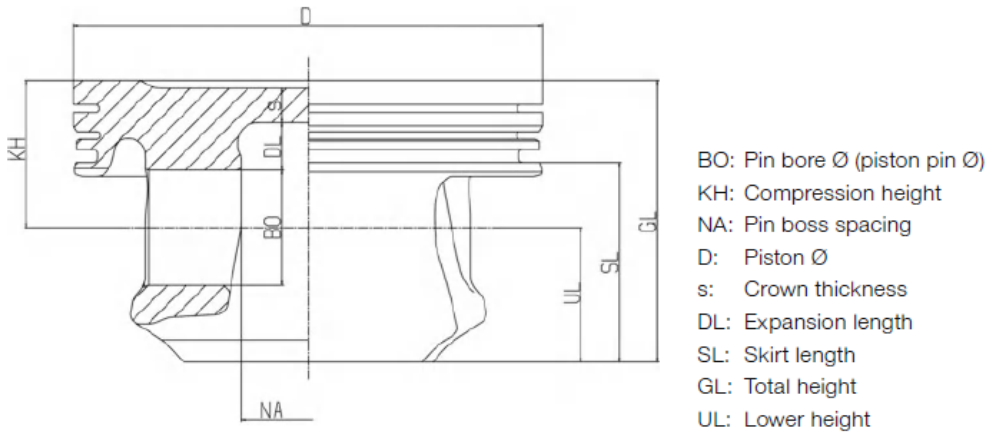

Figure 4. Piston major dimensions [2].

The piston crown transfers the gas forces resulting from the combustion of the fuel-air mixture via the pin boss, the piston pin, and the connecting rod, to the crankshaft. As a moving and force-transmitting component, the piston, with the piston rings, must reliably seal the combustion chamber against gas passage and the penetration of lubricating oil under all load conditions. This task can be achieved only if a hydrodynamic lubricating film is present between the piston rings or skirt and the cylinder bore. At four-stroke engines, the piston crown also

supports the mixture formation. It has a partially jagged shape, with exposed surfaces that absorb heat and reduce the load capacity of the component [2].

1.2.1. Piston tasks and requirements

The most important task that piston should achieved are [2]:

- to transfer the force of gas pressure to the conrod
- sealing off the working chamber
- guiding the sealing elements (piston rings)
- guiding the conrod
- controlling charge exchange (two-stroke engines)
- support of mixture formation (shape of piston head)
- heat dissipation
- variable bounding of the working chamber

To be able to achieve all tasks, piston must fulfill following features [2]:

- structural strength
- adapting to operating conditions
- low friction
- low wear
- low weight with sufficient shape stability
- low oil consumption
- low pollutant emission values

The optimum solution is difficult to achieve because piston requirements are partly contradictory, both in terms of design and material.

1.2.2. Gas pressure and temperature in diesel engines

The maximum gas pressure in the combustion cycle has critical significance for the mechanical loads. Gas pressures occur depending on the combustion process and charge intake (naturally aspirated/turbocharger). In diesel naturally aspirated engine maximum gas pressure achieves value of 80 – 100 bar, and in turbocharged engines the gas pressure increases up to 140 – 240 bar.

The peak temperatures of the exhaust gas can reach levels in excess of 2200°C. The exhaust gas temperature range between 600 to 850°C for diesel engines. Average temperatures on piston crown is 200 – 500 °C (depend on material), 150 – 260 °C on pin boss and 120 – 180 °C

on piston skirt. The amplitude of the temperature fluctuations is only a few °C at the piston surface and drops off rapidly toward the interior. Heat flows that lead to characteristic temperature fields result from the material cross sections heat are determined by the design [2].

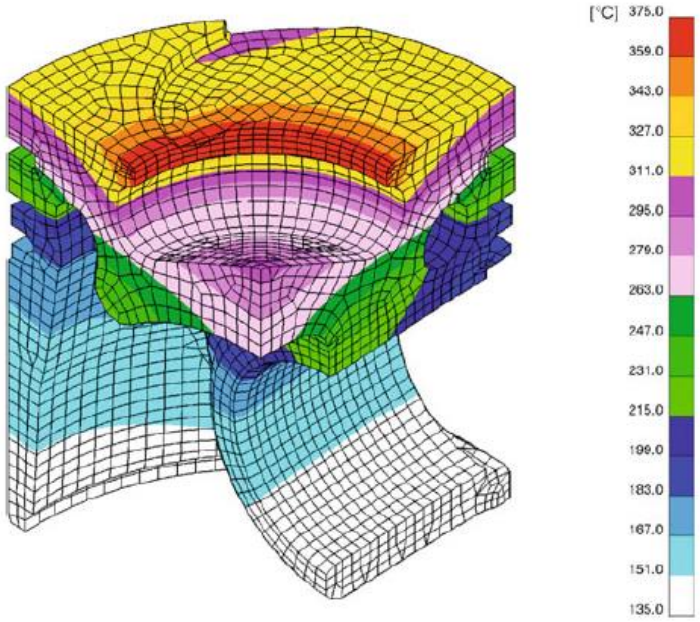

Figure 5. Temperature distribution on piston for diesel engine [2].

The temperature level and distributions in the piston depends on [2]:

- Operating principle (two or four stroke)
- Combustion process (direct/indirect injection)
- Operating point of the engine (speed, torque)
- Engine cooling (water/air)
- Friction between piston skirt/lands and liner
- Design of the piston and cylinder head (location and number of gas channels and valves, type of piston, piston material)
- Piston cooling (spray jet cooling, cooling channel, cooling channel location, etc.)

The strength properties of the piston materials are very dependent on the temperature. High thermal loads cause a drastic reduction in the fatigue resistance of the piston material. The critical locations for diesel engines with direct injection are the boss zenith and the bowl rim. The temperatures in the first piston ring groove are significant in terms of oil coking. If certain limit values are exceeded, the piston rings tend to “lock up” (coking) due to residue build-up in the piston ring groove, which leads to an impairment of their functionality.

1.2.3. Piston clearance and ovality

The piston deforms and stretches under the influence of the gas pressure and gas temperatures. This change in shape must be considered in advance to prevent binding at operating temperatures. This is done with a piston shape that deviates from the ideal circular cylinder. The piston must therefore be installed with some clearance in the cold state, which takes the expected deformation and the secondary piston motion into consideration. The piston profile (micro piston contour) deviates from the ideal circular cylinder in the axial direction (conicity, barrel shape) and in the circumferential direction (ovality) [2].

Pistons typically have a slightly smaller diameter in the piston pin axis than in the thrust – antithrust plane due to ovality. The oval shape of the crown and skirt provides many design opportunities. The skirt ovality creates space for thermal expansion in the piston pin axis direction. The ovality can be varied to generate an even wear pattern with sufficient width. It is typically (diametric) 0.3–0.8% of the piston diameter. In addition to the normal ovality, ovalities with superposition are also possible, such as double or tri-ovality. For double ovality, in the form of a positive or negative superposition, the local piston diameter is greater or less than for normal ovality. The positive superposition widens the wear pattern relative to normal ovality, and the negative makes it narrower. Tri-ovality widens the wear pattern, which is limited due to a reduced local piston diameter starting at about 35° from the thrust – antithrust axis [2].

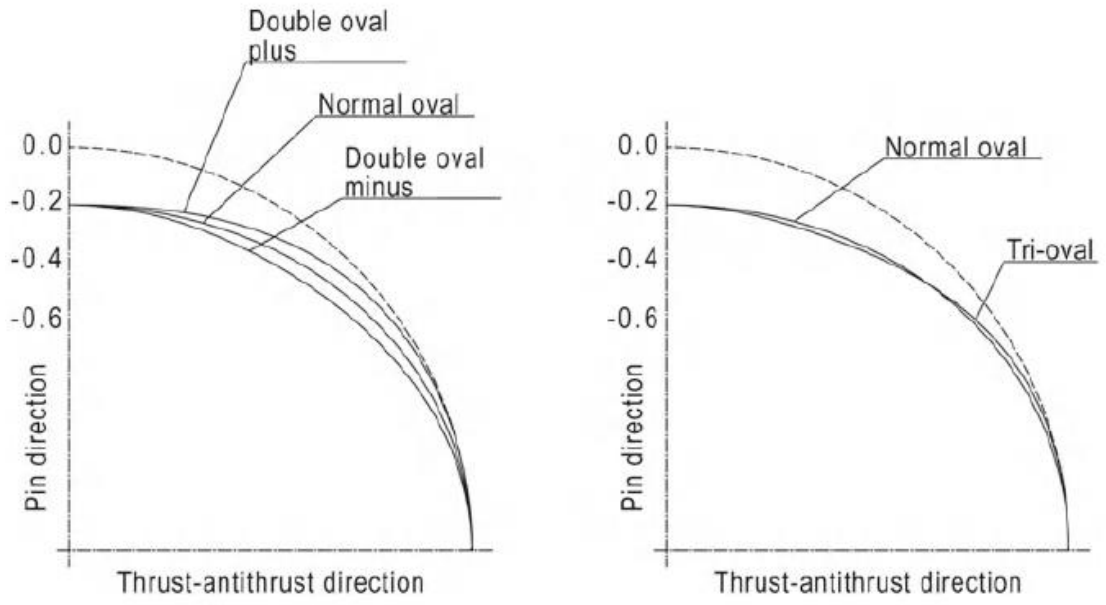

Figure 6. Ovality and superposition [2].

1.2.4. Diesel piston types

The piston shape is determined by the combustion process. In Diesel engines with directed injection of fuel into the cylinder, the combustion chamber is located in the dent of the piston head. Diesel engines with split combustion chamber have a shallow dent at the head of the piston, which enhances the swirling of the fuel mixture that flows from the antechamber or swirling chamber to the cylinder.

1.2.4.1 Ring carrier pistons

The ring carrier is made of an austenitic cast iron with a similar coefficient of thermal expansion to that of the piston material. The material is particularly resistant to frictional and impact wear. The first piston ring groove is protected with ring carrier against excessive wear. This is particularly advantageous at high operating temperatures and pressures, which are particularly prevalent in diesel engines [2].

Figure 7. Ring carrier piston [2].

1.2.4.2 Piston with cooled ring carrier

The cooled ring carrier significantly improves the cooling of the first piston ring groove and the thermally highly loaded combustion bowl rim. The intensive cooling of this ring groove makes it possible to replace the usual double keystone ring with a rectangular ring [2].

Figure 8. Piston with cooled ring carrier [2].

1.2.4.3 Piston with bushing in the pin bore

One of the most highly stressed areas of the piston is the piston pin bearing. Temperatures of up to 240°C can occur in this area, a range at which the strength of the aluminum alloy starts to drop off considerably. For this reason, is developed a reinforcement of the pin bore, using shrink-fit bushings made of a material with higher strength (CuZn31Si1) [2].

Figure 9. Piston with bushing in the piston bore [2].

1.2.4.4 FERROTHERM piston

FERROTHERM piston is commercial name for pistons that are designed by manufacturer MAHLE. This piston has two parts, piston crown and piston skirt and they are implemented separately. The piston crown, made of forged steel, transfers the gas pressure to the crankshaft via the piston pin and connecting rod. The aluminum skirt bears the lateral forces that arise due to the angle of the connecting rod and can therefore support the piston crown with an appropriate design. The FERROTHERM piston exhibits good wear values in addition to high strength and temperature resistance. Its consistently low oil consumption, small dead space, and relatively high surface temperature provide good conditions for maintaining low exhaust emissions limits. FERROTHERM pistons are used in highly loaded commercial vehicle engines [2].

Figure 10. FERROTHERM piston. [2]

1.2.4.5 MONOTHERM piston

MONOTHERM piston is commercial name for pistons that are designed by manufacturer MAHLE. This piston type is a single-piece forged steel piston that is weight optimized. With a small compression height (to less than 50% of the cylinder diameter) and machining above the pin boss spacing (internal), the piston mass, including the piston pin, is nearly that of the mass of a comparable aluminum piston with piston pin. The MONOTHERM piston is used in commercial vehicle engines with peak cylinder pressures of up to 20 MPa [2].

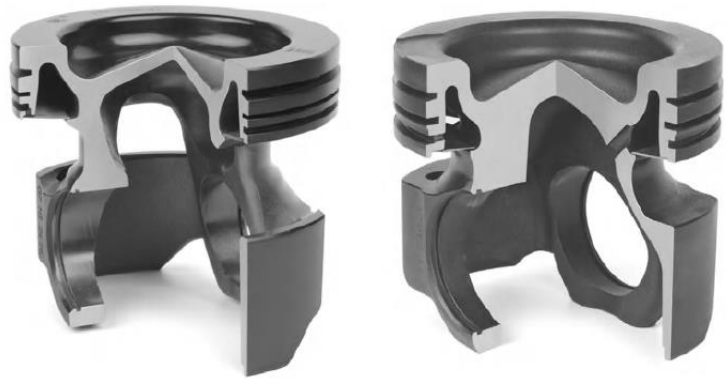

Figure 11. MONOTHERM piston (left) and optimized MONOTHERM piston (right) [2].

On the right picture is shown MONOTHERM optimized piston. The advantages of the optimized MONOTHERM piston are:

- Stiffening of the structure (reduced deformation and greater load capacity)
- Reducing the secondary piston motion, resulting in both a reduced tendency to cavitate and improved guide properties, particularly for the piston rings
- Smoothing of surface pressure on the skirt
- Additional surface and additional cross section for heat dissipation
- Advantages in forging and machining

The optimized MONOTHERM piston is used for peak cylinder pressures of up to 25 MPa [2].

1.2.4.6 MonoXcomp piston

MonoXcomp piston is commercial name for pistons that are designed by manufacturer MAHLE. This piston is a composite piston consisting of several parts:

- The piston crown with integrally formed antifatigue shaft and screw thread
- The thrust sleeve, which features a nut thread and an elastically deformable part with contact zone for transmitting power to the piston skirt
- The piston skirt with the counterpart to the contact zone.

It has an integrally formed antifatigue collar, and the interior is deformable like a Belleville spring washer. The ability to use different materials for the piston crown, piston skirt, and thrust sleeve enables the optimal utilization of material potentials. For piston crowns, the use of highly temperature-resistant and oxidation-resistant materials allows for extreme loads. The structure, which is very rigid due to its closed form, reduces deformations in the piston and thereby enables

thin walls and peak cylinder pressures greater than 25 MPa. The thin walls in the bowl area, in turn, improve the piston cooling and thus allow greater heat flow [2].

Figure 12. MonoXcomp piston [2].

1.2.4.7 Monosteel piston

Monosteel piston is commercial name for pistons that are designed by manufacturer Federal – Mogul. This is dual friction-welded construction, enabling large cooling galleries for high – temperature resistance and strength. The two-piece welded piston design allows the cooling gallery to be closer to the top of the piston, resulting in significant piston temperature reduction [4].

Figure 13. Monosteel piston [4].

Monosteel Magnum is optimized Monosteel piston by manufacturer Federal – mogul. It

is a first diesel piston with double – band piston skirt. This piston has friction reduction of 17% when compared to conventional steel pistons.

Figure 14. Monosteel Magnum [5].

1.2.5. Piston materials

The functions of the piston and the loads that act on it present a set of requirements for the piston material. If low piston weight is the goal, then a low-density material is preferred. Besides its design shape, the strength of the material is the deciding factor for the load capacity of the piston. The change in loads over time requires both good static and dynamic strength.

The thermal conductivity of the material is of significance for the temperature level. As a rule, a high thermal conductivity is advantageous, because it promotes uniform temperature distribution throughout the piston. Low temperatures not only allow greater loading of the material, but also have a beneficial effect on the process parameters at the piston crown, such as the volumetric efficiency and knock limit.

Static and dynamic strength values describe material behavior under isothermal conditions. Pistons are exposed to severe changes in temperature at times. The transient heat stresses that arise place cyclical loads on the material that can sometimes exceed the elastic limit, so materials must be resistant to these stresses. Due to the motions and forces that occur at the sliding and sealing surfaces, piston materials must also meet high requirements for seizure resistance, low friction, and wear resistance.

The requirements for the thermal expansion behavior of the piston material depend on the material pairings of the cylinder and the piston pin. Differences in thermal expansion coefficients

should be kept as low as possible in order to minimize changes in clearance between the cold and warm states.

A material with good machining properties supports cost-effective production in large quantities. The manufacture of the raw part should be as near to net shape as possible and should contribute to high material quality. Suitable processes include gravity die casting and forging. The sliding and sealing surfaces demand high-precision finishing, which requires suitable machinability of the material [2].

1.2.5.1 Aluminium materials

As a light alloy with high thermal conductivity, aluminum is often used as a piston material. In the unalloyed state, its strength and wear resistance are too low. Alloys that are suitable for pistons mainly have aluminum-copper-magnesium and aluminum-magnesium silicon solid solutions.

Figure 15. Aluminum pistons for diesel engines [6].

Pistons are almost exclusively made of aluminum-silicon alloys of eutectic, and partly hypereutectic composition, which can be cast easily and nearly always can be forged as well. Aluminum-silicon piston alloys are employed mainly for cast pistons. They can also be forged for special purposes, which leads to somewhat different microstructures and properties. Compared to the cast state, the material in the forged state exhibits greater strength and greater plastic deformability (greater elongation after fracture). The strength advantage of the forged material structure is greatest in the lower and middle temperature ranges, up to about 250°C, and drops off at high temperatures [2].

1.2.5.2 Cast iron materials

Cast iron materials generally have a carbon content of > 2%. MAHLE uses high-quality cast iron with lamellar and spherolithic graphite for its products. For the materials used in piston casting, the basic material of the structure is largely perlitic, due to its good strength and wear properties. Pistons in highly stressed diesel engines and other highly loaded components in engines and machine design are predominantly made of M-S70 spherolithic cast iron. This material is used for single-piece pistons and piston skirts in composite pistons. Due to their relatively high thermal expansion in comparison to cast irons with perlitic or ferritic basic structures, austenitic cast iron materials are of great significance to produce ring carrier pistons [2].

Figure 16. Cast iron piston [7].

1.2.5.3 Steel materials

Steels used for components generally have a carbon content of less than 0.8%. For very highly stressed pistons and piston components, the chromium-molybdenum alloy of heat-treated steel 42CrMo4 is used. Both alloying elements promote carbide formation to improved full hardenability, and molybdenum also increases strength at elevated temperatures. Decrease in strength toward the core area must be expected for very large heat-treatment cross sections or changes in cross section [2].

Material, 38MnVS6 is preferably used in steel pistons for commercial vehicle engines and for forged steel skirts in composite pistons. This steel material is built with technology for

increasing the strength of metallic materials, and this technology is called precipitation hardening. Precipitation-hardened ferritic-perlitic steels exhibit small amounts of vanadium or niobium added. This material is preferably used in steel pistons for commercial vehicle engines and for forged steel skirts in composite pistons. The advantages of this group of materials, compared to heat-treated steels, are improved machinability of the ferritic-perlitic structure and the elimination of costly subsequent heat treatment [2].

Both steel grades, 42CrMo4 heat-treated steel and 38MnVS6 AFP steel, are suitable for use at temperatures of up to 450°C regarding strength at elevated temperatures and oxidation resistance.

Bolts that connect the piston crown of a composite piston to the piston skirt are generally made of 42CrMo4 heat-treated steel. They must comply with the highest DIN 267 strength classification of 10.9. Sometimes, 34CrNiMo6 heat-treated steel is used, which has even greater full hardenability due to the addition of nickel [2].

1.2.6. Coatings on steel pistons used in diesel engines

Coating of the piston skirt is intended to prevent local welding between the piston and the cylinder, or piston seizing. Under moderate operating conditions, a piston does not require a skirt coating if its dimensions are designed carefully and correctly. Risk of seizing does exist under extreme operating conditions [2]:

- Lack of local clearance caused by mechanical and/or thermal deformation of the cylinder
- Insufficient oil supply, such as during cold start
- Insufficient lubrication capability of the engine oil, caused by fuel contamination, extremely high operating temperature, or excessive aging of the oil
- In brand-new condition, when the piston and cylinder have not yet been run in

A coating on the piston skirt provides protection in such extreme situations. It is important that the skirt coating be tribologically matched to the cylinder bore (cast iron or aluminum).

1.2.6.1 Grafal 255

The standard coating for the piston skirt is GRAFAL, for pistons of all sizes and types that are paired with cast iron cylinders. GRAFAL 255 is commercial name for piston coating created by manufacturer MAHLE. GRAFAL is an approximately 20-µm thick sliding lacquer coating with fine graphite particles embedded in a polymer matrix. It withstands temperatures of up to 250°C that can occur at the piston skirt and is resistant to oils and fuels. The film-forming

polymer matrix supports the action of the solid graphite lubricant during dry running, with advantageous tribological properties. This provides great seizure resistance for very low clearances and a lack of oil. Under normal loading conditions, the coating does not wear. Under extreme loads, particularly in case of high local surface pressure, it can be partially worn off locally. Due the self-lubricating properties of GRAFAL, pistons can exhibit very low clearances, which produces favorable acoustic properties with low friction [2].

1.2.6.2 Grafal 210

GRAFAL 210 is commercial name for piston coating created by manufacturer MAHLE. The layer consists of a highly temperature-resistant polymer matrix, in which graphite particles and molybdenum sulfide pigments added as a pressure resistant component are embedded. The layer thickness is about 8 μm and provides longer antiscuffing/-seizing protection in the piston pin bore during the run-in phase. This coating is used for steel piston in heavy duty Diesel engines of commercial vehicles [2].

1.2.6.3 Phosphate

Phosphate coatings can provide effective protection against seizing and scuffing between sliding pairs, especially in run-in phases. This effect can also be exploited for pistons, particularly for diesel engine pistons to protect the pin boss. Thick layers (averaging 5 μm) of manganese-iron mixed phosphates are deposited on steel pistons (MONOTHERM, FERROTHERM). They enable direct pairing with hardened steel pins, without the use of pin bore bushings [2].

1.2.6.4 EvoGlide

EvoGlide was developed to improve the sliding lacquer layer wear resistance in the piston/cylinder bore system over the service life of the engine. The sliding lacquer layer should be improved because the lateral forces on the piston skirt are increased when implementing a downsizing concept. The addition of certain additives makes the resin matrix more wear-resistant. EvoGlide is an approximately 15-μm thick sliding lacquer coating [2].

1.2.7. Differences between aluminium and steel pistons

This chapter describes differences in design, temperature field, cooling, friction and fuel consumption between steel and aluminium pistons.

1.2.7.1 Comparison of the steel and aluminum piston designs

Steel is characterized by the following properties as compared with aluminum:

- reduced thermal expansion
- increased strength
- greater density
- reduced thermal conductivity

Compared to aluminum, steel possesses a higher fatigue strength, which allows it to fulfill the demands placed on modern passenger car diesel engines peak cylinder pressures of up to 250 bar. This is one of the main reasons why is today often used steel piston in comparison to the aluminum pistons in diesel engines.

For the steel piston, the wall thickness can be reduced greatly due to its higher strength. Consequently, the weight of the piston group can be the same or even lower with a steel piston concept. The reduced oscillating masses may make it possible to eliminate the balance shafts. The reduced compression height can be used to extend the length of the conrod in an existing engine concept, while keeping the swept volume the same. This reduces the maximum lateral forces and therefore the friction forces on the piston skirt. It is also possible to take advantage of the reduction in compression height by adjusting the displacement of the engine and the combustion chamber geometry. It appears possible to reduce compression height by up to 30 % and top land height by up to 50 %. For a new development of an engine series, the reduced compression height can directly reduce the overall height of the engine, thus decreasing the installation space required. This can have a positive effect on the c_w value and pedestrian protection for the vehicle [8].

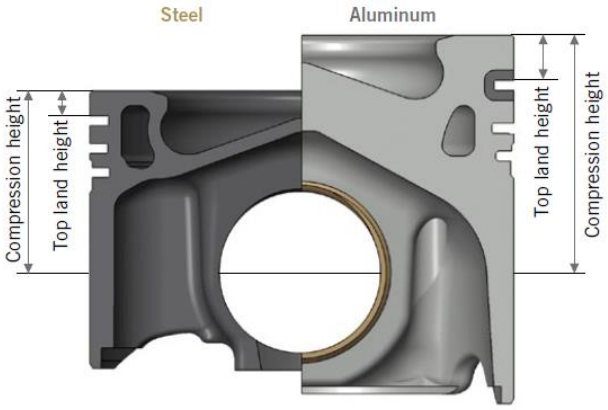

Figure 17. Geometrical comparison of steel and aluminum pistons [8].

Reducing the top land volume, the first piston ring on the steel piston can be placed at a higher position than on the aluminum piston. The smaller top land volume is advantageous for CO emissions of the steel piston and has a positive influence on the effective compression ratio for the same combustion chamber geometry. It is beneficial to reduce this volume, which makes this a system advantage of the steel piston [8].

For measurements with identical ring packs, the steel piston results in 15 to 45 % less blow-by. About 30 % (at partial load) or 10 % (at high load) of the advantages in fuel consumption can be ascribed to the difference in blow-by.

1.2.7.2 Piston cooling

Key factors in designing the cooling gallery include a small distance from the bowl rim as well as thermal shielding of the first ring groove. The steel piston allows the cooling gallery to be positioned higher thus reducing the top land height. Compared to aluminum pistons the cooling gallery volume is 57 % larger, and the effective gallery heat transfer surface 54 % larger. Also important is the free inner cooling gallery height, which enables high heat flows during the piston stroke by convection. The lower temperature level in the ring zone compared with aluminum pistons according to the analysis reduces ring groove carbonization as well as groove and piston ring wear over piston lifetime [8].

An optimized oil flow rate provides the opportunity to adjust the piston temperature in a targeted manner with a reasonable level of effort. This is better achieved for the steel piston than for the aluminum piston. For small oil flow volumes, the steel piston exhibits a friction advantage of 0.04 bar (corresponding to 1 g/ kWh BSFC). This is because the temperature at the skirt rises

by 15 °C for a smaller oil volume flow, and the reduced oil viscosity has a positive effect on friction. In contrast, small oil volume flows are critical for steel pistons with respect to cooling channel coking and surface scaling [8].

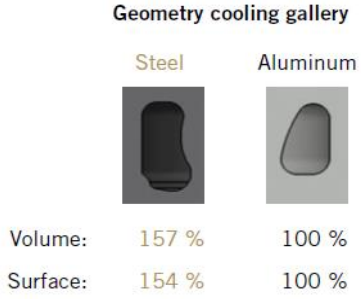

Figure 18. Geometry cooling gallery [8].

1.2.7.3 Temperatures on pistons

The temperature distribution in the aluminum and steel piston are fundamentally different. In the aluminum piston, the heat is distributed more uniformly due to the high thermal conductivity and larger material cross sections and is then dissipated by the cooling oil. The heat transport in the steel piston, in contrast, is rather limited and takes place primarily by means of the cooling oil. The lower thermal expansion of steel furthermore allows the installation clearance to be tight, while maintaining sufficient operating clearance, when the piston is hot. Due to the difference in thermal expansion between steel piston and aluminum cylinder block, the operating clearance increases as the temperature rises, and the piston may strike the cylinder wall with greater impact. This can be counteracted by optimizing the piston installation clearance, the shape of the piston, and the piston pin offset.

Bowl rim temperatures ranging from 360 to 420 °C are attained with aluminum pistons, whilst steel piston temperatures here range from 385 to 450 °C. Due to lower thermal conductivity of steel an approximately 30 °C higher temperature occurs at the bowl rim. An approximately 50 °C lower temperature in the first ring groove is a characteristic feature of passenger car steel pistons. While aluminum pistons exhibit groove temperatures of 260 to 300 °C, the groove temperatures determined for steel pistons reach a lower level of 220 to 245 °C as a result of longer heat conduction path between combustion bowl and ring zone, lower thermal conductivity of steel and a large cooling gallery with increased cooling oil flow. Pin boss temperatures measured for aluminum pistons are 230 to 250 °C. The significantly reduced compression height of steel pistons and the resulting lower distance between pin boss and combustion bowl lead to pin boss temperatures of 290 to 320 °C [8].

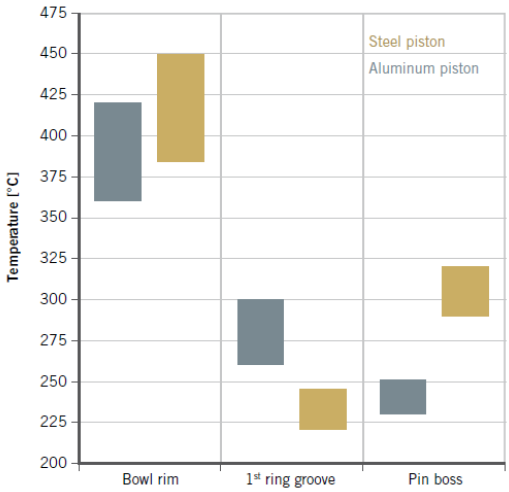

Figure 19. Measured temperatures of aluminum and steel pistons [8].

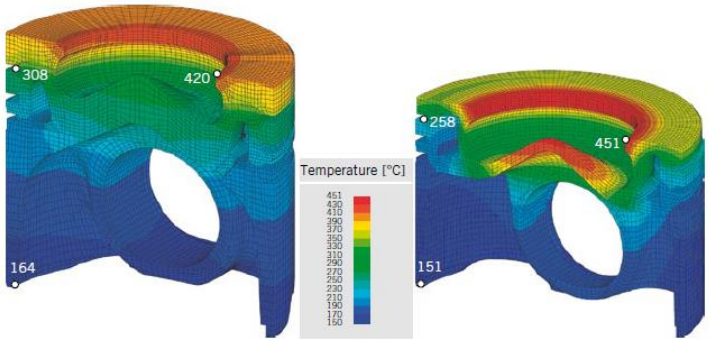

Figure 20. Measured temperature distribution on aluminum and steel piston [8].

The Figure 20. shows the temperature distribution for both piston designs for identical engine performance demonstrates the influence of significantly lower thermal conductivity of steel. The larger cooling gallery in the steel piston shields the ring zone from the heat input into the combustion chamber bowl, such that the groove temperatures are more than 50 °C lower than with aluminum pistons. Temperature levels more than 30 °C higher arise in the bowl rim and bowl bottom.

1.2.7.4 Friction losses

Steel piston have reduction of friction losses in comparison to aluminum pistons. There is a less thermal overlap in cylinder block because steel have reduced thermal elongation.

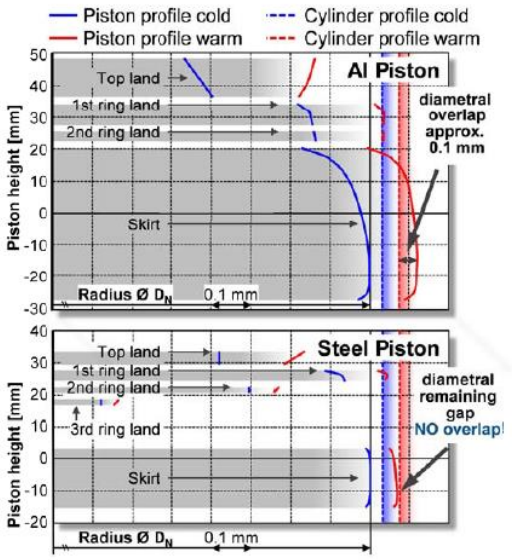

Figure 21. Thermal expansion behavior of the aluminum piston (top) and steel piston (bottom) [10].

In connection with the minimized area and asymmetric design of the piston skirt surfaces, this effect leads to a 50 % decrease in average friction power at the observed partial load point [8].

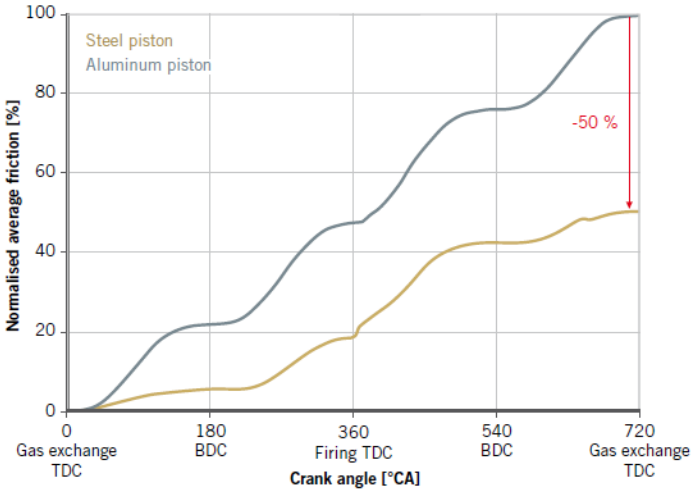

Figure 22. Normalized average friction between aluminum and steel pistons [8].

The steel piston has a friction advantage under high loads of up to 0.1 bar friction mean effective pressure (FMEP), which corresponds to as much as 3 g/kWh break specific fuel consumption (BSFC). Under low loads, the frictional loss behavior of the steel and aluminum variants can be considered essentially comparable (measurement accuracy $\Delta FMEP = \pm 0.03$ bar). The equivalent level of friction in this comparison is achieved with an aluminum piston with relatively high installation clearance. As the clearance is reduced, the frictional loss advantage of the steel piston becomes more pronounced [8].

1.2.7.5 Emission

The higher surface temperatures of the steel piston have a positive effect on the HC, CO and carbon particles emissions at partial load. This can be attributed to better fuel mixture preparation and more complete combustion. The reduction of HC emissions by 76 % at a constantly maintained EGR rate is significant, but the lowering of soot emissions by 50 % as well as the CO emissions by 23 % also demonstrate a clear advantage for the steel piston. Increased surface temperatures and improved fuel utilization however result in higher combustion temperatures, which lead to 29 % higher NOx emissions. In combination with longer connecting rods, which reduce lateral forces and piston skirt friction, the improved fuel utilization also leads to an advantage in specific fuel consumption of up to 4 % [8].

Measurements under full load show that NOx emissions are on the same level as for aluminum pistons when operating under the same boundary conditions as steel pistons (peak cylinder pressure, turbocharger speed). The cause for this is the dominant combustion temperature at full load as compared to the temperature on the piston surface. An exhaust temperature increases of only 1 %, caused by thermal flow restriction, results in an advantage for steel pistons in the order of 20 % regarding soot emissions. HC and CO emissions only play a subordinate role under full load in the range of only a few ppm [8].

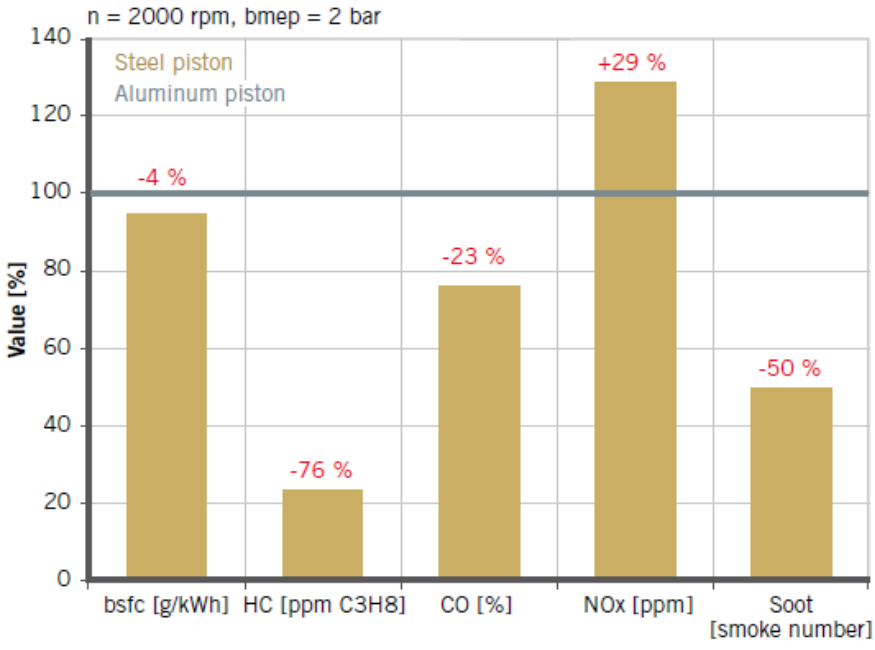

Figure 23. Engine operating performance with aluminum and steel pistons [8].

1.3. PISTON RINGS

A piston ring is a split ring that fits into a groove on the outer diameter of a piston in an internal combustion engine. Piston ring are the most endangered in the Diesel engines, and the most endangered is the first piston ring (compression ring) because it is exposed to the highest pressure and the highest combustion temperatures. Except the compression ring, pistons are with oil ring and mostly with second compression ring assembled [9].

Piston rings main functions are [9]:

- sealing the gap between moving piston and cylinder liner surface to prevent the combustion gases from penetrating into the crankcase
- to provide a uniform oil film on the cylinder gore surface
- to prevent the oil passing from the crankcase to the combustion chamber
- assuring the heat flow from the piston to the cylinder

Piston rings main target are [9]:

- blow-by reduction based on optimized ring conformability and overall balance between piston and rings
- friction loss reduction by optimizing tangential forces and piston ring profiles
- oil consumption reduction by optimizing bore distortion and tangential forces
- running face wear reduction based on improved material properties

The top ring seals the ring-liner interface to prevent high pressure gas from escaping from the cylinder into the lower parts of the ring pack. The oil control ring regulates the amount of oil that passes the ring-liner interface to lubricate the upper rings. A second ring is also present in most engines. This ring scrapes down excessive oil that passes the oil control ring-liner interface.

1.3.1. Piston rings design

The top two rings are designed with a diameter that is larger than the size of the cylinder bore in which they are to be installed. They are made with a gap in their circumference so that they can be compressed to fit into the cylinder bore during installation. Once they are installed, their own tension allows them to maintain an effective seal against the liner.

The top ring has a barrel-shaped face profile, which has been shown to be most effective for lubrication. Sufficient lubrication is critical for the top ring as it is subjected to the high cylinder pressures, which can result in large radial forces acting on the back of the ring. If there is no lubrication between the top ring and the liner, large contact pressures can be generated, and this can result in significant wear and an increase in the top ring gap over time. This will result

in higher power losses due to the larger amount of high-pressure gases in the cylinder that can escape through the larger gap. Cast iron Goetze KV4 or KV1 with flash chrome plated side faces or steel nitride with 18% chrome (X90CrMoV18) is often used for manufacturing first piston ring [12].

The second ring, also called the scraper ring, has a tapered face so that it cannot accumulate oil on its upper edge to scrape it in the upward direction towards the combustion chamber. However, it can very effectively accumulate oil on its lower edge to scrape it down toward the crankcase to prevent excessive oil from reaching the top ring.

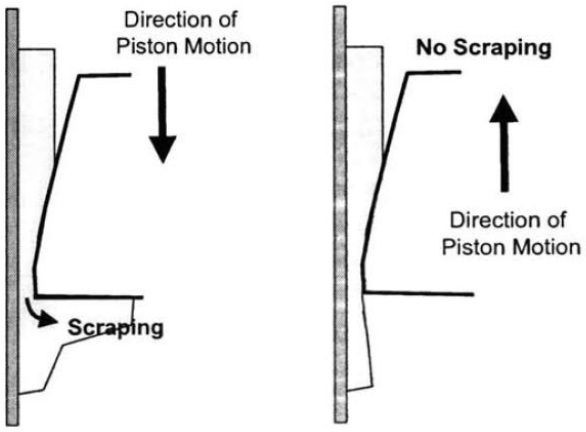

Figure 24. Effect of taper face ring profile on oil transport [11].

The design of the oil control ring is quite different from that of the compression rings. The twin-land oil control ring is one of designs of oil control rings and it is typically used in large diesel engines. This ring consists of a spring mounted inside two rails to ensure adequate conformability to the liner. The circumferential length of the spring determines the tension of the oil control ring once installed in the cylinder bore. The high-tension force from the ring on the liner created by the spring is necessary to achieve adequate conformability when thermal and mechanical deformation of the cylinder bore occurs during engine operation. Cast iron or steel nitride are used for manufacturing oil ring.

Piston rings are designed to have positive ovality or negative ovality. High speed gasoline engines usually have rings with positive ovality since this condition has a damping effect on the vibration of the ring thus reducing ring flutter. If rings having excessive negative ovality, then blow-by past the ring can be high with subsequent loss in performance and possible wear.

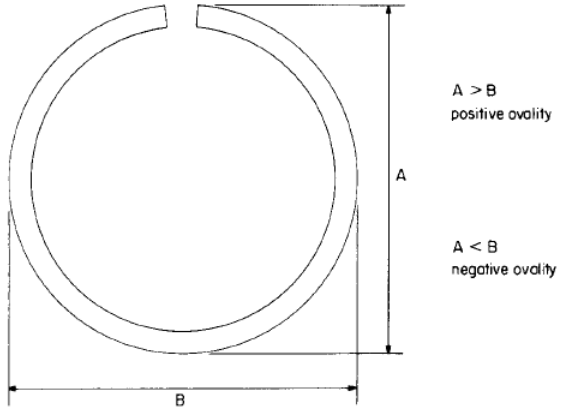

Figure 25. Piston ring ovality [2]

On the Figure 26. and figure 27. are shown different types of compression and oil ring profiles. These profiles are developed for different piston and for friction reduction and different lubrication performance.

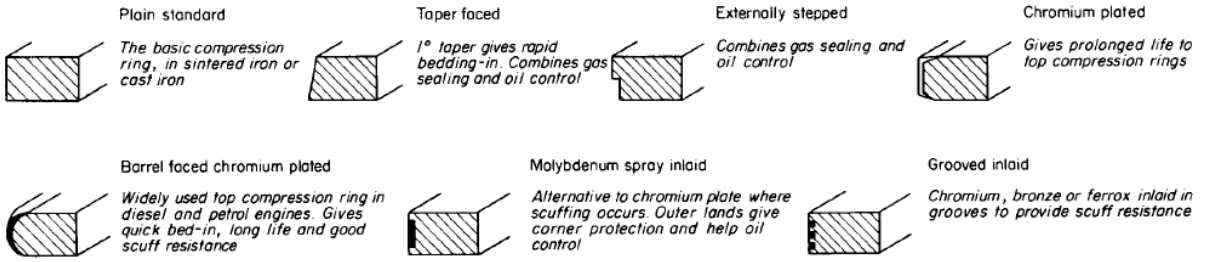

Figure 26. Compression rings [13].

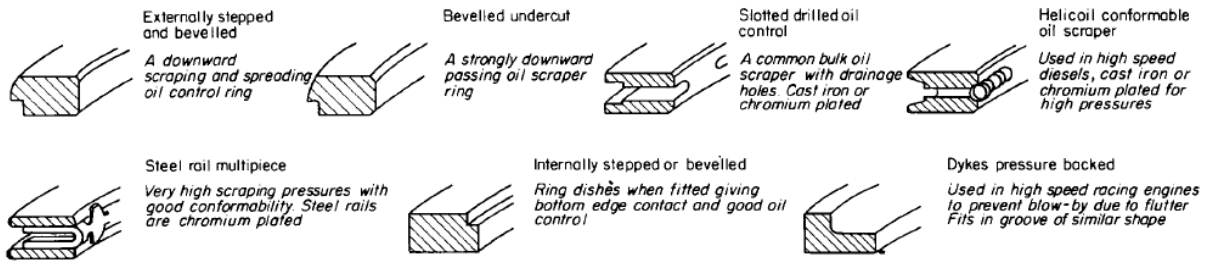

Figure 27. Oil control rings [13].

1.3.2. Piston rings materials and manufacturing

The rings are manufactured with different materials depending on the type of engine in which they are to be installed. In larger diesel engines, the rings are typically made of ductile cast iron due to the high thermal stability of the material, which makes it suitable to the high operating

temperatures in these engines. Steel is the more popular material for rings to be used in smaller gasoline engines because it is stronger than cast iron, and therefore, the size of the rings can be reduced, and conformability improved without a reduction in ring life. High strength, thermal conductivity, thermal expansion, corrosion resistance and resistance to micro welding are properties that determine the characteristics of piston ring materials [13].

Typical axial heights of piston rings range from 1 mm to 4 mm. As a result, machining the rings to precisely match the design specifications is difficult, and tolerances are often on the order of the design values themselves.

Grey cast iron is universally used for the manufacture of piston rings. It's had good mechanical properties, friction and wear characteristics and it is cheap and readily available material. Some cast irons are manufactured containing controlled amounts of carbides obtained by adding chromium, molybdenum and vanadium. Malleable and nodular irons are used where higher strength and fatigue resistance is required but they have the least satisfactory wear characteristics [13].

Material Specification Material	Minimum Bending Strength **) (N/mm^2)	Modulus of Elasticity **) 10^3 x (N/mm^2)	Grade
	Tensile strength *)		
GOE 61 - 18% Cr-Steel GOE 65C - 13% Cr-Steel GOE 64 - SAE 9254	1300 1150 1020	230 210 206	Martensitic Chromium Steel Spring Steel
GOE 52 - KV1 GOE 56 - KV4	1300 1300	>150 >150	Nodular Cast Iron, unalloyed, heat-treated
GOE 44	800	>165	Malleable Cast Iron
GOE 32 - F14	650	130 - 160	Grey Cast Iron, alloyed, heat-treated
GOE 12 - STD GOE 13	350 420	85 - 115 95 - 125	Grey Cast Iron, unalloyed, pearlitic

*) Bending strength not measurable on steel rings
**) as per GOE Specification

Figure 28. Federal Mogul piston rings materials [14].

Cast iron piston rings are manufactured by casting. There are different types of casting methods, and every method depend on piston ring type. Some of this casting methods are: centrifugal, sand, or individually casting. Except casting, piston ring can be manufactured by powder metallurgy. This manufacturing method is suitable for small piston rings, and the iron, carbon, copper and molybdenum powders are blended together and cold pressed in metal dies to produce ring blanks. The rings are sintered, repressed, resintered, oil impregnated and finish machined. After casting or sintering, piston ring plots must be machined on the highspeed lathes.

The various shapes used for oil control rings are milled out and the ring gap is cut out. Steel piston ring are made from a profiled wire. The rings are first coiled into the circle shape and then the gap is cut out. The necessary shape is obtained using a heat treatment process in which the rings are mounted onto a spindle appropriately designed to impart the required radial pressure distribution [13].

1.3.3. Blow - by

One of most important aspects about analyzing piston rings dynamics is blow – by. Blow – by is a part of the total amount of engine gas that flows from combustion chamber into the crankcase. In addition to the resulting energy loss, blow – by also poses a risk to the piston and piston ring lubrication due to contamination and displacement of the lubricating film, and due to oil coking as a result of overheated temperatures at the locations in contact with the combustion gases. Sealing against gas penetration is mainly accomplished by the first piston ring, which is a compression ring. For naturally aspirated engines, the quantity of blow-by is a maximum of 1%; for turbocharged engines, it is a maximum of 1.5% of the theoretical air intake volume.

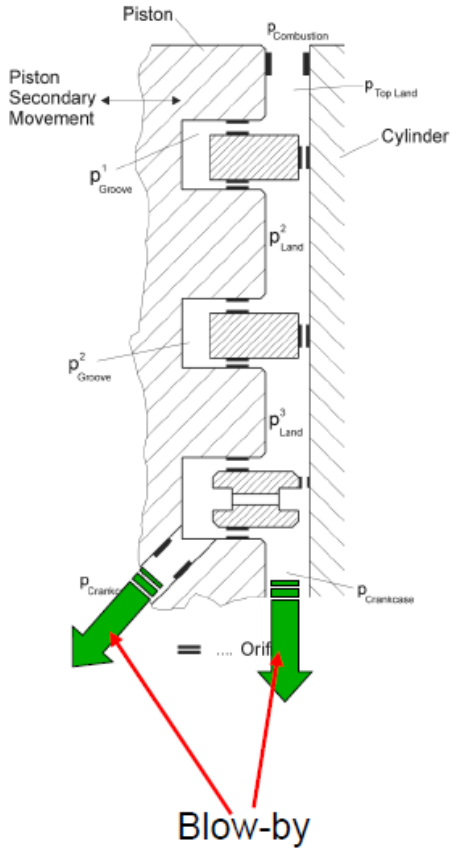

Figure 29. Gas flow in crankcase [9].

1.4. LUBRICATION AND ENGINE FRICTION

Oil consumption is the change of amount of oil in the sump during time. Lube oil consumption occurs due the turbo system, valves, camshafts and the main contributor is piston bore interface. Oil emission is the loss of lube oil through the exhaust system

1.4.1. Lube oil consumption

Lube oil consumption results caused by piston bore interface are:

- total and current lube oil consumption due to evaporation of lube oil from liner wall
- oil throw – off from accumulated oil above the top ring due to inertia forces
- oil blow through the end gap of the top ring into to combustion chamber due to a negative pressure gradient
- oil scraping at piston top land's edge

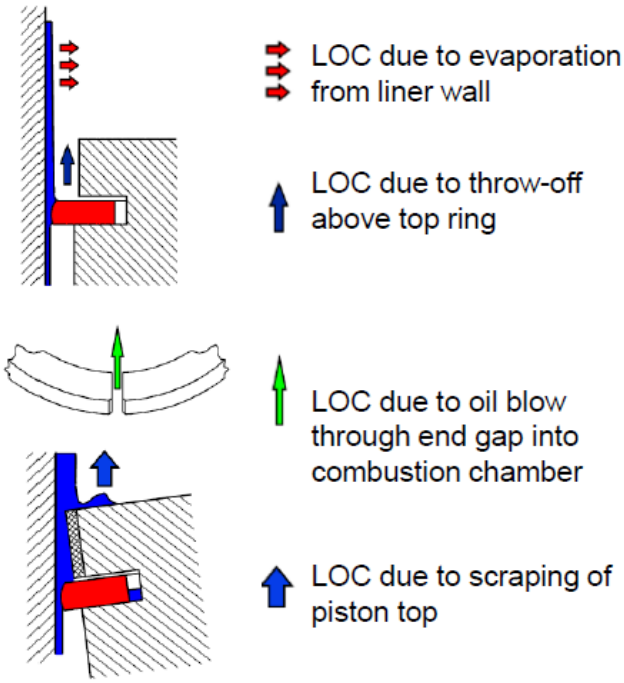

Figure 30. Lube oil consumption [9].

The lubricant itself is a multi-constituent fluid that strongly influences the lubrication regime of the lubricated parts. Various additives provide different functions in the oil: to maintain the temperature sensitivity of the oil viscosity, to protect against wear through formation of surface films, and to reduce solid-to-solid friction by making the surfaces more slippery. In addition, other additives keep the component surfaces clean and maintain the oil properties to within acceptable levels. In recent years, lubricant additive derived ash in the exhaust stream has become

an important issue in advanced diesel engines equipped with emission after treatment control systems. Engine design and the lubricant-additive formulation need to be optimized to simultaneously protect both the engine and the emission-control system from contamination by ash, sulfur and phosphorous originating in the oil.

1.4.2. Lubrication in piston assembly

Due to the variation in oil supply to the different piston rings throughout the engine cycle, each ring encounters different modes of lubrication while traveling along the liner. When the lubricant can separate the surfaces, the friction is considerably less in comparison with the situations at which the surfaces are in direct contact. If the surfaces are separated by fluid film due to motion, the lubrication mechanism is called hydrodynamic lubrication (HL) and when the contacting bodies deform elastically due to the contact pressure the lubrication mechanism refers to as elasto-hydrodynamic lubrication (EHL).

When the sliding velocity between 2 surfaces in contact is high, due to the hydrodynamic effects, the 2 surfaces are fully separated by the lubricant. In this situation the pressure of the fluid in the contact is high enough to separate the surfaces (EHL regime) and the friction coefficient is governed by lubricant properties and is typically of the order of 0.01.

When the velocity decreases the pressure of the fluid in the contact decreases and consequently the asperities of the surfaces start to touch each other and part of the load is carried by the asperity which leads to an increase in the friction. In this situation the friction is carried out by the shear between the interacting asperities as well as by the shear of the lubricant. The lubrication regime in this region is called mixed lubrication (ML). Decreasing the sliding velocity further, the pressure of the lubricant at the contact region approaches the ambient pressure and the total normal load is carried by the interacting asperities. The lubrication regime is called boundary lubrication (BL). Boundary lubrication usually occurs under high-load and low-speed conditions in machine components such as bearings, gears and traction drives. It is the regime which controls the lifetime of the mechanical system.

Figure 31. Lubrication modes [9].

In Hydrodynamics lubrication friction depends on oil film formation (oil viscosity). In this mode of lubrication, the oil supports the load from the ring on the liner, and therefore the amount of friction generated by the ring-liner interaction depends on the properties of the lubricant as well as the film height and width under the ring surface. In Mixed lubrication friction depends on separation of solid and hydrodynamic contact. In Boundary lubrication friction depends on solid contact (surface treatment and oil additives) [11].

Micro-EHL can be of great importance for the functioning of a rough surface operating in the BL and ML regime. This can be seen not only as a primary point of interest of the surface life, but also with respect to the performance of rough surfaces in general. As is shown on Figure 32., in BL and ML regime are two curves.

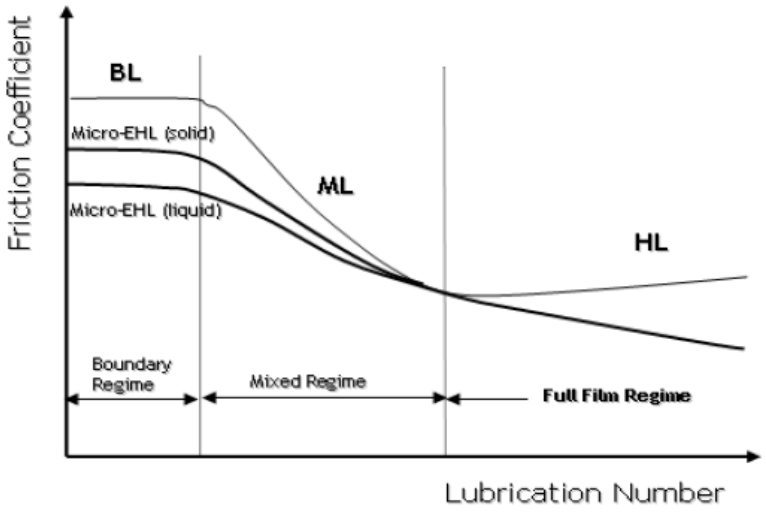

Figure 32. Friction coefficient depend on modes of lubrication. [11]

The lower curve indicates the occurrence of micro-EHL at the interacting asperities. Since shear stress in an asperity contact operating under micro-EHL conditions is less than the shear

stress in boundary lubricated micro-contacts, one may notice that the coefficient of friction increases at a smaller rate as HL decreases. The lower curve observed phenomenon is the micro-EHL (solid). If the load is completely carried by the asperities, the coefficient of friction does not depend on a lubrication number. The reason is the very high pressure at the micro contacts. As a result, the lubricant may act as a solid. In this case the shear does not depend on the shear rate and the friction coefficient is constant.

Most of the piston assembly friction comes from either piston-skirt/ liner interaction, or ring-pack/liner interaction. There is also lubrication and friction as the rings slide radially against the inside surfaces of the ring grooves in which the rings reside. However, the ring-groove interactions are only intermittent and do not contribute significantly to energy losses, but rather to ring-grooves wear issues.

1.4.3. Piston – liner friction

The lubrication regimes and friction losses in the piston-skirt-liner subsystem are significantly influenced by the piston secondary motion. Piston secondary motion results primarily in a variable slight tilt of the piston as it rotates about the piston-pin, and an impact force, commonly called piston slap, of the piston as it switches from sliding up on one side of the sliding down on the other side of the liner. Skirt-liner friction is higher when there is solid-solid contact in the boundary lubrication and mixed lubrication regimes. The axially barrel-shaped skirt profile is expected to provide the hydrodynamic pressure to sufficiently separate the skirt from the liner in maintaining hydrodynamic lubrication. However, when the piston speed approaches zero at the ends of the piston travel up or down strokes, the squeeze-film damping there remains as the essential mechanism to maintain a reasonably oil film, often not thick enough to avoid solid-solid contact [15].

The important parameters governing piston skirt-liner friction include the surface characteristics, such as textures or waviness patterns on the skirt and surface roughness; piston – liner arm clearances (material combination), skirt design details such as ovality and axial profile, and lubricant thickness and rheology. The key in reducing piston skirt-liner friction lies in maintaining hydrodynamic lubrication of the skirt. With an adequate oil supply to the skirt, most other issues of skirt profile design and surface characteristics affecting boundary lubrication would disappear or diminish [15].

1.4.4. Piston ring – liner friction

Except piston – liner friction, one of the most influence contributors of increasing friction power loss in ICEs are friction between piston ring and liner. The important parameters governing piston ring-liner friction include the surface characteristics, such as textures or surface roughness; piston rings design details such as piston ring cross section, and lubricant thickness and rheology. Oil supply plays a very important role in ring-liner lubrication. For a single grade oil, the viscosity of the oil depends only on its temperature, which is controlled primarily by the temperature distribution along the liner. As piston speed increases, the liner temperature may increase, causing a reduction in lubricant viscosity. Therefore, for the case of single grade oils, friction power losses only increase with higher engine speeds if the reduction in lubricant viscosity does not offset the increase in piston speed [15].

1.4.5. Engine friction reduction

The industry has made large improving in energy consumption by lowering friction in passenger cars. The turbocharged, direct-injection spark ignition engine with downsizing is one of the technical solutions that have been used in the market. In the case of diesel engines, the turbocharger had to be utilized to meet strict emissions regulations along with fuel economy improvement requirements.

General the relative friction losses of an engine can be reduced by increasing the engine load. This is since the load on the engine has low influence on the friction power losses. Increasing the load often means changing gear ratio such that the engine runs at lower RPM, while still providing the same vehicle speed. This can be beneficial also because the friction power loss is highly dependent on velocity and can be reduced with lower engine speed.

Surface texturing has been recognized as a method for enhancing the tribological properties of sliding surfaces. After surface texturing, surface have a lot of dimples. The dimple (micropit, hole, oil pocket or cavity) can serve either as a micro-hydrodynamic bearing in cases of full or mixed lubrication, a micro-reservoir for lubricant in cases of starved lubrication or a micro-trap for wear debris in either lubricated or dry sliding. It was found that surface texturing of contacting elements reduced the frictional force substantially in comparison to untextured surfaces [16]. A lot of testing are made with laser textured surfaces and the laser textured surfaces showed less friction than surfaces manufactured by conventional honing.

Except surface texturing, piston rings coating is today a most useful method for reduction piston ring – liner friction [17]. Ever since coatings were acknowledged as an essential design

feature they have inevitably been a point for improving friction losses in the tribological system of piston ring and cylinder bore. Carbon-based, diamond-like coatings (Diamond-like Carbon, DLC) are particularly used for components which undergo solid-to-solid contact with other components during operation. The excellent properties of DLC coatings ensue from the generation of a thermally and mechanically induced transformation of the top layer of the DLC film into a material of lower shear strength than the layer itself, and which therefore becomes self-lubricating. Traditional DLC coatings are limited in their application on piston rings by the following features. Typical layer thicknesses are lying in the region of a few microns, which limits coating lifetimes. If the coating is thicker the risk of delamination increases due to typical internal stresses. Hard DLC coatings make it difficult to achieve very smooth piston ring running surfaces to ensure excellent friction levels and avoid cylinder bore wear. DLC piston ring coatings currently are often used as a running-in layer on other wear-resistant coatings [17].

DuroGlide is a commercial name for DLC coating manufactured by Federal – Mogul. This coating suitable for lifetime use in highly loaded gasoline and diesel engines. Due to the high amount of sp3-hybridised carbon (tetrahedral structure) DuroGlide can be applied with a layer hardness of up to 5000 HV 0.2. The coating has a layer thickness of up to 25 µm with an excellent adhesion to cast iron and or steel surfaces. The temperature resistance of up to 500°C allows the application in diesel engines. Figure 33. shows a relative comparison of the coefficients of friction found in the piston ring coatings used today in gasoline and diesel engines. The coefficient of friction was measured outside the engine under test conditions which represent a high mixed friction share while using oil without additives. Compared to chromium-based coatings such as chrome ceramic coating (Chrom-Keramik-Schicht: CKS) and Goetze diamond coating (GDC) as well as physical vapor deposition (PVD) coatings such as CrN, the use of DuroGlide reduces the coefficient of friction by up to 60 % [17].

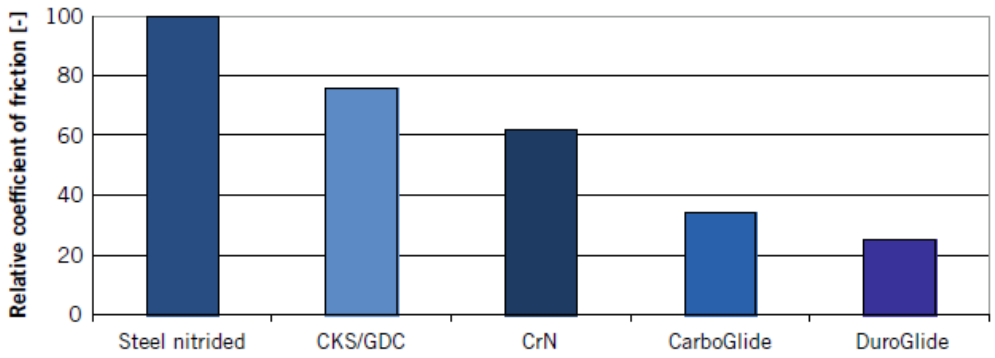

Figure 33. Relative comparison of the friction coefficient of various piston ring coatings [17].

As DuroGlide can be applied to base materials such as cast iron and steel and is feasible for different running surface designs, it is equally suited for compression rings and oil rings. Figure 33. shows a conceptual setup of a piston ring pack for passenger car diesel and gasoline engines. As the top compression ring and the oil ring each contribute around 40% to the mechanical friction loss, DuroGlide is preferred for these two ring types. The coated piston rings show the highest level of wear and scuff resistance when compared to all conventional piston ring coatings and thus contribute to a fuel efficiency improvement of up to 1.5%. This is equivalent to a reduction of CO_2 emissions by up to 3g/km, depending on the engine application [17].

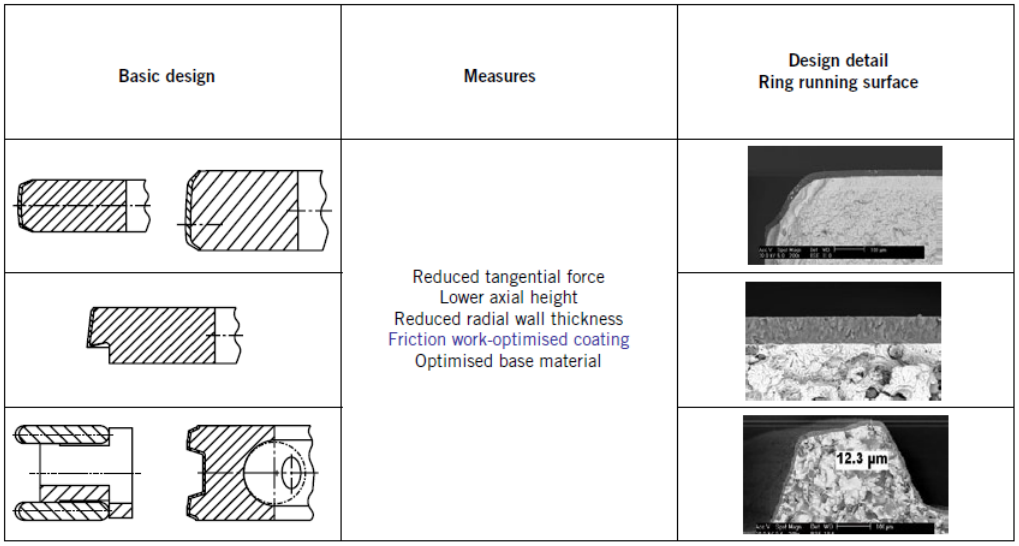

Figure 34. Example of low – friction piston ring packages for passenger car engines [17].

1.5. Objective of the thesis

The objective of this thesis is to correlate results of simulation models and available results given from measurement on an AVL FRISC engine. This includes influence of tangential force on friction and differences between simplified and advanced modeling. Simulation models are created in software's *AVL EXCITE™ Piston&Ring* (piston ring dynamic) and *AVL EXCITE™ Power Unit* (piston dynamic). Also, sealring and cylinder head are implemented in EXCITE™ Power Unit models and influence on friction behavior caused by stick slip effect is observed. In results, friction force, side force, LOC, blow-by and FMEP values are compared.

2. AVL FRISC Engine – friction measurement

AVL FRISC engine ((FRIction Single Cylinder) is the name for the research engine with a floating liner concept. On Figure 35., AVL FRISC engine concept is presented.

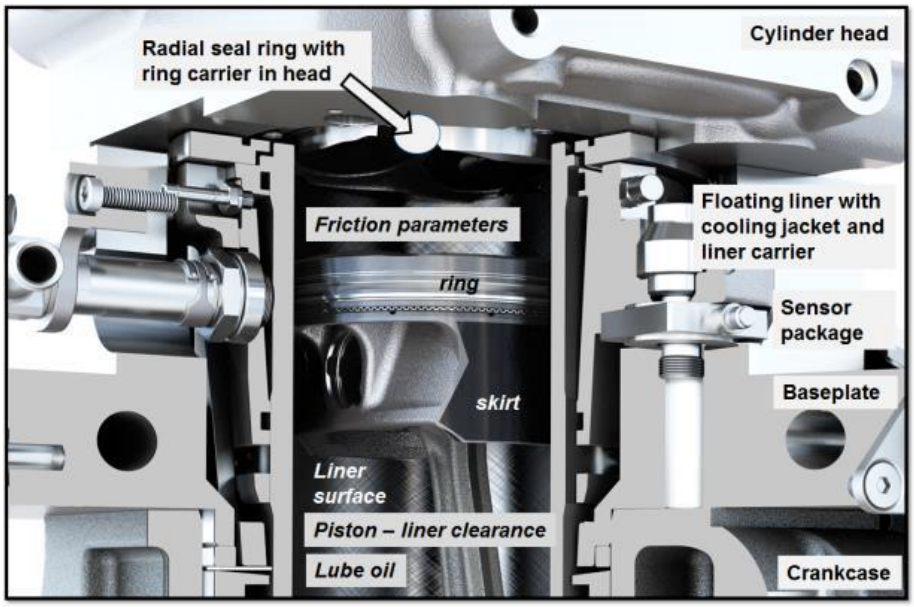

Figure 35. AVL FRISC engine concept [18].

2.1. AVL FRISC engine and floating liner in general

AVL FRISC engine is in fact a single cylinder engine, which has a quite robust and stable design for the base engine consisting of crank-case, mass balancing system (up to second order), auxiliary devices and power cell [19]. The measurement of piston to liner friction is done with the "floating liner" engine concept. One aim of friction measurement is to evaluate the force data for the FMEP (friction mean effective pressure) evaluation. Such design requires the liner to be mounted via force sensors onto the crankcase. Contact forces between the liner and cylinder head or any other part of the engine must be reduced to minimum. With this design the liner is "floating" on its force sensors and any dynamic force introduced into the liner is recorded as an add-on to the static force required to hold the liner in place. The practicality of engine testing requires a floating liner engine design capable of operation at relevant engine conditions and providing mechanical interfaces for an easy exchange of piston or liner without compromising the setup of the sensor system [20]. Figure 36 shows the schematic view of AVL FRISC engine.

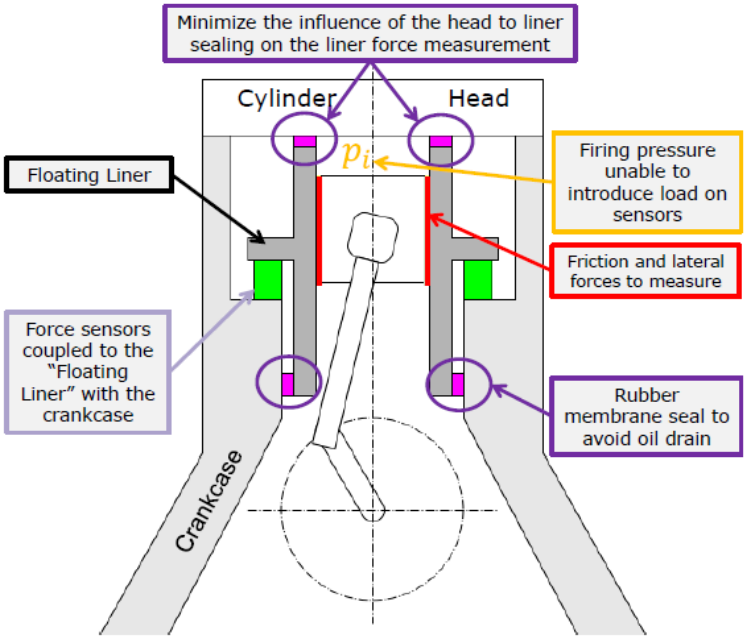

Figure 36. Schematic view of AVL FRISC engine [21].

The functional principle is as follows: If one imagine the force sensors being springs (because of their elasticity) and a piston with ring pack, guided by the liner, is going up and down, friction forces occur due to the contact between liner and piston skirt as well as rings. Simultaneously mechanical forces arise which act normal to the liner surface and in direction of the liner surface (into direction of the liner axis). These forces into z – direction (friction forces) will modify the spring length (because of the elasticity of the sensors there will be a displacement in z – direction) what is the signal measured. Because of the friction forces acting on the liner surface the whole floating liner system will also move (mainly into z – direction). This movement is first of all the reason for the name "floating liner" [19].

2.2. Mechanical system and resonance cases

The power cell is moving according kinematics of the crank drive. The dynamics of the FRISC engine can be defined with the following action and reaction forces. Direction of this forces can be seen on Figure 37.

Action forces [19]:

- Friction forces between piston skirt, rings and inner liner surface: $F_R(t)$,
- Contact normal forces between piston skirt, rings and inner liner surface: $F_N(t)$,
- Gas forces from the chamber acting on top of the liner $F_G(t)$,

- Normal and friction force of the sealing ring on top of the liner: $F_{RS}(t)$ and $F_{NS}(t)$,
- Gas forces from crankcase are acting on bottom of the liner $F_{GC}(t)$.

Reaction forces:

- The force sensors are reacting with "spring" forces $F_S(t)$,
- The friction force is $F_R(t)$.

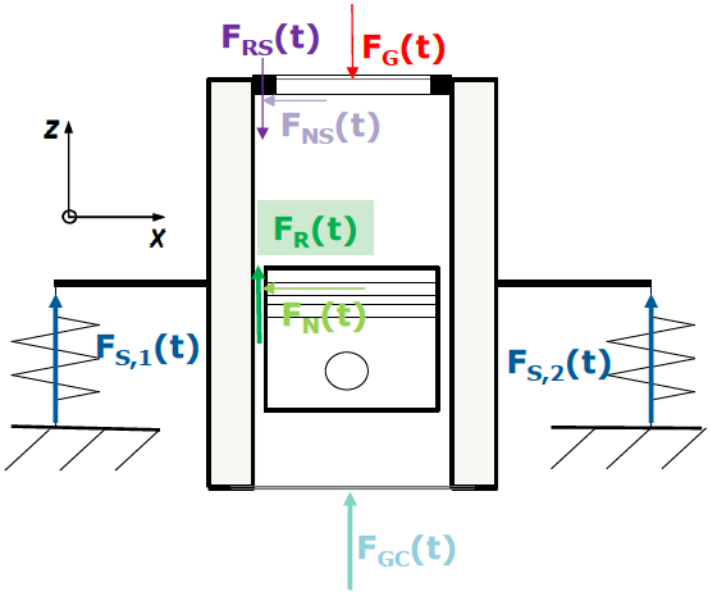

Figure 37. Forces acting on liner and liner carrier [19].

According the principle of linear momentum we have the following equation in global z - direction [19]:

$$m \cdot \ddot{z}(t) + D \cdot \dot{z} = \sum F(t) = F_G(t) + F_{GC}(t) + F_{rS}(t) + F_R(t) + F_S(t) \qquad \textbf{(1)}$$

The FRISC system is highly dynamic, in that it has time varying movement and forces. One has to take into account also that the FRISC engine consists of a large number of different parts out of different materials. These parts are flexible bodies (not infinitely stiff) and as such have their own individual frequency response. In addition, there are fluids in the joints and gas in the combustion chamber and surrounding volumes all of which alters the frequency response of the system. As the engine speed increases the signal amplitudes increase and it is necessary to detect those operating points where eigen frequencies and harmonics of the individual parts, or those of the system as a whole, may occur. Generally speaking these so-called resonance cases can never be avoided but they have clearly be observed [19].

2.3. FRISC engine design

Figure 38. shows the floating liner assembly. Main part of the design will be described at the following section. With this design, the exchange of piston, piston rings and liner without interference to the sensor package installation is accomplished.

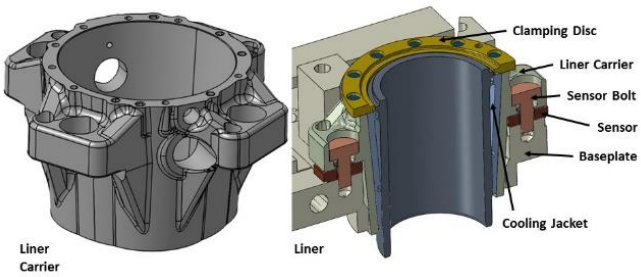

Figure 38. Floating liner assembly [22].

Liner carrier and floating liner:

This part connects the liner and its cooling water jacket with the engine block via the force sensors central screws. The mounting screws are tightened for a precisely defined static pre-load. Together with the cooling jacket, the liner is inserted into the carrier and fixed with a clamping disk [21].

The floating liner is a part which is inserted into the cooling jacket. It is disjointed from the cylinder head with a seal ring. For a high-precision evaluation of piston to liner clearance effects, a form honing procedure at the liner is applied to achieve the original liner distortion, thus maintaining correct clearance dimensions.

Sensor package:

The selection of force sensor stiffness and sensor positions within the engine structure ensures the static stability of the liner [21]. The sensors' dynamic response and sensitivity are key to providing accurate dynamic force measurements. The sensor package is tightened to the baseplate with bolts.

The sensor package includes four force sensors, each providing force signals in the axial, lateral and longitudinal direction. Each sensor signal component includes force components

acting along the respective axis as well as residual components because of the sensor element's cross-talk sensitivity.

Handling the 12 force signal components is accomplished with a multichannel data recorder. The sensor package sensitivity matrix (comprised of 36 sensitivity matrix elements in total) is used in a real time analyzer to provide instantaneous output of engine force components [21].

Seal ring

The radial seal ring is one of the most important parts of the AVL FRISC engine because it enables the sealing between the liner and the cylinder head. The seal ring's contact to the liner together with gas pressure acting on the ring surface imposes residual force components acting along the liner axis [21]. Even if this axial force can be minimized with the selection of seal ring design parameters, the measurement system's high sensitivity shows its effects as a residual force superimposed on the basic friction signal components. The friction signal shows a negative spike around the crank angle position of the maximum cylinder pressure. In the fired operation, the response of the ring to the rising pressure together with the downward motion of the piston introduces a microscopic stick – slip motion with a consequent reaction force seen in the force signals. This small microscopic motion is known as the "stick-slip" effect and results will show an influence of this motion for friction. The signal appears as a spike superimposed and counteracting to the friction signal of the accelerating piston after combustion TDC. Seal ring tension and contact force to the liner are the parameters of influence. The stick-slip effect will be described later in the thesis.

Cylinder head:

Prototype or mass production cylinder heads need a minor modification to provide the space for mounting the seal ring between head and liner. Camshaft operation is achieved with a tooth belt. Tooth wheels are mounted on to the front end of the camshafts. Original cylinder head bolts and bolt positions are maintained. Coolant and lubrication are provided via suitable hose connections to the base engine and further on to the media supply unit. With such modifications, a multicylinder head is operated as a single cylinder engine, and engine operation can use original stationary engine calibration parameters [21].

Crankcase:

The crankcase provides a module to allow the mechanical interface to the cylinder head bolts, the interface to the force sensors between crankcase and floating liner, and the housing for cranktrain and balancer shafts. Side openings provide a mechanical window to access the conrod screws. The engine uses first and second order balancer shafts to minimize crankcase vibrations [21].

2.4. FRISC engine parameters and cases

In this chapter parameters and measurement cases of FRISC engine will be represented. Parameters are given in Table 1. FRISC measurements were made for full load and for partial load. Friction force result, blow-by and lube oil consumption are calculated from cases given in Table 2. Cases are named by speed and BMEP values in bar.

Table 1. FRISC engine parameters.

Properties	Unit	Value
Bore	mm	77
Stroke	mm	80
No. cylinders	-	1
Volume/cylinder	ltr	0,37
Fuel type	-	Diesel
Coolant temperature	°C	90
Oil temperature	°C	90

Table 2. Measurement and simulation cases.

Load type	CASE	Engine speed [rpm]	BMEP [bar]
Full load	3000_15p5	3000	15.5
Full load	2500_15p4	2500	15.4
Full load	2000_15p2	2000	15.2
Full load	1500_14p8	1500	14.8
Partial load	3000_9p3	3000	9.3

Partial load	3000_5p3	3000	5.3
Partial load	3000_2p9	3000	2.9
Partial load	2500_9p2	2500	9.2
Partial load	2500_2p8	2500	2.8
Partial load	2000_8p6	2000	8.6
Partial load	2000_2p7	2000	2.7
Partial load	1500_8p8	1500	8.8
Partial load	1500_4p7	1500	4.7
Partial load	1500_2p3	1500	2.3

Measurement is performed for two ring packages. Differences are in the tangential force on the top and second ring and in the width of the second ring. Running faces of the piston ring are the same. Tangential force, F_t, is a force which is sufficient to compress the ring to the specified closed gap. Knowing the value of the tangential force, contact pressure can be calculated. The equation for calculating contact pressure is [23]:

$$\boldsymbol{p = \frac{F_t}{r \cdot h}} \qquad \textbf{(2)}$$

Where r is the radius of piston ring and h is the piston ring axial width.

Figure 39. shows constant contact pressure and tangential force. Except for constant contact pressure, contact pressure can also be a variable.

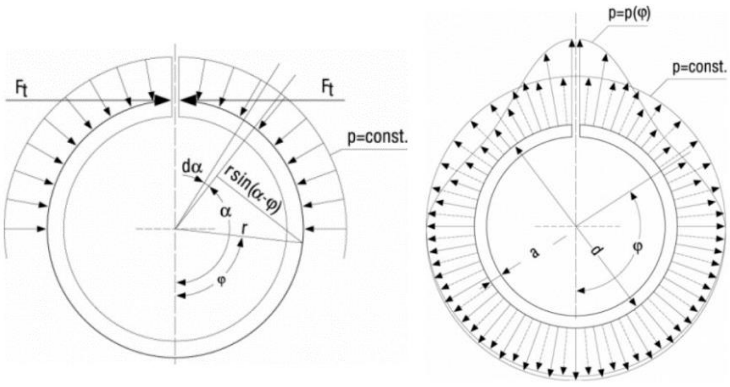

Figure 39. Tangential force and contact pressure distribution [23].

The contact pressure determines how high the ring is pressed against the cylinder wall. This pressure is governed by the dimensions and total free gap of the ring and by the modulus of

elasticity of ring material. The total free gap is defined as the distance, measured along the neutral axis, between the ends of a piston ring in its uncompressed state [23].

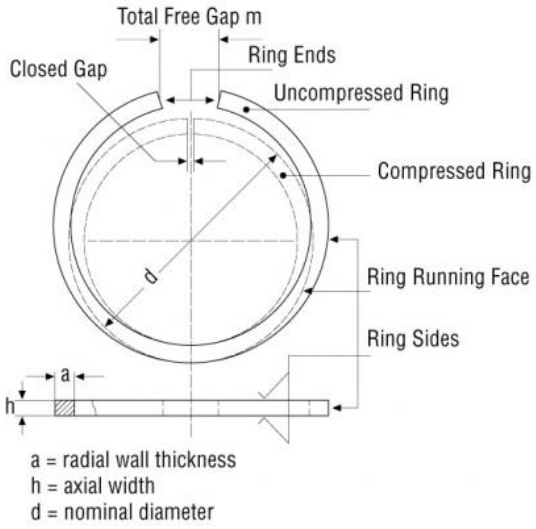

Figure 40. Total free and closed gap [23].

Table 3. shows differences in parameters between ring packages.

Table 3. Difference in parameters in cases.

CASE name	Tangential force (Top and 2nd ring)	Radial Thickness (2nd ring)
BASIC	6 N	2.7 mm
LOW FT	5 N	2.6mm

3. SIMULATION MODELS

Simulation models are made in AVL EXCITE™ software in two modules: PowerUnit and Piston&Rings. Models are created in a simplified and in an advanced way. Guidelines and recommendations for an efficient modelling will be presented.

3.1. General about analysis in Piston & Rings.

In AVL EXCITE™ Piston&Rings module two types of analysis are considered: piston ring dynamics and lube oil consumption.

Piston ring dynamics was developed to analyze effects of design modifications of piston and piston rings in view of low LOC, blow-by and friction values. For the determination of the dynamic loads upon the rings, the piston ring dynamics considers forces and moments due to inertia, friction and the flow of the gas from the combustion chamber through the inter-ring volumes into the sump. The calculation is simultaneously done at TS (thrust side) and ATS (anti-thrust side), the mutual influence being considered ("quasi three-dimensional"). Along the circumference direction, constant conditions are assumed. The simulation also gives values for blow-by, inter-ring pressures and oil film thickness between the rings and liner over crank angle. The main characteristics of the Piston ring dynamics are the following [24]:

- Each ring is modelled as a single mass. The interaction between the thrust and anti-thrust sides is given by a beam model and a model for pressure compensation. Twisting, (including the pre-twist angle) is considered.
- For the calculation of the gas flow through the rings, inter-ring areas are considered as volumes, which are given by the piston and ring geometries and the actual clearances between piston and liner. The volumes are connected due to the actual clearances of ring end gaps and the actual position of the rings in the grooves. The possible gas flow behind the rings and between ring and groove flanks is considered.
- The oil film is considered between the ring running surface and liner by calculating the pressure distribution in the clearance according to the liner and ring contours.

The Lube Oil Consumption Module was developed to calculate the lube oil consumption in the piston-ring-liner group. Any losses in the shafts of the valves, in the turbo charger or general leakages of the entire engine are not considered. The following consumption mechanisms are considered [24]:

- Evaporation at the oil film from the liner surface
- Oil transport around the first piston ring – including oil throw off
- Oil blow through the gap of the first ring from and into the combustion chamber
- Oil scraping at the top land's top edge (considering deposits)

3.1.1. Piston ring dynamics and gas flow models

In piston ring dynamics, there are forces acting on the piston ring in the axial and radial direction. The schematic display of forces is given in Figure 41.

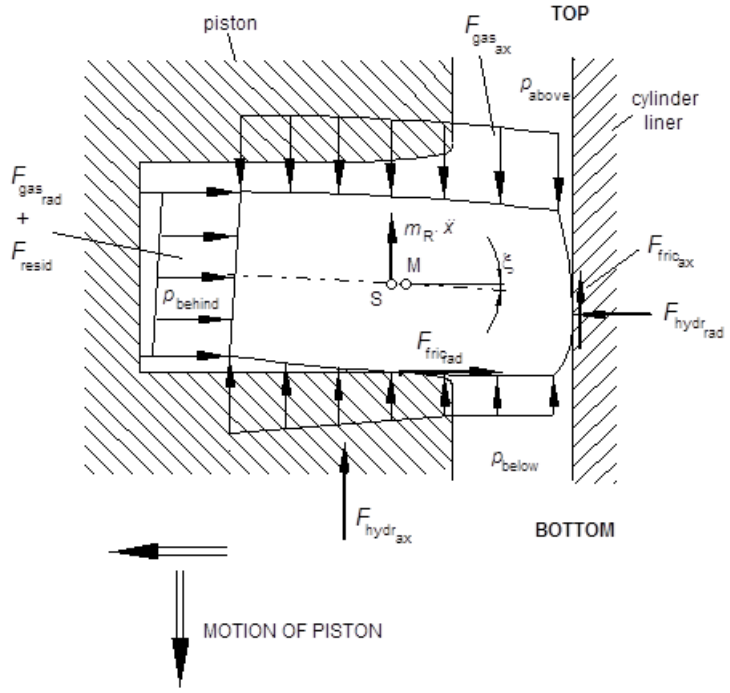

Figure 41. Piston ring forces [9].

In the axial direction, the forces acting on the piston ring are [9]:

- mass force (including gravity and piston tilting motion)
- friction force between liner and ring running surface: $F_{\text{fric\_ax}}$
- gas force: $F_{\text{gas\_ax}}$
- damping force caused by the oil filling of the groove: $F_{\text{hydr\_ax}}$
- bending force caused by the interaction between TS and ATS: F_{bend}

According to the equilibrium of dynamic forces acting upon the ring, the equation of motion in the axial direction is given by [9]:

(3)

$$m_{\text{ring}} \cdot \ddot{x}_{\text{ring}} = \sum F = F_{\text{mass}_{\text{ax}}} + F_{\text{fric}_{\text{ax}}} + F_{\text{gas}_{\text{ax}}} + F_{\text{bend}} + F_{\text{hydr\_ax}}$$

The contact force F_{contact} between the ring and ring groove, if the ring is in contact with the groove flank will be [9]:

$$F_{\text{contact}} = F_{\text{mass\_ax}} + F_{\text{fric\_ax}} + F_{\text{gas\_ax}} + F_{\text{bend}} + F_{\text{hydr\_ax}} \quad \textbf{(4)}$$

If the $F_{\text{contact}} > 0$ ring is moved with the piston and if the $F_{\text{contact}} < 0$ ring is lifted from the groove flank [9].

In the radial direction, the forces acting on the piston ring are:

- force caused by the tension of the ring: F_{tension}
- gas force: $F_{\text{gas\_rad}}$
- friction force between ring and ring groove: $F_{\text{fric\_rad}}$
- force caused by the hydrodynamic pressure in the gap between liner and ring running surface (incl. radial damping force): $F_{\text{hydr\_rad}}$

The contact force between the liner and ring running surface is given by:

$$F_{\text{contact\_rad}} = F_{\text{fric\_rad}} + F_{\text{gas\_rad}} + F_{\text{tension}} + F_{\text{hydr\_rad}} \quad \textbf{(5)}$$

If the $F_{\text{contact\_rad}} < 0$ ring is lifted from liner.

The friction force $F_{\text{fric\_rad}}$ is calculated using Stribeck model based on the relative radial velocity between ring and piston. The relative radial velocity is the result of the radial velocity due to piston secondary motion and the one due to ring dynamics.

For the calculation of the gas forces acting upon the piston rings, the pressures resulting from the gas flow must be known. For this, the entire ring package will be divided into chambers (volumes behind and between the rings), which are connected one to another by throttling points. Starting upon the known pressures p_{comb} on the piston top land and p_{crankc} below or behind the oil ring, the pressures in the chambers will be determined in a quasi-stationary way by means of a step-by-step calculation of the gas masses flowing through the throttling points [9]. Gas flow model for entire ring package is shown on Figure 42.

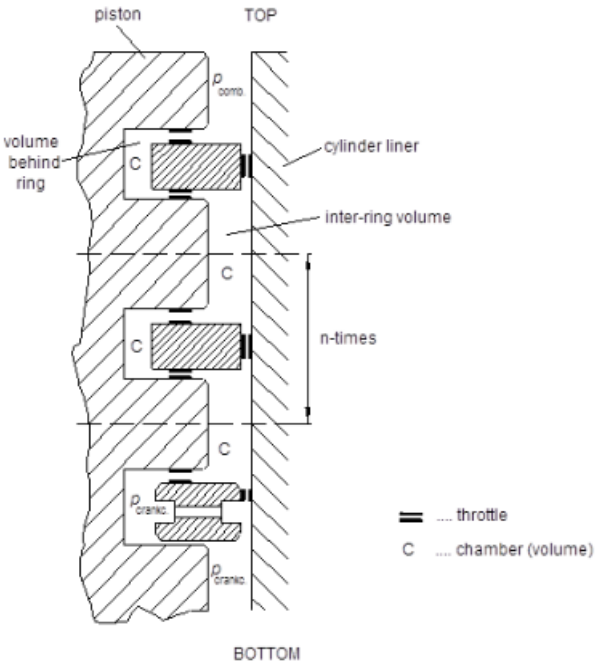

Figure 42. Gas flow model for entire ring package [9].

For the flow processes, an isothermal change in the state is assumed, the max. velocity of flow is limited to the sound velocity in the throttle. Mass flow change of mass and pressure in the chamber are calculated as follows [9]:

$$\dot{m} = A \cdot \psi \cdot p_{\mathrm{C}} \cdot \sqrt{\frac{2}{R \cdot T_{\mathrm{C}}}} \cdot \sqrt{\frac{\kappa}{\kappa - 1} \cdot \left(\left(\frac{p_0}{p_{\mathrm{C}}} \right)^{\frac{2}{\kappa}} - \left(\frac{p_0}{p_{\mathrm{C}}} \right)^{\frac{\kappa+1}{\kappa}} \right)} \tag{6}$$

where $\dot{m}$ is mass flow,

$$\Delta m = \dot{m} \cdot \Delta t \tag{7}$$

where Δm is change of mass,

$$p_{\mathrm{C}} = \frac{R \cdot T_{\mathrm{C}}}{V_{\mathrm{C}}} \cdot (m + \Delta m) \tag{8}$$

where p_{C} is pressure in the chamber.

For the calculation of the pressures, the gas flows over the following throttling point are considered [24]:

- ring running surface
- ring end gap

- ring top and bottom flanks

Throttling points and discharge areas are shown in Figure 43.

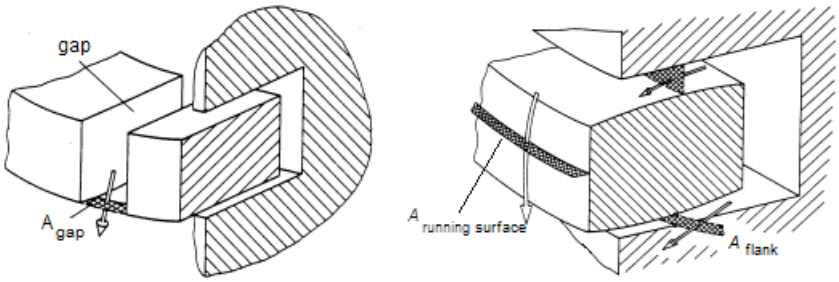

Figure 43. Throttling points and discharge areas [24].

3.2. EXCITE Piston & Ring models

Piston ring model is shown in Figure 44. For creating the model, AVL EXCITE™ 2018b software is used. The model is created from the liner and ring package (top ring, 2nd ring and oil ring). Each part is filled with parameters which are mostly calculated from piston, liner and piston rings drawings. Other parameters are either set as default or calibrated for good overlapping between simulation and measurement results.

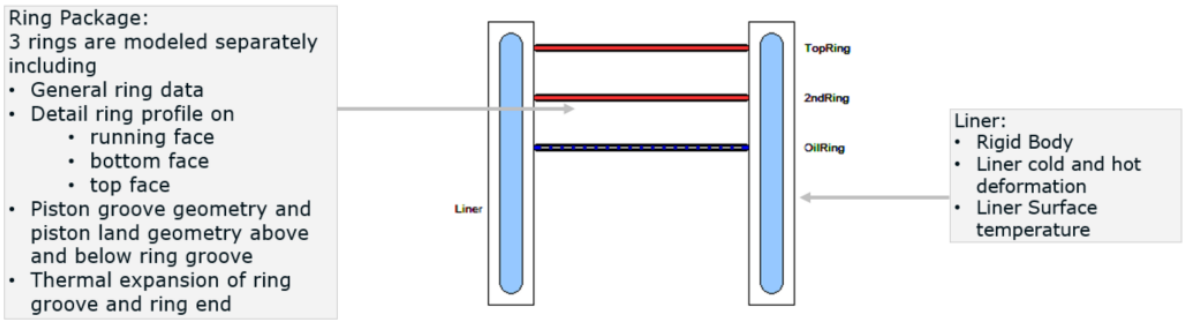

Figure 44. Simulation model

The solving of simulation model will be considered in two ways: 2D enhanced and 3D approach. The input data between the two approaches are the same, only difference is the simulation solver. Simulation solver selection is shown in Figure 45.

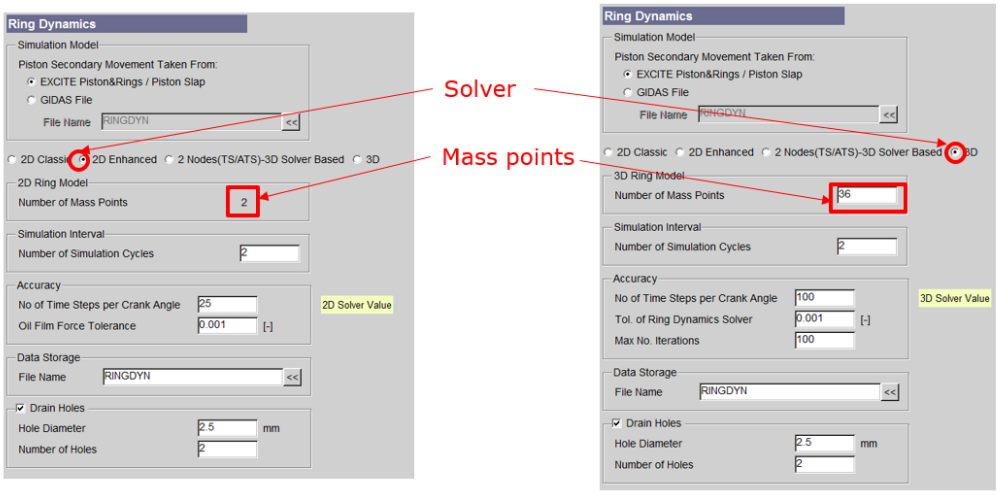

Figure 45. Selection of simulation solver

In 2D enhanced module, the balance of the forces applied on the ring cross section is considered in both radial and axial direction. In the circumferential direction, only two elements are considered. One of them is at the thrust side and other on the anti-thrust side. The calculation is carried out by solving the equations of motion of forces and moments equilibrium conditions on each ring. The explicit integration method in time domain is used to solve the resulting dynamic equation. The forces applied on the ring, which depend on the position of the piston ring in groove, are calculated iteratively. The hydrodynamic contact between the ring running face and liner is calculated using the Reynolds equation [24].

In the 3D module, the 3rd dimension, which is the circumferential direction, is added to the piston ring analysis domain. The 3D ring model is based on the finite-element (FE) beam-mass formulation. The ring is divided into equal segments in the circumferential direction. The mass of each segment is concentrated at its center (mass lump) and is associated with the mass and inertia tensor of that segment. Each mass section contains one node connected with that section with RBE2 (kinematic coupling). It is recommended to use one mass point on every 5 to 10 degrees, result in 36 to 72 mass points. Increasing the number of mass points, the liner and ring contact have better conformation, but simulation time increases significally. The center of the ring segment has 6 degrees of freedom, 3 translational and 3 rotational DOFs. This results in 12x12 stiffness and mass matrices for each element. The stiffness and mass matrices, as well as the force vector, are assembled, and the resulting system of equation is solved iteratively. The hydrodynamic and asperity contacts are evaluated at each ring segment [24].

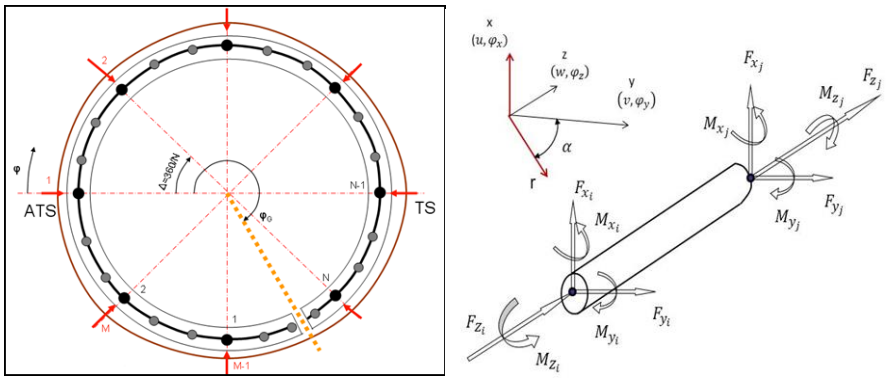

Figure 46. Ring partitioning into equal mass lumps connected beam [9].

3.3. Input data for piston & ring model

This chapter describes main input data such as load, data necessary for describing surface contact, piston ring profile and liner profile.

3.3.1. Load data

Load input data is divided into two types: cylinder pressure curve data and thermodynamic data. For each operating point, cylinder pressure curves are different, and they are taken from the measurement on the AVL FRISC engine. In the following figures, cylinder pressure curves for full and partial load are shown.

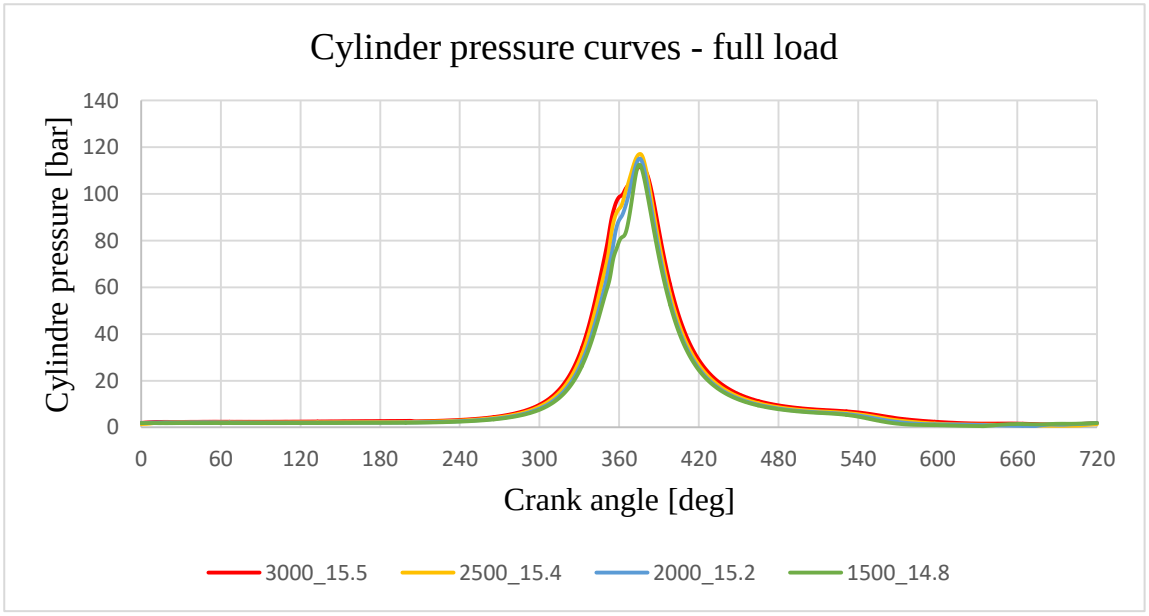

Figure 47. Cylinder pressure curves for full load.

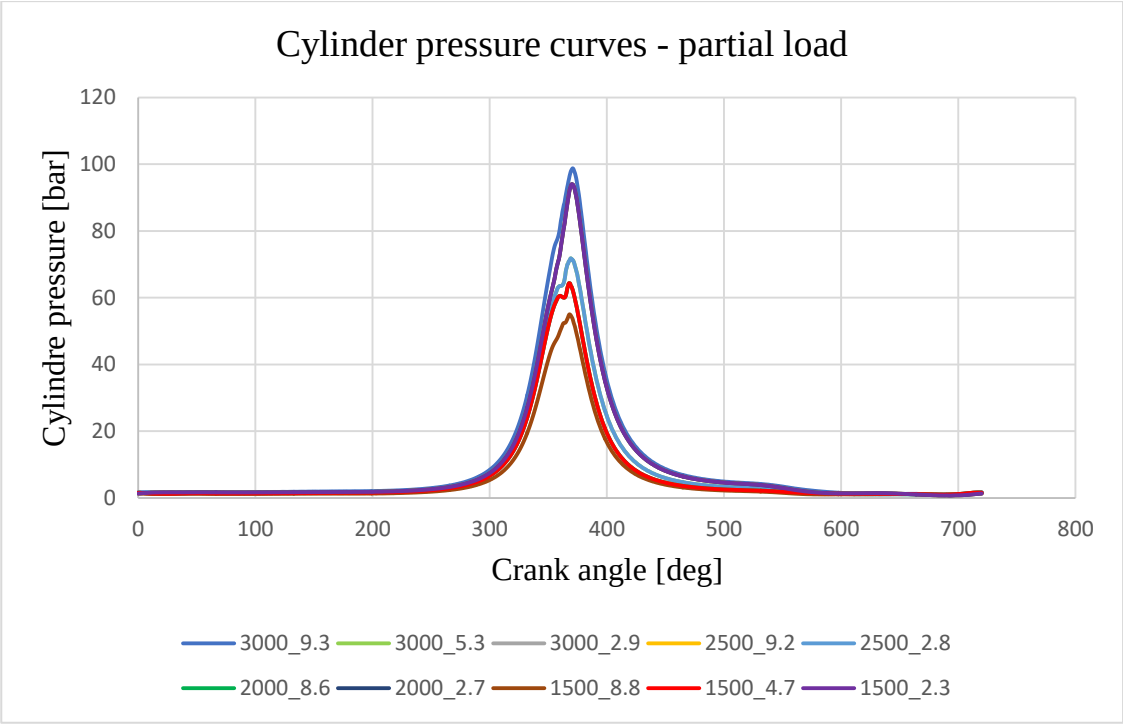

Figure 48. Cylinder pressure curves for partial load.

This pressure curves are also used in Power Unit model and they are shifted for 2.266 deg because of piston pin and crankshaft offset. In Piston & ring model, pressure curves are shifted for 362.266 deg and ignition start at 0 deg.

Thermodynamic data used for the LOC simulation are the same for all cases and they are taken from benchmark. In Figure 49. The combustion gas temperatures, liner heat coefficient and cylinder swirl number are shown.

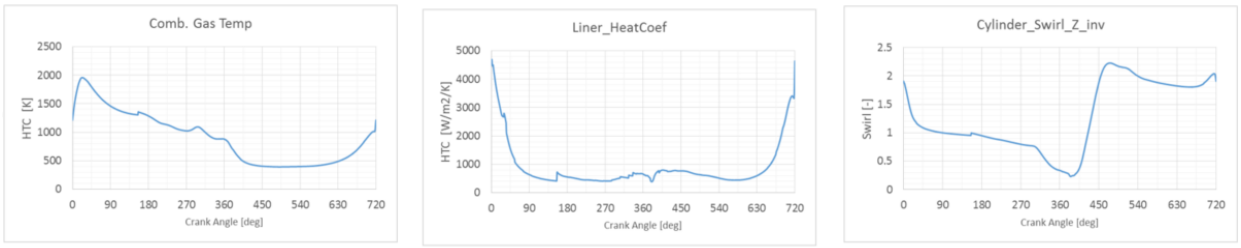

Figure 49. Thermodynamic load.

3.3.2. Surface contact

For calculating friction between piston ring running face and liner it is very important to know the material properties and the surface roughness between the parts. Figure 50. shows surface roughness for the liner and top ring. The EHD contact is described by Asperity Contact

– Greenwood/Tripp approach and the averaged Reynolds equation is described by the Patir and Cheng model.

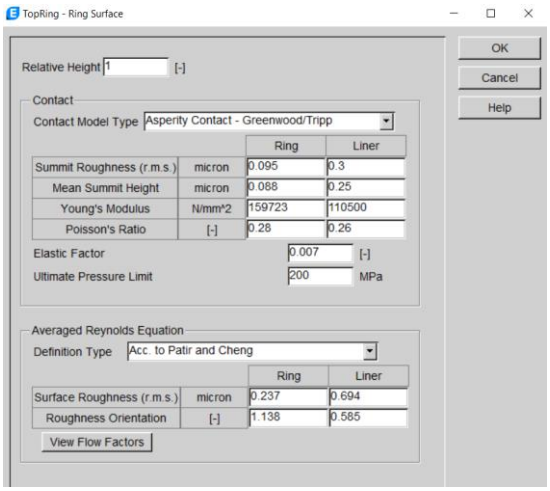

Figure 50. Surface contact for Top ring.

The contact between the interacting roughness summits is a combination of micro-hydrodynamic contact and partly local solid contacts. The ratio between micro-HD and solid contact depends on the local gap size between the asperity summits h_L. The asperity interaction gap size h_L depends on the local asperity contact lubrication number L_N. Lubrication number depends on mean dynamics viscosity, sliding speed, asperity contact pressure and reference length for summit contact. Main lubrication number contributor is sliding speed [24]. Increasing sliding speed, lubrication number increase, and micro-HD friction coefficient also increase. Lubrication asperity friction model is shown in Figure 51. Constants a, b, c and reference length are mainly used for model calibration. Influence of abrasive coefficient was not considered in the simulation. Default value for adhesive coefficient is 0.1, and maximum value is 0.15 for dry/dry contact.

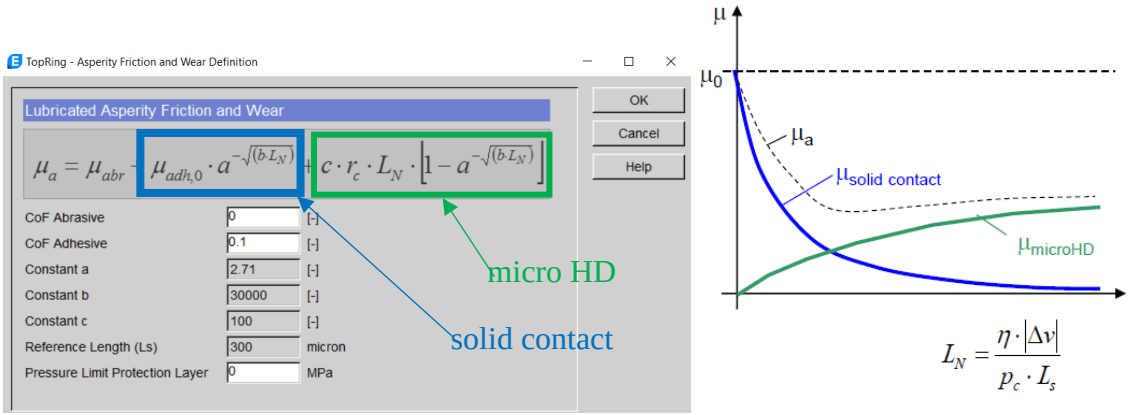

Figure 51. Lubricated asperity friction model [9].

Constants a, b, c and reference length for each ring are shown in Table 4.

Table 4. Values of friction constants in Piston & rings model.

	Constant a	Constant b	Constant c	Reference length
Top ring	2,71	30000	100	300
2nd ring	2,718	30000	100	100
Oil ring	2,718	40000	350	200

3.3.3. Piston & rings profiles

In the EXCITE Piston&Rings module, the profiles of piston rings and liner must be inserted. After creating a profile in ASCII format, the files are imported into software.

Piston ring profiles are separately created for each piston ring and loaded in to the software. These profiles represent the cross section of piston rings. For the top, second and oil ring, it is necessary to import profiles in three positions. These three positions are the profile of ring face, top side face and bottom side face. First, these profiles are created in Excel, CAD software or in some other program (MatLab). For each ring, main dimension of profile is known on drawing and all other profile points are interpolated between the known points. Figure 52. shows the cross-section profile of the top ring, Figure 53. shows the profile of the second ring and Figure 54. shows the profile of the oil ring.

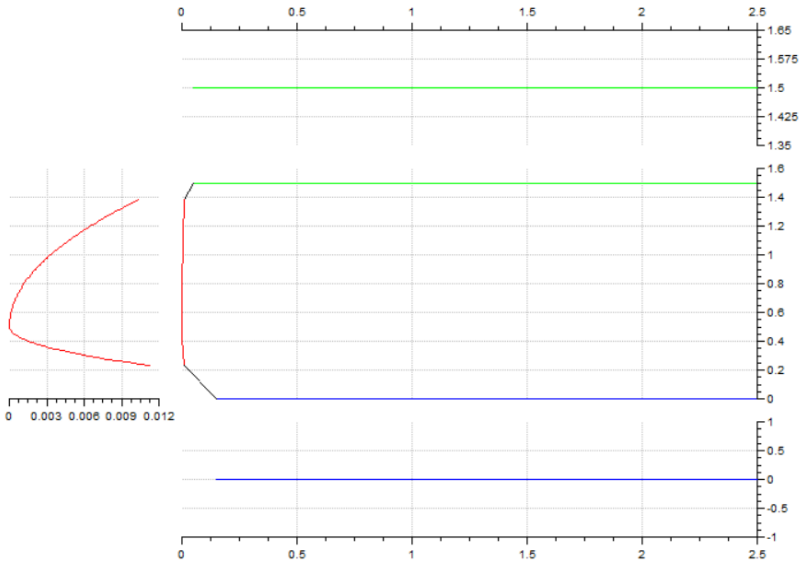

Figure 52. Cross section of top ring.

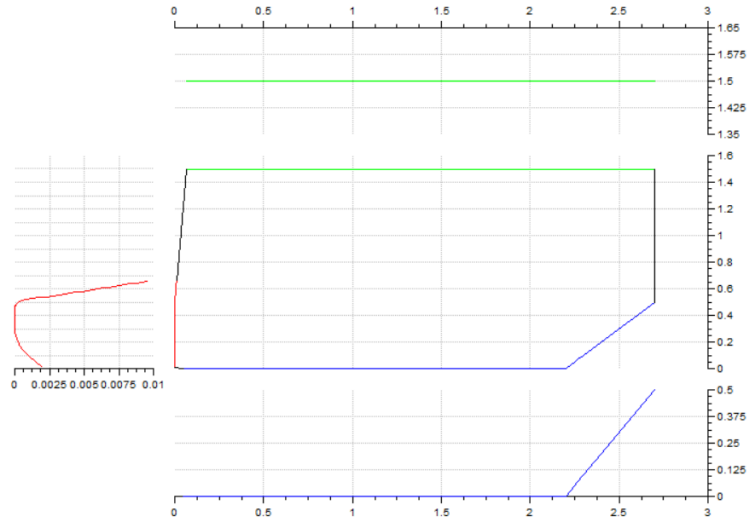

Figure 53. Cross section of second ring.

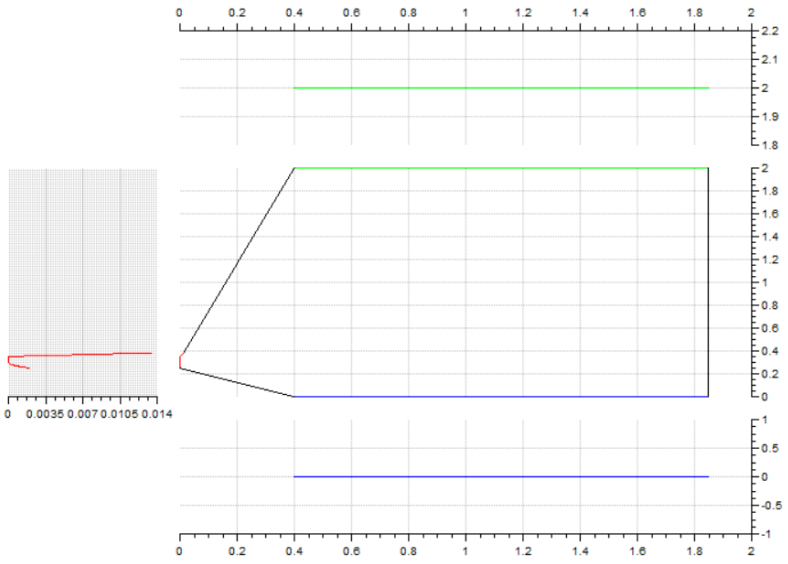

Figure 54. Cross section of oil ring.

Liner profiles are calculated in cold and warm conditions. The cold liner profile describes the radial and circumferential deformation from an ideal cylinder at assembling the liner in engine. The cold liner deformation is constant for all operating conditions. Cold profile can be imported in one ASCII file or created via meridians in circumferential direction. Figure 55. shows the cold profile of liner created in liner profiler via meridians. All meridians together create a patch which is displayed on Figure 56. Input data for creating meridians are taken from benchmark.

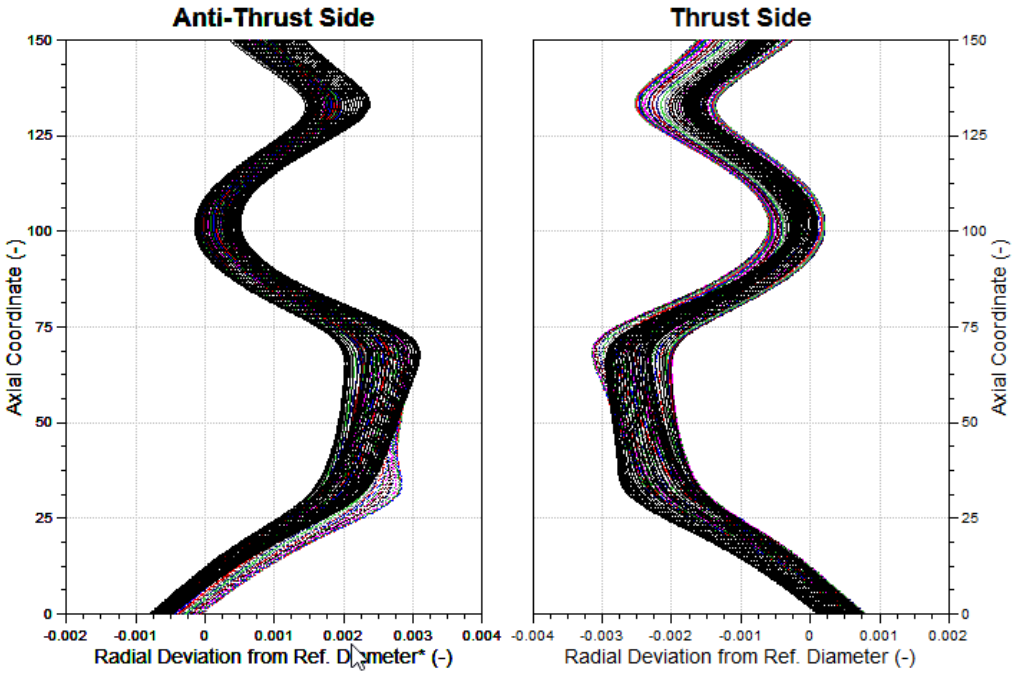

Figure 55. Liner meridians.

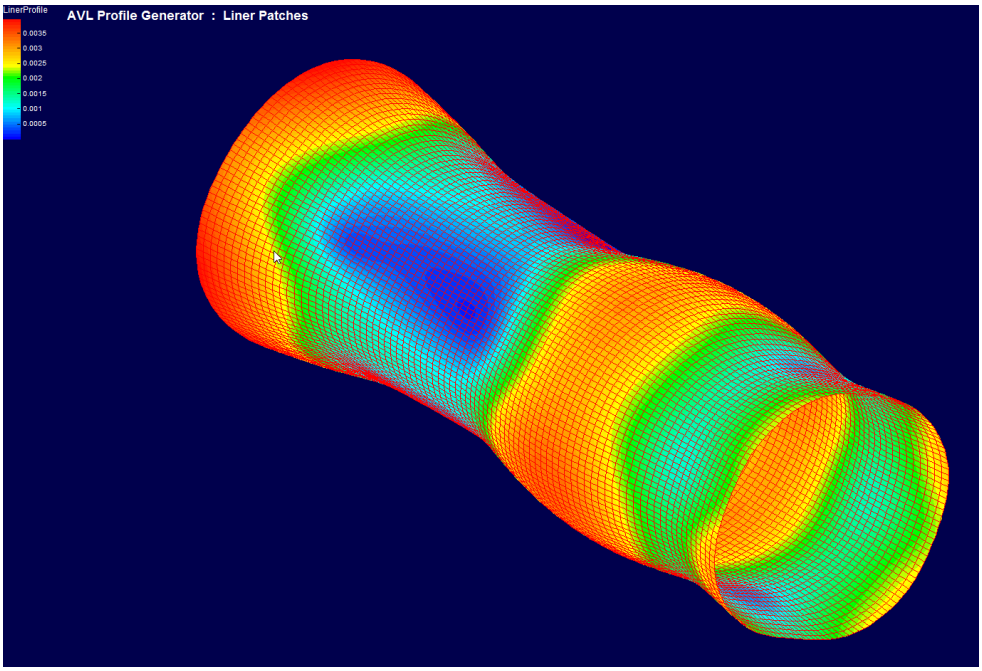

Figure 56. Liner patches.

The warm liner profile is calculated equally in the circumferential direction for a different liner height. To calculate it, it is important to know the temperature field over liner height. These temperatures can be taken from the thermal simulation or from measuring points at the liner on test bed. For this simulation, temperatures are imported from measurement. Temperatures are

measured on liner top, middle and bottom position in four circular points for all cases. The average temperature value of this circular point is calculated for each position on the liner. The temperature fields from measurement are shown in Table 5.

Table 5. Temperature fields from measurement.

CASE	TOP [°C]	MIDDLE [°C]	BOTTOM [°C]
3000_15p5	168	112	113
2500_15p4	158	111	112
2000_15p2	158	110	111
1500_14p8	160	110	111
3000_9p3	142	110	110
3000_5p3	132	108	105
3000_2p9	122	103	101
2500_9p2	140	109	108
2500_2p8	116	100	99
2000_8p6	135	107	106
2000_2p7	109	97	96
1500_8p8	143	112	109
1500_4p7	121	105	101
1500_2p3	107	97	96

The warm profile is described by the thermal radial deviation. This value can be calculated or defined directly. For calculation, liner temperature field (LinerT) and thermal expansion coefficient of liner wall should be imported as shown in Figure 57. Except LinerT, which represents the mean temperature of the liner wall, the temperature of the liner surface (SurfT) should also be imported. The surface temperatures will be used on determination of lube oil viscosity for the hydrodynamics between the ring running face and liner wall and the surface temperature of the oil vapor used for the simulation of the evaporation rate in lube oil consumption. The surface temperature will not influence the radial profile of liner specified in the liner profile.

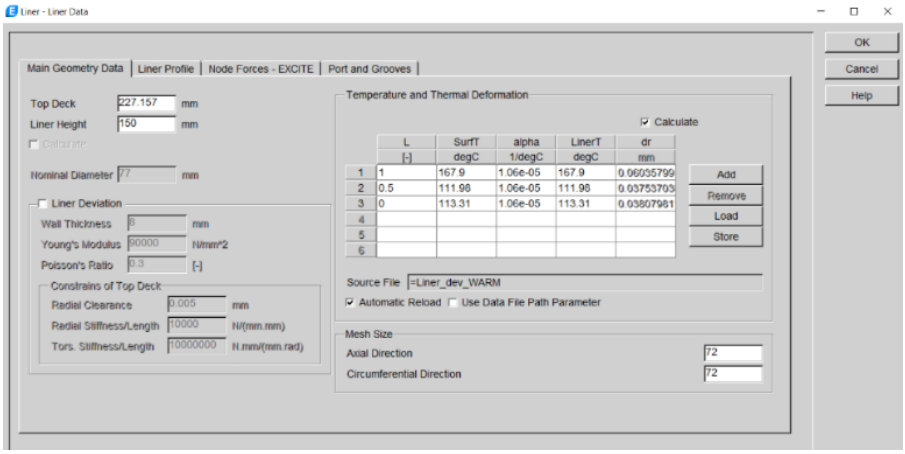

Figure 57. Calculation of radial thermal deviation in case 3000_15p5.

3.4. EXCITE™ Piston&ring simulation results

This chapter describes simulation results of piston and rings models. Results are presented for basic and low friction ring package. Except different ring package, results are also presented for different simulation solver (2D or 3D solver).

3.4.1. EPR results - basic ring package

Results of piston ring dynamics, friction characteristics, blow – by and lube oil consumption for basic ring package are presented only for engine speed 3000rpm for all load cases. At appendix A, the results for 2500, 2000 and 1500 rpm for basic ring package are documented.

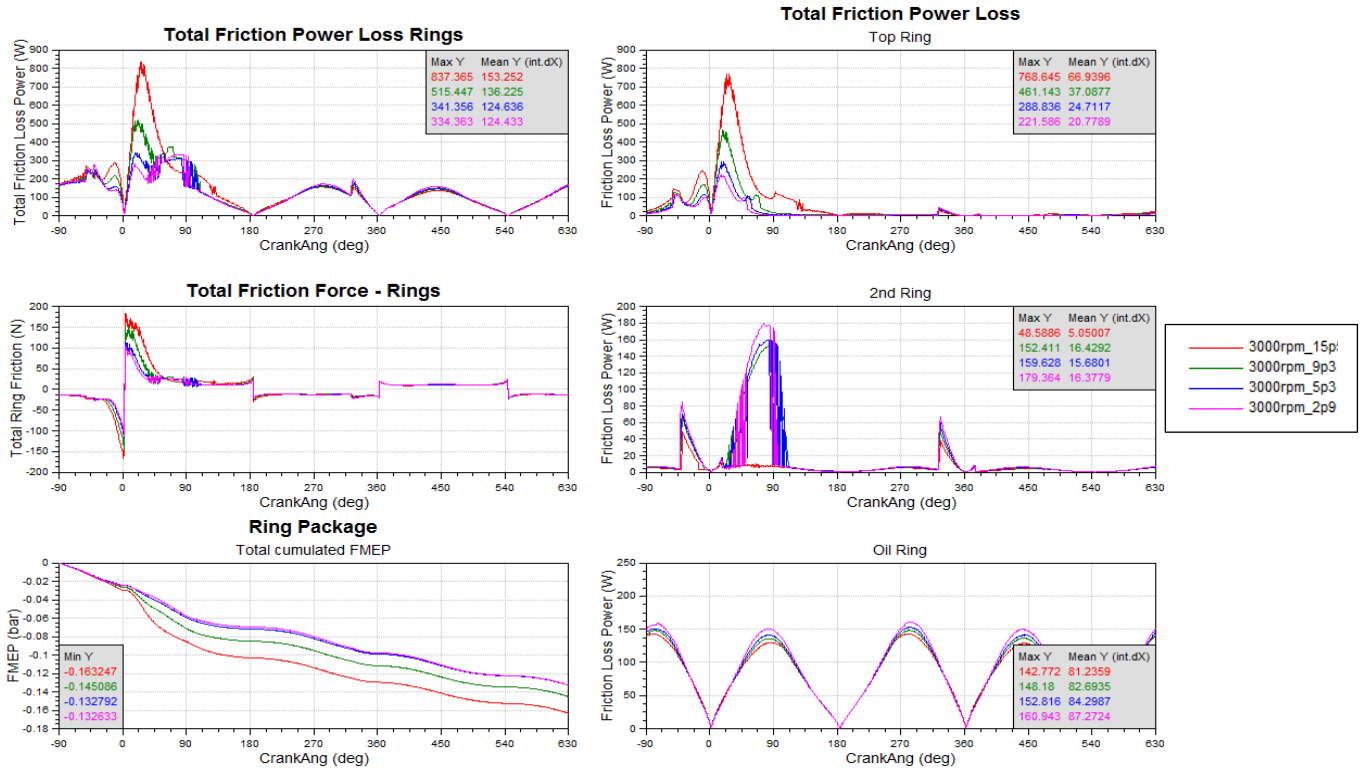

Figure 58. Basic ring package – Friction characteristics overview.

Above Figure 55. shows total friction power loss which is sum of friction power losses on top, second and oil ring. On figure are also calculated mean integration values of friction power loss over degree crank angle. Total cumulated FMEP values of all cases are also presented. Friction forces between piston rings and liner are also shown.

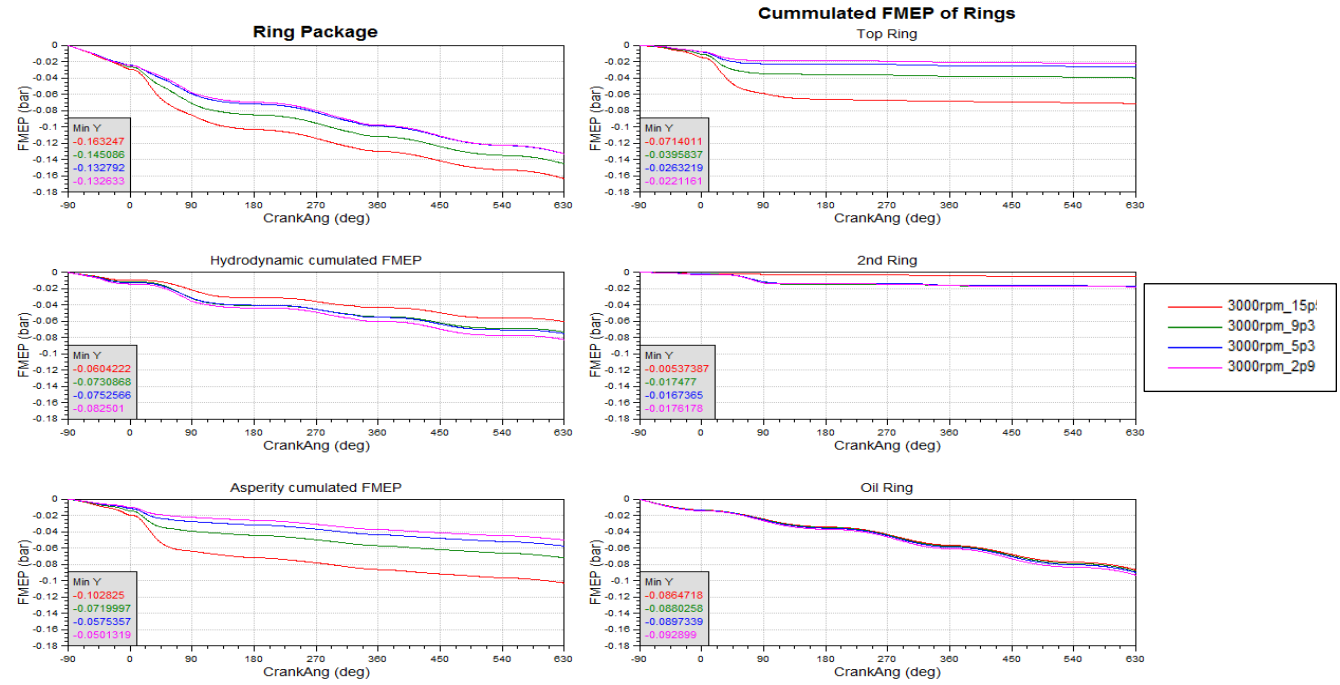

Figure 59. Basic ring package – FMEP overview.

Above Figure 59. represents FMEP contribution of each piston ring. Total FMEP value for each case and contribution of hydrodynamic and asperity cumulated FMEP are presented.

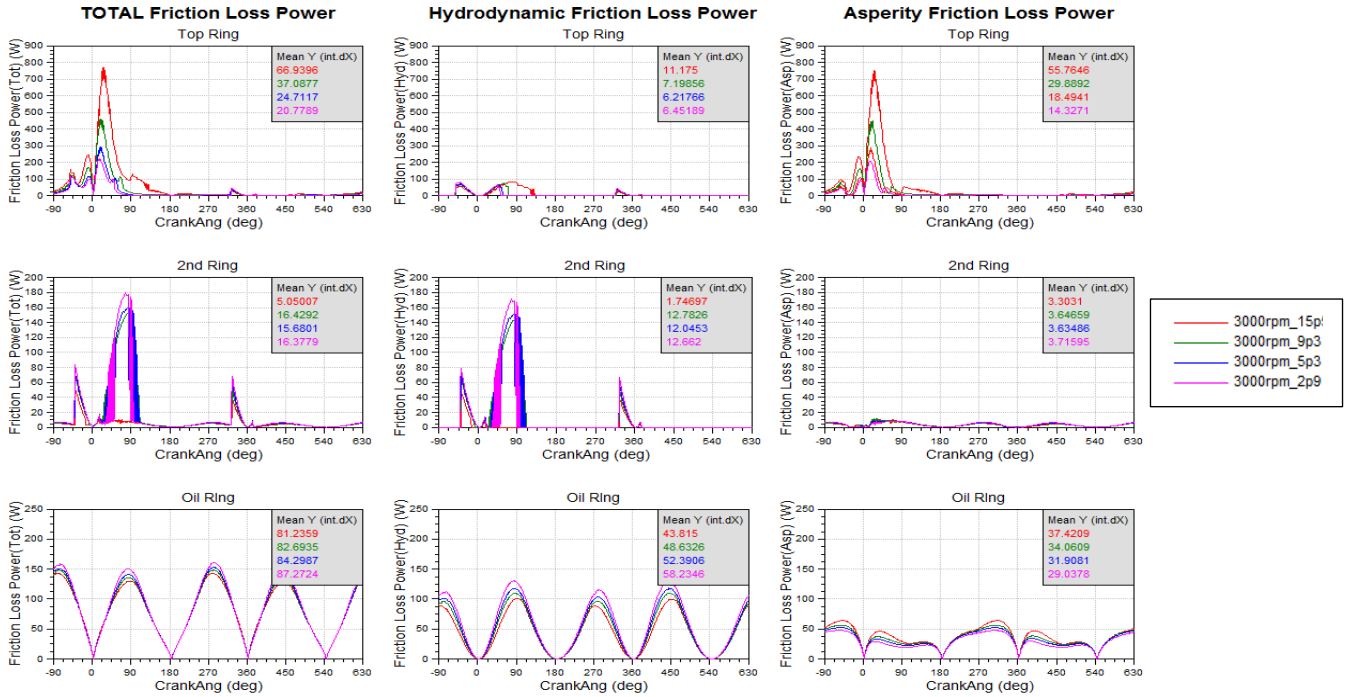

Figure 60. Basic ring package – Friction Power Loss overview.

Above Figure 60. represents friction power loss contribution of each piston ring. Contribution of hydrodynamic and asperity friction power loss is presented.

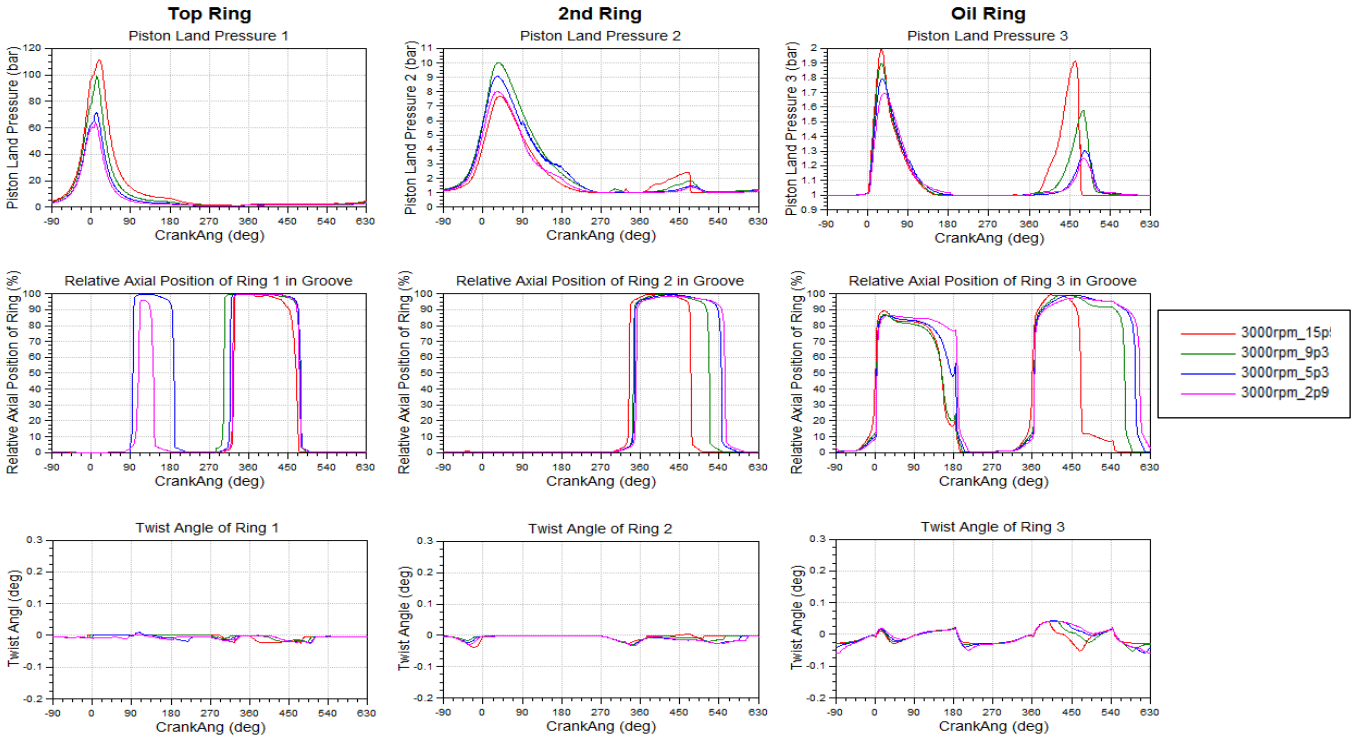

Figure 61. Basic ring package – Piston ring dynamics overview.

Above Figure 61., presents piston land pressure between piston ring and piston groove. Relative axial position of ring represents axial position of piston ring inside piston groove. When is ring on bottom position in groove value is 0 and when is ring on top position in groove, value is 100. Twist angle of piston ring regarding x-axis is presented.

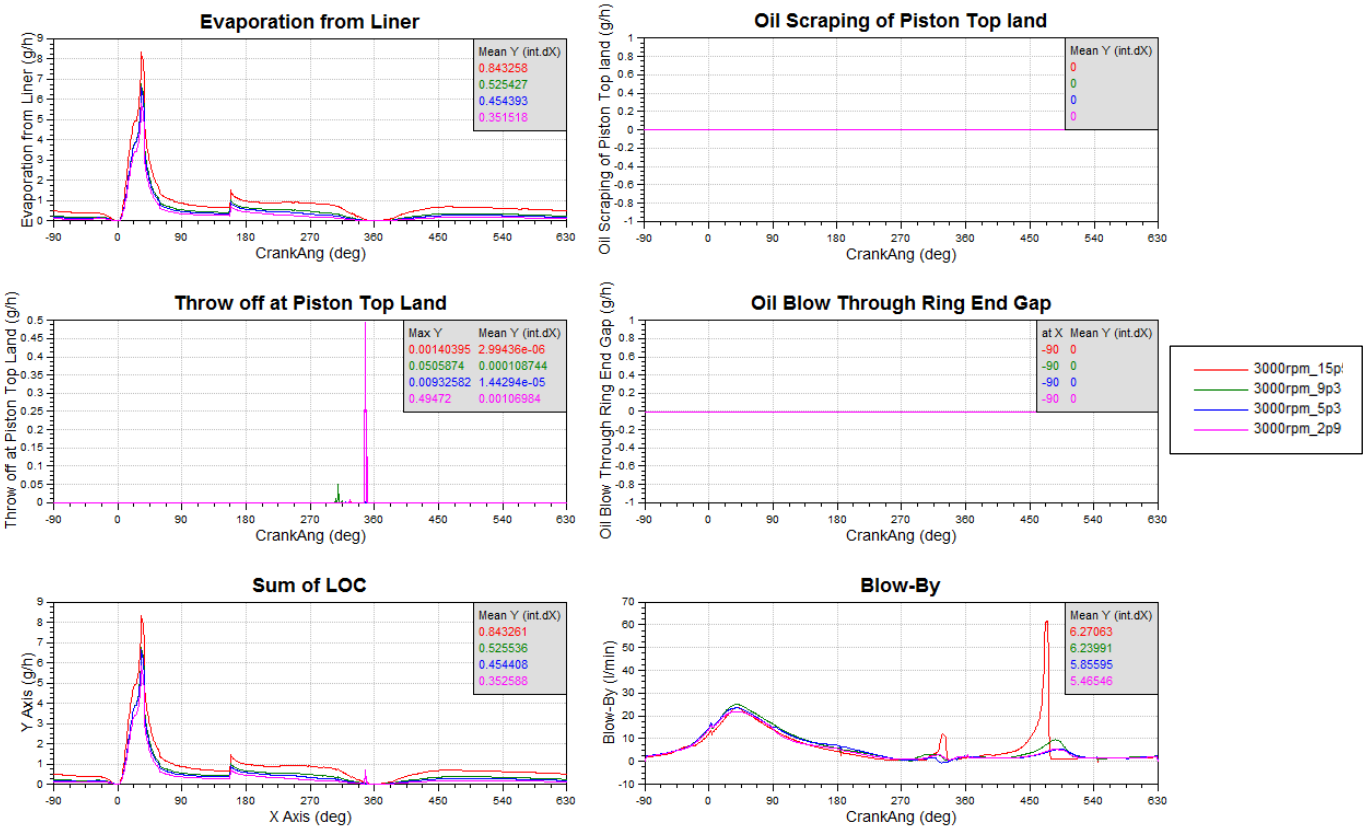

Figure 62. Basic ring package – Lube Oil Consumption and Blow-by overview.

Above Figure 62., presents total lube oil consumption and contribution of each lube oil consumption segements caused by piston bore interface. Total blow-by in crankcase is also presented.

Results summary – basic ring package

Above results shows that friction power loss at top ring increases with load for the same operating speed. Friction power loss of oil ring have cycle behavior through engine cycle and friction power loss of top ring increased after ignition in combustion chamber. Friction power loss of top ring is load dependent and friction power loss of oil ring are more speed dependent. Friction mean effective pressure are higher if load increased and the most contributor of FMEP comes from oil ring. Top and oil ring change relative axial position in groove 4 times and second ring change 2 time. After first change of oil ring the axial position is not defined in the groove. Also, twist angle of oil ring has the higher value every time in changing movement of piston in

liner. Lube oil consumption and blow–by values are higher if load increases. The most contributor of lube oil consumption is evaporation from liner.

3.4.2. EPR results - comparison basic and low friction ring package

In following figures results of basic and low friction force ring package is shown. Low friction package has reduced tangential force on top and second ring by 17%. Results are displayed only for one operating point (3000rpm_15.5) and other results for different load cases at speed 3000 rpm are shown in appendix B.

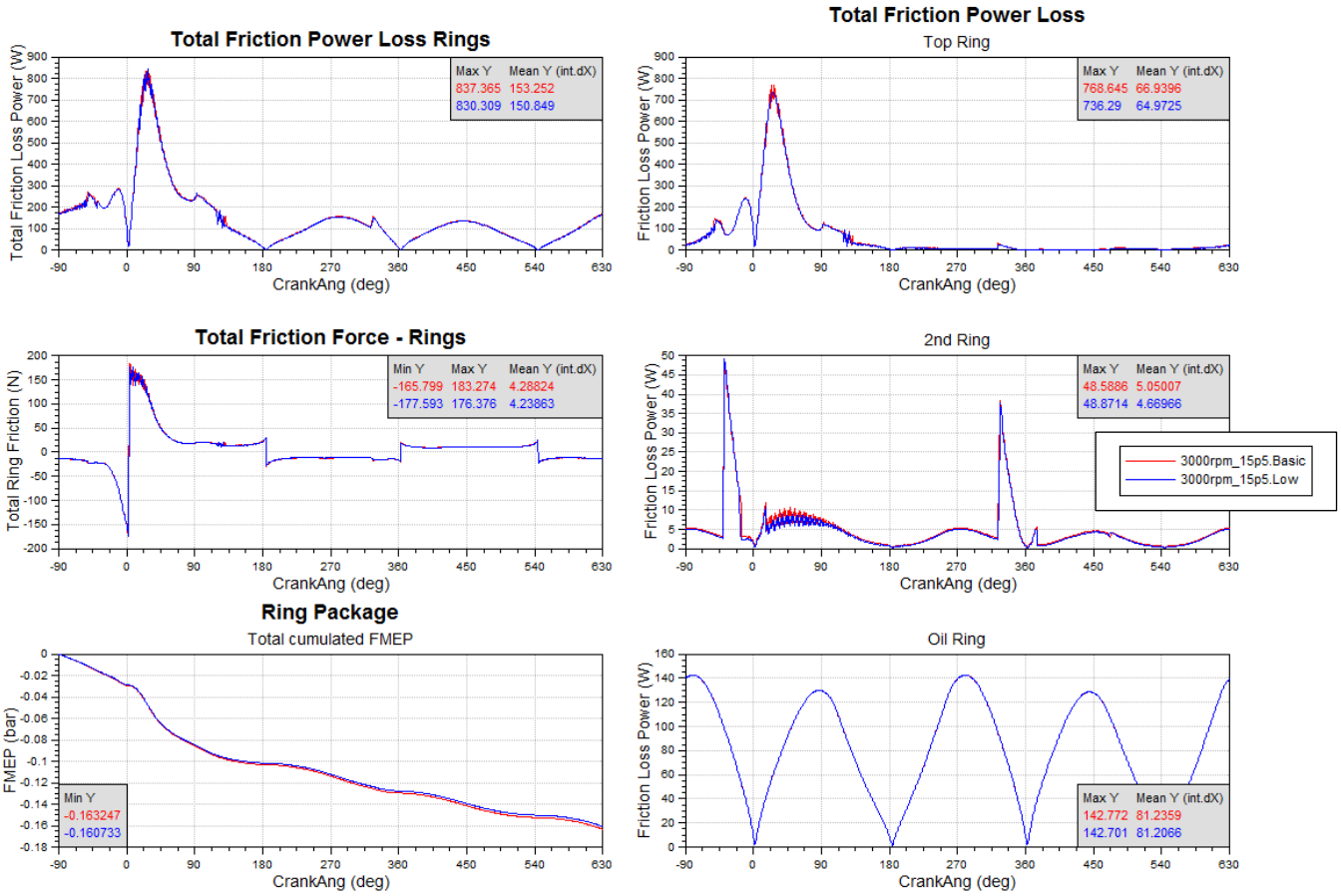

Figure 63. Comparison between BASIC and LOW FT ring package - Friction characteristics overview.

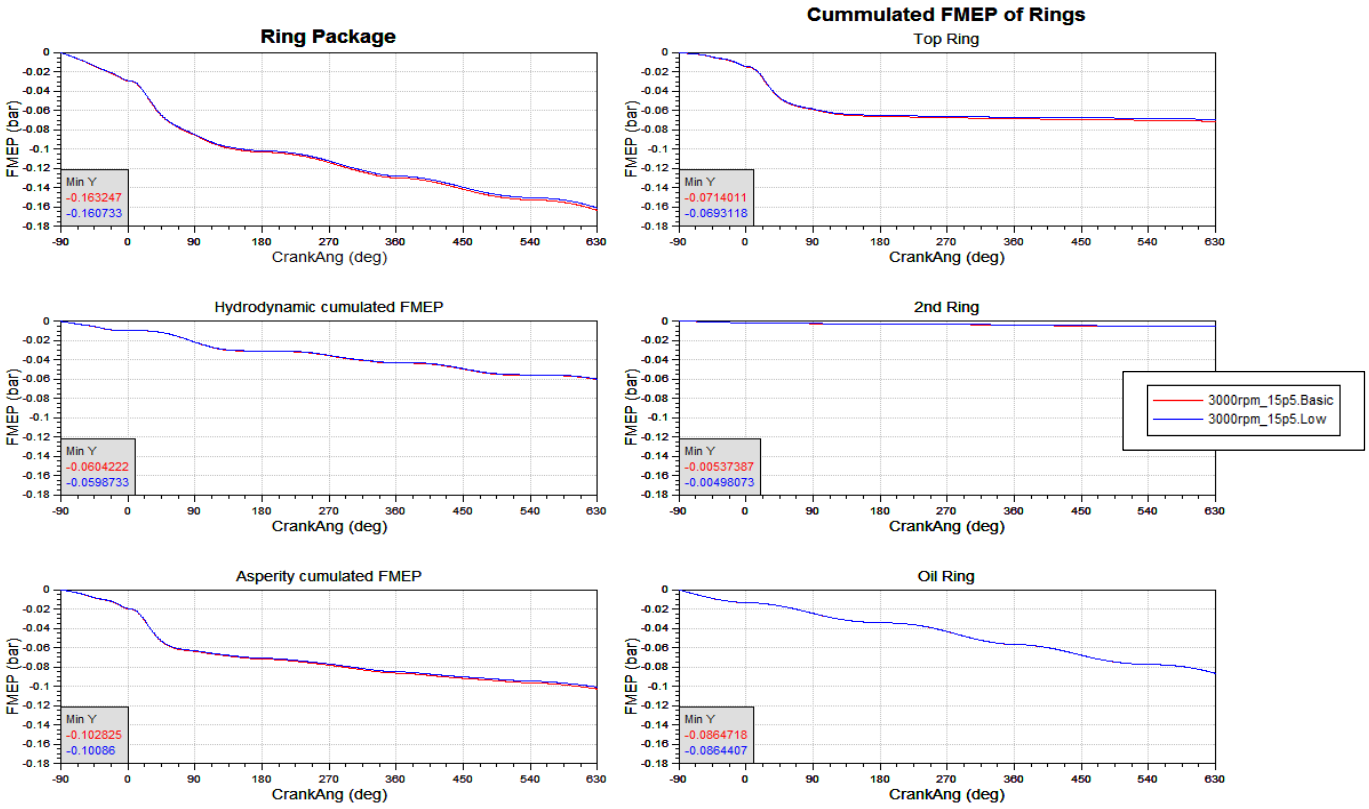

Figure 64. Comparison between BASIC and LOW FT ring package - FMEP overview.

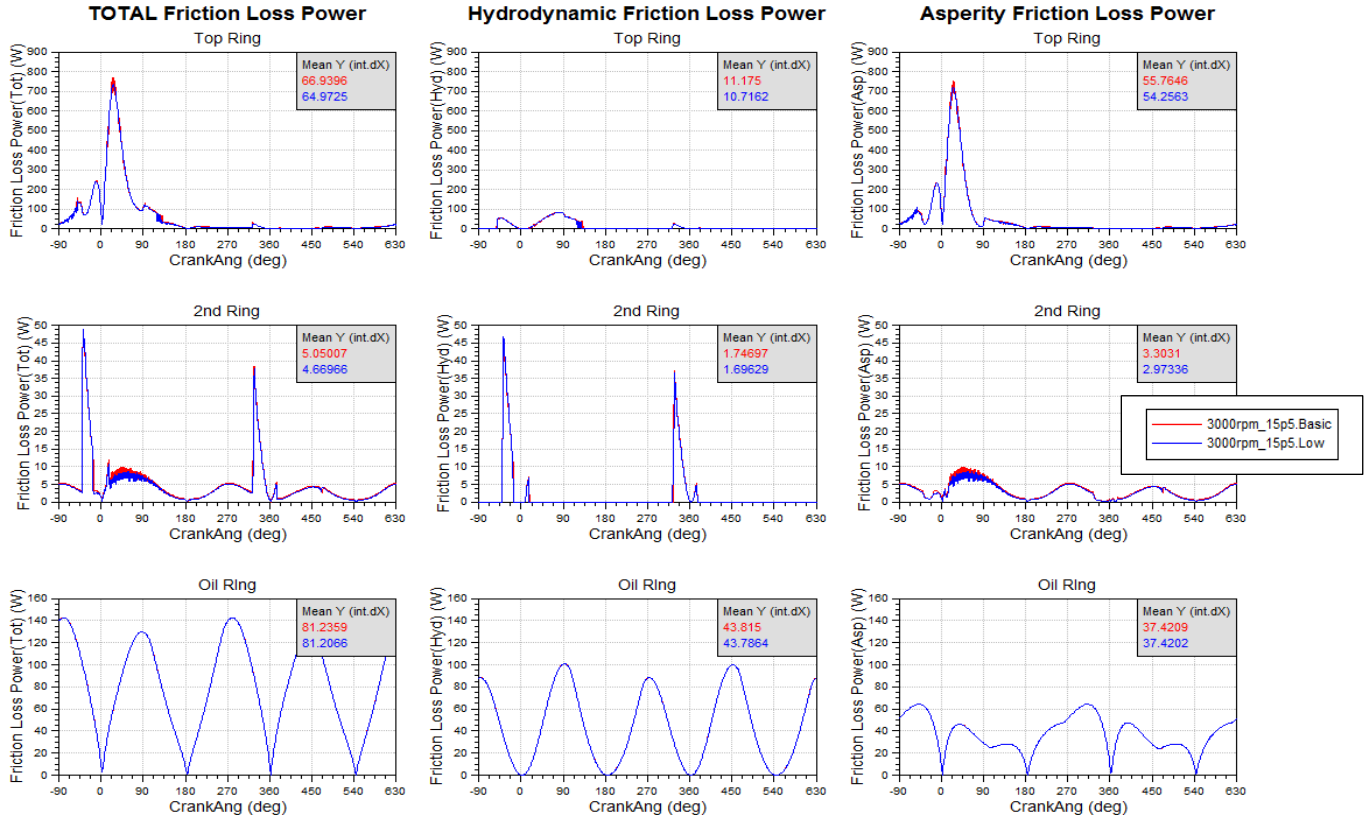

Figure 65. Comparison between BASIC and LOW FT ring package – Friction Power Loss overview.

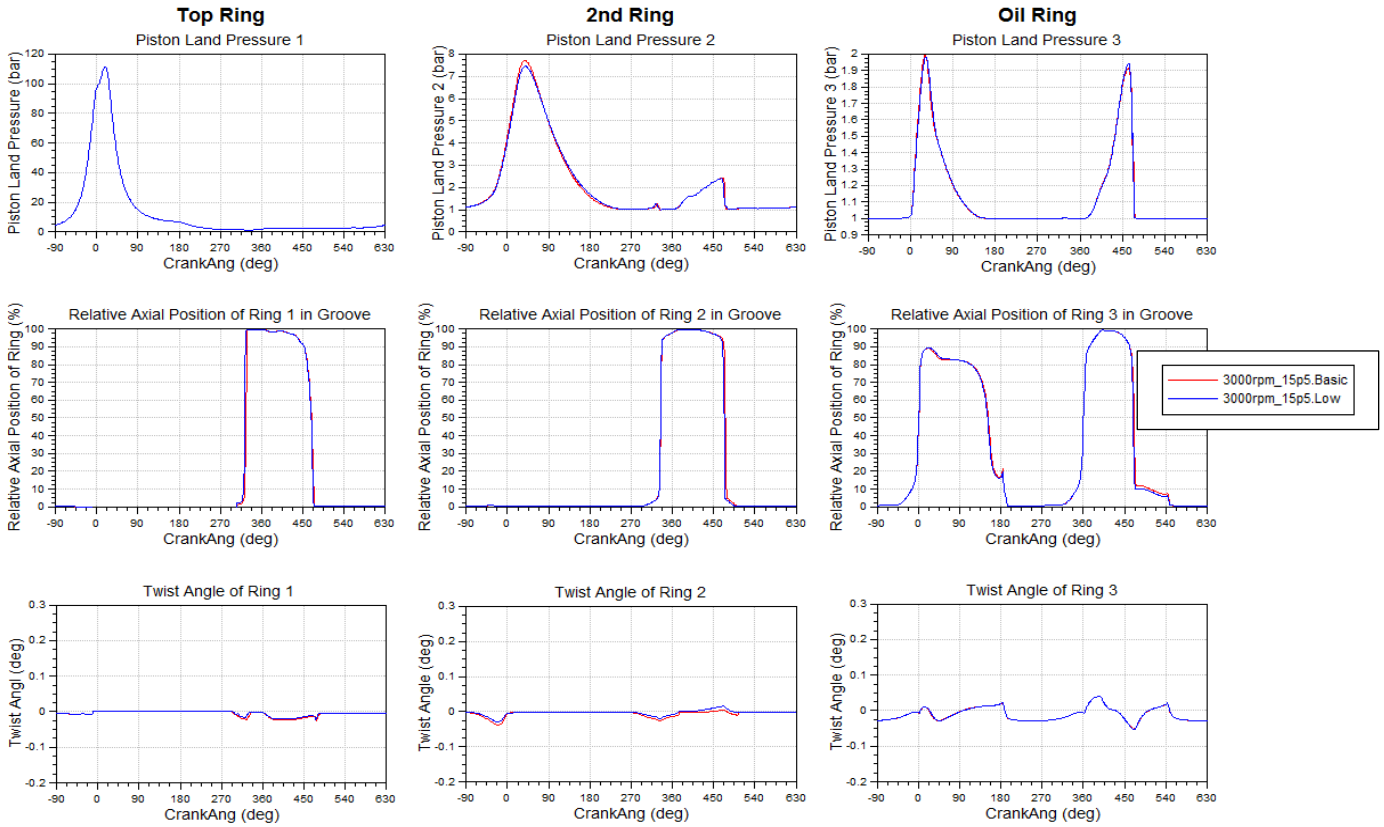

Figure 66. Comparison between BASIC and LOW FT ring package – Piston rings dynamics overview.

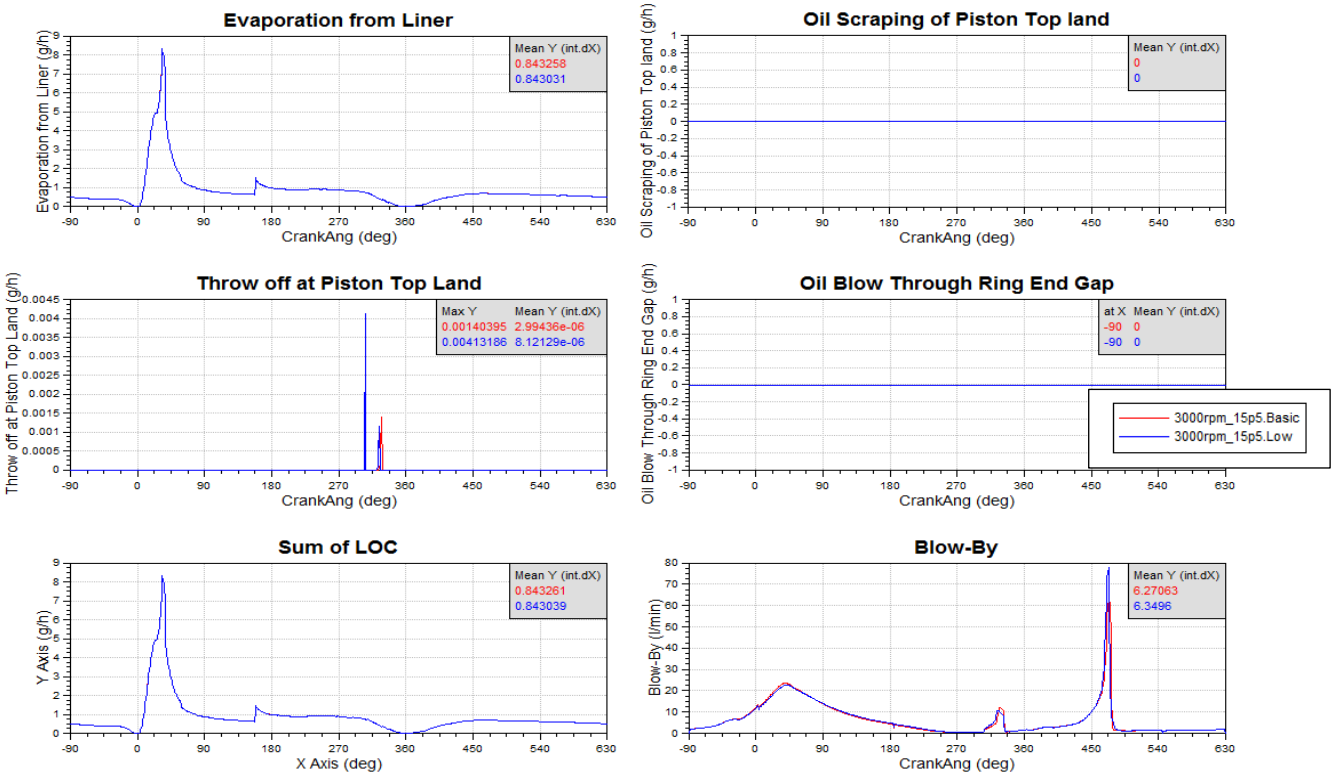

Figure 67. Comparison between BASIC and LOW FT ring package – Lube Oil Consumption and Blow-by overview.

Results summary – comparison between basic and low friction ring package

Above results shows that friction power loss and FMEP values slightly decreased with reduced tangential force ring package. Axial movement and twist angle only show minor differences both ring packages. Lube oil consumption is little bit lower in ring package with reduced tangential force. Blow-by values are higher in ring package with reduced tangential force. This trend of results is the same in other operating points of engine. In Appendix B, results of this comparison for different load cases at 3000rpm are shown.

3.4.3. EPR results – comparison between 2D and 3D solver

In following figures results of 2D and 3D simulation solver for basic ring package will be shown. In 2D approach piston ring dynamic is calculated only with 2 mass point and in 3D approach, piston ring dynamic is calculated with 36 mass point. Results are displayed only for one operating point (3000rpm_15.5) and other results for different load cases at speed 3000 rpm are shown in Appendix B.

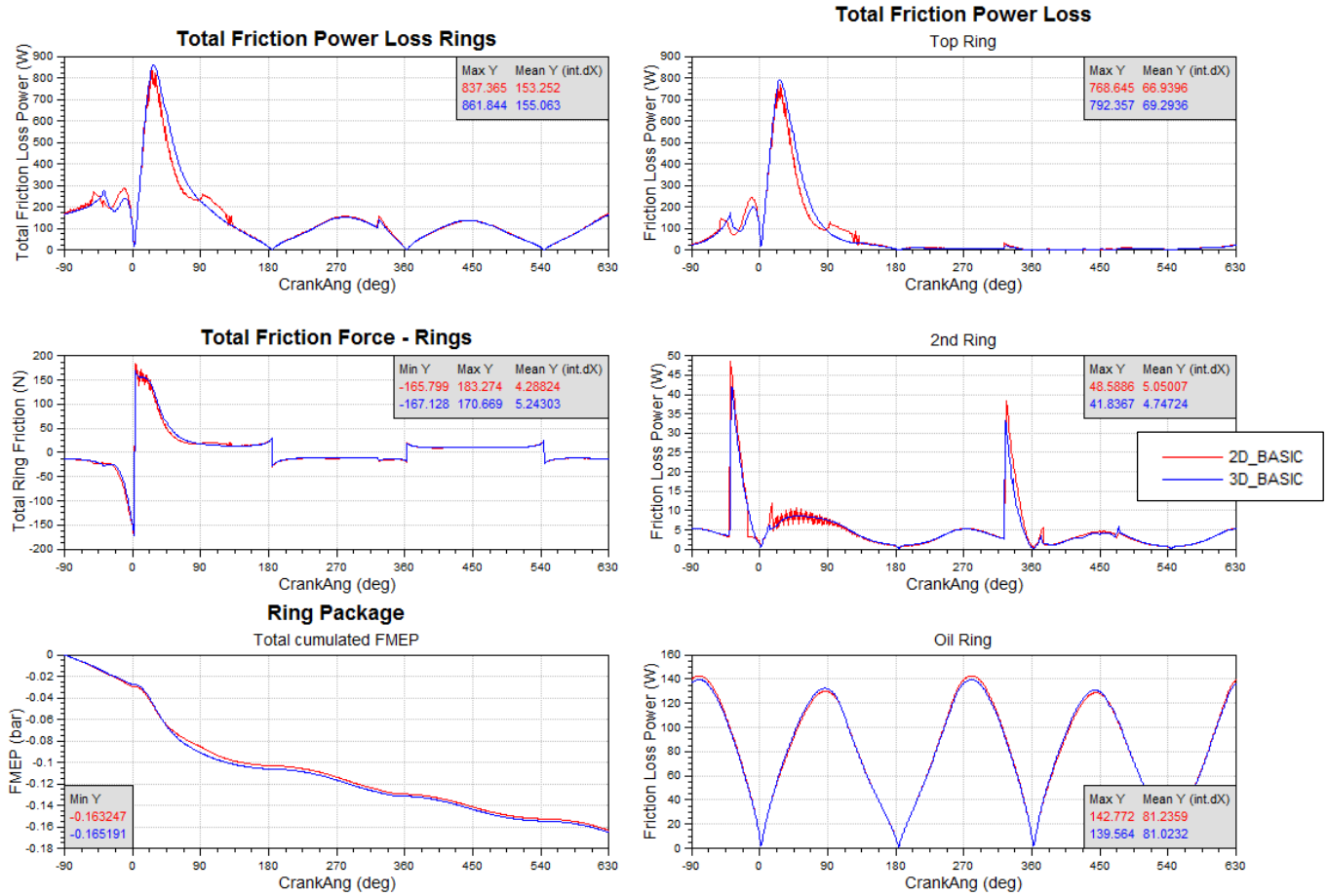

Figure 68. Comparison between 2D and 3D basic ring package - Friction characteristics overview.

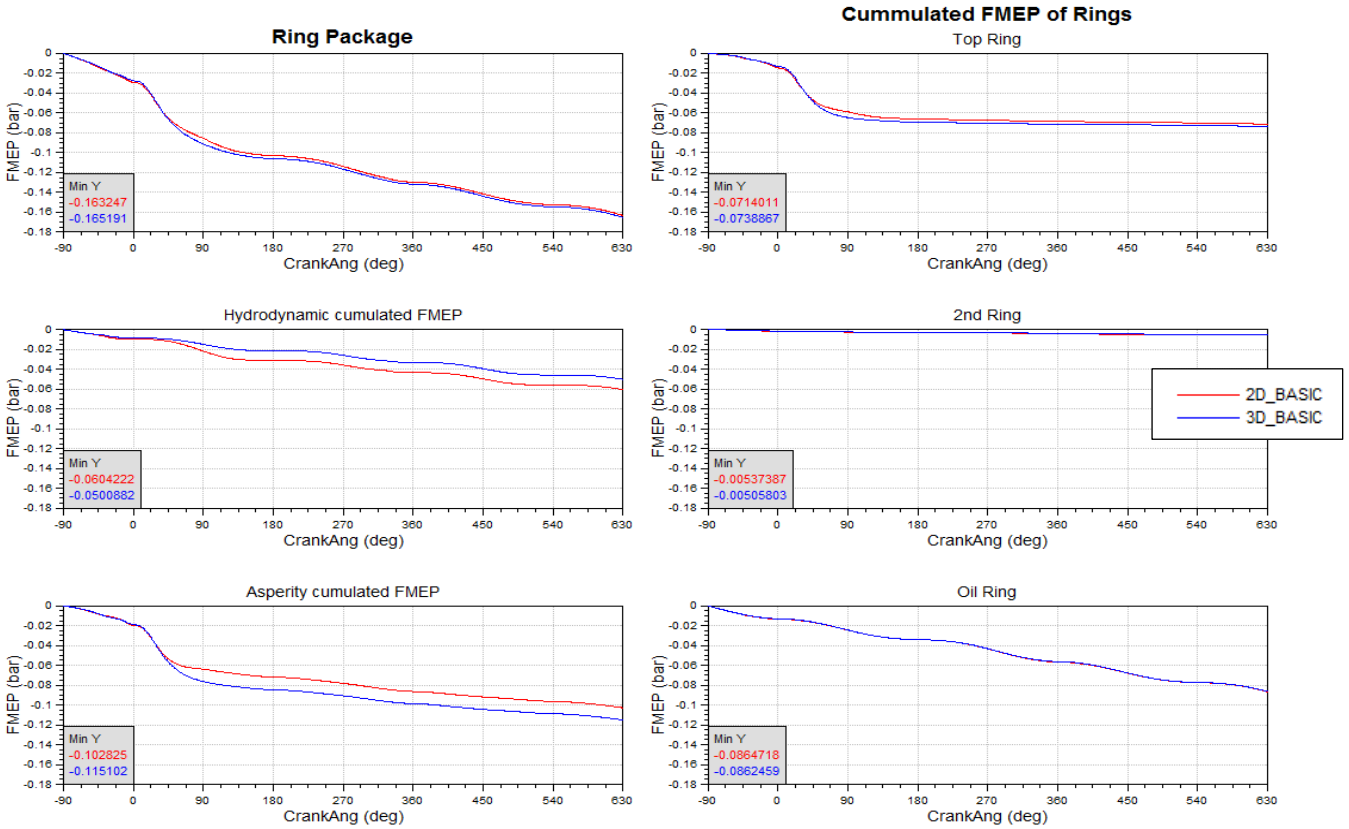

Figure 69. Comparison between 2D and 3D basic ring package - FMEP overview.

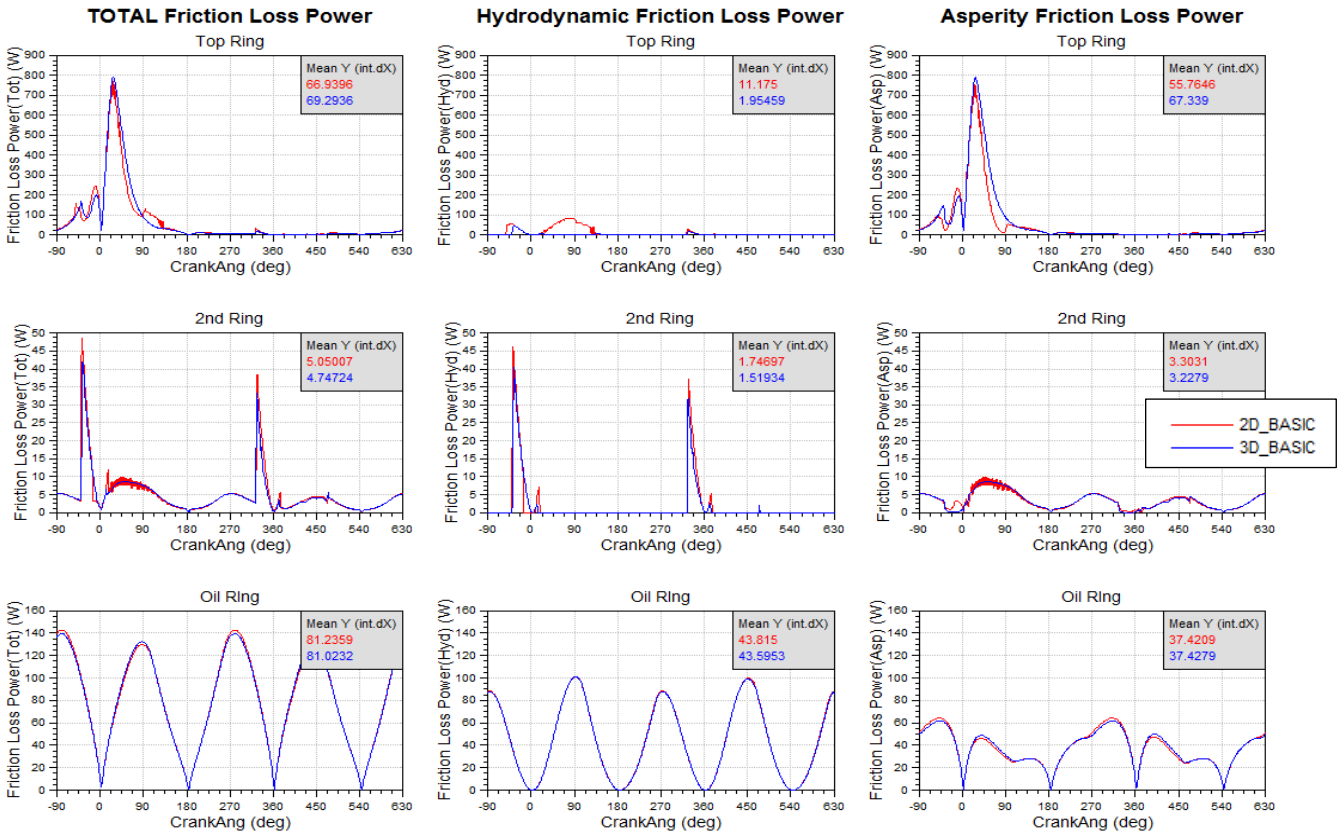

Figure 70. Comparison between 2D and 3D basic ring package - Friction Power Loss overview.

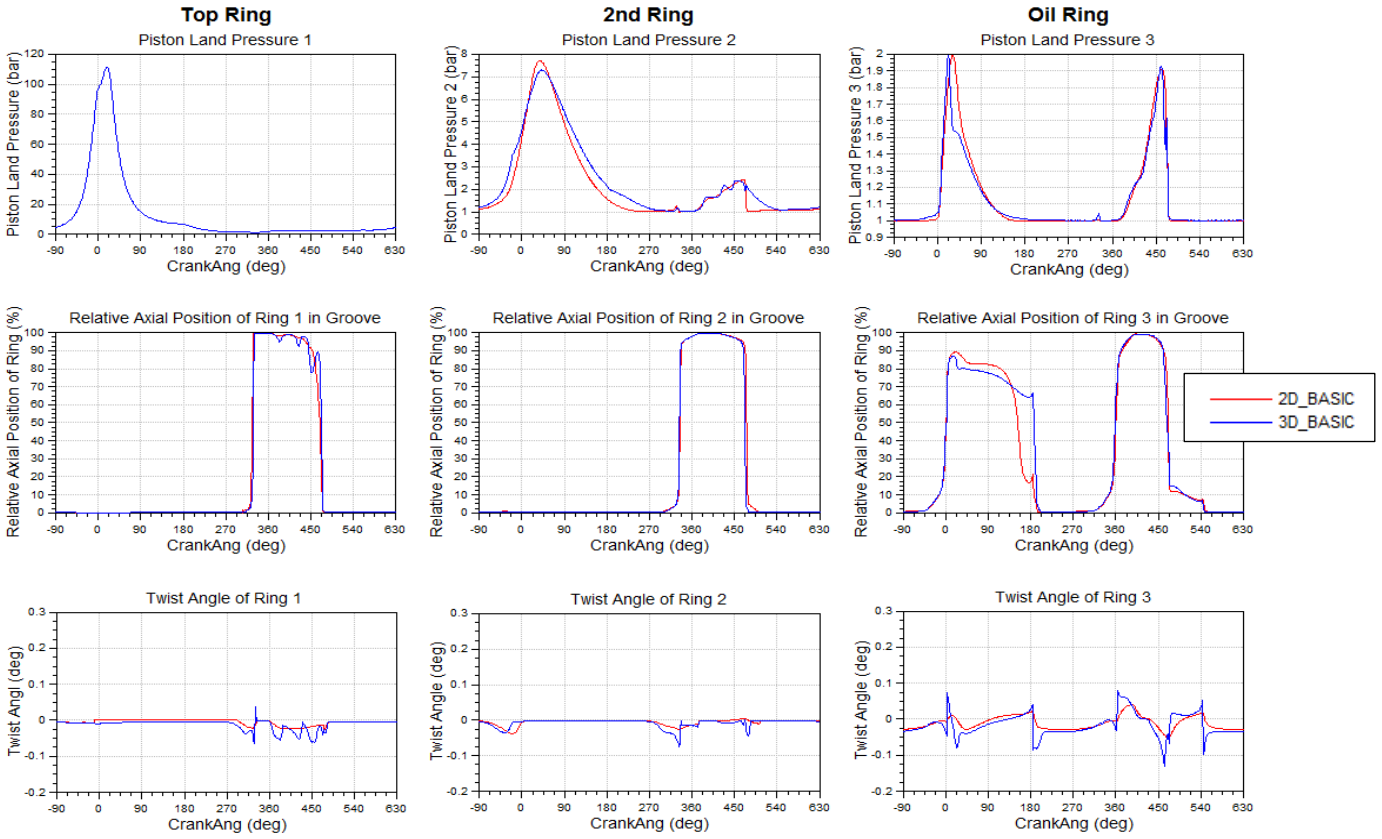

Figure 71. Comparison between 2D and 3D basic ring package – Piston ring dynamics overview.

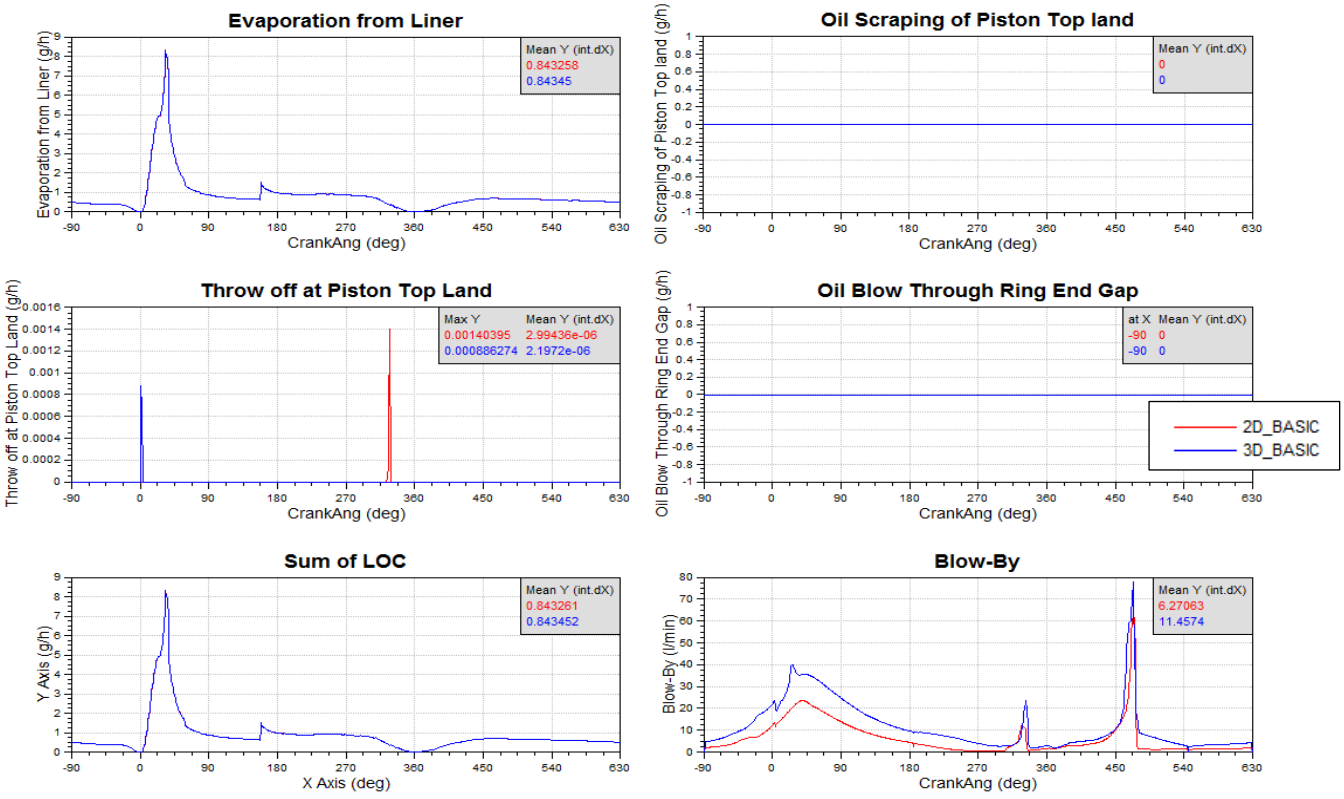

Figure 72. Comparison between 2D and 3D basic ring package – Lube oil consumption and Blow-by overview.

Results summary – comparison between 2D and 3D

Above results shows that friction power loss and FMEP values slightly increased with 3D simulation solver. Visible is difference in hydrodynamics and asperity cumulated FMEP value. Hydrodynamic cumulated FMEP have higher values with 2D solver and asperity cumulated FMEP have higher value with 3D solver. Friction ring forces have slightly higher value with 3D simulation solver. Axial movement of piston ring in groove are pretty the same in both cases and twist angle is slightly higer in case with 3D simulaton solver. Lube oil consumption are the same in both cases and blow by results significaly increased in model with 3D simulation solver. In other lower speed cases (1500 rpm) in simulation with 3D solver ring end shut of top ring. This phenomenon is very bad for engine because that phenomenon significaly increased friction losses in cylinder. The reason of ring end shut on lower engine speed is probably caused because 3D approach calculated liner deformation and shapes in all circumferential direction and 2D approach calculated liner deformation and shapes only in one point on TS and on point on ATS.

3.5. General about analysis in modul EXCITE™ Power Unit.

AVL EXCITE™ Power Unit is a multi dynamic simulation tool for engine design and for the analysis and optimization of existing engines and power units. This module is used for analyzing dynamics of cranktrain components, 3D piston dynamics, engine NVH, detailed bearing analaysis, acustics etc. The simulation concept is based on dividing the non-linear mechanical system into subsystems with linear elastic behavior and non-linearities occurring only at the connections between these subsystems. Therefore, in the simulation model, linear elastic bodies interact through highly non-linear connections. Since the system is nonlinear the equations of motion are solved in time domain. An effective time integration procedure with adjusted step size is provided. The results can be transformed into the frequency domain afterward [24].

The elastic bodies are represented by Finite element models using reduced structure matrices. FE- models have a large number of degrees of freedom (DOF) which are not practical to use in multibody dynamics calculations. Assuming small displacements, modal superposition can be used to significantly reduce the number of DOF and therefore the size of the model. The main idea of modal superposition is that the deformation behavior of a component with a very large number of degrees of freedom (DOF) can be captured with a much smaller number of modal DOFs. The main assumption behind working with flexible bodies is that the procedure is valid only for small, linear body deformations relative to a local frame of reference, while that local

reference frame is undergoing large, non-linear global motions. The data transfer to EXCITE™ Power Unit is organized by interfaces to FE-solvers [25].

In the graphics window, the user can switch between the 2D (block model) view and the 3D view. Both - the uncondensed (or any surface) mesh and the condensed mesh - can be displayed for a body. Joints are displayed by lines between the connected nodes. Once the 2-D representation of the system is defined, the properties of the bodies and joints can be defined. The Crank Train Globals tool is used to define various specifications of the system, such as engine speed, bore, stroke, etc [24].

3.6. EXCITE™ Power Unit models

In this chapter, simulation model, based on full engine models, will be described. There are created two simulation models in EXCITE™ Power Unit module: a simplified and an advanced model. Differences in models are in using different joint connections between bodies. After in this chapter, those joints will be described. In next figures, 2D view of AVL FRISC simulation model are presented.

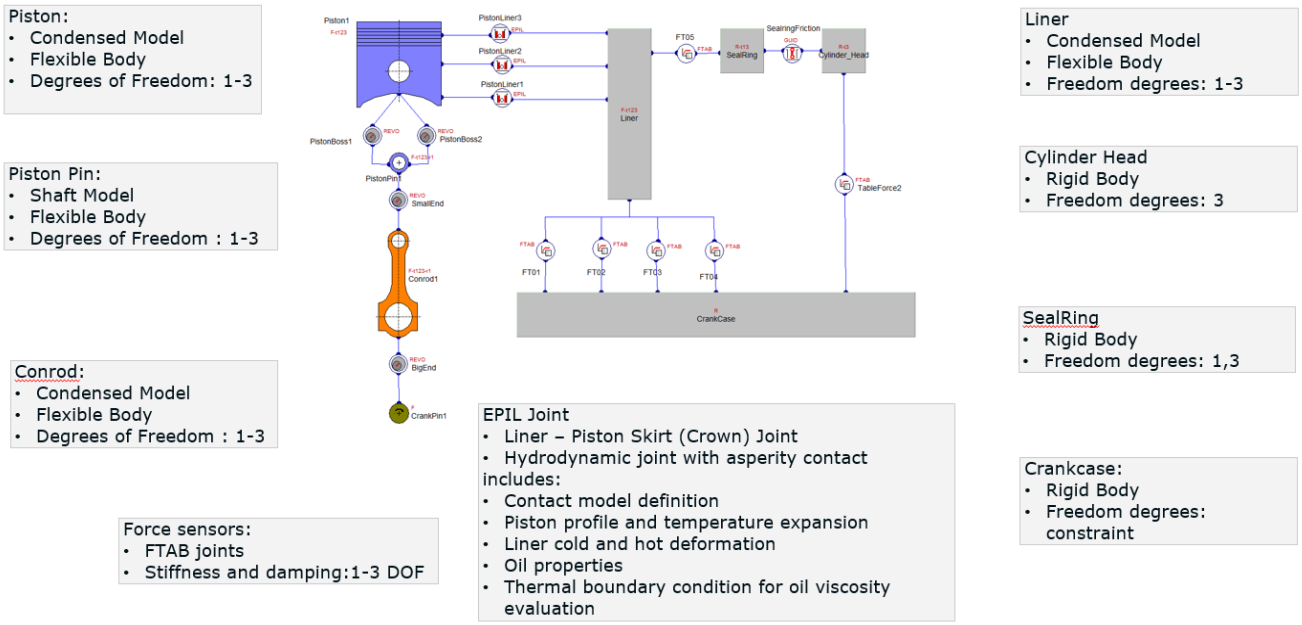

Figure 73. EXCITE™ Power Unit FRISC engine.

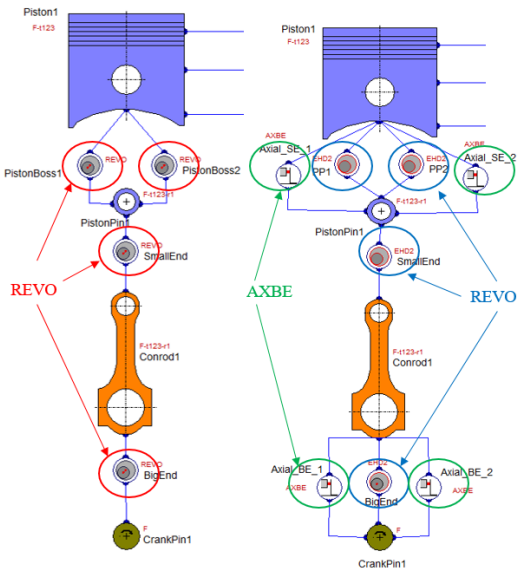

Figure 74. Differences between simplified and advanced model.

In above figures, body and joint elements can be seen. Piston, conrod, liner and piston pin are flexible bodies. In advanced model this bodies are FE models with reduced structure matrices, and before that they are meshed in SimLab software. In simplified model, piston pin is created via Shaft Modeler. Liner mesh are the same in both models, but piston and conrod mesh models are different between simplified and advanced model. Crankcase is creted like rigid body. Rigid body is not deformable body in which displacement of all nodes of that body are the same. In model are also implemented bodies of cylinder head and sealring. That are dummy rigid bodies with mass, moments of inertia and initial position in engine. They are imported to investigate "stick-slip" effect of sealring and vertical movement of the cylinder head. In chapter about comparison between simulation and measuremet results of friction caused by "stick-slip" effect will be shown.

Condensed nodes of piston and liner are connected with EPIL joints on top land, second land and skirt. Piston and piston pin are in simplified model connected with REVO joints (marked with red circle) and in advanced with EHD joints (marked with blue circle). Conrod in simplified model is connected to piston pin and crank pin with REVO joint (marked with red circle) and in advanced model with EHD joint (marked with blue circle). Main difference between REVO and EHD joint is that EHD model consider elasto-hydrodynamic contact which depend on oil viscosity, temperature, surface properties and REVO model describe contact with spring and damper. Also, REVO model connect only one node of connected bodies and EHD joint connect surfaces or nodes between bodies. On Figure 75. are presented differences in connections in joints.

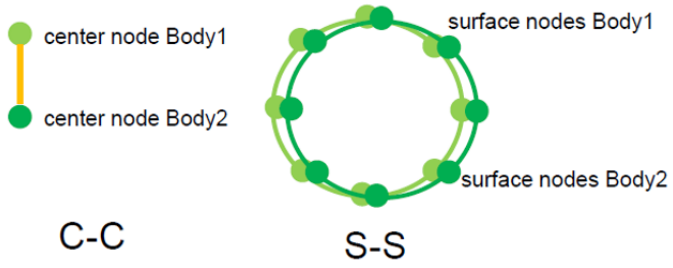

Figure 75. Connections between jonits [26].

It is important to note that EHD joints allows axial movement so axial thrust bearing must be implemented inside model (marked with green circle). Liner and crankcase are connected with FTAB joints on 4 symmetrical positions and they represent force sensors in real engine model.

3.6.1. FTAB joint

FTAB joint, or full name Table Force/ Moment Jonits, defines the properties of a user-defined spring force/moment versus relative displacement and/or a user-defined damping force/moment versus relative velocity. Optionally, the force/moment can also be speed dependent. This joint represent linear or nonlinear static siffness between bodies.The model force is interpolated from the defined table values. Interpolation of the input table values can be linear or cubic. For the purpose of cubic interpolation at least 3 data points need to be defined. This joint can connect one node of one body with one node of another body in the same DOF [24].

In this model, same values of stiffness and damping are given for all 4 FTAB jonits whose connect liner and crankcase correnspondig to stiffness of the force sensors. Each FTAB have given valus for stiffness and damping in 3 directions: axial, longitudional and vertical.

3.6.2. REVO joint

REVO joint, or full name Revolute Joint is joint who connect one node of a body with another node of another body. The initial distance of the two connected nodes has to be zero. Main aplication of this joint is for main bearings, big and small end bearing. On Figure 76. connection between two bodies with REVO joint are presented [24].

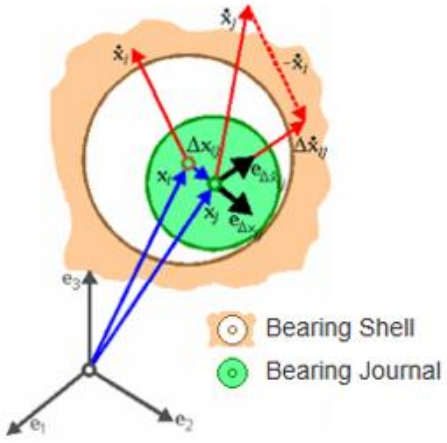

Figure 76. Connection of bodies with a REVO joint [24].

Connection between two nodes is describes via spring – damper functions. A formula for the computation of an unknown force *f* (a moment computation can be written analogously) is depicted in equation (9):

$$f = k_{\text{joint}} \cdot \Delta x + d_{\text{joint}} \cdot \Delta \dot{x}, \tag{9}$$

where Δx and $\Delta \dot{x}$ denote the distance and its first derivative in time of the connected nodes. In the case of a linear spring damper model, the coefficients k_{joint} and d_{joint} are constant. For non-linear modeling, k_{joint} and d_{joint} are determined via the non-linear equations [24].

3.6.3. EHD and EPIL joint

The Elasto-Hydro-Dynamic journal sliding bearing (EHD2) is joint which can connect a number of bearing pin nodes of a body with a number of bearing shell nodes of another body. This joints defines the properties of a journal sliding bearing using the Reynolds equation with a mass conserving cavitation model under constant or variable viscosity. The viscosity depends on the temperature, pressure and shear rate of the lubricant. The model force is a highly nonlinear function depending on the relative displacement (clearance), the relative velocity of the connected nodes and the oil film history in terms of the fill ratio.

The Elastic Piton-Liner Contact (EPIL) is a joint which can connect several numbers of piston skirt nodes with several numbers of liner nodes. This joint defines the properties of an elastic piston-liner contact using the Reynolds equation. Constant oil film height and a constant or pressure dependent viscosity is considered. The joint force is a highly nonlinear function of

the relative displacement (clearance), the relative velocity of the connected nodes and the oil film history in terms of fill ratio.

For both joints, the excitation joint forces are computed from hydrodynamic pressure and hydrodynamic friction via integration. The hydrodynamic pressure distribution of the oil film in a lubrication region between two bodies can be calculated using a modified Reynolds equation derived from the Navier-Stokes equation and the equation of continuity. In equation (10) is presents modified Reynolds equation for EHD joint given in shell body fixed coordinate system. For EPIL joint this equation is the same, only difference is that the EPIL jonits equation is given in piston body fixed coodinate system.

$$-\frac{\partial}{\partial \bar{x}}\left(\bar{\theta}\cdot\alpha_x^2\frac{\partial \bar{p}}{\partial \bar{x}}\right)-\frac{\partial}{\partial z}\left(\bar{\theta}\cdot\alpha_z^2\frac{\partial \bar{p}}{\partial z}\right)+\frac{\partial\left(\theta\cdot\beta_R\right)}{\partial \bar{x}}+\frac{\partial\left(\theta\cdot\gamma_R\right)}{\partial t}=0 \qquad \textbf{(10)}$$

The Elastohydrodynamic Lubrication (EHL) contact model is used to evaluate contact pressures, which is distributed over a large contact area (journal contact) and contact which is concentrated on a very small area and generates very high pressures, with high pressures and thin oil films while taking local elastic deformations into account. These two features are combined by solving the Reynolds equation for the pressure distribution together with the film thickness equation for the elastic deformation [24]. Asperity contact can be modeled in different ways: Greenwood/Tripp, composite, microslide import and user define. If Asperity Contact - Greenwood/Tripp is selected, the solid-to-solid contact of the asperity summits is modeled by force-compliance relationship, which is based on a statistical evaluation over all contact spots. Each individual conjunction is approximated by a Hertzian contact of a sphere with a rigid plane, where the contact condition between the two rough surfaces is implicitly considered.

3.7. Input data for EXCITE™ Power Unit simulation

This chapter decribed main input data such as load, data necessary for describing surface contact, piston profile and liner profile.

3.7.1. Load data

In EXCITE™ Power Unit models, the same pressure curves like in EXCITE™ Piston&Rings model are used. In Chapter 3.3.1. the pressure curves are shown. Besides pressure curves in EXCITE™ Power Unit models, the friction forces calculated from EXCITE™ Piston&Rings simlation are acting on the liner. Those friction forces are shown in results in

Chapter 3.4. and in Appendix A for basic ring package. At the sealring a cylinder pressure dependant normal force is acting on radial area of sealring. On the cylinder head an axial force is modeled from cylinder pressure. This force curves are shown in Figures 77. and 78.

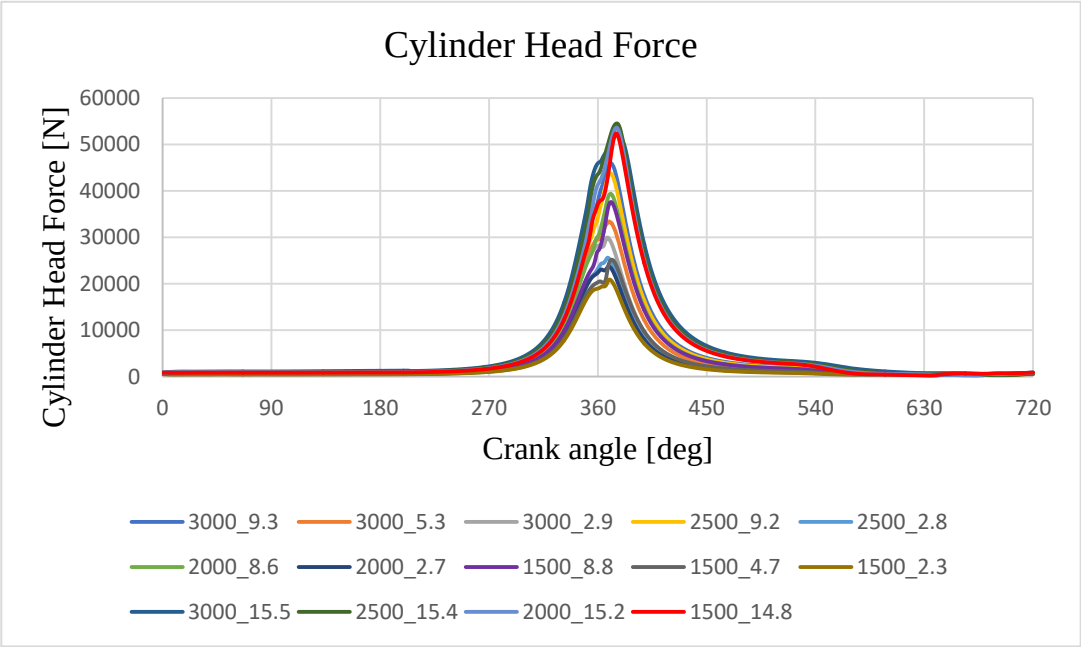

Figure 77. Load curves acting on cylinder head.

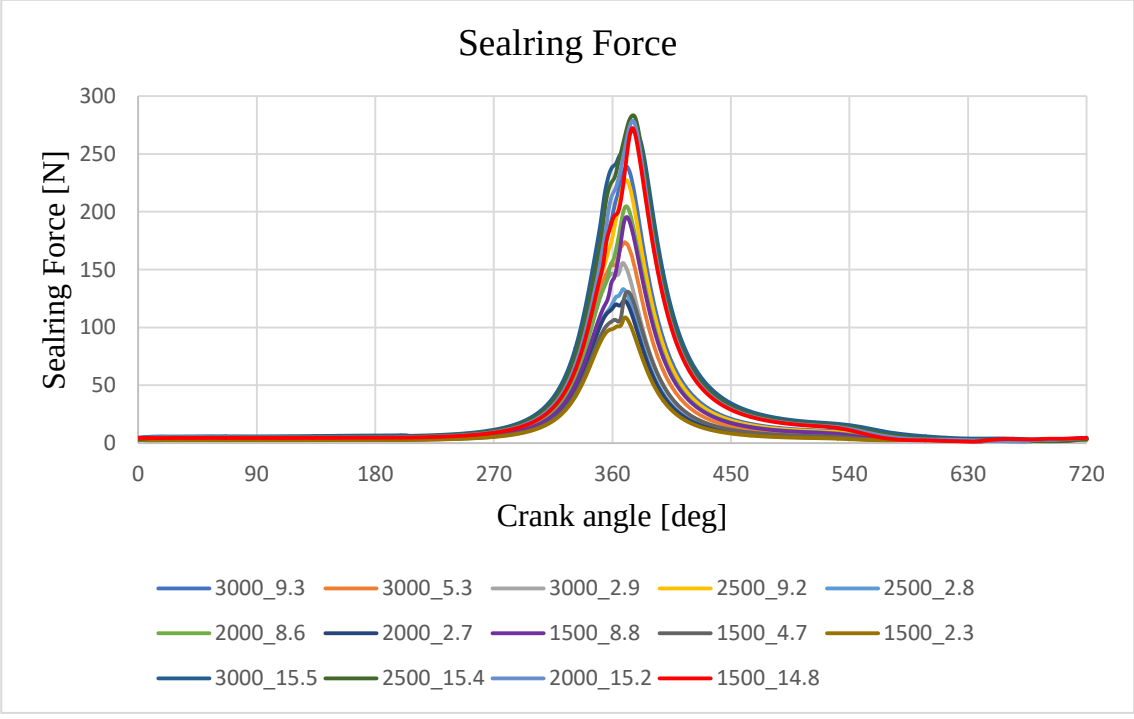

Figure 78. Load curves acting on sealring.

3.7.2. Surface contact

For calculating friction between piston and liner it is very important to know the material properties and the surface roughness between them. Figure 79. shows surface roughness for the liner and piston skirt. Surface contact are modeled in three EPIL jonits. On top and second land contact on EPIL joint are modeled like dry asperity contact without hydrodynamics. Piston skirt contact is modeled like hydrodynamics with or without asperity contact. The EHD contact is described by Asperity Contact – Greenwood/Tripp approach and the averaged Reynolds equation is described by the Patir and Cheng model.

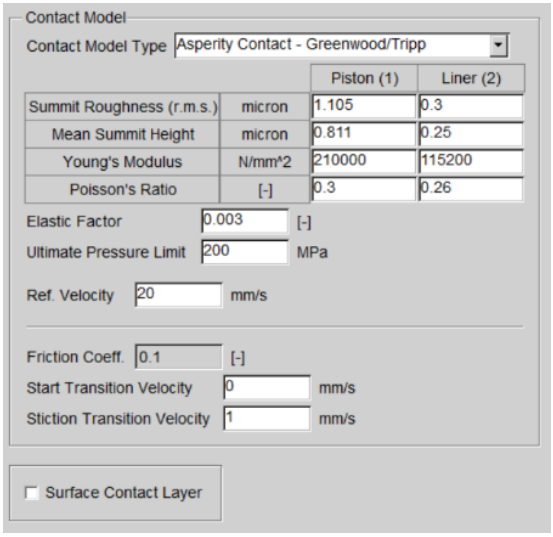

Figure 79. Surface contact for second land.

The contact between the interacting roughness summits is a combination of micro-hydrodynamic contact and partly local solid contacts. This type of contact is explained in Chapter 3.3.2. In Power Unit model, this contact is modeled on piston skirt. Top and second land have standard value of friction coefficient set as default value (0.1).

Constants a, b, c and reference length for piston skirt are shown in Table 6.

Table 6. Values of friction constants in Power Unit model.

	Constant a (-)	**Constant b (-)**	**Constant c (-)**	**Reference length (micron)**
Piston skirt	2.71828	1000	1000	2

For calculation friction between piston and liner is very important to know nominal radial clearance of piston skirt, second and top land. This value represent distance between liner and piston segments. FE model of liner and piston should be created with the same diameter. Very important is to use correct values of nominal radial clearances because friction results would not be accurate, and it is possible that simulation will be failed. On Figure 80. is shown how nominal radial clearance is calculated.

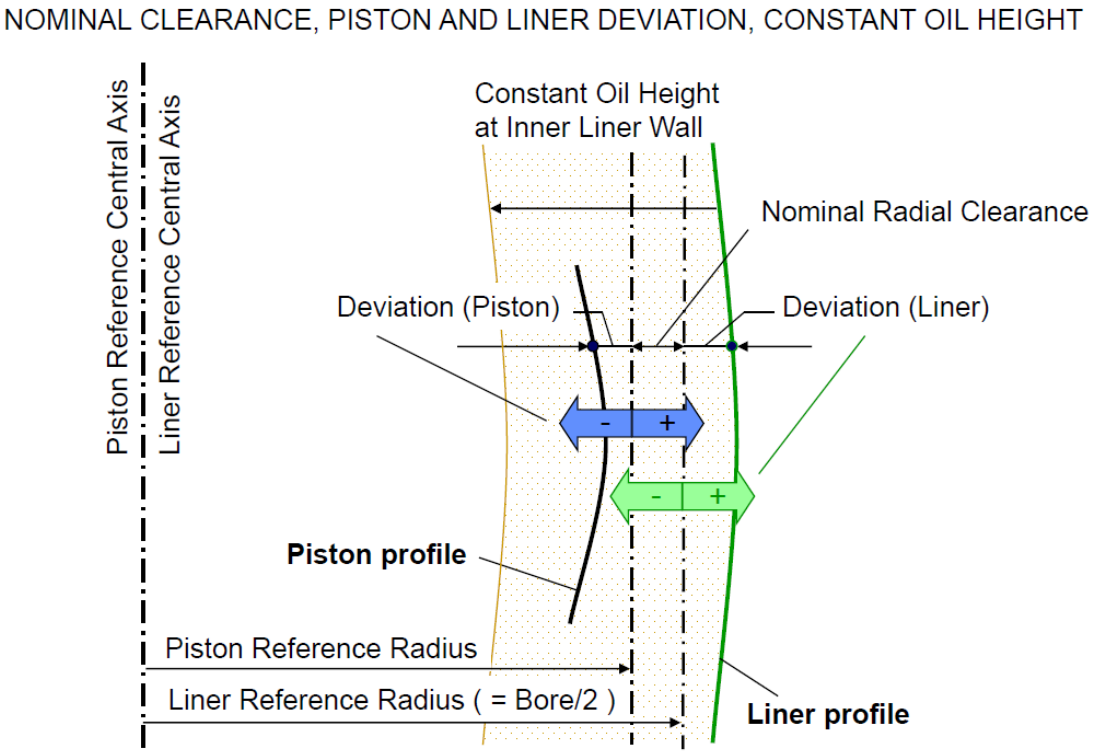

Figure 80. Nominal radial clearance display [9].

3.7.3. Power Unit Profiles

In the EXCITE™ Power Unit module, the profiles of piston and liner must be inserted. After creating a profile in ASCII format, the files are imported into software. The same liner profile described in Chapter 3.3.3. are used in Power Unit model.

Piston profiles are calculated in cold and warm conditions. The cold piston profile is a profile that describes how the piston profile differs in the radial and circumferential direction from an ideal cylinder in assembling piston in engine. In all cases the cold piston profiles is the same. Cold profiles are imported with .txt file. This piston has 2 cold profiles: piston skirt and second land profile. Top land doesn't have cold profile because there are no differences in radial and circumferential direction from ideal cylinder.

The warm profile is described by the thermal radial deviation. This value can be calculated from FE analysis or defined calculated by using temperature field. In this case, thermal radial deviation is calculated from temperature filed.

Table 7. Piston temperature field.

CASE	Skirt [°C]	Second Land Bottom [°C]	Second Land Top [°C]	Top Land Bottom[°C]	Top Land Top[°C]
3000_15p5	120	211	263	298	382
2500_15p4	115	211	263	298	382
2000_15p2	110	211	263	298	382
1500_14p8	100	211	263	298	382
3000_15p5	110	206	258	293	377
3000_5p3	106	201	253	288	372
3000_2p9	102	196	248	283	367
2500_9p2	108	206	258	293	377
2500_2p8	100	196	248	283	367
2000_8p6	106	206	258	293	377
2000_2p7	96	196	248	283	367
1500_8p8	97	206	258	293	77
1500_4p7	92	201	253	288	372
1500_2p3	87	196	248	283	367

For piston skirt a constant temperature field over skirt height is assumed. Top and second land was calculated with two temperatures, on bottom and top height of this piston segments. Thermal expansion coefficient of piston wall should be also defined. Figure 81. shows equation for calculating thermal deviation of piston profile with temperature field.

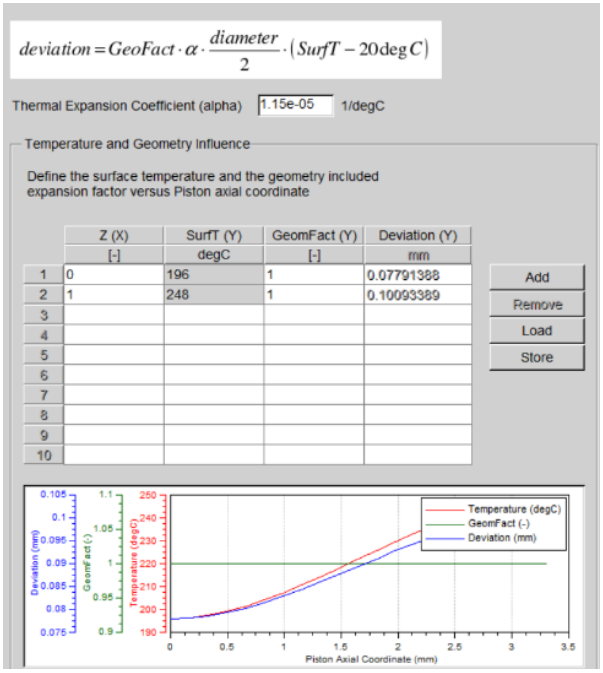

Figure 81. Calculation of thermal deviation.

After importing cold and warm piston profiles, total piston profile is sum of both profiles. In next Figure 82., piston profiles of top land, second land and piston skirt are displayed. This Campbell diagrams represent piston radial and circumferental deformation over piston height for each piston segment. At figure, 180 degree represent piston TS and ATS is presented with 0 and 360 degree.

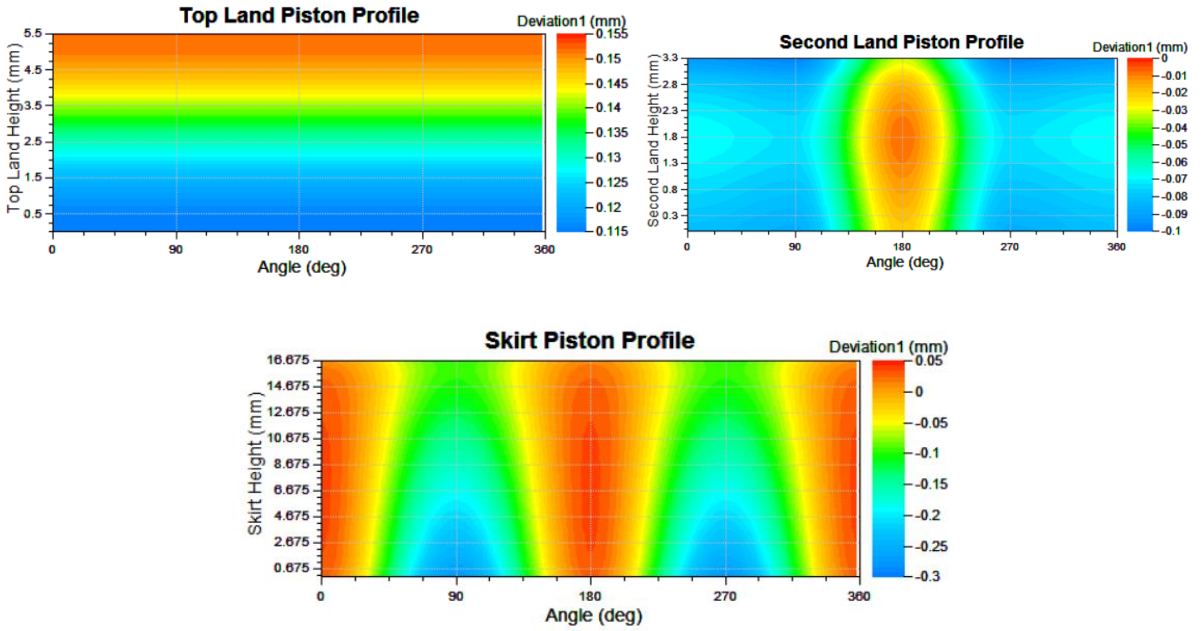

Figure 82. Piston profiles.

3.8. EXCITE™ Power Unit simulation results

This chapter describes simulation results of EXCITE™ Power Unit models. Results are presented for basic and low friction ring package. Except different ring package, results are also presented for simplifies (REVO) and advanced (EHD) model.

3.8.1. EPU results – basic ring package

This chapter describes results of piston movement, pressures, force in FTAB joint and friction power losses for basic ring package with REVO joints. Reasults are presented only for load case 3000_15.5. At Appendix D, other lower load cases for engine speed 3000rpm with basic ring package are shown.

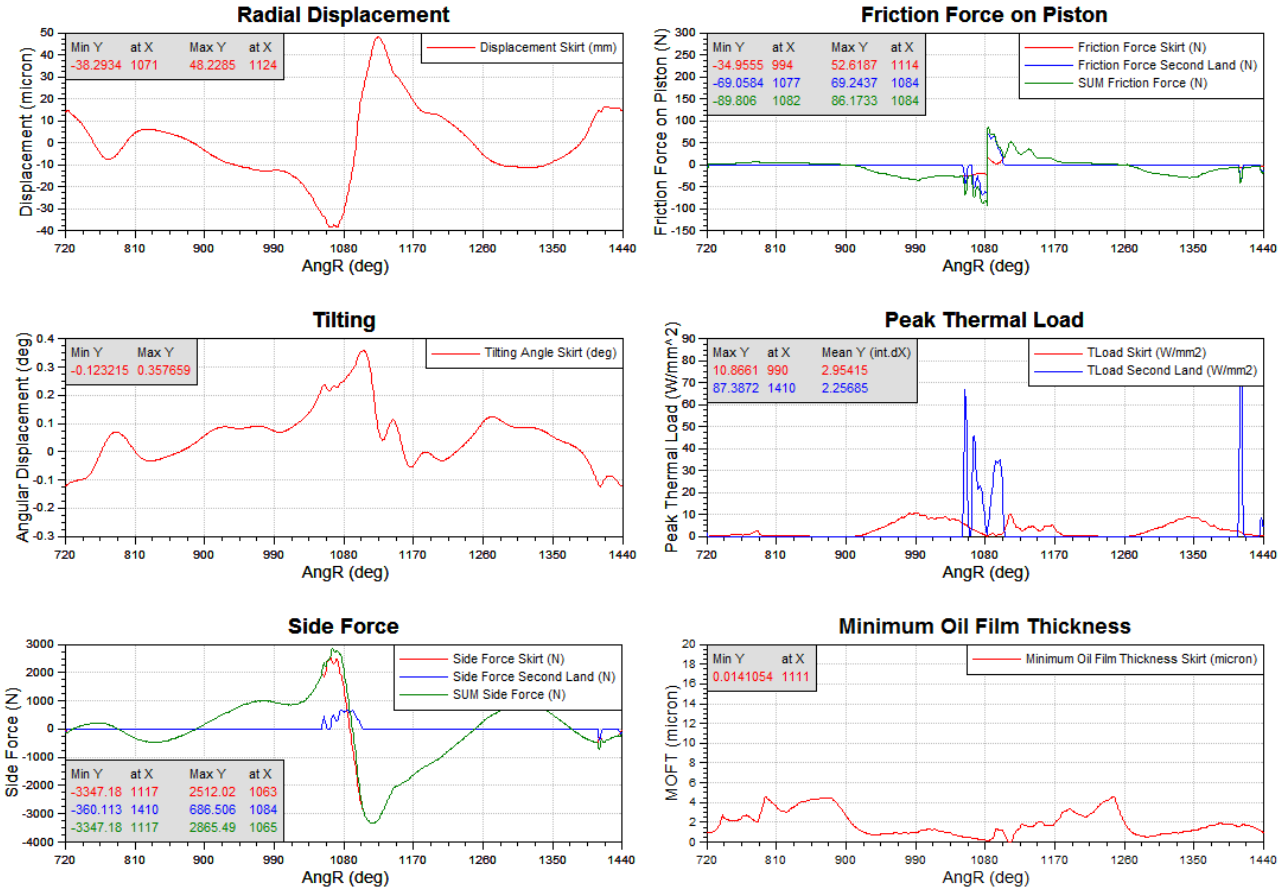

Figure 83. Piston results overview – 3000_15.5.

Above figure presents radial displacement ot piston motion between ATS and TS side. Movement of piston is also described with tilting around the piston pin ratotation axis. Lateral force whose act on skirt and second land are presented with side forces. Sum of friction forces on skirt and second land at TS and ATS can be also seen. Peak thermal load represents friction

energy which is applied at a certain spoat at the skirt and second land. Minimum oil film thickness describes oil film thickness between liner and skirt over crank angle.

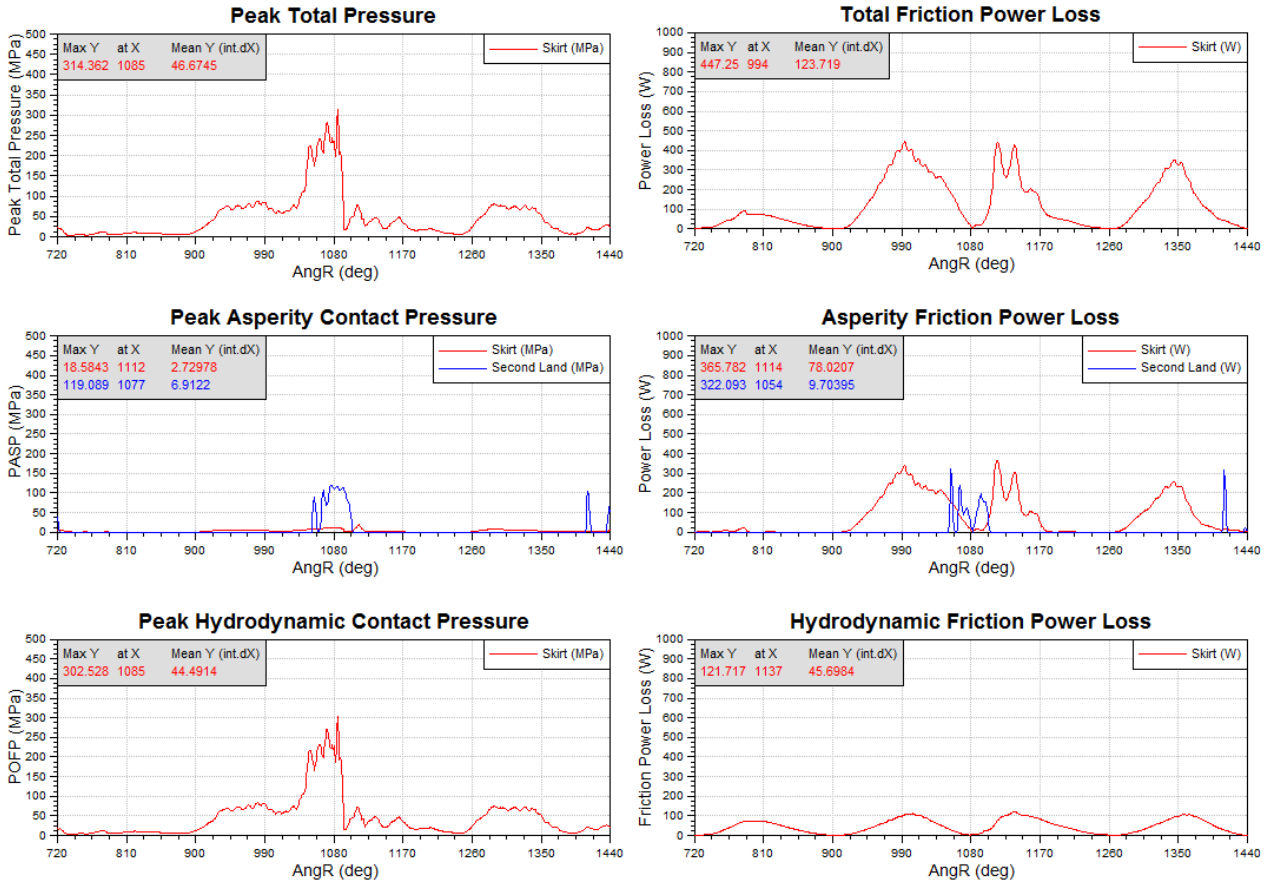

Figure 84. Pressure and friction results – 3000_15.5.

Peak total pressure describes maximum pressure at the contact between liner and skirt – second land over crank angle. Peak total pressure is the sum of peak asperity and peak hydrodynamic contact pressure whose are presented above. Total friction power loss are the sum of asperity and hydrodynamic friction power loss.

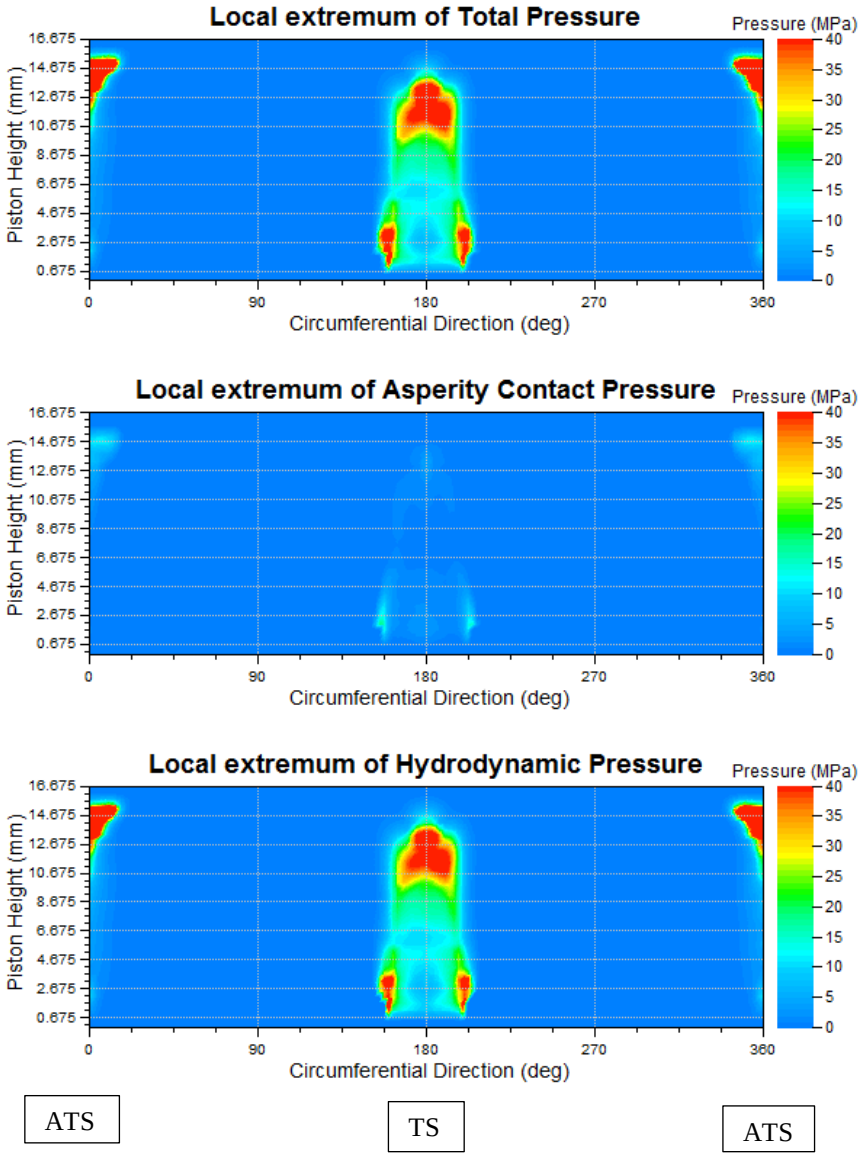

Figure 85. Campbell pressure distribution– 3000_15.5.

Local extremum of total pressure present points on piston skirt where the highest pressure occure. This pressure is combination of asperity and hydrodvnamic pressure.

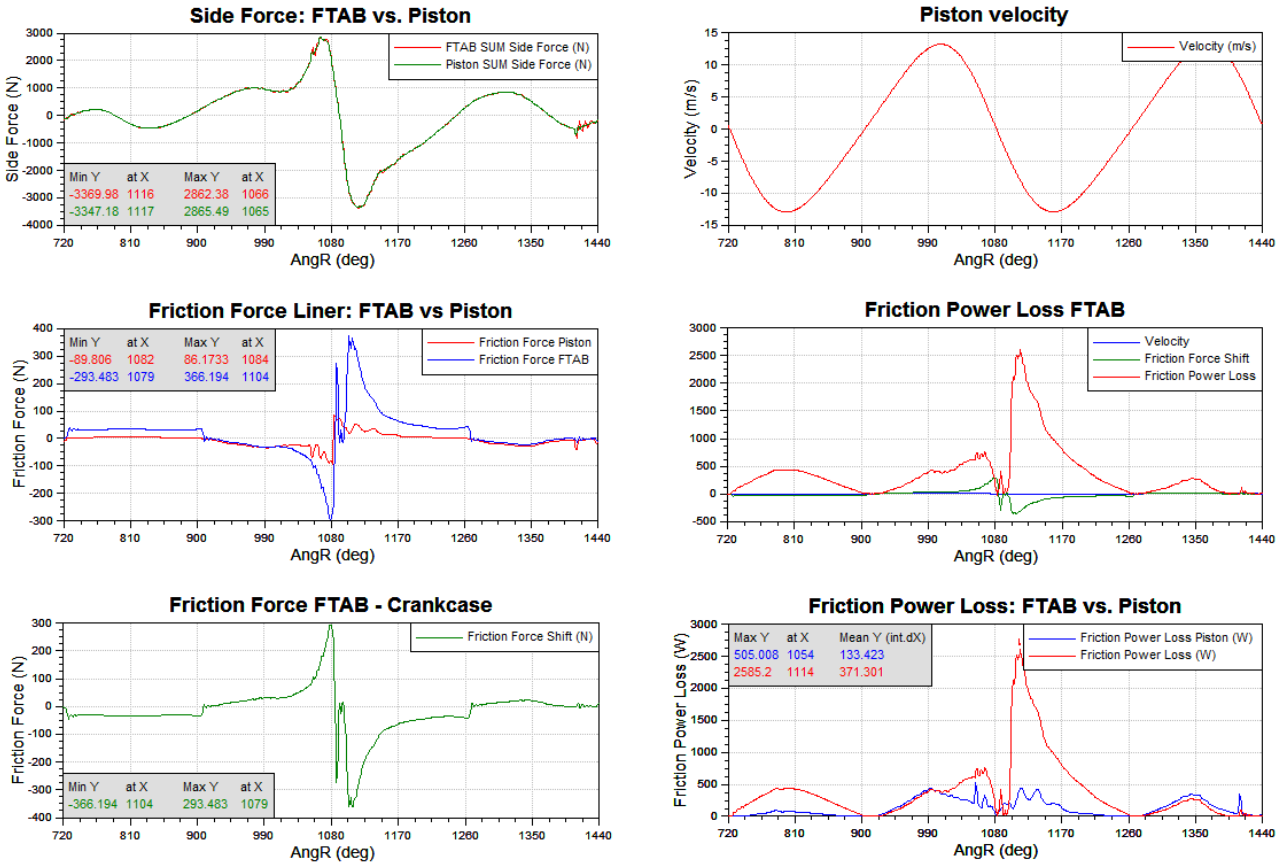

Figure 86. FTAB forces and friction power loss – 3000_15.5.

Above figure presents comparison between side forces generated on piston and calculated sum of lateral force in y – direction from FTAB joints (force signals). Comparison between friction forces generated on piston and calculated sum of vertical forces in z – direction can be seen. Friction forces at FTAB included piston ring friction forces, forced caused by stick slip effect (cylinder head vertiacal displacement), piston skirt and second land friction forces. Reaction friction force which act on crankcase is also shown. Total friction power losse are calculated like the product of friction force and piston velocity of midpoint. Profile of piston velocity are shown. After calculating total friction power loss, comparison with piston friction power loss are made.

Results summary – basic ring package, REVO

Above figures shows results of piston simulation with REVO joints. Radial displacement amplitude is inside AVL guideline area (+/- 0.2% of bore radius = 77microns). Tilting angle are slightly above AVL guideline (0.33deg). Friction force which acting on piston are higher on second land and peak of that force appear at FTDC. Pressure at skirt are mostly influenced by hydrodynamics pressure. On second land, around FTDC, asperity contact is visible. Minimum

oil film thickness appears also around FTDC in the area of high asperity pressure. Due to high tilting, local high pressure appears at top of skirt height on ATS. On piston skirt a small constant value of asperity pressure occurs on a long period around TDC asperity contact at of second land appears. Side force calculated from EPIL and from FTAB joint have the same values. Difference, between friction force a EPIL and FTAB are caused by friction forces from piston rings simulation and vertical force from cylinder head movement in opposite direction after FTDC included at FTAB joint. Total friction power loss is calculated like product of piston velocity and sum of friction forces in FTAB joint. In results are also visible big difference in total friction power loss and friction power loss only generate from piston. Friction power loss are used for calculation of FMEP values, but more about that topic will be described in next chapter.

3.8.2. EPU results - comparison basic and low friction ring package

In following figures results of basic and low friction force ring package for REVO model are shown. Results are displayed only for one operating point (3000rpm_15.5) and other results for different load cases at speed 3000 rpm are shown in Appendix E. Solid curves represents results with basic ring package, and dotted curves represents results with reduced tangential force package.

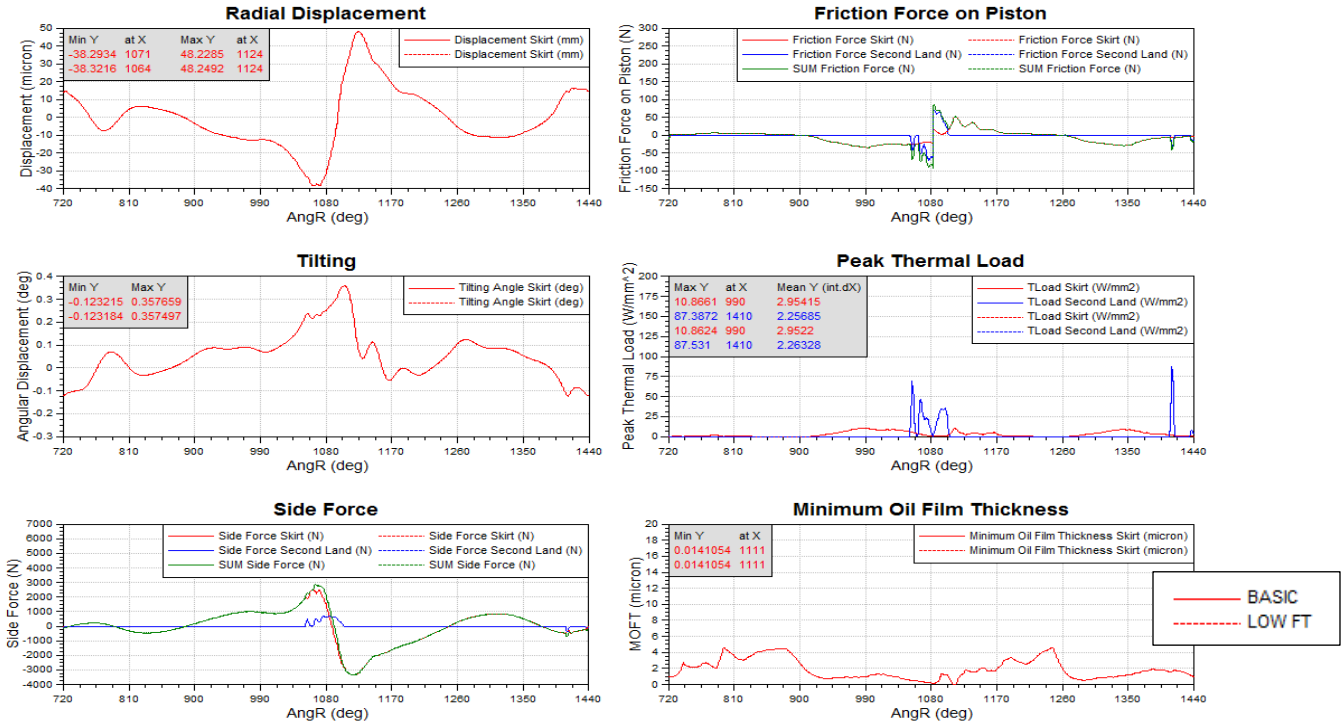

Figure 87. Comparison between basic and low friction ring package, REVO model, piston results overview – 3000_15.5.

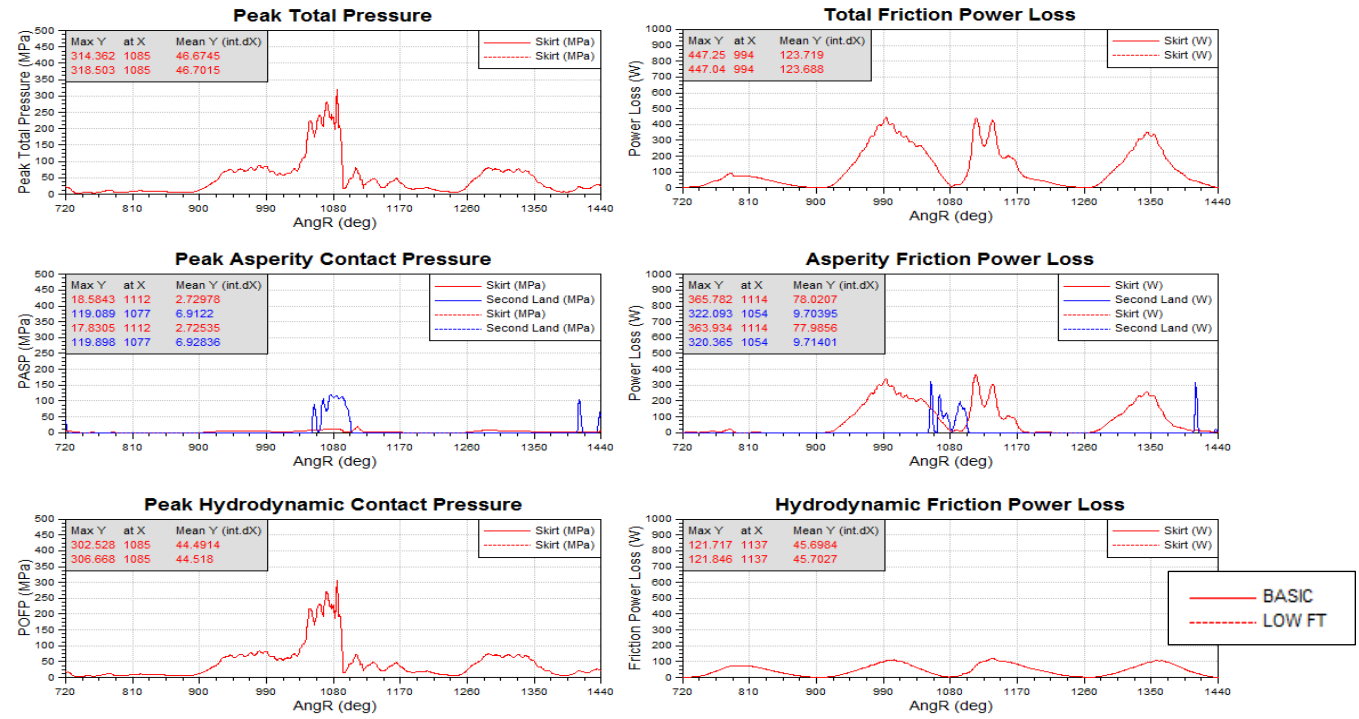

Figure 88. Comparison between basic and low friction ring package, REVO model, Pressure and friction results – 3000_15.5.

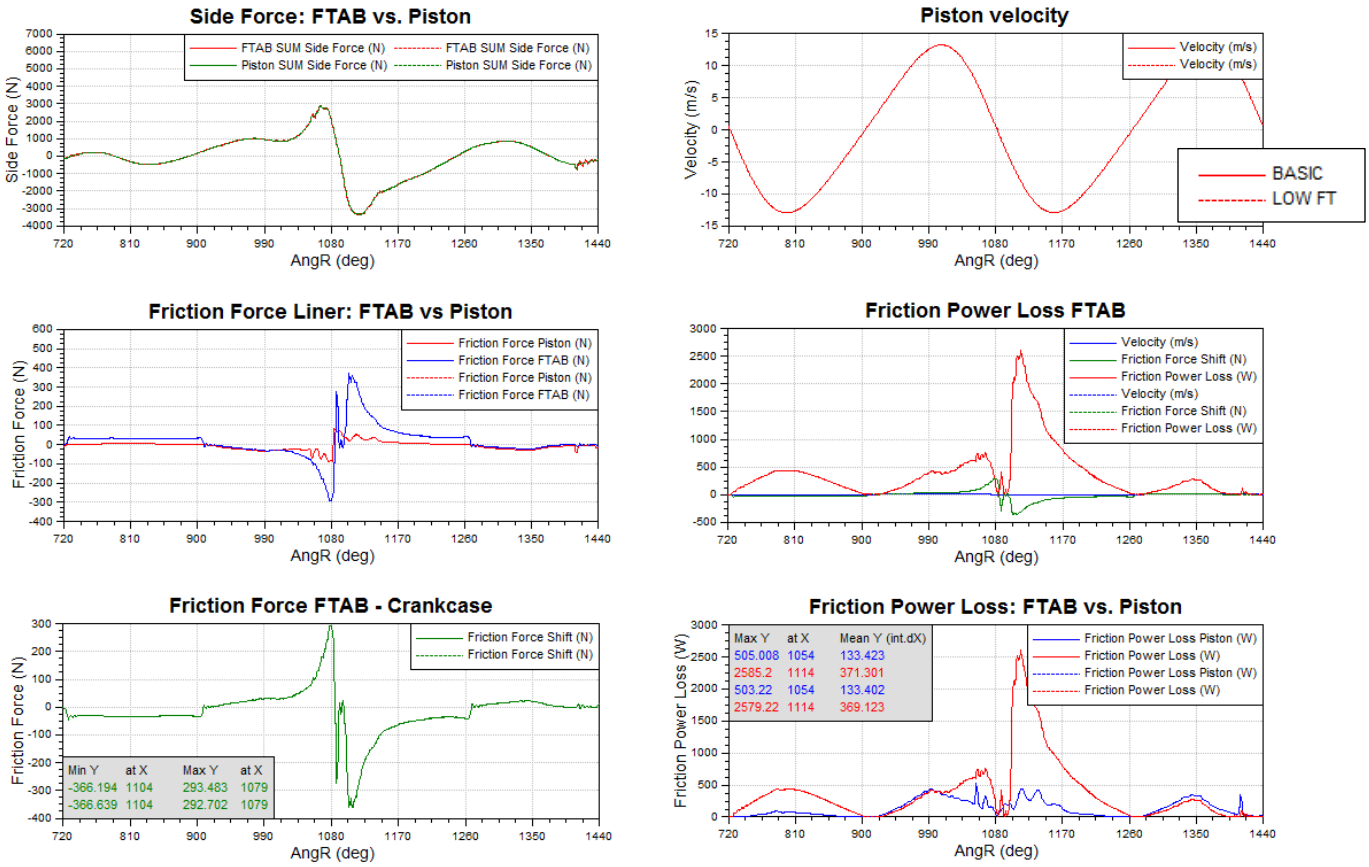

Figure 89. Comparison between basic and low friction ring package, REVO model, FTAB forces and friction power loss – 3000_15.5.

Results summary – comparison between basic and low friction ring package, REVO

In above figures, results of piston simulation models with basic ring package and low friction ring package connected with REVO jonits are displayed. There are no big differences between results of this models. Fricton and side force have the same trend line. Model with low friction ring package shows slightly lower values of total friction power loss, and piston friction power loss are the same. It can be concluded that this slightly lower values of total friction power loss are caused only by piston ring package.

3.8.3. EPU results – comparison between simplified and advanced model

In following figures results of simplified (REVO) and advanced (EHD) simulation models for basic ring package are shown. Results are shown only for one operating point (3000rpm_15.5) and other results for different load cases at speed 3000 rpm are shown in Appendix F. Solid curves represents REVO results, and dotted curves represents EHD results.

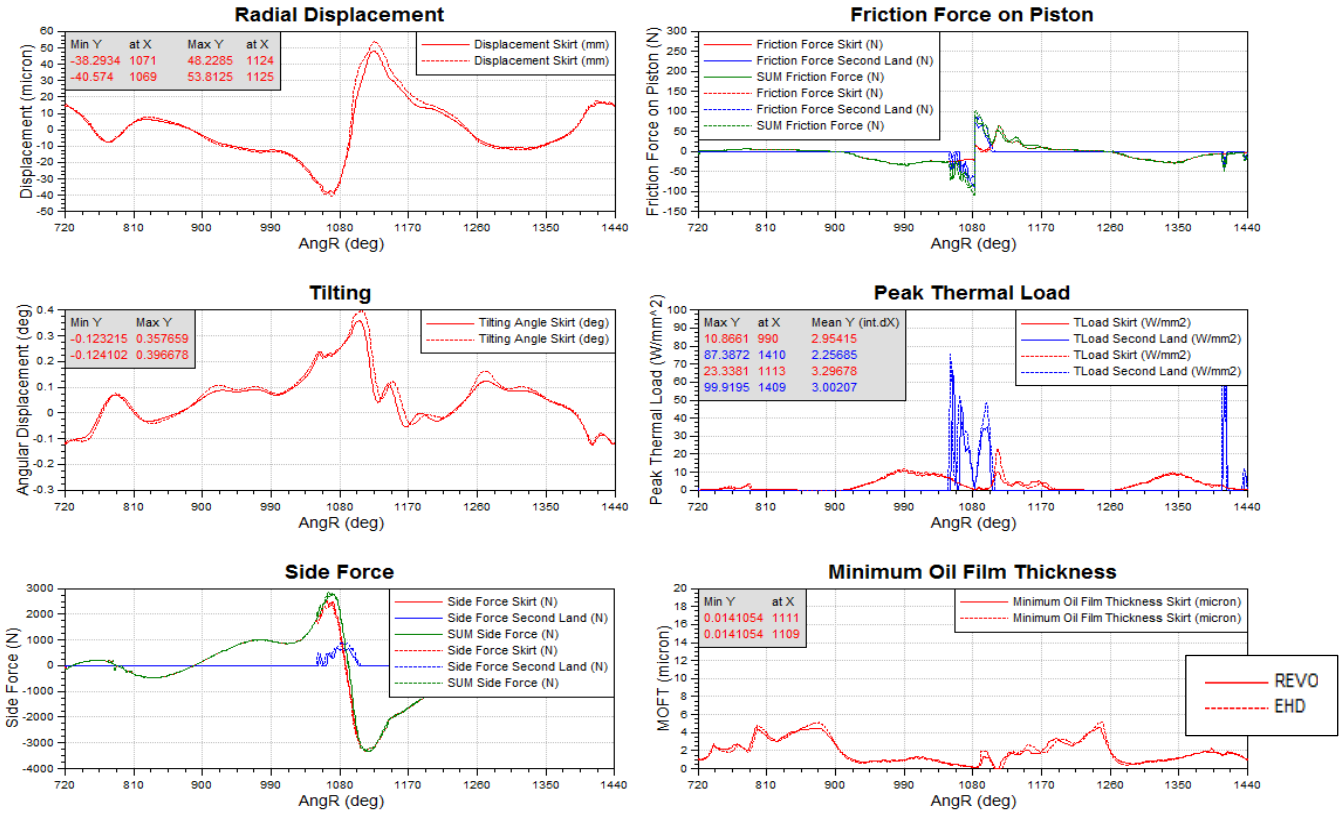

Figure 90. Comparison between REVO and EHD model, basic ring package, piston results overview – 3000_15.5.

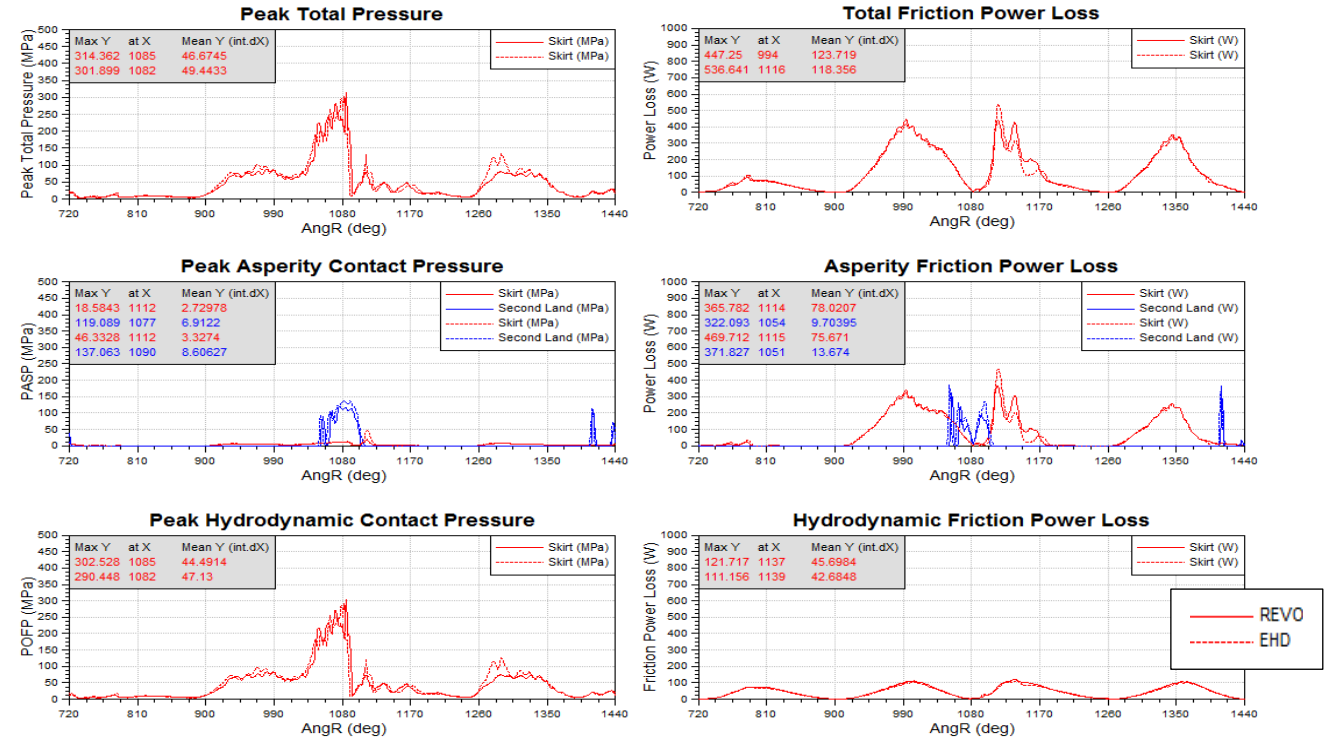

Figure 91. Comparison between REVO and EHD model, basic ring package, pressure and friction results – 3000_15.5.

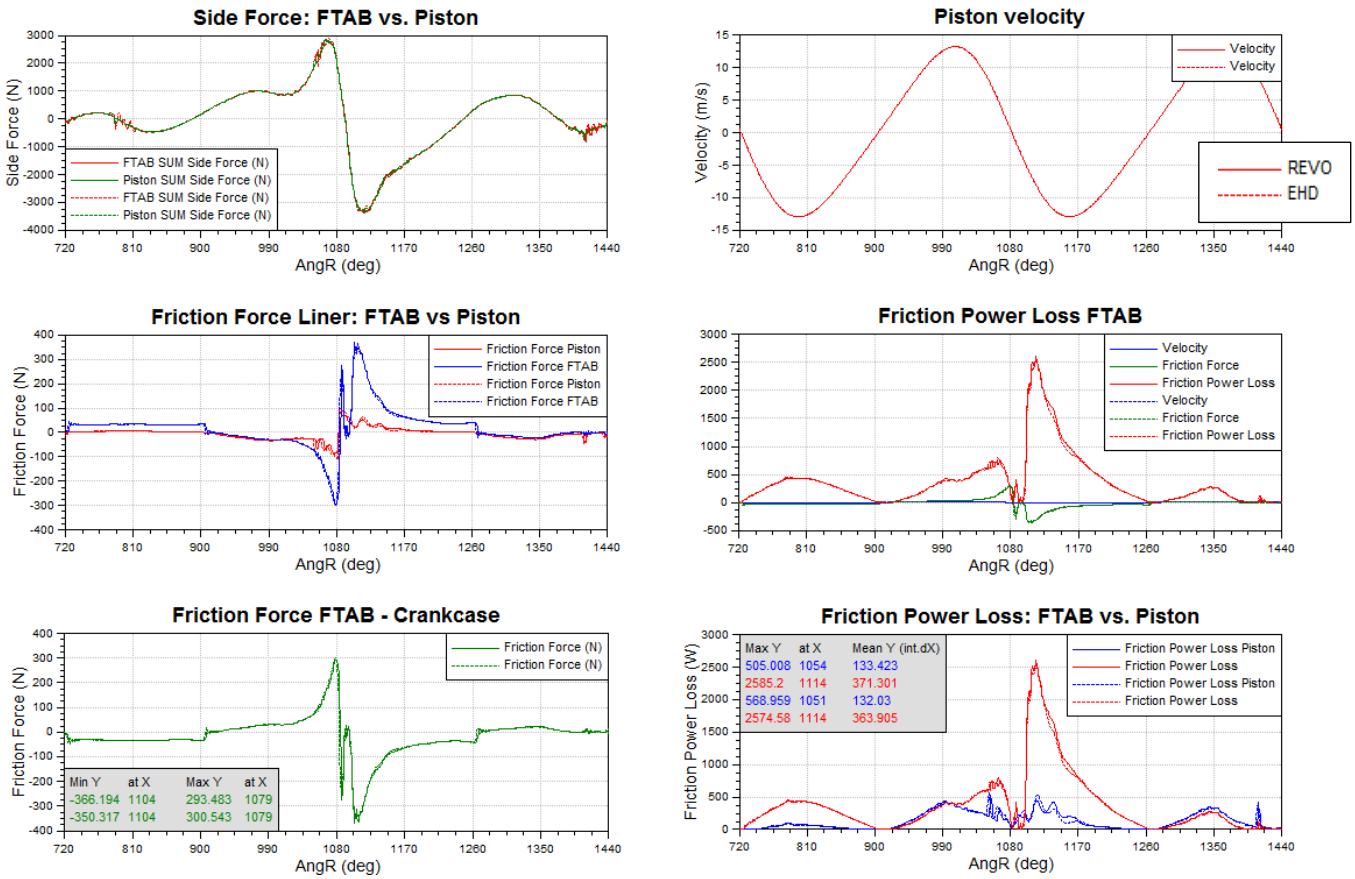

Figure 92. Comparison between REVO and EHD model, basic ring package, FTAB forces and friction power loss – 3000_15.5.

Results summary – comparison between REVO and EHD model, Basic ring package

In above figures, results of piston simulation of models with REVO joints and EHD joints are displayed. There are no big differences between results of this models. Some differences are visible in tilting where EHD model has higher peak of tilting angle and radial displacement than REVO model. Reason of that is caused by different stiffness and damping behavior in joints. Also, is visible that REVO model have slightly lower value of friction power loss, so FMEP values will be also lower in that case.

3.8.4. "Stick slip effect"

In above results is visible that friction force changes direction around FTDC. Friction force signal depends on ignition pressure and on friction of the FRISC sealring. Lubrication on FRISC sealring reduces friction force peak values. In this case, this phenomenom of changing direction is so called "stick slip effect" of sealring and marked at Figure 93.

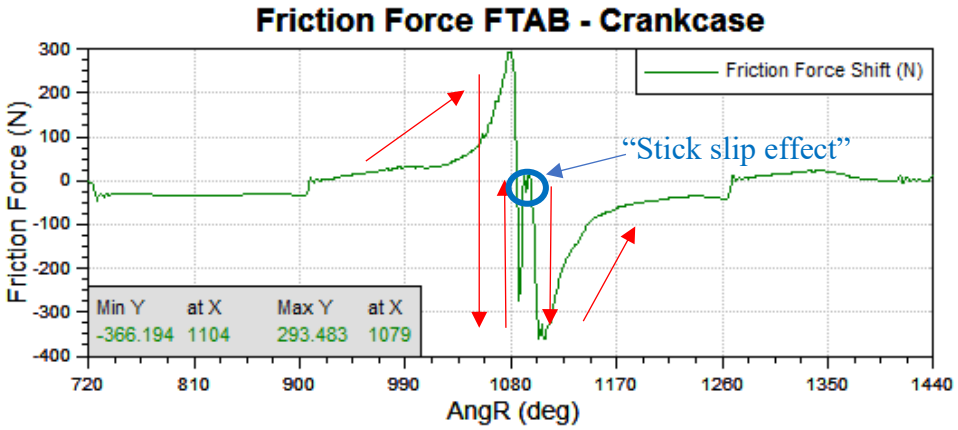

Figure 93. Position of "stick slip effect".

Stick slip effect can be described as surfaces alternating between sticking to each other and sliding over each other, with a corresponding change in the force of friction. Typically, the static friction coefficient (a heuristic number) between two surfaces is larger than the kinetic friction coefficient. If an applied force is large enough to overcome the static friction, then the reduction of the friction to the kinetic friction can cause a sudden jump in the velocity of the movement [27]. Stick-slip causes a single impulse or a series of impulses which will excite surrounding structures to respond with resonance vibrations. Stick-slip behaviour depends on surface topography and on the elastic and plastic properties of the sliding materials [28].

Effect on Stick slip of sealring is primary caused by cylinder head movement upwards. This movement is based on elongation of cylinder head bolts and bending of cylinder head. This thesis will be observed influence on that cylinder head movement on friction. In that case, validation of model with measurement should be done. Results of cylinder head movement of full REVO model will be compared with simplified EXCITE model and MATLAB Simulink model. Simplified EXCITE model and MATLAB Simulink model are dynamic systems with one degree of freedom (vertical axis). This model has one mass, which represent mass of cylinder head, one spring (stiffness of cylinder head bolts) and one damper (damping coefficient of cylinder head bolts). On Figure 94., MATLAB Simulink model are presented and on Figure 95. is simplified EXCITE model. Full REVO model is shown at Figure 73. Load are implemented on cylinder head and values are given in time domain. Load curves are shown on Figure 77.

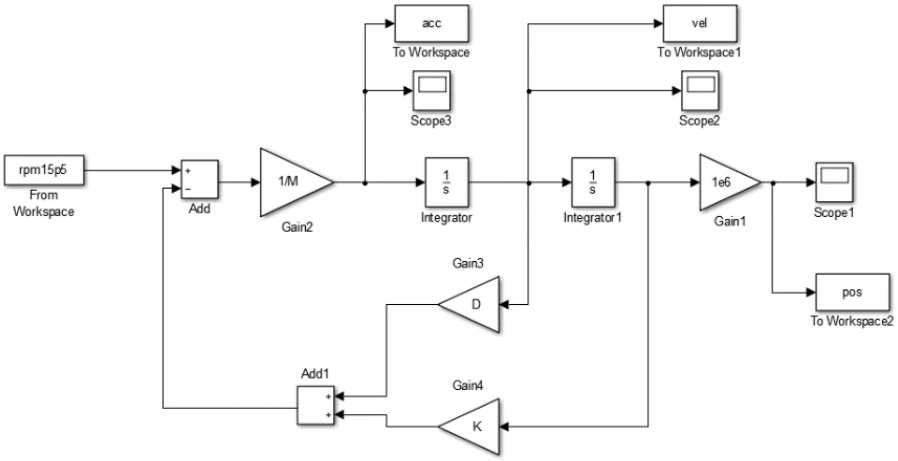

Figure 94. Simulink model.

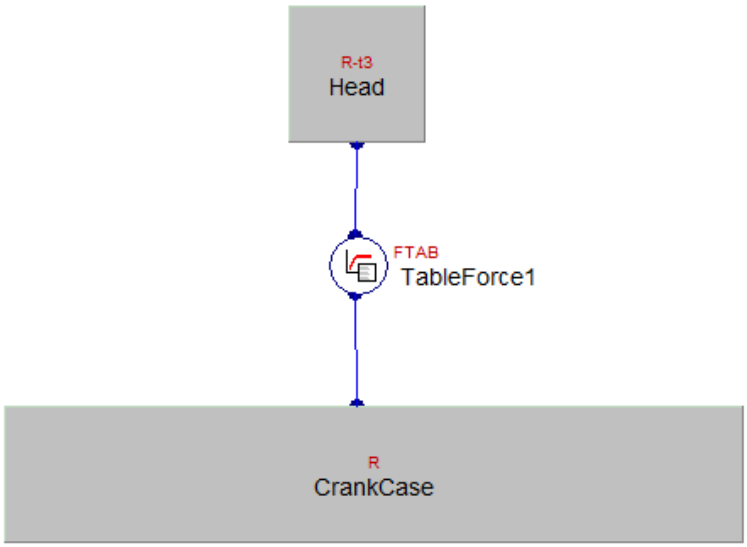

Figure 95. Simplified EXCITE model.

In following figures, comparison between Simulink, simplified EXCITE and full REVO model are shown. On following figures, cylinder head displacement, velocity and acceleration are presented for two operating points.

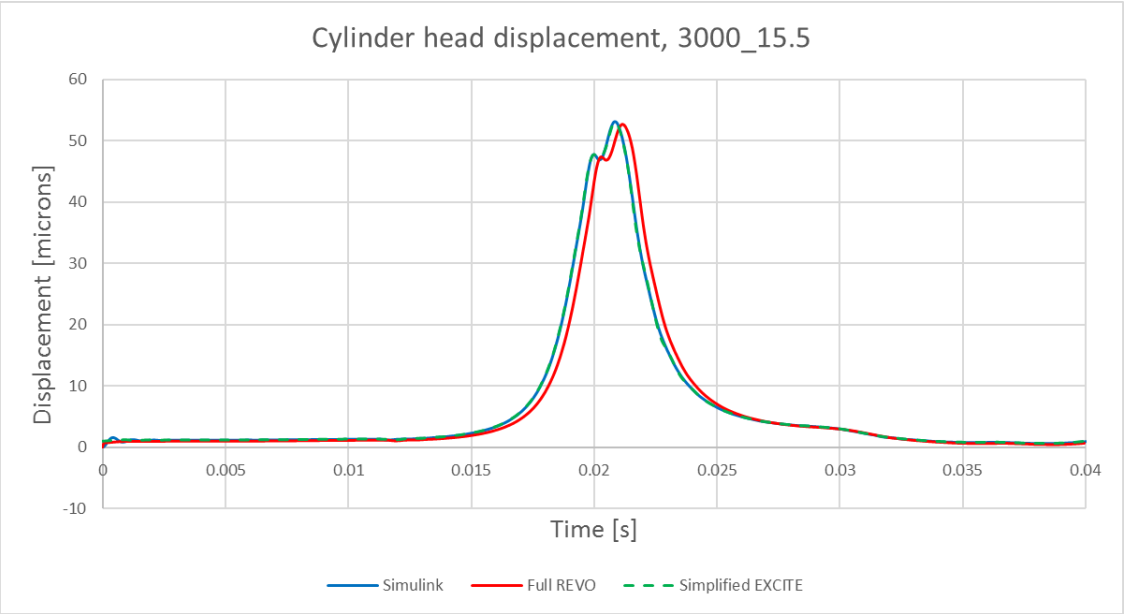

Figure 96. Cylinder head displacement, 3000rpm15.5.

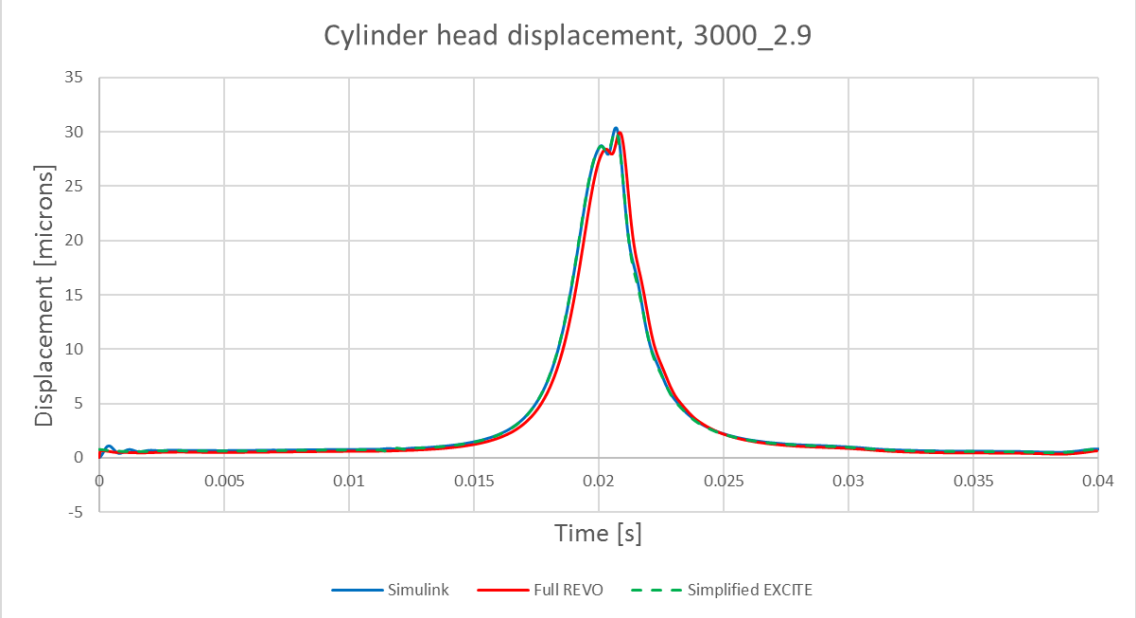

Figure 97. Cylinder head displacement, 3000rpm2.9.

Peak of cylinder head displacement is the same for al models. There is visible that full model has shifted curves for both cases. Reason of that is that full REVO model has implemented sealring into model and applied normal force on sealring which caused this shift. Also, it can be seen that shift is lower if is load lower. It can be concluded that shift doesn't have big influence on results of cylinder head displacement and full REVO model is validated.

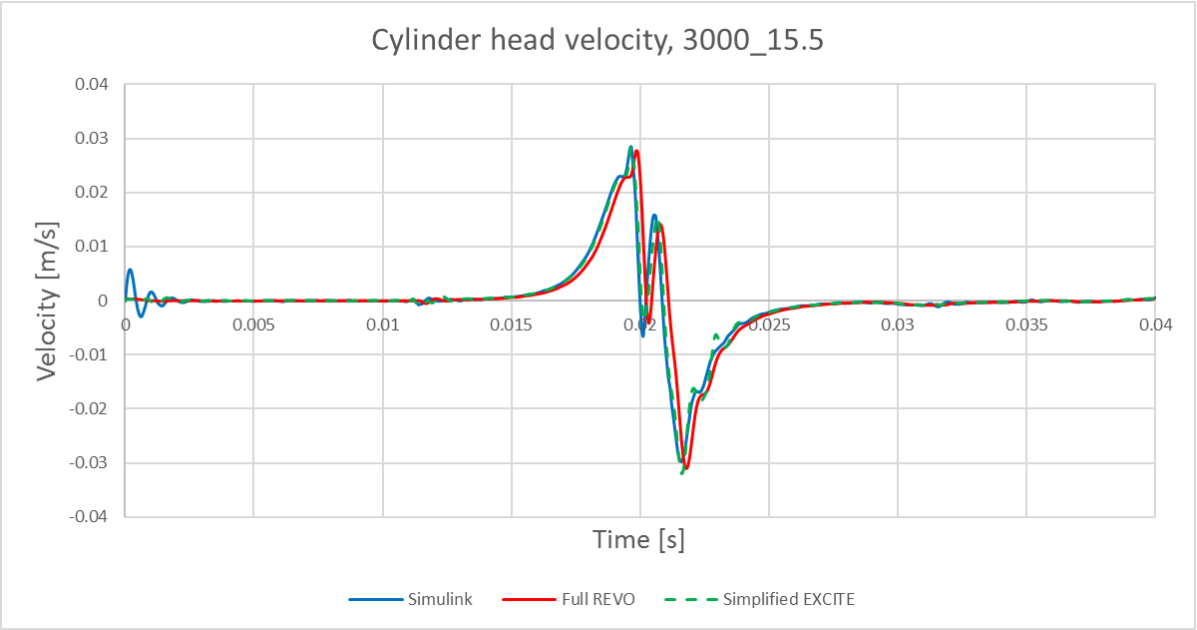

Figure 98. Cylinder head velocity, 3000rpm15.5.

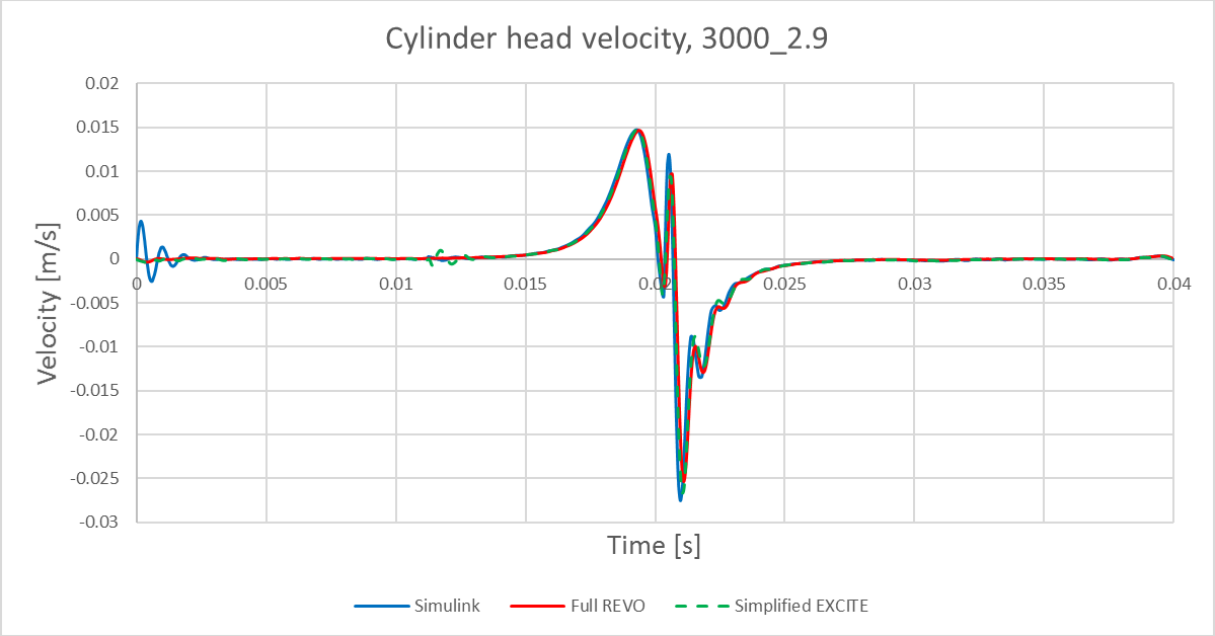

Figure 99. Cylinder head velocity, 3000rpm2.9.

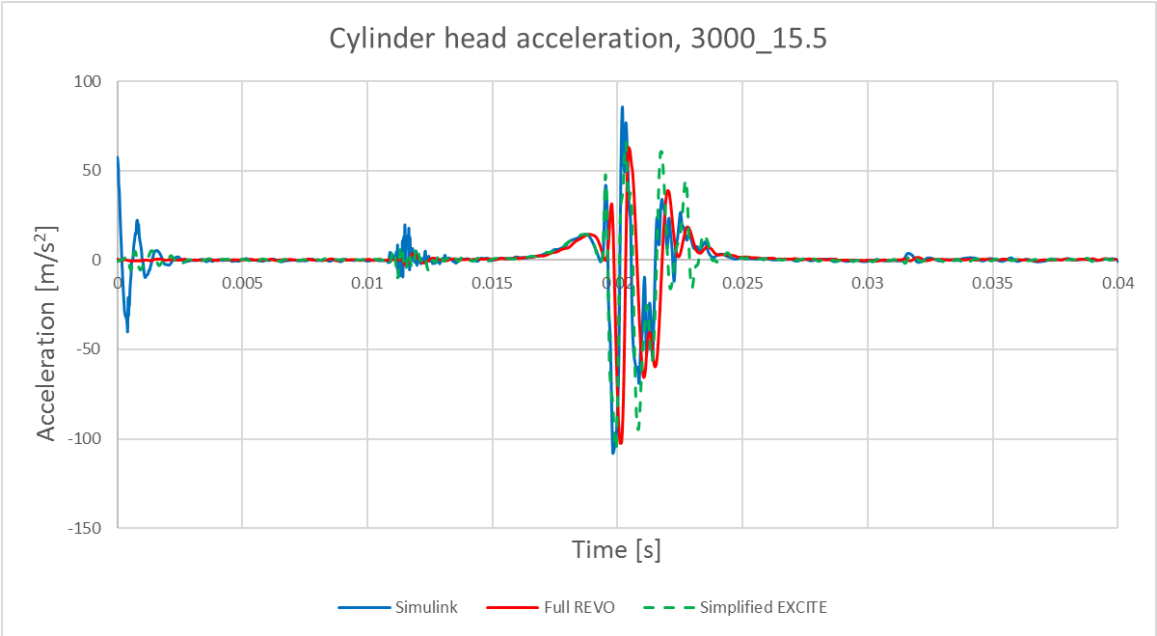

Figure 100. Cylinder head acceleration, 3000rpm15.5

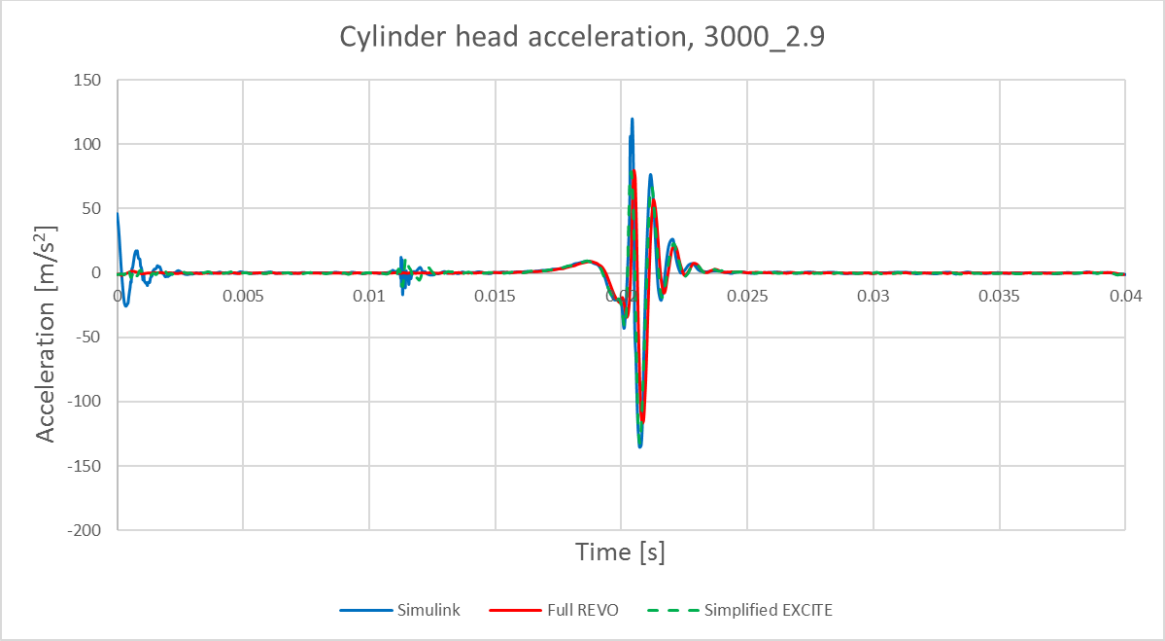

Figure 101. Cylinder head acceleration, 3000rpm2.9

Above figures presents cylinder head velocity and acceleration. Shift of full REVO model curves are also presented like in cylinder head displacement. Except that shift, visible is that Simulink curves have higher values of acceleration peak points on lower operating point. The biggest differences can be seen on cylinder head acceleration for full load at speed 3000 rpm.

4. CORRELATION BETWEEN MEASUREMENT AND SIMULATION

In this chapter, correlation between measurement on FRISC and results from simulation are shown. Values of friction forces, side force, FMEP, LOC and blow-by are correlated. Results are presented for basic and low friction ring package.

In EXCITE™ Piston&Ring simulaton, FMEP and friction power loss values of each ring are calculated. Piston simulation in EXCITE™ Power Unit represent only values of friction power loss, so FMEP values has to be calculated. Equation (11) described the method of calculating FMEP from friction power loss values.

$$FMEP = \frac{FPL \cdot 60}{0{,}5 \cdot n \cdot V_{\mathrm{H}}} \ [\mathrm{Pa}], \tag{11}$$

where: FPL is Friction Power Loss [W], n is engine speed [rpm] and V_{H} is cylinder volume [m^3]

Side force is force which act lateral on liner wall. This force is generated from lateral up and down movement of the piston in the liner. This force depends on inertia force (oscillating masses), load force (generated from cylinder pressure) and offsets (piston pin, crankshaft offset). Side force can be calculated analytical, so results of side force given in simulation and measurement will be compared with analytical side force. In equations (12) are presented method of calculating analytically side force.

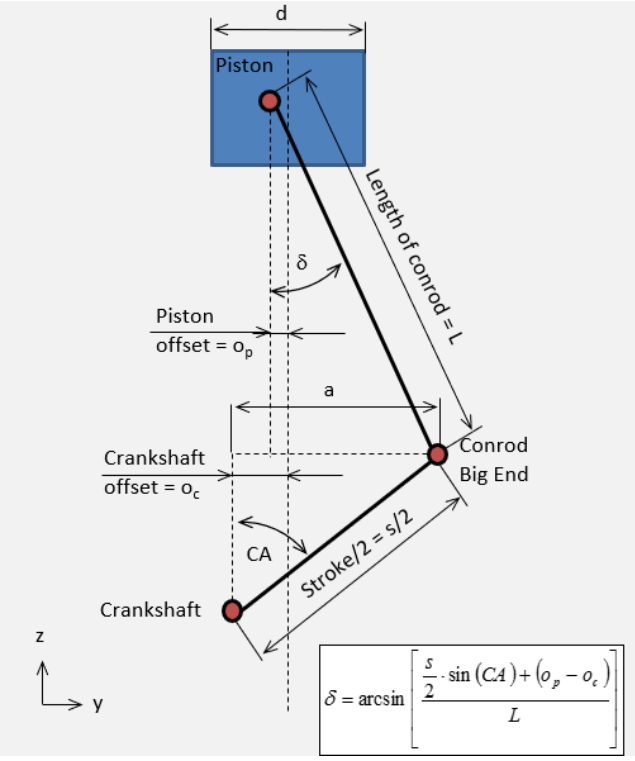

Figure 102. Dimensions necessary for calculation side force.

Side force is calculated like component of difference between cylinder pressure force and oscillating inertia force.

$$F_y = (F - F_{iner}) \cdot \tan(\delta) \ [\mathrm{N}], \tag{12}$$

Where, F is cylinder pressure force [N], F_{iner} is oscilating inertia force [N] and δ is shifted angle [deg].

Cylinder pressure force is calculated like:

$$F = \frac{D^2 \cdot \pi}{4} \cdot p(\alpha) \ [\mathrm{N}], \tag{13}$$

where, D is cyliner bore [m] and $p(\alpha)$ is cylinder pressure [Pa].

Inertia force caused from oscillating masses is calculated like:

$$F_{iner} = m_{osc} \cdot a \ [\mathrm{N}], \tag{14}$$

where, m_{osc} is oscilating mass [kg] and a is piston accelereation [m/s^2].

Piston acceleration is calculated like:

$$a = \omega^2 \cdot \frac{s}{2} \cdot \left[\cos(\alpha) + \frac{\cos(2\alpha) \cdot \frac{s}{2}}{L} \right] \ [m/s^2], \tag{15}$$

where ω is engine speed [rad/s], s is stroke [m] and L is conrod length [m].

Shifted angle is calculated like:

$$\delta = \arcsin \cdot \left[\frac{\frac{s}{2} \cdot \sin(\alpha) + (o_p - o_c)}{L} \right] \ [\mathrm{deg}], \tag{16}$$

where, s is stroke [m], L is conrod length [m], o_c is piston pin offset [m] and o_p = crankshaft offset [m].

4.1. Blow-by and LOC results

In Table 8., results of blow-by are shown. Those results are calculated from Piston & ring module for basic and low friction package and for different simulation solver (2D or 3D).

Table 8. Blow-by results.

	SIMULATION				MEASUERMENT	
Blow by	BASIC		LOW FT		BASIC	LOW FT
CASE	2D	3D	2D	3D		
3000/15,5	6.27	11.46	6.35	11.46	6.70	10.95
3000/9,3	6.05	11.09	6.11	11.13	6.41	6.55
3000/5,3	5.90	10.96	5.90	10.95	6.11	6.82
3000/2,9	5.47	9.00	5.39	8.90	5.77	6.83
2500/15,4	7.51	12.41	7.47	12.42	7.67	9.99
2500/9,2	7.56	13.57	7.51	14.31	7.50	8.03
2500/2,8	5.09	8.42	5.17	8.41	5.40	7.09
2000/15,2	8.50	68.02	9.87	69.72	11.36	13.48
2000/8,6	10.63	12.67	6.95	12.77	10.29	12.86
2000/2,7	5.98	9.34	5.63	9.19	8.06	8.17
1500/14,8	9.69	54.25	9.03	55.52	9.08	8.11
1500/8,8	5.32	39.39	8.54	40.74	6.57	10.31
1500/4,7	4.30	30.66	4.15	31.16	5.13	6.22
1500/2,3	3.30	30.66	8.02	24.05	4.38	4.61

In Figure 103., results of camparison between measurement and simulation for basic ring package with different simulation solver are shown.

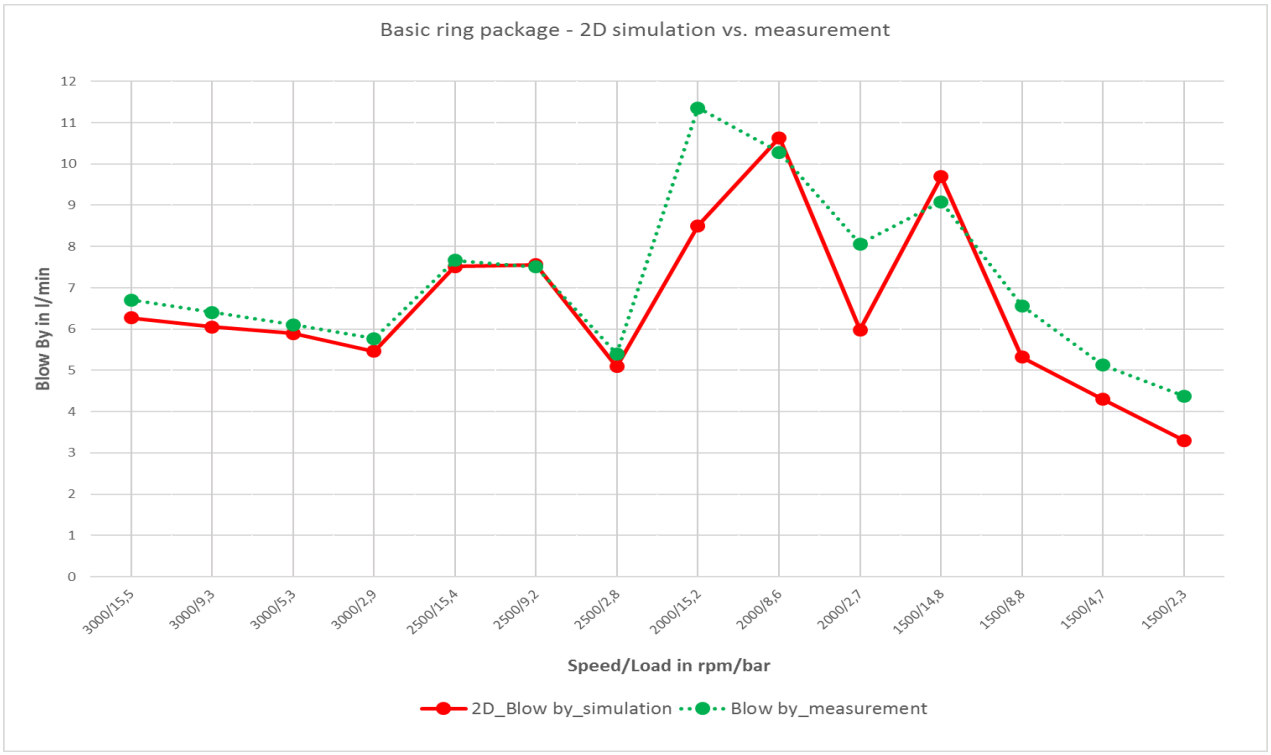

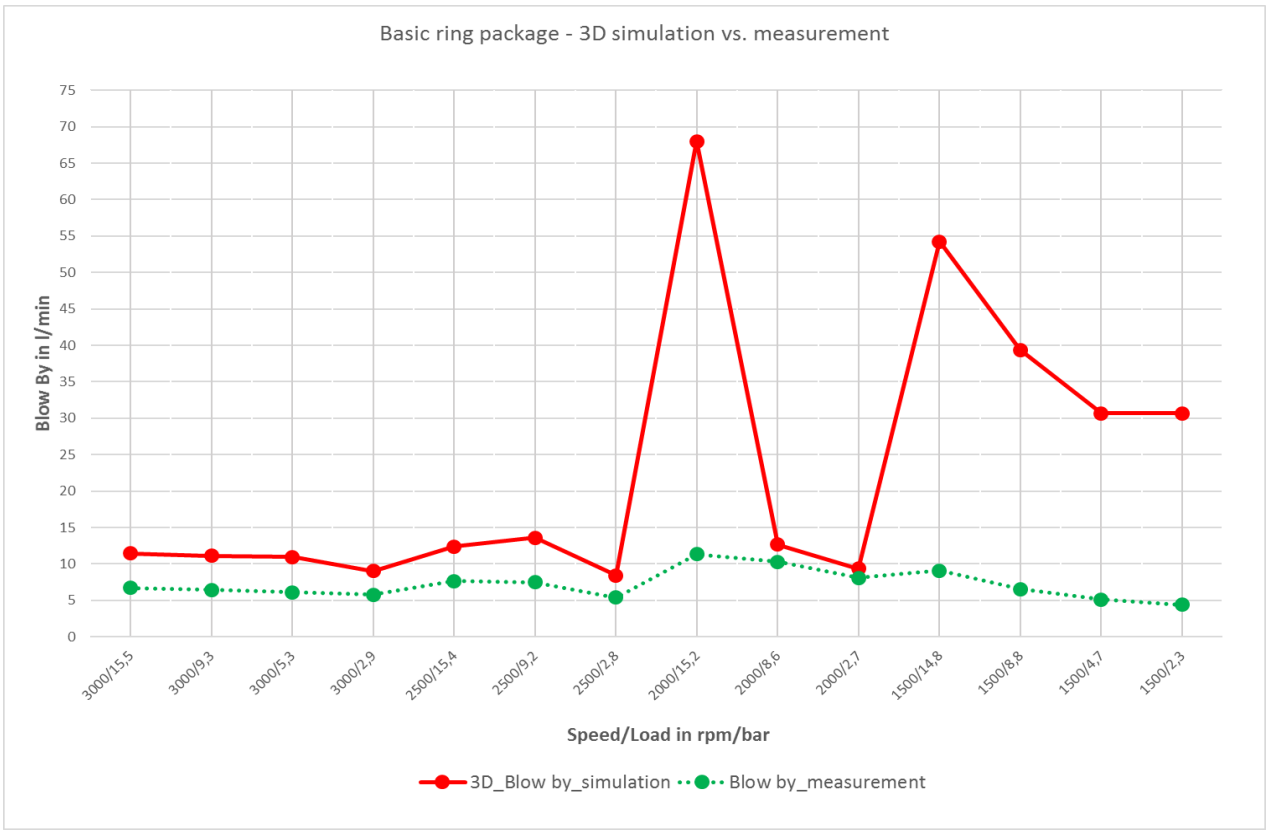

Figure 103. Comparison blow-by between measurement and simulation for basic ring package.

In Figure 104., results of camparison between measurement and simulation for low friction ring package with different simulation solver are shown.

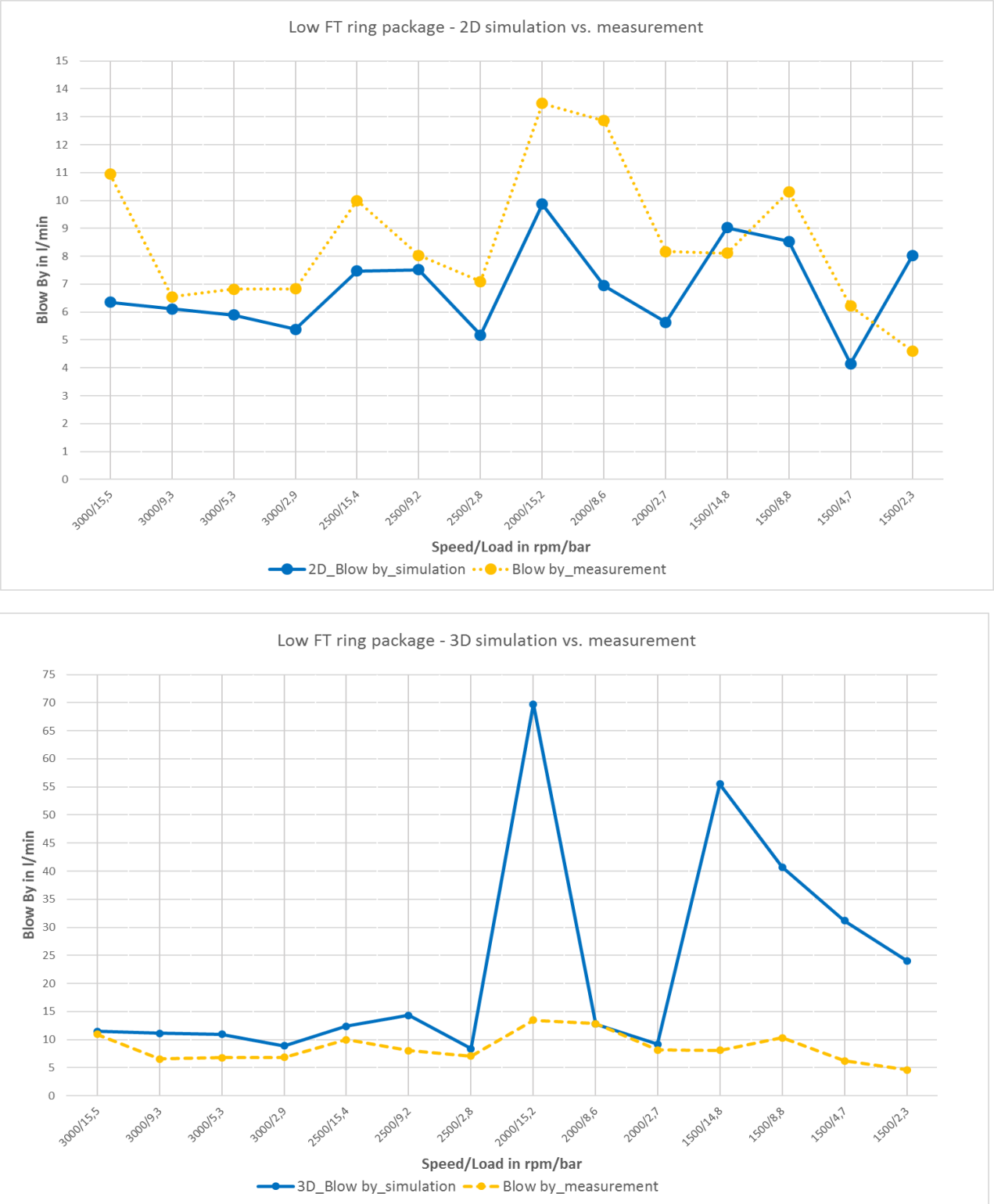

Figure 104. Comparison blow-by between measurement and simulation for low friction ring package.

In Figure 105., results of camparison between simulation results for basic and low friction ring package with different simulation solvers are shown.

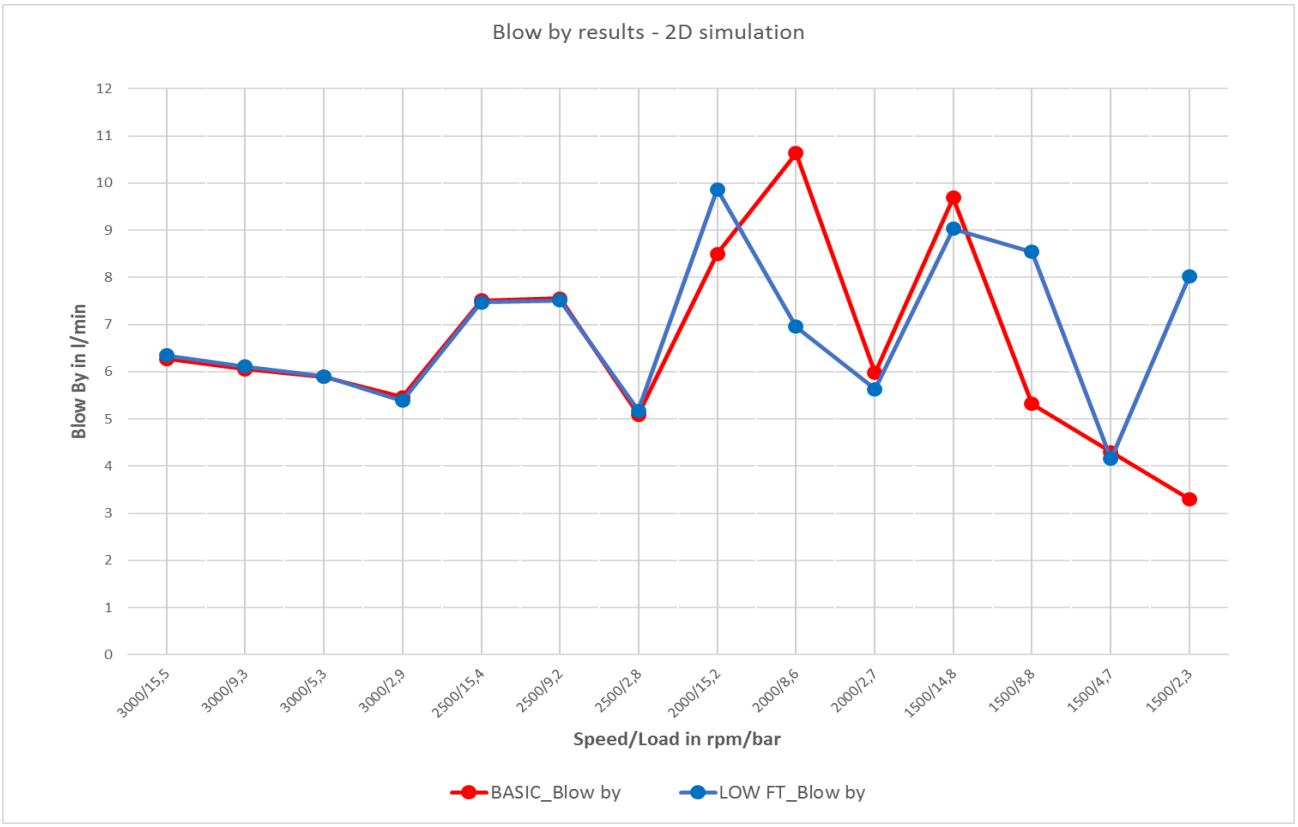

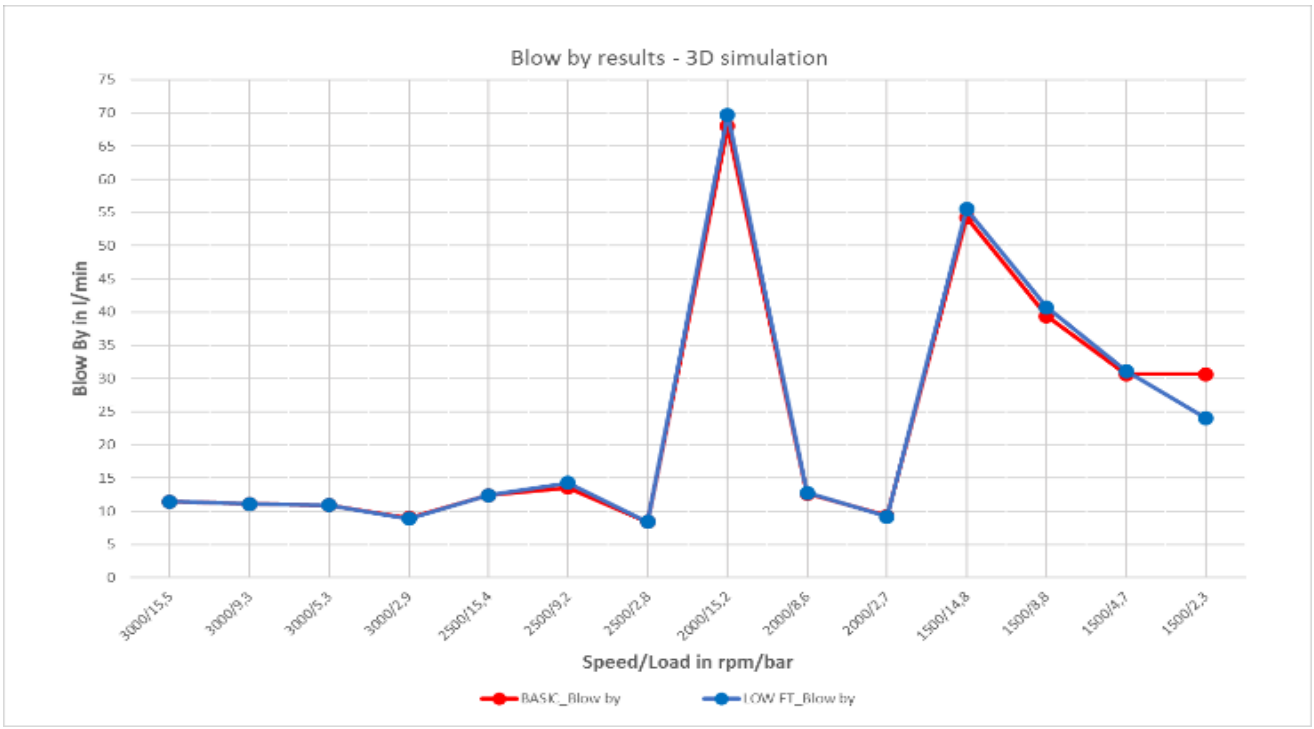

Figure 105. Comparison blow-by simulation results between basicand low friction ring package.

In Table 9., results of LOC are shown. Those results are calculated from Piston & ring module for basic and low friction package

Table 9. LOC results.

CASE	2D_BASIC	2D_LOW FT	Measurement_B	Measurement_L
1500/2,3	0.27	0.27	0.51	0.42
1500/4,7	0.37	0.37	0.47	0.36
1500/8,8	0.63	0.63	0.55	0.30
1500/14,8	0.79	0.78	0.99	0.79
2000/2,7	0.31	0.31	0.43	0.34
2000/8,6	0.54	0.54	0.56	0.35
2000/15,2	0.83	0.83	0.80	0.57
2500/2,8	0.42	0.42	0.61	1.49
2500/9,2	0.74	0.75	1.36	1.93
2500/15,4	1.02	1.02	1.58	2.25
3000/2,9	0.53	0.53	0.63	0.85
3000/5,3	0.67	0.68	1.04	1.31
3000/9,3	0.79	0.79	1.13	1.40
3000/15,5	1.26	1.26	1.21	2.27

In Figure 106., results of comparison between measurement and simulation for basic and low friction ring package are shown.

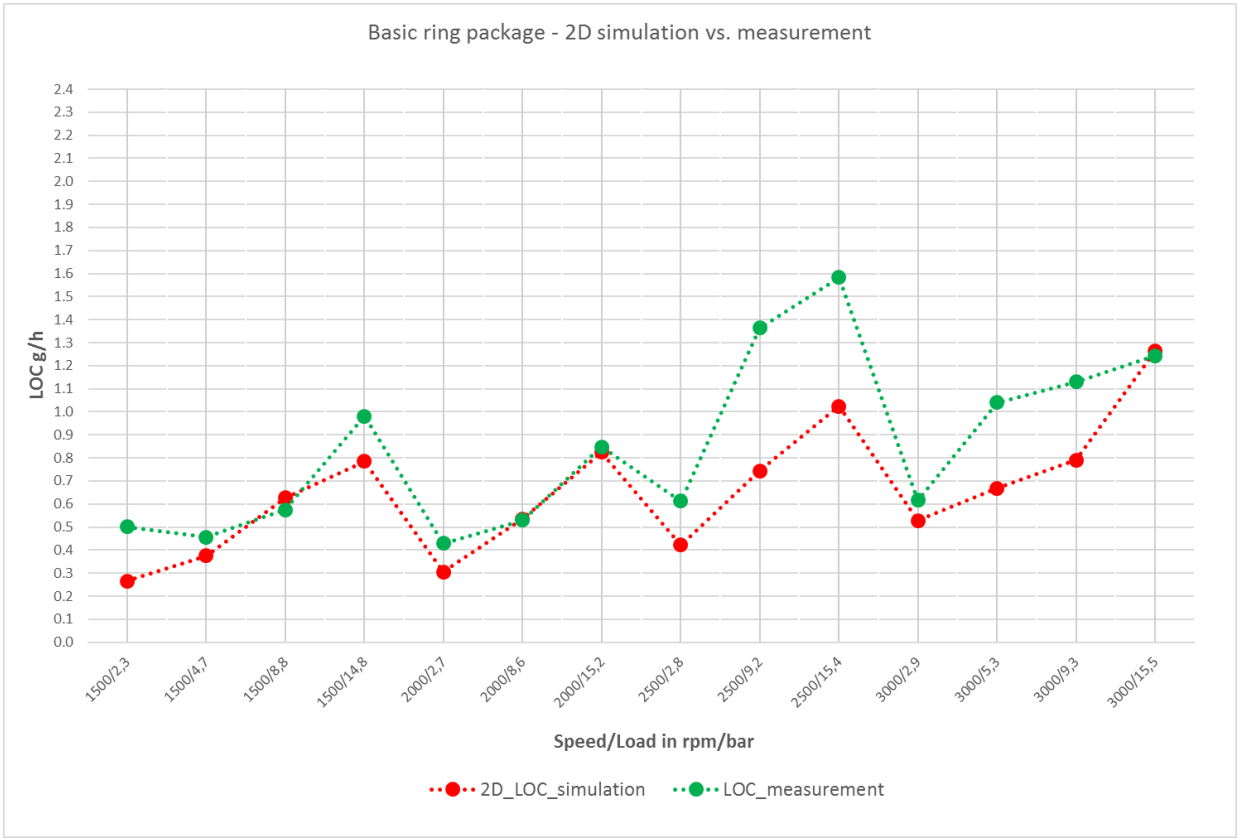

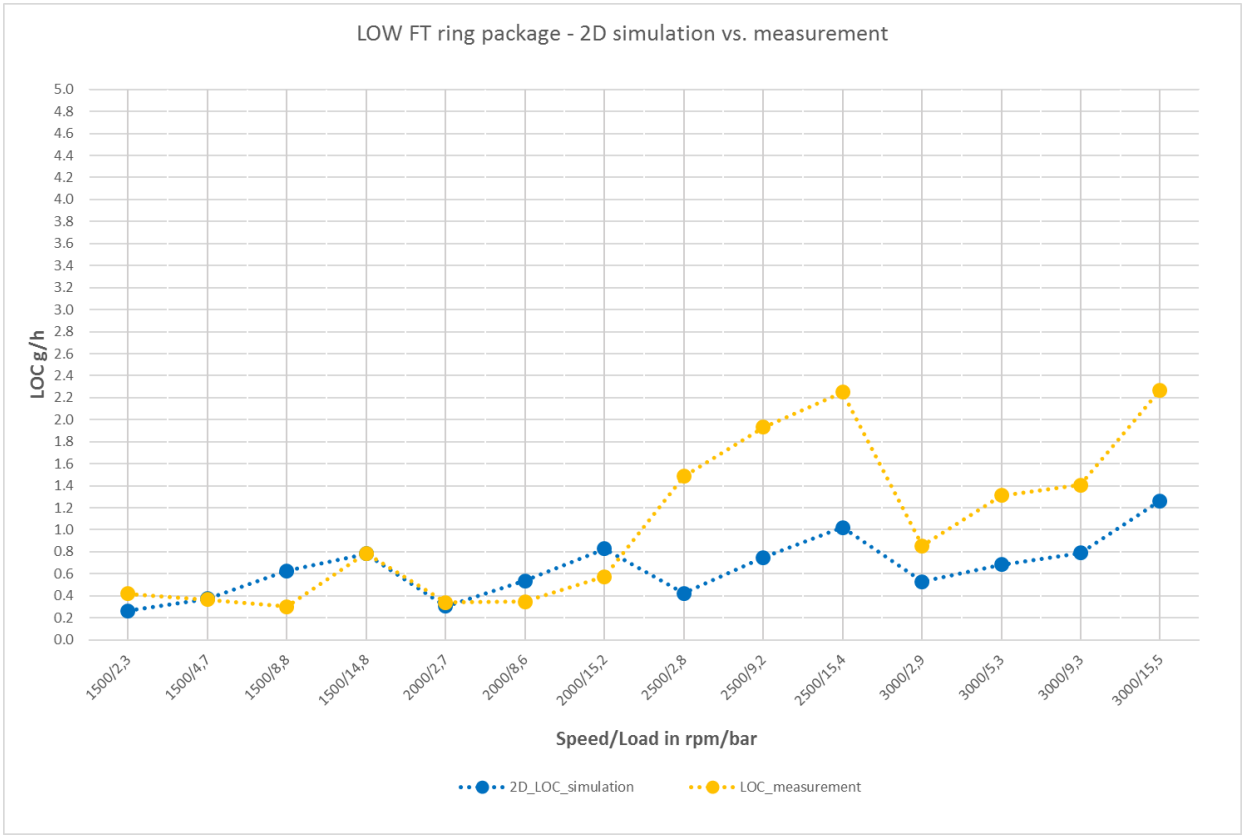

Figure 106. Comparison of LOC results between measurement and simulation for basic and low friction ring package.

Results summary – LOC and blow-by

In above figures and tables, blow-by and LOC results are presented. Simulation model with basic ring package and calculated with 2D solver is calibrated to measurement. Exceptions can be seen on lower speed and on speed 2000 rpm with full load where is measured the biggest blow-by. There are not big differences between 2D simulation models with basic and low friction ring package. Low friction ring package shows slightly higher blow-by compared to basic ring package and bigger differences regarding to measurement. Between 2D and 3D simulation solver big differences are presented. Also, on lower speed (1500rpm) in simulation with 3D solver piston ring end shut occurs and that lead to significant increase of blow-by value. The reason of that effect in 3D simulation are not further evaluated. Lube oil consumption results are not fully calibrated because thermodynamic data are taken from older similar project and all cases have the same thermodynamic data. It can be seen that at lower speeds (1500 and 2000 rpm) are the smaller LOC differences in simulation with basic ring package and measurement.

4.2. Friction and side forces

In this chapter, correlation of friction and side forces between simulation and measurement are described. Friction force results are presented for basic and low friction ring package for simplified (REVO) and advanced (EHD) models. Measurement and simulation side forces are compared with analytical calculated side forces and they are presented only for simplified model with basic ring package. Reason of that is because side force only depends on engine design, cylinder pressure and oscillating mases and in all other cases (advanced model, low friction ring package) those parameters are the same. Results are presented only for engine speed 3000rpm for all load cases. At appendix G, friction forces with basic ring package are shown and at appendix H friction forces with low friction ring package are shown for other laod cases. Side forces for other load cases are shown at appendix I.

Friction forces with basic ring package

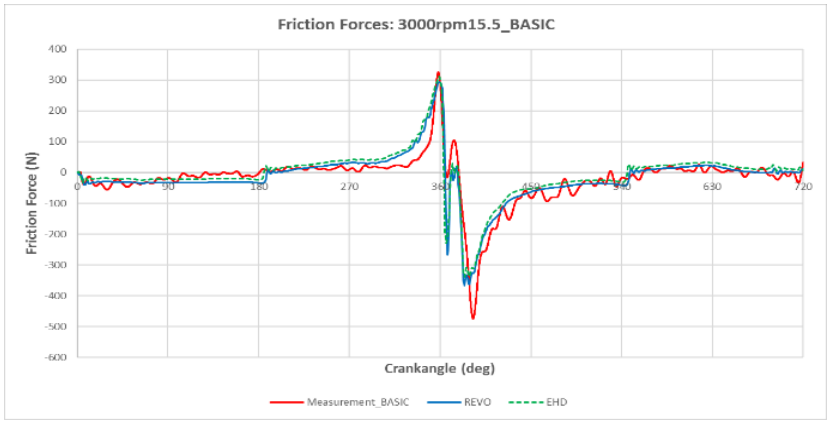

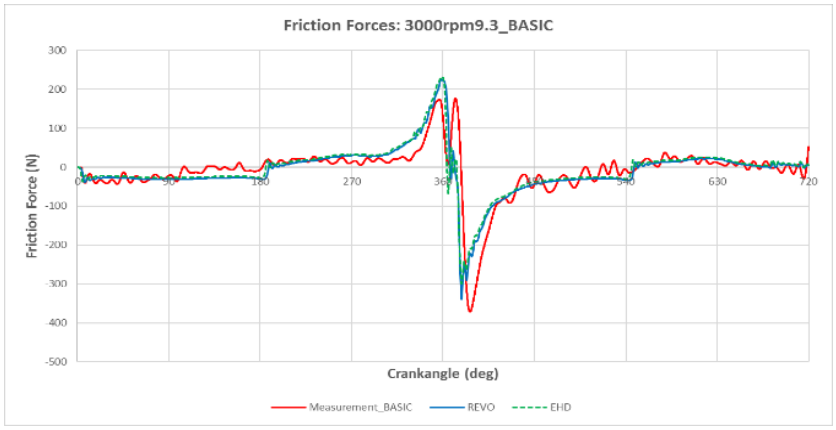

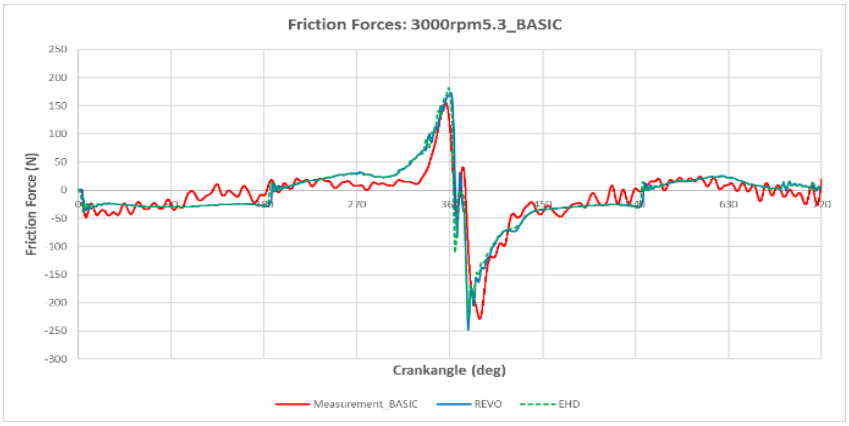

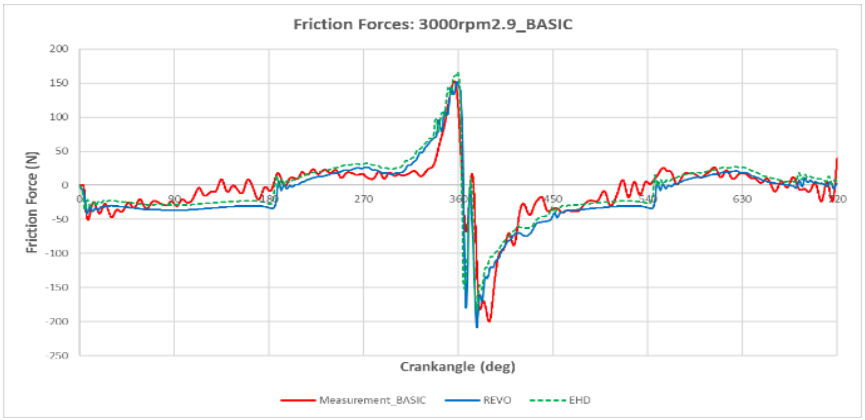

Figure 107. Comparison of friction forces, basic ring package, 3000rpm.

Friction forces with low friction package

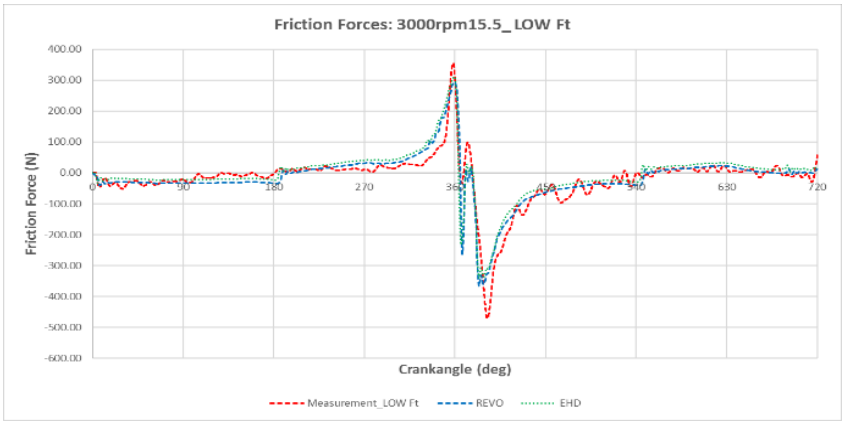

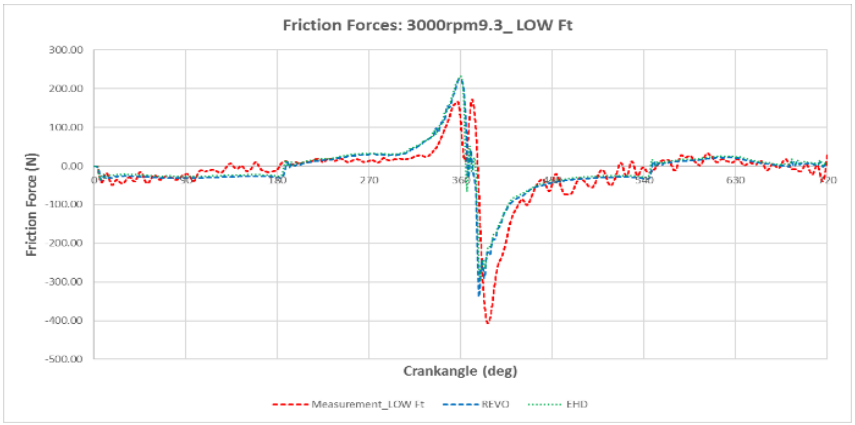

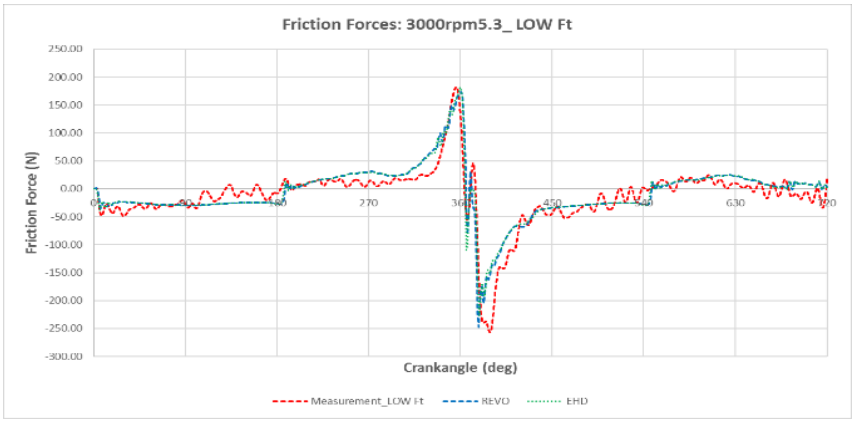

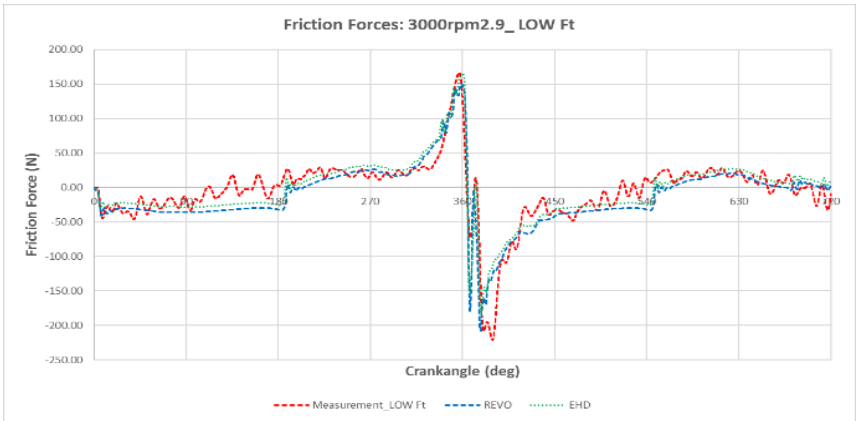

Figure 108. Comparison of friction forces, low friction ring package, 3000rpm.

Side forces with basic ring package

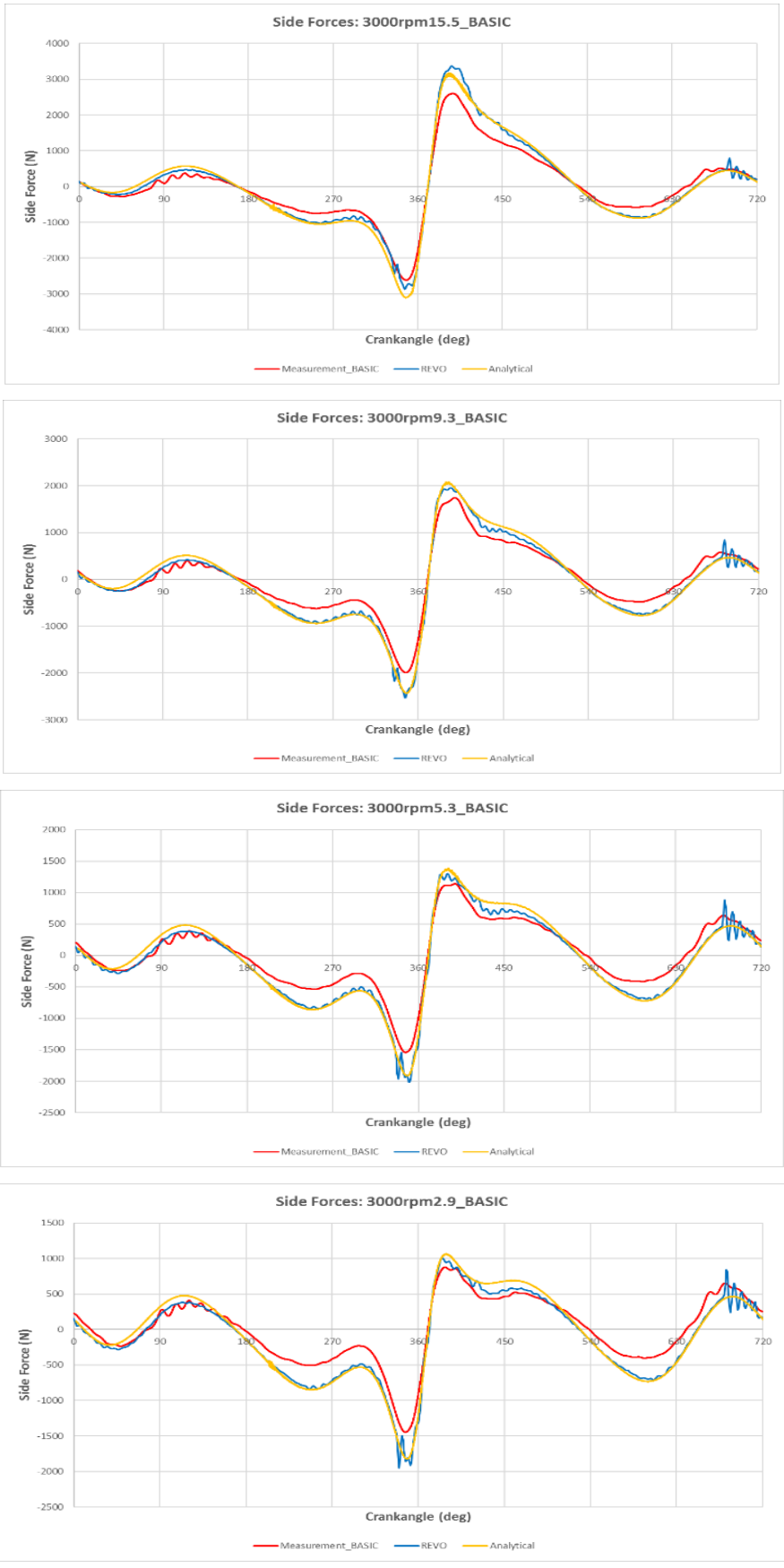

Figure 109. Comparison of side forces, basic ring package, 3000rpm.

Results summary – friction and side forces

In above figures, friction and side forces are presented. Friction force calculated in REVO model have similar behavior like friction forces given from measurement. Second peak after FTDC, caused by cylinder head movement, is visible in simulation results. There are differences in peak values between simulation and measurement results. Friction forces calculated from EHD model have the same trend line as forces calculated with REVO model. Peak values of EHD model are slightly higher than forces given from REVO simulation model. Friction forces calculated with basic and low friction package are very similar. Analiticaly calcualted side forces have same trend line compared to simulation. Only minor differences in peak values are visible. Differences are caused by piston dynamic beahviour in simultion model. Measured side forces have big differences compared to simulation or analitical side forces. Reason of that behavior is not further investigated.

4.3. Friction mean effective pressure (FMEP)

In this chapter, the correlation of FMEP between simulation and measurement are described. FMEP results are presented with basic and low friction ring package for simplified (REVO) and advanced (EHD) models. Except FMEP values, friction power loss (FPL) is also displayed. In Table 10, comparison between measurement and REVO model with basic ring package is shown.

Table 10. Comparison between measurement and REVO model with basic ring package.

REVO_BASIC ring package									
CASE	n (rpm)	FPL SUM (W)	FPL Piston (W)	FPL Piston Rings (W)	FPL Cylinder Head (W)	Total FMEP (Pa)	Total FMEP (bar)	Measurement (bar)	Difference
3000rpm_15p5	3000	371.3	133.4	153.3	84.6	40141	0.401	0.409	-2%
3000rpm_9p3	3000	301.2	111.5	130.8	58.9	32565	0.326	0.310	-6%
3000rpm_5p3	3000	265.2	105.0	119.9	40.2	28669	0.287	0.261	-12%
3000rpm_2p9	3000	265.5	105.6	124.4	35.5	28704	0.287	0.248	-14%
2500rpm_15p4	2500	286.0	96.9	124.7	64.4	37104	0.371	0.364	-6%
2500rpm_9p2	2500	229.7	80.7	105.6	43.4	29798	0.298	0.274	-10%
2500rpm_2p8	2500	187.2	72.3	91.5	23.5	24290	0.243	0.212	-15%
2000rpm_15p2	2000	201.9	61.9	96.0	44.0	32741	0.327	0.309	-7%
2000rpm_8p6	2000	163.8	54.5	79.8	29.4	26560	0.266	0.239	-11%
2000rpm_2p7	2000	137.6	49.4	71.3	16.9	22317	0.223	0.188	-16%
1500rpm_14p8	1500	143.6	37.9	75.0	30.7	31054	0.311	0.339	4%
1500rpm_8p8	1500	109.4	30.3	59.5	19.6	23657	0.237	0.221	-8%
1500rpm_4p7	1500	94.6	28.9	53.3	12.5	20463	0.205	0.179	-12%
1500rpm_2p3	1500	89.8	29.6	50.6	9.6	19419	0.194	0.177	-13%

In Table 10. results of total friction power loss (generated in FTAB), piston friction power loss (piston skirt and second land), piston rings friction power loss (calculated in EXCITE Piston&Rings) and cylinder head friction power loss are visible. Cylinder head friction power loss is calculated as difference between total friction power loss and friction power loss generated from piston and piston ring. Total FMEP values are calculated with equation (11) and they are

compared with measurement. Difference between total FMEP given from simulation (red) and measurement (green) is shown in percentage (blue).

In Table 11., comparison between measurement and REVO model with low friction package is shown.

Table 11. Comparison between measurement and REVO model with low friction ring package.

REVO_LOW FT ring package									
CASE	n (rpm)	FPL SUM (W)	FPL Piston (W)	FPL Piston Rings (W)	FPL Cylinder Head (W)	Total FMEP (Pa)	Total FMEP (bar)	Measurement (bar)	Difference
3000rpm_15p5	3000	370.0	133.4	150.8	85.7	39997	0.400	0.409	-1%
3000rpm_9p3	3000	297.5	111.5	127.1	58.9	32163	0.322	0.339	4%
3000rpm_5p3	3000	261.4	104.9	116.3	40.2	28264	0.283	0.293	1%
3000rpm_2p9	3000	258.0	105.6	118.1	34.3	27888	0.279	0.285	-1%
2500rpm_15p4	2500	278.4	92.9	121.6	63.9	36118	0.361	0.369	2%
2500rpm_9p2	2500	226.4	80.7	102.3	43.4	29370	0.294	0.310	2%
2500rpm_2p8	2500	184.2	71.7	89.5	23.0	23898	0.239	0.247	-1%
2000rpm_15p2	2000	197.8	61.9	91.9	44.0	32070	0.321	0.328	2%
2000rpm_8p6	2000	159.6	54.5	75.8	29.4	25889	0.259	0.262	-2%
2000rpm_2p7	2000	134.4	49.1	68.4	17.0	21800	0.218	0.212	-4%
1500rpm_14p8	1500	142.7	37.9	74.1	30.6	30848	0.308	0.328	2%
1500rpm_8p8	1500	106.0	30.3	56.4	19.3	22928	0.229	0.234	0%
1500rpm_4p7	1500	93.6	28.9	52.2	12.5	20242	0.202	0.186	-8%
1500rpm_2p3	1500	88.4	29.6	49.5	9.3	19123	0.191	0.173	-9%

In Table 12., comparison between measurement and EHD model with basic friction package is shown.

Table 12. Comparison between measurement and EHD model with basic ring package.

EHD_BASIC ring package									
CASE	n (rpm)	FPL SUM (W)	FPL Piston (W)	FPL Piston Rings (W)	FPL Cylinder Head (W)	Total FMEP (Pa)	Total FMEP (bar)	Measurement (bar)	Difference
3000rpm_15p5	3000	363.6	132.0	153.3	78.3	39303	0.393	0.409	1%
3000rpm_9p3	3000	294.6	110.4	130.8	53.4	31848	0.318	0.310	-4%
3000rpm_5p3	3000	260.1	103.7	119.9	36.5	28124	0.281	0.261	-10%
3000rpm_2p9	3000	260.9	105.4	124.4	31.1	28204	0.282	0.248	-13%
2500rpm_15p4	2500	273.6	91.3	124.7	57.5	35493	0.355	0.364	-2%
2500rpm_9p2	2500	223.2	78.3	105.6	39.4	28959	0.290	0.274	-7%
2500rpm_2p8	2500	184.6	71.8	91.5	21.3	23946	0.239	0.212	-14%
2000rpm_15p2	2000	197.4	61.4	96.0	40.1	32015	0.320	0.309	-4%
2000rpm_8p6	2000	159.0	52.7	79.8	26.5	25788	0.258	0.239	-8%
2000rpm_2p7	2000	136.1	49.4	71.3	15.4	22076	0.221	0.188	-15%
1500rpm_14p8	1500	142.4	39.5	75.0	27.9	30781	0.308	0.339	5%
1500rpm_8p8	1500	106.8	30.6	59.5	16.6	23086	0.231	0.221	-6%
1500rpm_4p7	1500	92.3	28.3	53.3	10.7	19952	0.200	0.179	-10%
1500rpm_2p3	1500	87.6	29.0	50.6	8.0	18943	0.189	0.177	-11%

In Table 13., comparison between measurement and EHD model with low friction package is shown.

Table 13. Comparison between measurement and EHD model with low friction ring package.

EHD_LOW FT ring package									
CASE	n (rpm)	FPL SUM (W)	FPL Piston (W)	FPL Piston Rings (W)	FPL Cylinder Head (W)	Total FMEP (Pa)	Total FMEP (bar)	Measurement (bar)	Difference
3000rpm_15p5	3000	361.2	132.0	153.3	75.9	39045	0.390	0.409	2%
3000rpm_9p3	3000	290.9	110.4	130.8	49.8	31452	0.315	0.339	7%
3000rpm_5p3	3000	256.5	103.6	119.9	32.9	27726	0.277	0.293	3%
3000rpm_2p9	3000	254.6	105.4	124.4	24.8	27520	0.275	0.285	1%
2500rpm_15p4	2500	270.5	91.3	124.7	54.4	35086	0.351	0.369	5%
2500rpm_9p2	2500	220.0	78.2	105.6	36.1	28535	0.285	0.310	5%
2500rpm_2p8	2500	182.6	71.8	91.5	19.3	23687	0.237	0.247	-1%
2000rpm_15p2	2000	193.3	61.3	96.0	36.0	31345	0.313	0.328	5%
2000rpm_8p6	2000	155.1	52.7	79.8	22.6	25146	0.251	0.262	1%
2000rpm_2p7	2000	133.2	49.4	71.3	12.5	21608	0.216	0.212	-3%
1500rpm_14p8	1500	139.9	39.5	75.0	25.4	30244	0.302	0.328	4%
1500rpm_8p8	1500	103.3	30.6	59.5	13.2	22344	0.223	0.234	3%
1500rpm_4p7	1500	91.1	28.3	53.3	9.6	19708	0.197	0.186	-6%
1500rpm_2p3	1500	86.4	29.0	50.6	6.8	18687	0.187	0.173	-7%

In Figures 110. and 111., total FMEP values from measurement and simulation models are shown.

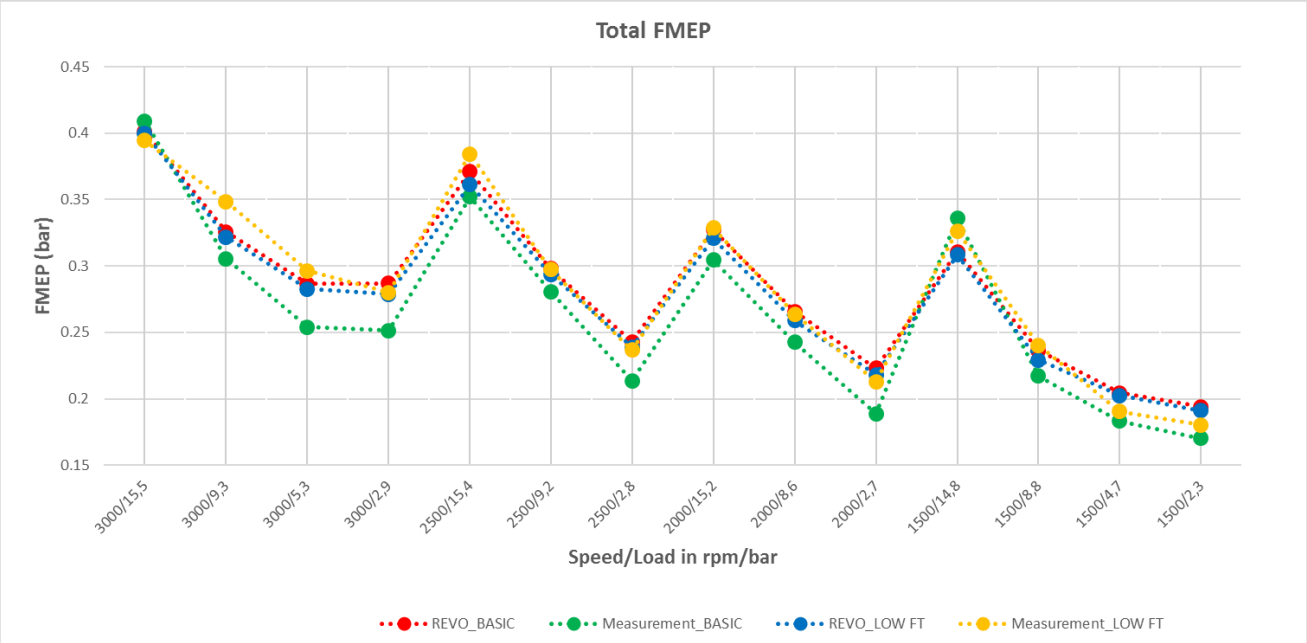

Figure 110. Comparison of FMEP values between measurement and REVO simulation model with basicand low friction ring package.

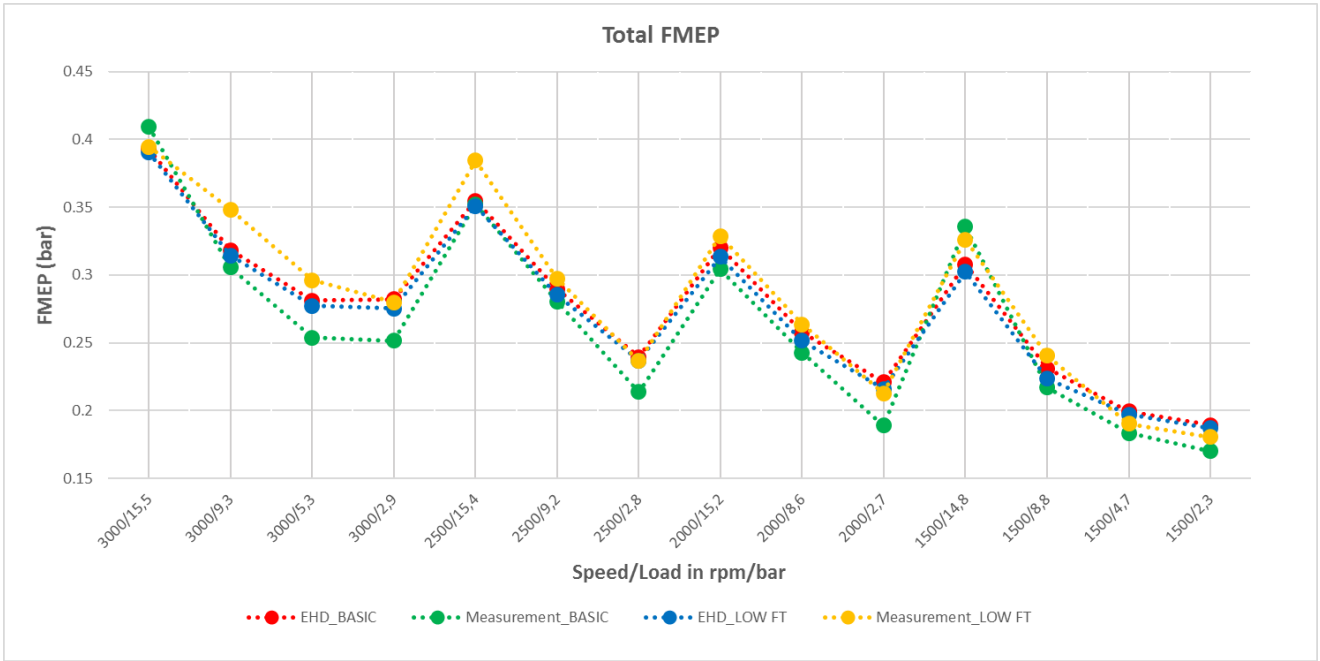

Figure 111. Comparison of FMEP values between measurement and EHD simulation model with basic and low friction ring package.

Above figures and tables show differences between simulation model and measurement. It is visible that the highest deviation from measurement is coming from REVO simulation model

with basic ring package. The major deviations are visible on lower load operating points. Model with REVO joints and low friction ring package shows lower FMEP values over all engine operating points. In other hand, measurement with low friction ring package shows higher values than measurement with basic ring package. Reason of this measurement results are not clear. Model with EHD joints shows slighty lower FMEP values compared to model with REVO joints with both ring packages.

Distribution of FMEP values

In following figures and tables, distribution of FMEP values are shown. Distribution is presented for piston, cylinder head and ring package for REVO model with basic and low friction ring package.

Table 14. Distribution of FMEP values for REVO model with basic ring package are shown.

REVO_BASIC ring package						
CASE	n (rpm)	Piston FMEP (bar)	Head FMEP (bar)	FMEP_Top ring (bar)	FMEP_2nd ring (bar)	FMEP_Oil ring (bar)
3000rpm_15p5	3000	0.144	0.094	0.071	0.005	0.086
3000rpm_9p3	3000	0.121	0.066	0.043	0.008	0.088
3000rpm_5p3	3000	0.114	0.045	0.028	0.010	0.090
3000rpm_2p9	3000	0.114	0.040	0.022	0.018	0.093
2500rpm_15p4	2500	0.126	0.086	0.059	0.016	0.085
2500rpm_9p2	2500	0.105	0.058	0.036	0.014	0.085
2500rpm_2p8	2500	0.094	0.032	0.019	0.008	0.090
2000rpm_15p2	2000	0.100	0.074	0.061	0.009	0.084
2000rpm_8p6	2000	0.088	0.051	0.033	0.009	0.084
2000rpm_2p7	2000	0.080	0.029	0.018	0.010	0.087
1500rpm_14p8	1500	0.082	0.068	0.070	0.005	0.085
1500rpm_8p8	1500	0.066	0.044	0.038	0.005	0.084
1500rpm_4p7	1500	0.062	0.029	0.025	0.005	0.083
1500rpm_2p3	1500	0.064	0.022	0.019	0.005	0.084

Table 15. Distribution of FMEP values for REVO model with low friction ring package are shown.

REVO_LOW FT ring package						
CASE	n (rpm)	Piston FMEP (bar)	Head FMEP (bar)	FMEP Top ring (bar)	FMEP 2nd ring (bar)	FMEP Oil ring (bar)
3000rpm_15p5	3000	0.144	0.095	0.069	0.005	0.086
3000rpm_9p3	3000	0.121	0.066	0.041	0.006	0.088
3000rpm_5p3	3000	0.113	0.045	0.027	0.007	0.090
3000rpm_2p9	3000	0.114	0.039	0.021	0.012	0.093
2500rpm_15p4	2500	0.121	0.085	0.057	0.014	0.085
2500rpm_9p2	2500	0.105	0.058	0.034	0.012	0.085
2500rpm_2p8	2500	0.093	0.032	0.018	0.007	0.090
2000rpm_15p2	2000	0.100	0.074	0.058	0.005	0.084
2000rpm_8p6	2000	0.088	0.050	0.031	0.006	0.084
2000rpm_2p7	2000	0.080	0.029	0.016	0.006	0.087
1500rpm_14p8	1500	0.082	0.068	0.069	0.005	0.085
1500rpm_8p8	1500	0.066	0.043	0.031	0.005	0.084
1500rpm_4p7	1500	0.063	0.029	0.024	0.004	0.083
1500rpm_2p3	1500	0.064	0.021	0.018	0.005	0.084

Contribution of FMEP values in percentage are shown in pie charts for all operating points at engine speed 3000 rpm.

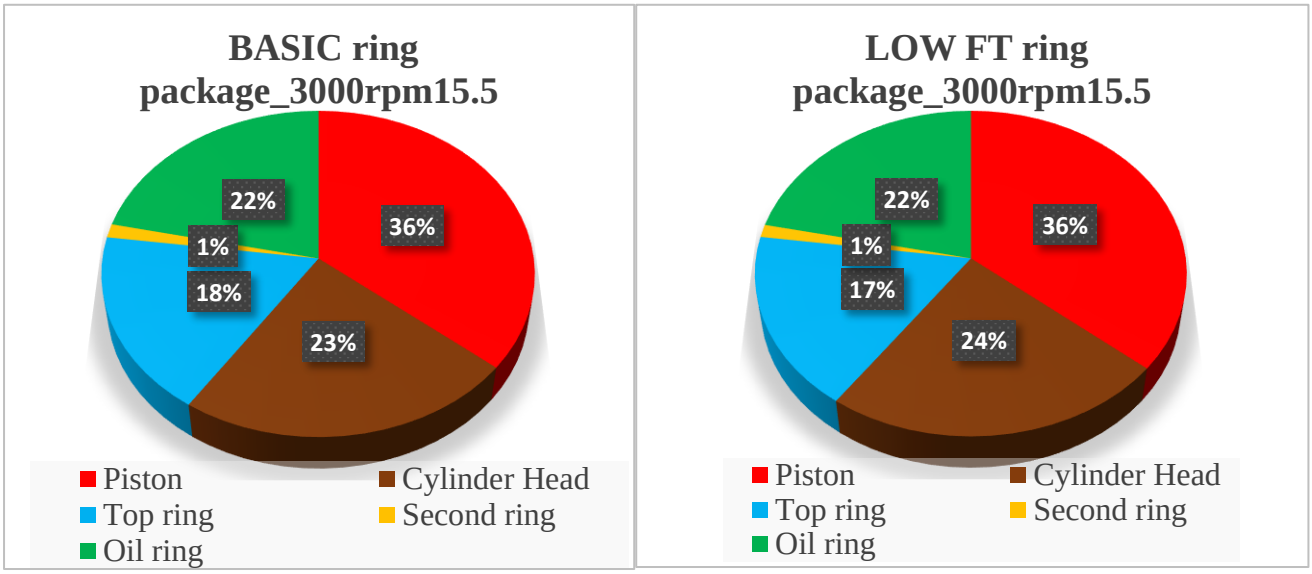

Figure 112. Comparison of FMEP distribution between basic and low friction ring package, 3000_15.5.

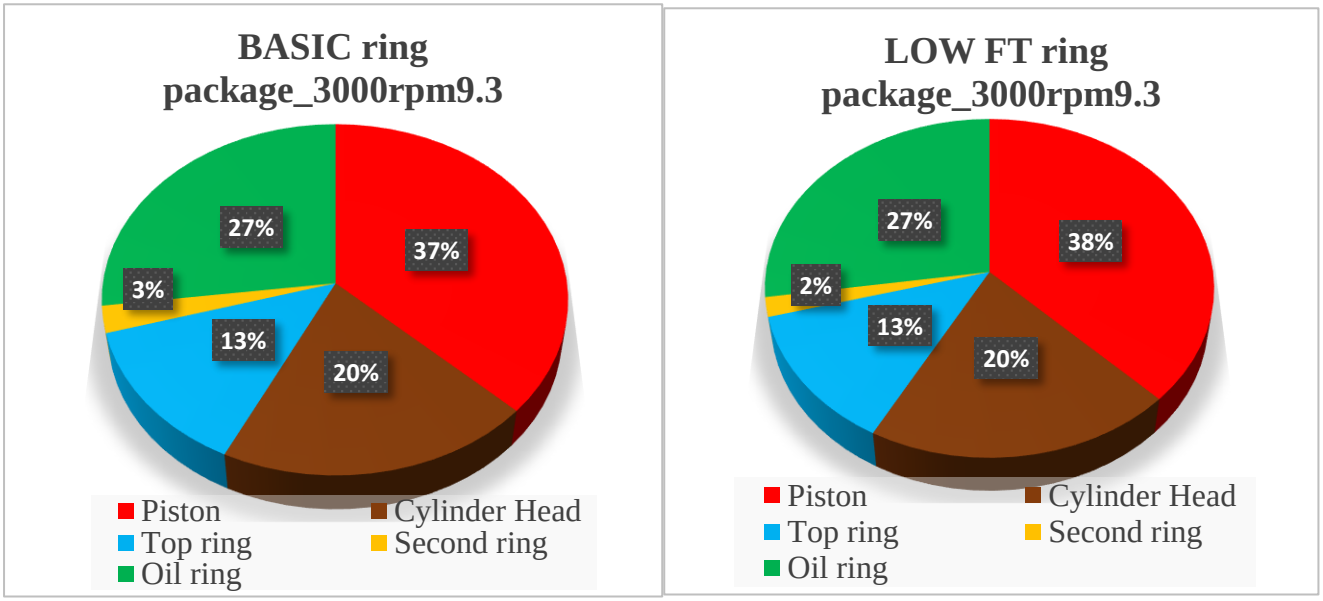

Figure 113. Comparison of FMEP distribution between basic and low friction ring package, 3000_9.3.

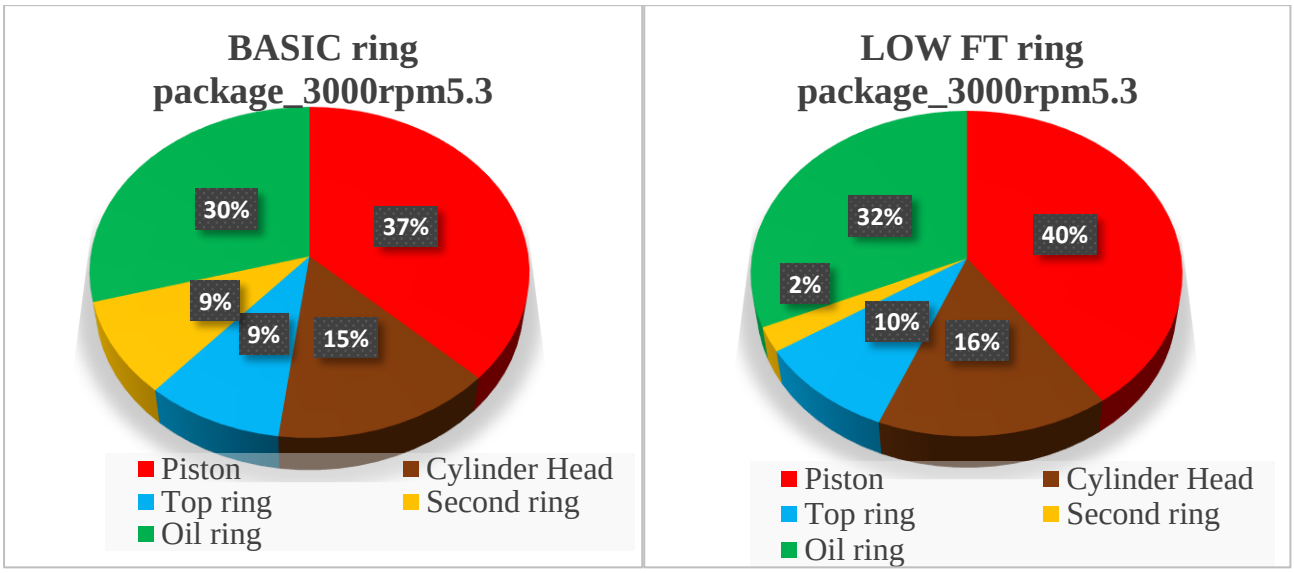

Figure 114. Comparison of FMEP distribution between basic and low friction ring package, 3000_5.3.

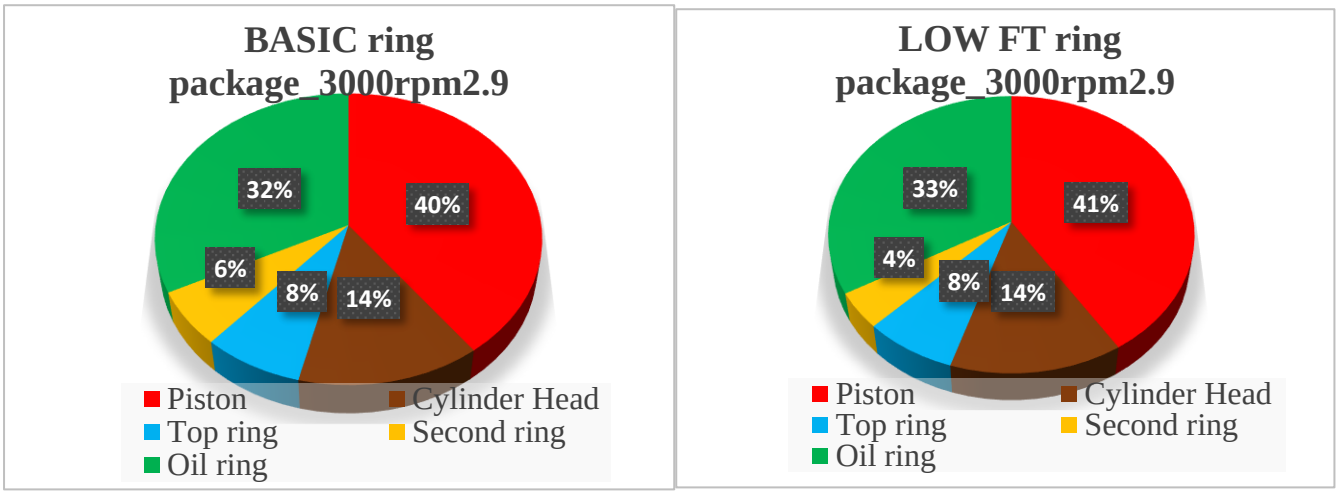

Figure 115. Comparison of FMEP distribution between basic and low friction ring package, 3000_2.9.

Above figures and tables show distribution of FMEP values generated from REVO simulation model with basic and low friction ring package. Is can be seen that FMEP generated from a whole piston ring package have the most influence on total FMEP value compared to other components. Biggest contribution on whole piston ring package FMEP come from oil ring and the second ring have the smallest contribution. Also, visible is that low friction package has slighty higder percentage FMEP values generated on piston compared to basic ring package. The reason of that is beacuase low friction package have lower piston ring FMEP values than basic

ring package and FMEP values generated on piston are the same for both ring packages. Increasing the load, FMEP values from cylinder head are higher and FMEP values generated from piston are lower.

4.4. Friction tuning parameters

This chapter describes sensitivity of tuning friction parameters. Those parameters have purpose for calibration simulation model with measurement results. Friction coefficients whose describe lubrication asperity friction model (Figure 51) are changed in EXCITE™ Piston&Ring and EXCITE™ Power Unit. For each model, two variants of parameters sets are tested.

In Table 16. the values of friction tuning parameters for 2D EXCITE™ Piston&Ring model with basic ring package are dislayed.

Table 16. Friction tuning parameters for EXCITE™ Piston&Ring model.

	Friction Coefficient	Constant			Reference Lenght
		a	b	c	
	[-]	[-]	[-]	[-]	[microns]
	AVL FRISC model				
Top Ring	0.1	2.71	30000	100	300
2nd Ring	0.1	2.718	30000	100	100
Oil Ring	0.1	2.718	40000	350	200
	Variant A				
Top Ring	0.125	2.718	30000	1000	300
2nd Ring	0.125	2.718	30000	2000	100
Oil Ring	0.125	2.718	40000	3500	200
	Variant B				
Top Ring	0.12	2.718	20000	10000	200
2nd Ring	0.125	2.718	20000	10000	200
Oil Ring	0.12	2.718	20000	10000	200

In Table 16. are presented changed values of friction coefficient for boundary condition, base for exponential function for solid contact (Constant a), exponent coefficient for exponential function of solid contact (Contants b), micro hydrodynamic coefficient (Constant c) and reference length for different piston ring. Variant A and B have higher values of friction coefficient for boundry condition and constant c than AVL FRISC model. Reference length and

constant b are the same for Variant A and AVL FRISC model and Variant B have smaller those values.

In Table 17. and on Figure 116. comparison of FMEP values of piston rings are presented for all operating points. Results are presented only for 2D simulation solver model with basic ring package.

Table 17. Comparison of piston rings FMEP values.

		Piston ring FMEP (bar)		
CASE	**n (rpm)**	**FRISC**	**Variant A**	**Variant B**
3000rpm_15p5	3000	0.163	0.244	0.337
3000rpm_9p3	3000	0.139	0.217	0.315
3000rpm_5p3	3000	0.128	0.205	0.305
3000rpm_2p9	3000	0.133	0.213	0.314
2500rpm_15p4	2500	0.159	0.235	0.326
2500rpm_9p2	2500	0.135	0.209	0.302
2500rpm_2p8	2500	0.117	0.191	0.290
2000rpm_15p2	2000	0.153	0.221	0.287
2000rpm_8p6	2000	0.127	0.195	0.281
2000rpm_2p7	2000	0.114	0.187	0.263
1500rpm_14p8	1500	0.160	0.238	0.294
1500rpm_8p8	1500	0.127	0.186	0.259
1500rpm_4p7	1500	0.113	0.174	0.251
1500rpm_2p3	1500	0.108	0.173	0.253

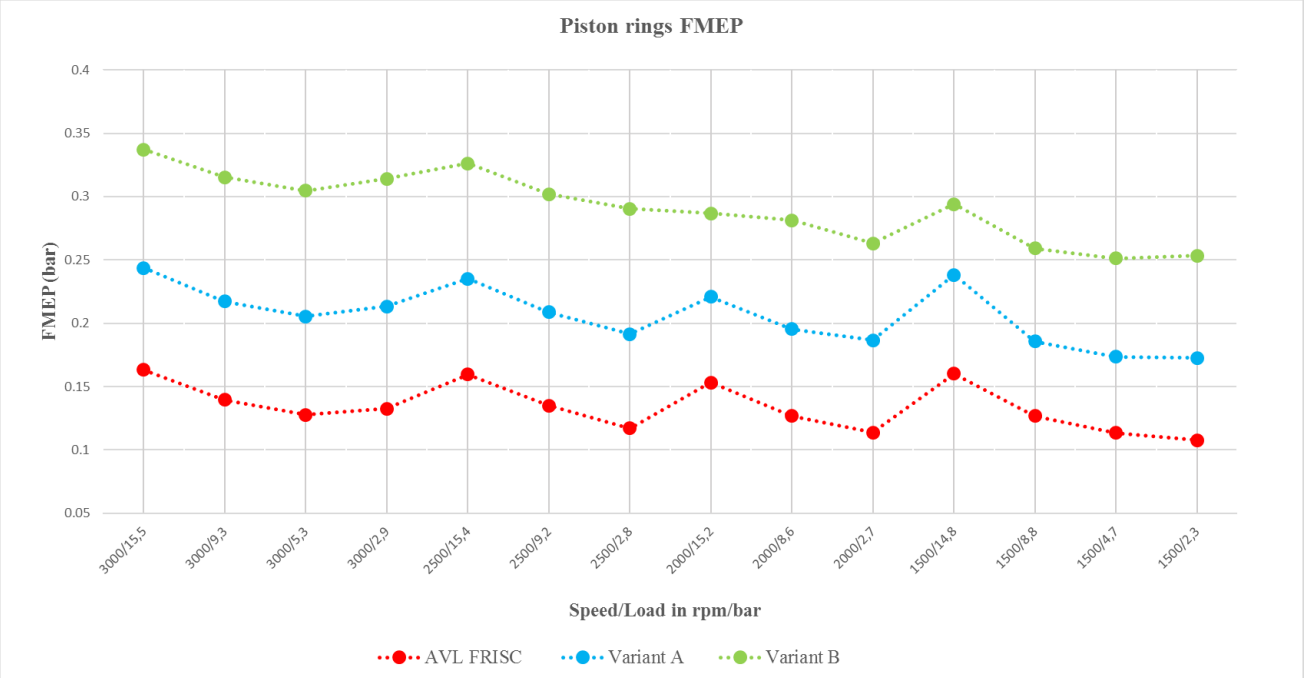

Figure 116. Comparison of piston rings FMEP values.

Variant A and B have higher FMEP values than AVL FRISC model. Comparing friction parameters is visible that value of Constant C has the biggest difference. In Variant B, on top and second ring, Constant c have 100-time higher value than in AVL FRISC model. It can be concluded that increasing Constant c lead to increasing FMEP values in EXCITE™ Piston&Ring.

In Table 18. shows values of friction tuning parameters for REVO EXCITE™ Power Unit model with basic ring package.

Table 18. Friction tuning parameters for EXCITE™ Power Unit model.

	Friction Coefficient	Constant			Reference Lenght
		a	b	c	
	[-]	[-]	[-]	[-]	[microns]
	AVL FRISC model				
Skirt	0.1	2.71828	1000	1000	2
	Variant C				
Skirt	0.15	2.71828	10000	10000	20
	Variant D				
Skirt	0.18	1.71828	1000	100000	200

Table 18. shows different values of friction coefficient for boundary condition, base for exponential function for solid contact (Constant a), exponent coefficient for exponential function of solid contact (Contants b), micro hydrodynamic coefficient (Constant c) and reference length for piston skirt. Variant C and D have higher values of friction coefficient for boundry condition, constant c and reference length than AVL FRISC model. Constant b is the same for Variant D and AVL FRISC model and lower than in Variant C. Constant a is the same for Variant C and AVL FRISC model and higher than in Variant C.

In Table 19. and on Figure 116. comparison of total FMEP values calculated from FTAB jonits are presented for all operating points. Results are presented only for REVO model with basic ring package.

Table 19. Comparison of total FMEP values.

	Total FMEP (bar)			
CASE	**n (rpm)**	**FRISC**	**Variant C**	**Variant D**
3000rpm_15p5	3000	0.401	0.411	0.415
3000rpm_9p3	3000	0.326	0.327	0.329
3000rpm_5p3	3000	0.287	0.288	0.285
3000rpm_2p9	3000	0.287	0.288	0.283
2500rpm_15p4	2500	0.371	0.368	0.386
2500rpm_9p2	2500	0.298	0.299	0.306
2500rpm_2p8	2500	0.243	0.243	0.242
2000rpm_15p2	2000	0.327	0.330	0.357
2000rpm_8p6	2000	0.266	0.267	0.283
2000rpm_2p7	2000	0.223	0.224	0.227
1500rpm_14p8	1500	0.311	0.314	0.349
1500rpm_8p8	1500	0.237	0.239	0.264
1500rpm_4p7	1500	0.205	0.206	0.221
1500rpm_2p3	1500	0.194	0.195	0.204

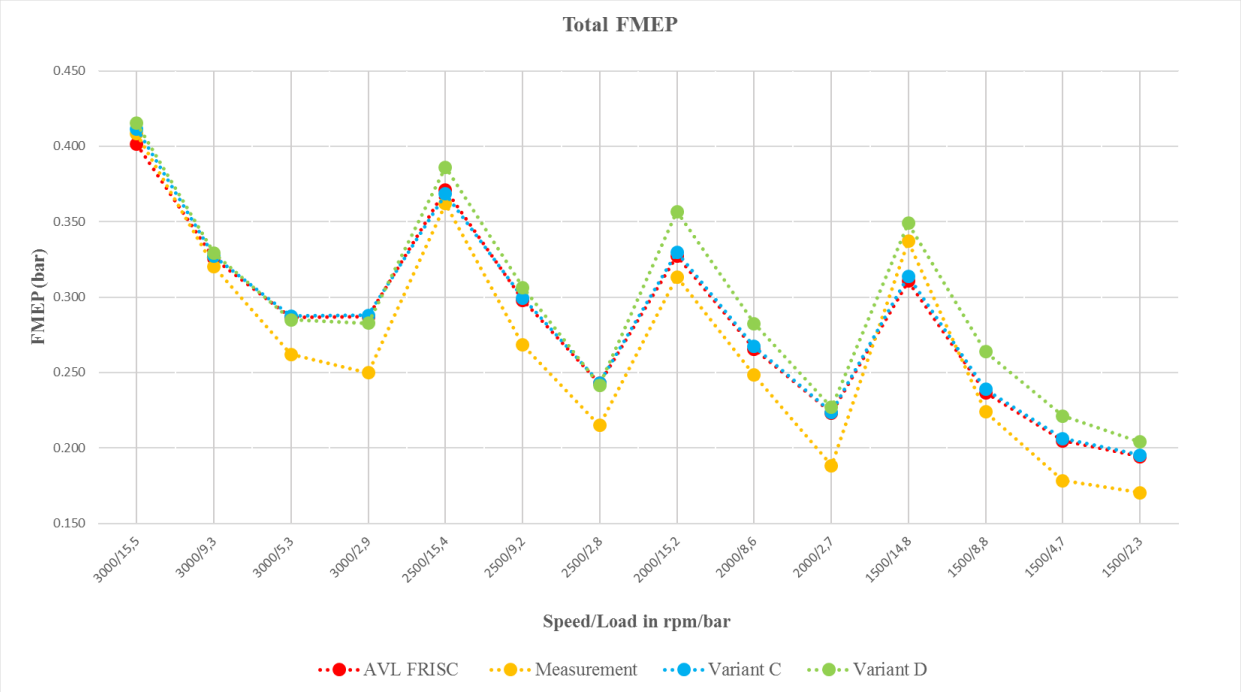

Figure 117. Comparison of total FMEP values.

Variant D have higher FMEP values than AVL FRISC model on full load operating points and Variant C have slightly higer FMEP values. Comparing friction parameters is visible that value of Constant C has the biggest difference. It can be concluded that increasing Constant c lead to increasing FMEP values in EXCITE™ Piston&Ring. Also, importat is to emphasize that changing of this friction tuning parameters have big influence on FMEP values on full operating point.

5. CONCLUSION AND RECOMMENDATIONS

The main goal of this thesis was to correlate results of simulation model and available results given from measurement on an AVL FRISC engine. Also, influence of tangential force on friction and differences between simplified and advanced modeling is presented. Simulation model are described, and main input data are presented. Simulation model with basic ring package and calculated with 2D solver is calibrated to measurement (blow-by). Sealring and cylinder head are implemented in EXCITE™ Power Unit models and influence on friction behavior caused by stick slip effect is accomplished. In results, friction force, side force, LOC, blow-by and FMEP values are compared.

5.1. Conclusions

Based on examined literature and results of this thesis some conclusions can be made. Firstly, conclusions of EXCITE™ Piston&Rings simulation results are presented:

- Friction power loss of top ring is load dependent and friction power loss of oil ring is more speed dependent. Also, friction power loss of top ring increases with load for the same operating speed. Piston ring FMEP is higher if the load is increased and the main contributor of FMEP comes from oil ring. Lube oil consumption and blow–by values are higher if load increases. The most contributor of LOC is evaporation from liner.
- Piston ring friction power loss and FMEP values slightly decreased with reduced tangential force ring package. Lube oil consumption is little bit lower in ring package with reduced tangential force. Blow-by values are higher in ring package with reduced tangential force. Axial movement and twist angle only show minor differences both ring packages.
- Hydrodynamic cumulated FMEP of piston ring package have higher values with 2D than 3D solver and asperity cumulated FMEP have higher value with 3D than 2D solver. Friction power loss of piston ring package and FMEP values slightly increased with 3D simulation solver. Friction ring forces have slightly higher value with 3D simulation solver. Axial movement of piston ring in groove is the same in both models (2D and 3D simulation solver). Blow by results significally increased in model with 3D simulation solver.

Conclusions of simulation results from EXCITE™ Power Unit models are:

- Tilting angle are slightly above AVL guideline Pressure on piston skirt is mostly influenced by hydrodynamics pressure. Minimum oil film thickness appears around FTDC where area of asperity pressure is presented. Asperity contact appear on second land of steel piston. Local high pressure appears at the top of skirt on ATS due to high tilting. Side force calculated from EPIL and from FTAB joint have the same values. Difference between friction force and friction power loss in EPIL and FTAB is visible in peak values.
- Simulation results of REVO model with basic and low friction ring package don't show significant differences. Friction and side force have the same trend line. Model with low friction ring package shows slightly lower values of total friction power loss, and piston friction power loss are the same. It can be concluded that this slightly lower values of total friction power loss are caused only by piston ring package
- Simulation results of REVO and EHD model with basic ring package don't show significant differences. Some minor differences are visible in tilting where EHD model have higher peak of tilting angle and radial displacement The REVO model have slightly lower value of friction power loss, so FMEP values are also lower in that case. Also, important is to emphasize that simulation time of EHD model is 2-3 time longer and therefore more computer resources is needed.

Conclusions of comparison between simulation and measurement results are:

- Minor differences in blow-by results of 2D simulation models with basic (calibrated to measurement) and low friction ring package. Simulation results of 2D model with low friction ring package shown lower values of blow-by compared to measurement. Results of blow-by calculated with 3D solver in both ring package cases are higher than measurement results. Lube oil consumption results are not fully calibrated and on lower speeds (1500 and 2000 rpm) are the smaller LOC differences in simulation with basic ring package and measurement.
- Friction force calculated in REVO model with both piston ring packages have similar behavior like friction forces given from measurement. Second peak after FTDC, caused by cylinder head movement, is visible in simulation results. Also, friction force calculated from EHD model have the same trend line as forces calculated with REVO model. Side forces analytical calculated and given from simulation have same trend line, only are visible little differences in peak values caused by piston dynamic. Measured side forces have big differences compared to simulation or analytical side forces.

- The highest deviation of FMEP values from measurement is coming from REVO simulation model with basic ring package. Model with REVO joints and low friction ring package shows lower FMEP values over all engine operating points. In other hand, measurement with low friction ring package shows higher values than measurement with basic ring package. Model with EHD joints shows slightly lower FMEP values compared to model with REVO joints with both ring packages.
- Is can be seen that FMEP generated from a whole piston ring package have the most influence on total FMEP value compared to other components. Biggest contribution on whole piston ring package FMEP come from oil ring and the second ring have the smallest contribution. Increasing the load, FMEP values from cylinder head are higher and FMEP values generated from piston are lower.

5.2. Recommendations and future work

Some recommendation for future work in this field:

- For better understanding friction force behavior, important is to know all parameters that are used on measurement. In further work on this model, bore distortion of liner should be calculated for used liner (in model are implemented liner profile from old similar FRISC model). Also, temperature field of piston is assumed from old project and thermal simulation of piston should be done for better input data.
- Results of friction force, side force and FMEP calculated with REVO joint model don't have significant differences compared to EHD model. For further investigation of similar FRISC project, REVO model should be used because simulation time is 2-3 times shorter.
- Further investigation of EXCITE Piston&Rings model should be done because in 3D model ring end shut appear at lower speeds. After implementing exact liner profile, this appearance of ring end shut could be solved.
- Cylinder head and sealring can be examined as finite element model and in that form can be implemented in numerical simulation software. In that way, influence of real distributed mass of cylinder head and saelring on stick-slip effect can be examine. This approach is more complicate approach and therefore more computer resources is needed.
- Further investigation of friction parameters whose describe lubrication asperity friction model.

REFERENCES

[1] AVL LIST GmbH (n. d.). *Basic Training Course - Piston Dynamics.* Unpublished manuscript.

[2] MAHLE GmbH (2012). *Piston and engine testing*. Stuttgart: Springer Fachmedien Wiesbaden GmbH.

[3] Rohr, W. F. (2013). *Experimental and theoretical investigations of lube oil performance and engine friction.* (Doctoral thesis, University of Tennessee, Knoxville)

[4] Business Wire (2006). Retrieved from: https://www.businesswire.com/news/home/20060405005975/en/Federal-Moguls-Monosteel-Piston-Wins-2006-Automotive-News

[5] OEM Off – Highway (2011). Retrieved from: https://www.oemoffhighway.com/engines/article/10250729/engine-piston-fuel-economy

[6] Diesel Net (n. d.). Retrieved from: https://www.dieselnet.com/tech/combustion_piston-cool.php#cool

[7] Everychina (2015). Retrieved from: http://enginepistons.sell.everychina.com/p-101827554-komatsu-cast-iron-pistons-6217-31-2130-diesel-engine-piston.html

[8] Ottliczky, E., Voigt, M., Weimar, H-J., & Weiss, E. (2011). Steel piston for passenger car diesel engines. *ATZ autotechnology*, *11*, 38-42. doi: 10.1365/s35595-011-0066-8

[9] AVL LIST GmbH (n. d.). *Basic Training Course - Ring Dynamics.* Unpublished manuscript.

[10] Schreer, K., Roth, I., Schneider, S., & Ehnis, H. (2013). *Analysis of aluminum and steel pistons—comparison of friction, piston temperature, and combustion.* ASME 2013 internal combustion engine division fall technical conference. Daerborn, Michigan, USA. doi: 10.1115%2Ficef2013-19114

[11] Smedley, G. (2004). *Piston ring design for reduced friction in modern internal combustion engines.* (Master thesis, Massachusetts Institute of Technology)

[12] Haslinger, R., (2010) *LOC requirements for Euro 6 engines.* Unpublished manuscript.

[13] Taylor, J. B., & Eyre, S. T. (1979) A review of piston ring and cylinder liner materials. *TRIBOLOGY international*, 79-89. doi 10.1016%2F0301-679x%2879%2990006-9

[14] Korihandbook (n. d.). http://korihandbook.federalmogul.com/en/section_41.htm

[15] Wong, V. W., & Tung, S. (2016*). Overview of automotive engine friction and reduction trends-Effects of surface, material and lubricant-additive technologies*. Friction, 4(1), 128. doi: 10.1007/s40544-016-0107-9

[16] Grabon, W., Koszela, W., Pawlus, P., & Ochwat S. (2012). *Improving tribologicalbehaviour of piston ring-cylinder liner frictional pair by liner surface texturing*. Elsevier, 102-108.

[17] Kennedy, M., Hoppe, S., & Esser, J. (2014). Lower friction losses with new piston ring coating*. MTZ eMagazine*, 75, 24-28.

[18] Winklhofer, E., Loesch, S., Satschen, S., Thonhauser, B. (2018). Reduction of friction losses by means of cylinder liner offset. *International Journal of Automotive Engineering, 9* (4), 304-309. doi: 10.20485/jsaeijae.9.4_304

[19] Lösch, S., Priestner C., Thonhauser B., Zieher F., Hick H. (2018). Advances in Determination of Piston Group Friction Losses at High Speeds and Loads using the AVL FRISC Single-Cylinder Engine (Zuverlässige Messung der Kolbengruppenreibung bei hohen Drehzahlen und Lasten mit dem AVL-FRISC-Einzylindermotor). In J. Liebl (Ed.), *Reibungsminimierung im Antriebsstrang 2015: Proceedings* (pp. 179–197). Wiesbaden: Springer Vieweg. doi: 10.1007/978-3-658-23189-7_11

[20] Winklhofer, E., Loesch, S., & Satschen S. (2016). High precision piston to liner friction measurement. *Proceedings of the JSAE Annual Congress 75-16*, 1864-1869

[21] Ming-Tang, M., C. Priestner C., Thonhauser B. (2017, September). *Advanced Piston Assembly Friction Evaluation Methods: CAE Simulation and Floating Liner Measurement.*

[22] AVL List GmbH (n.d.).

https://www.avl.com/-/the-avl-frisc-floating-liner%20engine?inheritRedirect=true

[23] Korihandbook (n. d.). http://korihandbook.federalmogul.com/en/section_8.htm

[24] AVL List GmbH, *AVL Excite 2017.1*, Documentation, www.avl.com

[25] Beloiu, M. D. (2012). Modeling and Analysis of Powertrain NVH. SAE International. 1 – 10. doi: 10.4271/2012-01-0888

[26] AVL LIST GmbH (n. d.). Basic Training Course – Power Unit. Unpublished manuscript

[27] Kligerman, Y.; Varenberg, M. (2014). Elimination of stick-slip motion in sliding of split or rough surface. *Tribology Letters.*

[28] Jiménez, A.-E., Bermúdez, M.-D. (2011). Friction and wear. 33-63.

APPENDICES

A EXCITE™ Piston&Rings simulation results – BASIC ring package

B EXCITE™ Piston&Rings simulation results – comparison between BASIC and LOW FT ring package

C EXCITE™ Piston&Rings simulation results – comparison between 2D and 3D simulation solver for BASIC ring package

D EXCITE™ Power Unit simulation results – BASIC ring package

E EXCITE™ Power Unit simulation results – comparison between BASIC and LOW FT ring package

F EXCITE™ Power Unit simulation results – comparison between 2D and 3D simulation solver for BASIC ring package

G Comparison of friction force between simulation and measurement – basic ring package

H Comparison of friction force between simulation and measurement – low frictionring package

I Comparison of side force between simulation, measurement and analytics – basic ring package

Appendix A

In this appendix EXCITE™ Piston&Rings results for other operating point of engine with basic ring package are performed.

Engine speed = 2500rpm

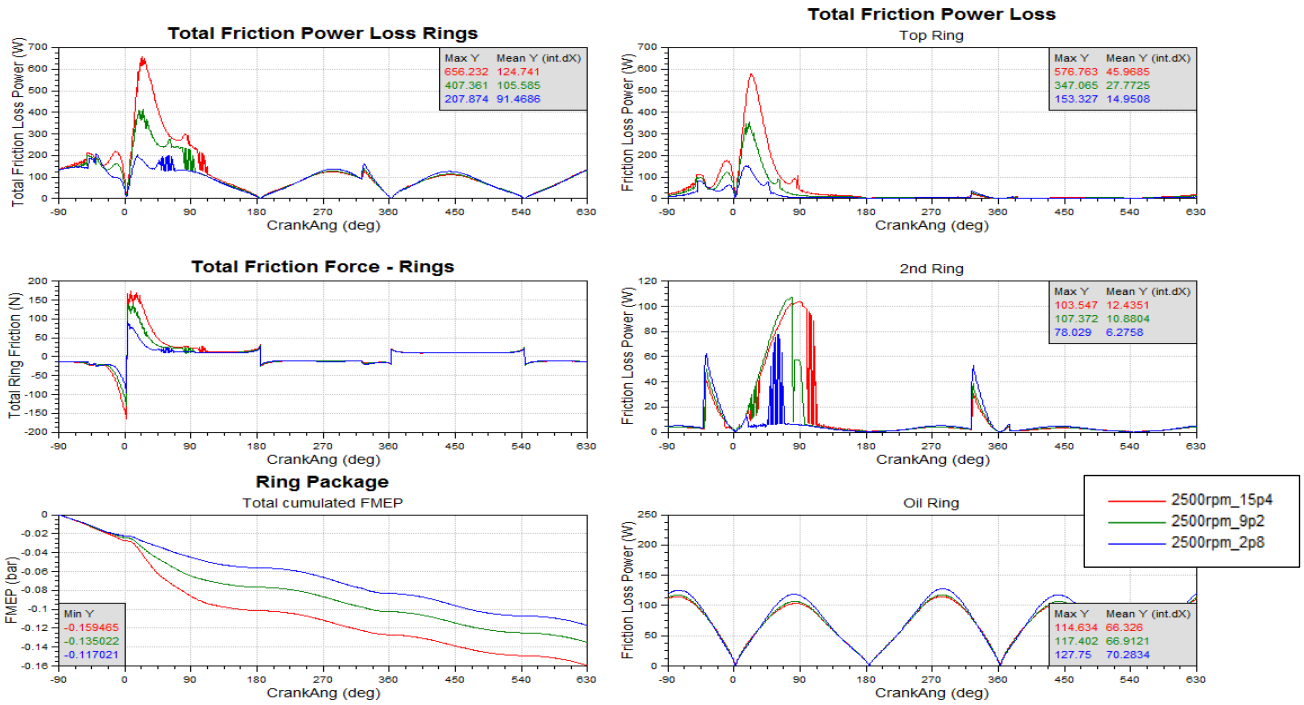

Figure A. 1 Basic ring package – Friction characteristics overview.

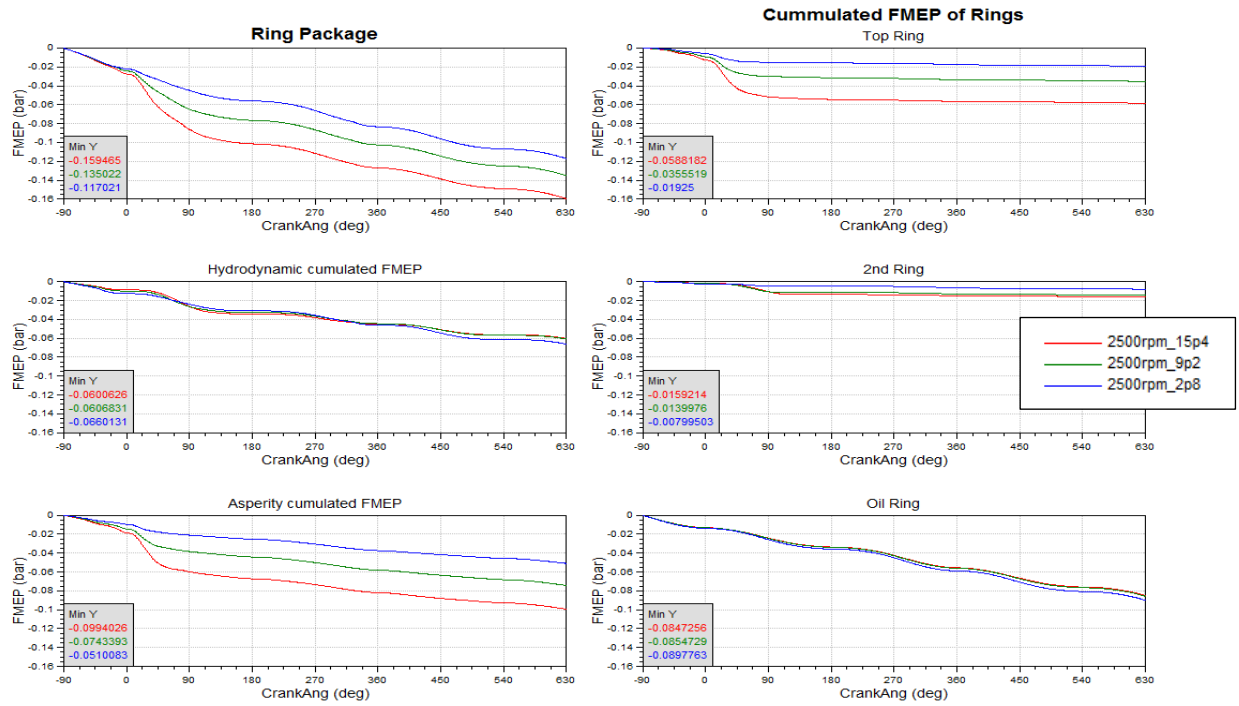

Figure A. 2. Basic ring package – FMEP overview.

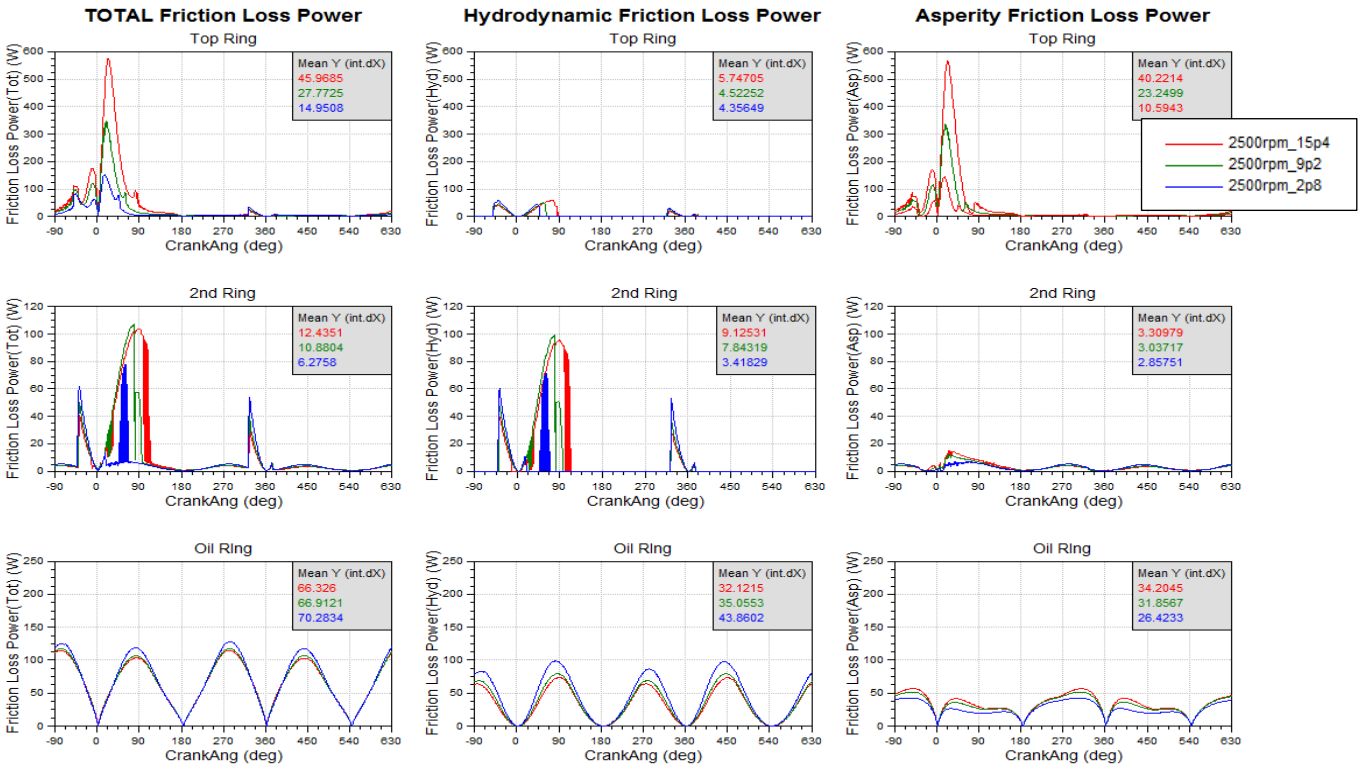

Figure A. 3. Basic ring package – Friction Power Loss overview.

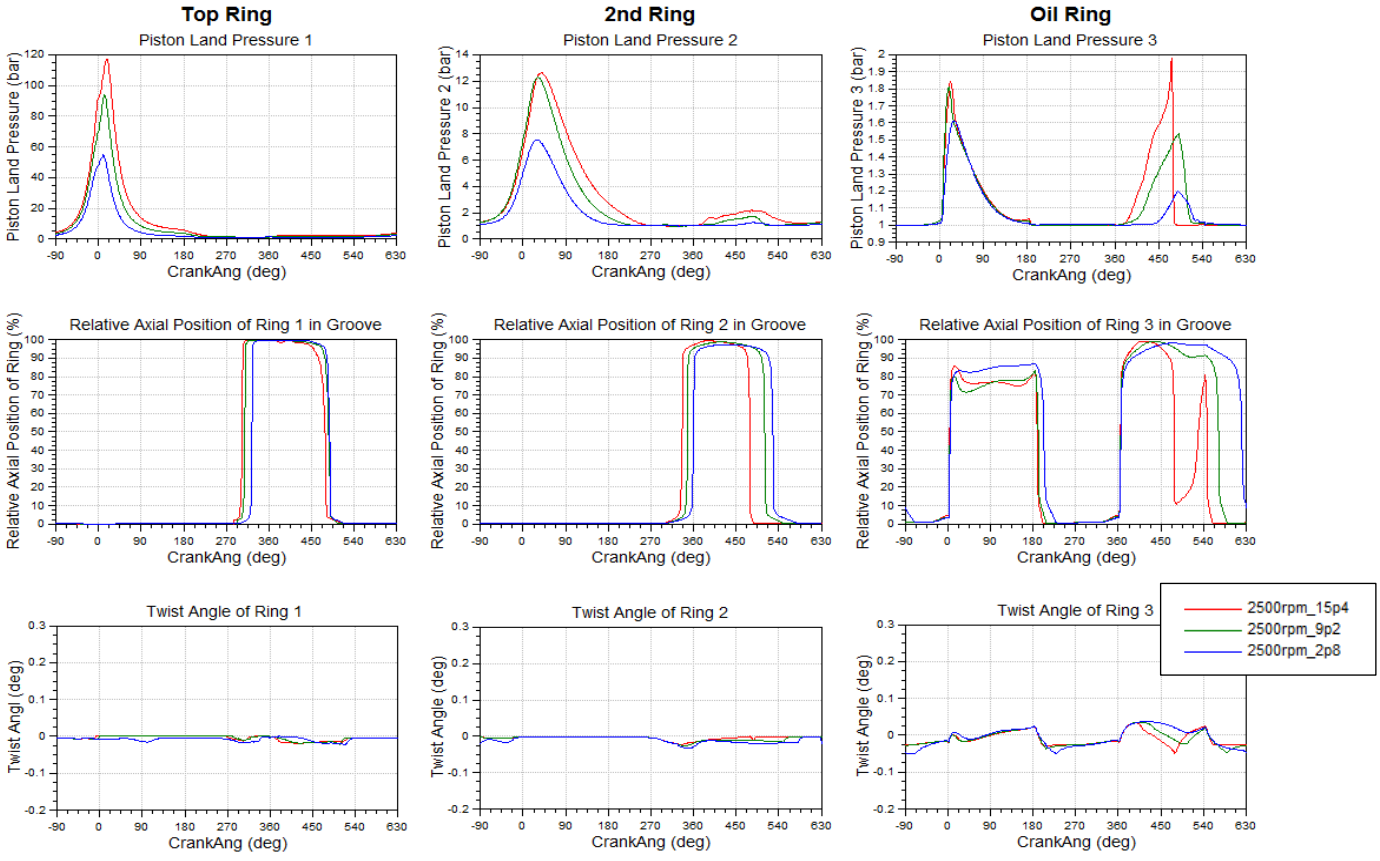

Figure A. 4. Basic ring package – Piston ring dynamics overview.

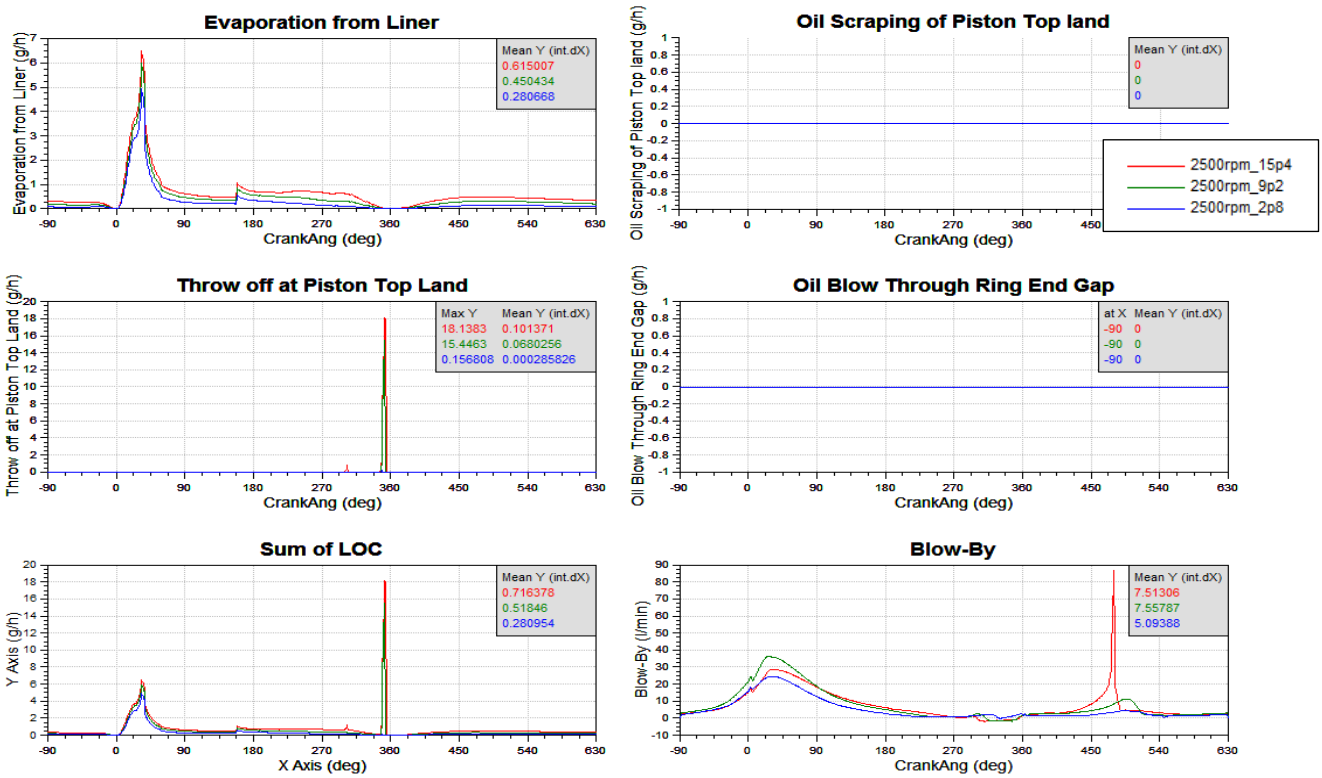

Figure A. 5. Basic ring package – Lube Oil Consumption and Blow-by overview.

Engine speed = 2000rpm

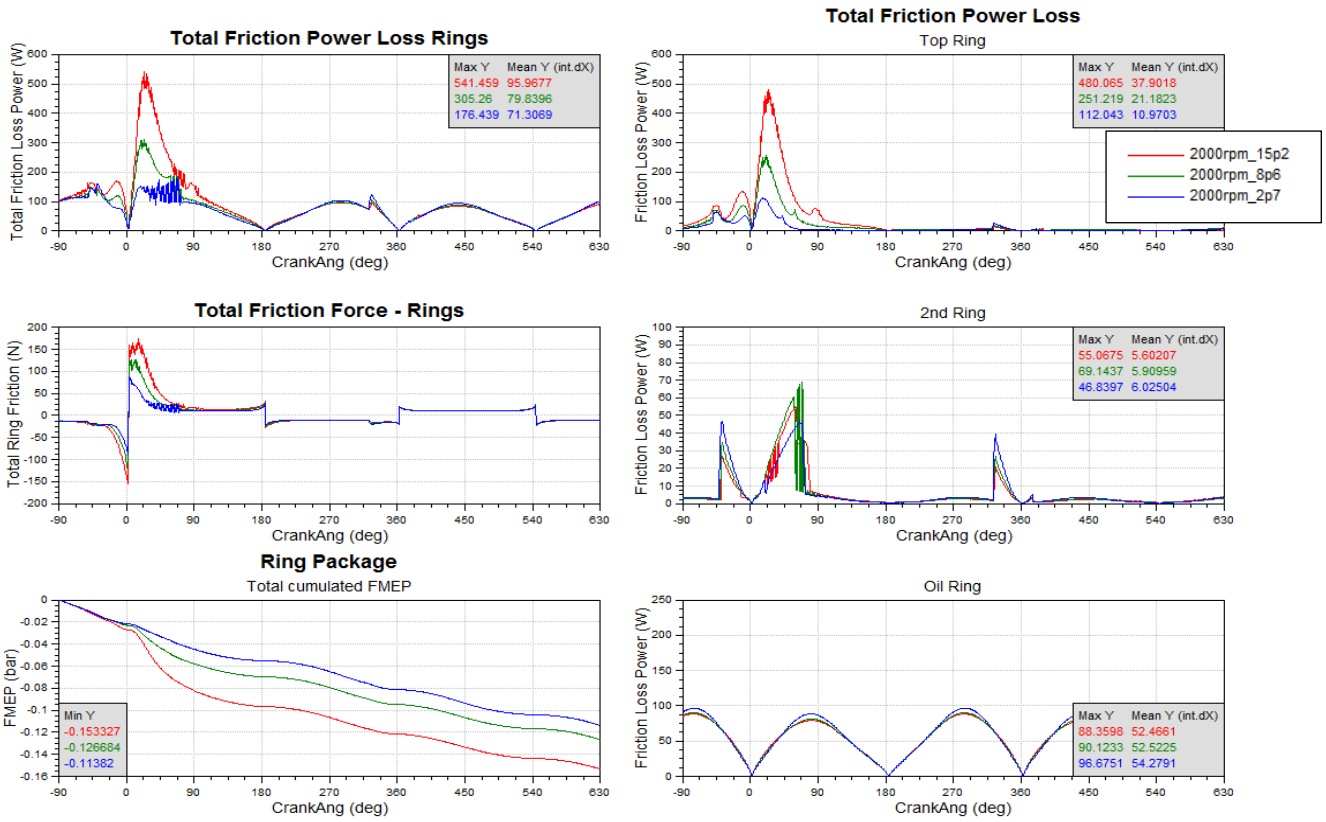

Figure A. 6. Basic ring package – Friction characteristics overview.

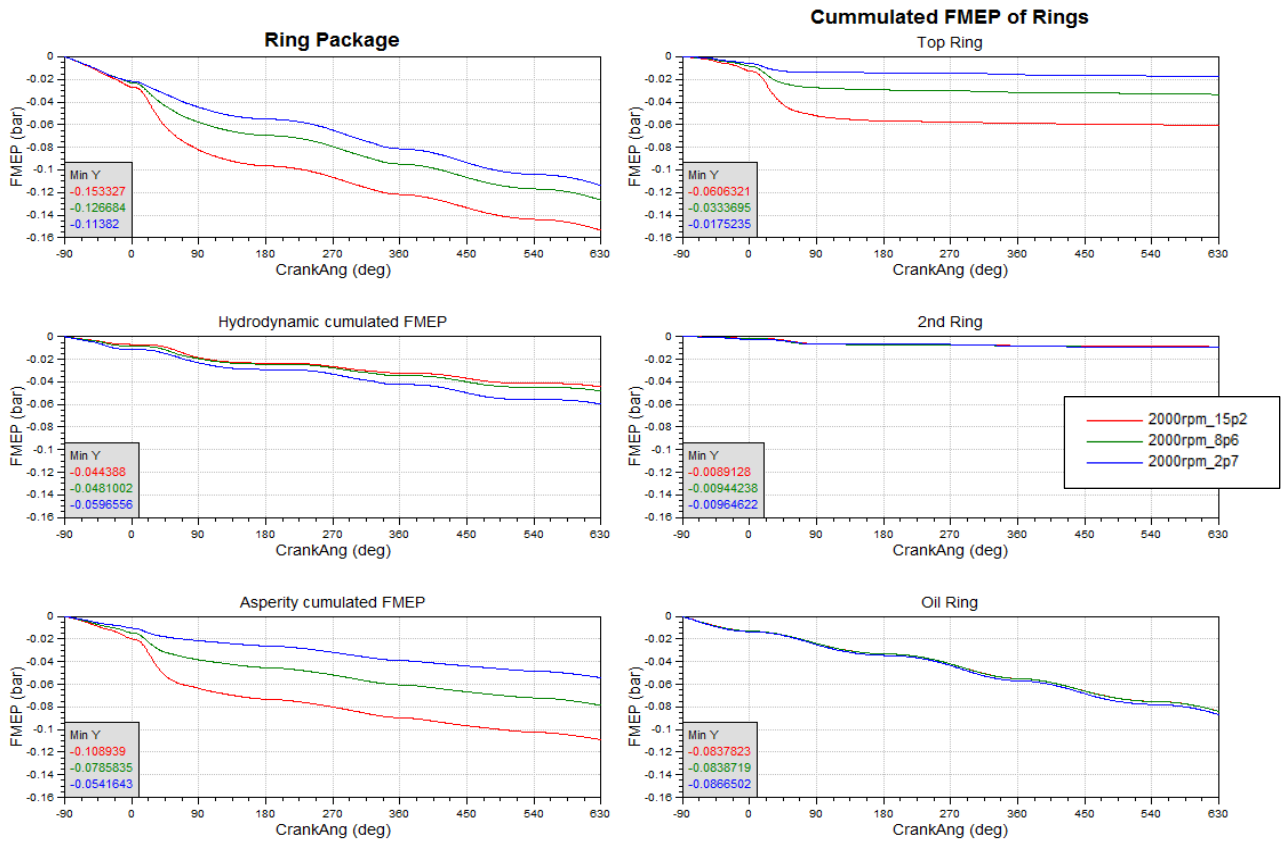

Figure A. 7. Basic ring package – FMEP overview.

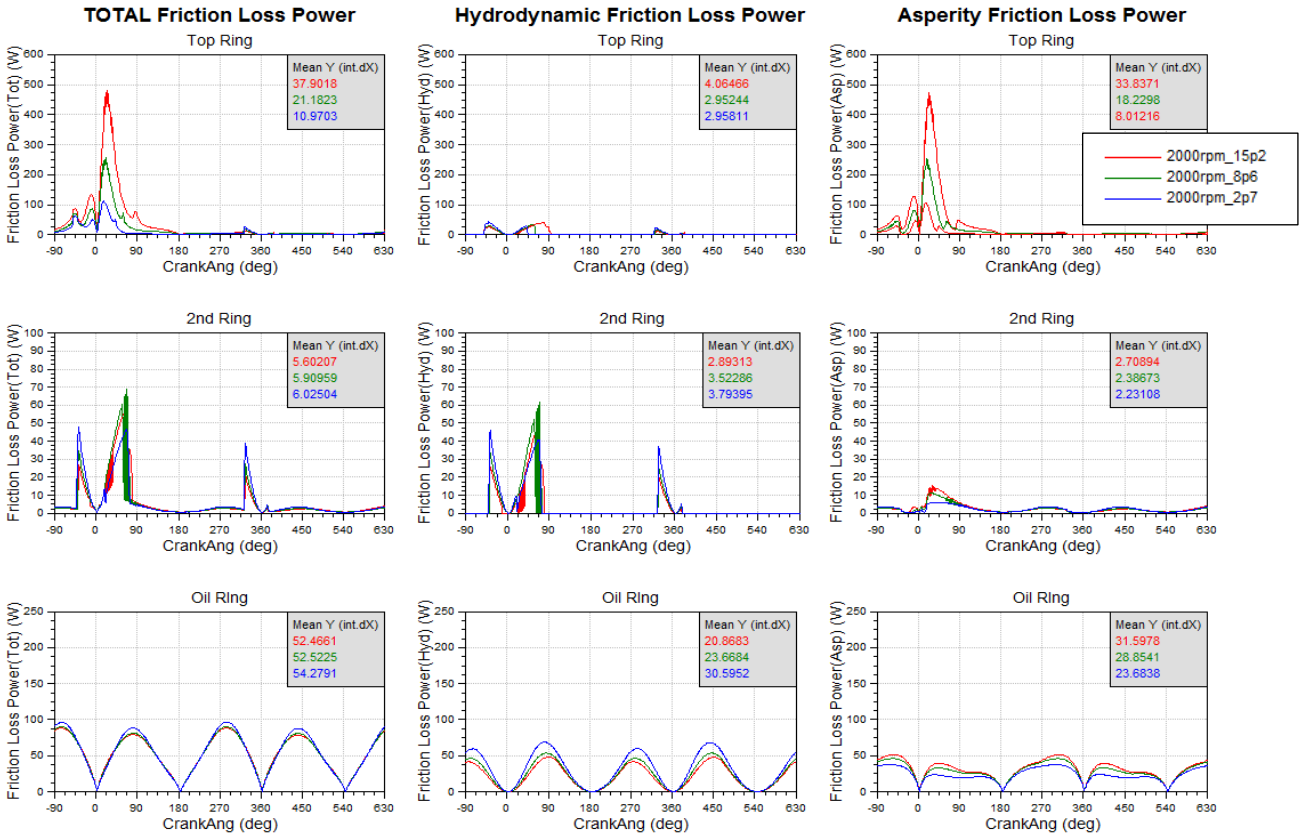

Figure A. 8. Basic ring package – Friction Power Loss overview.

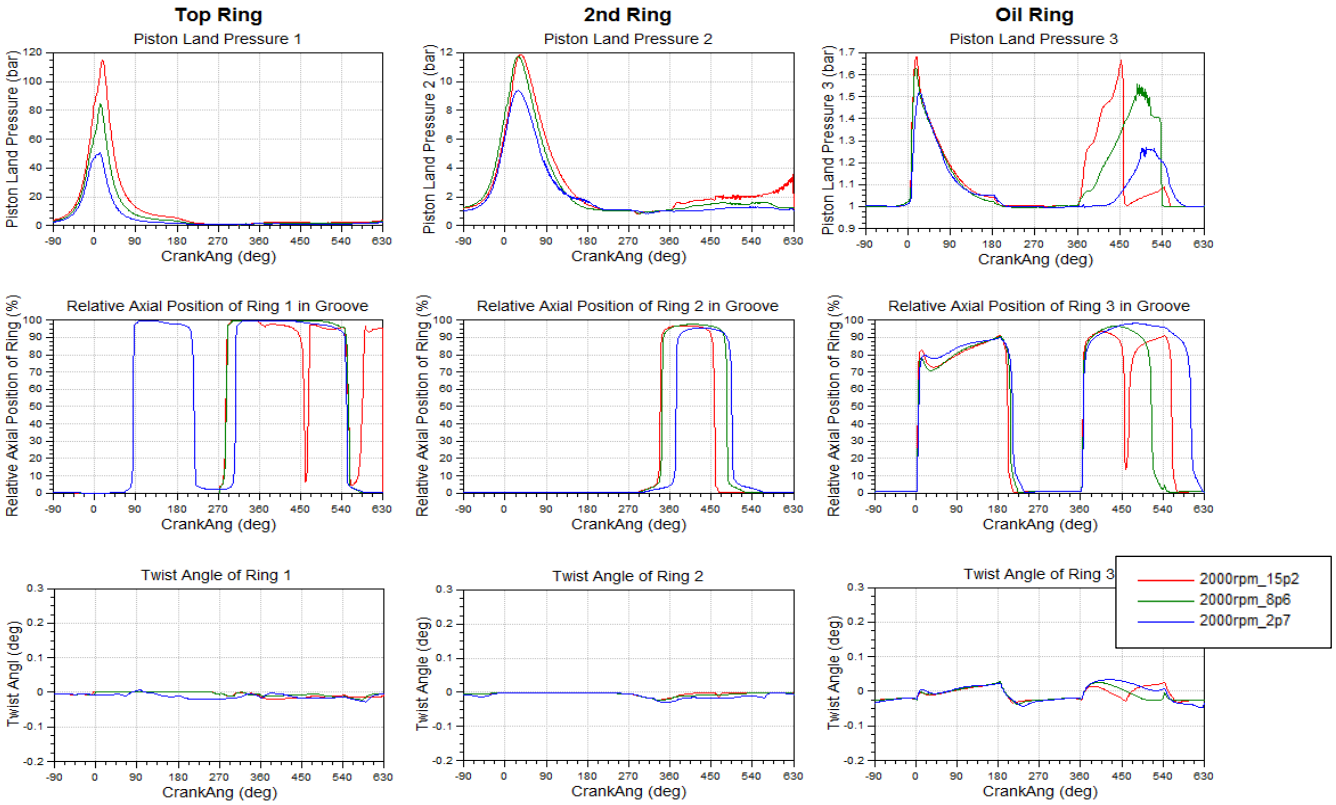

Figure A. 9. Basic ring package – Piston ring dynamics overview.

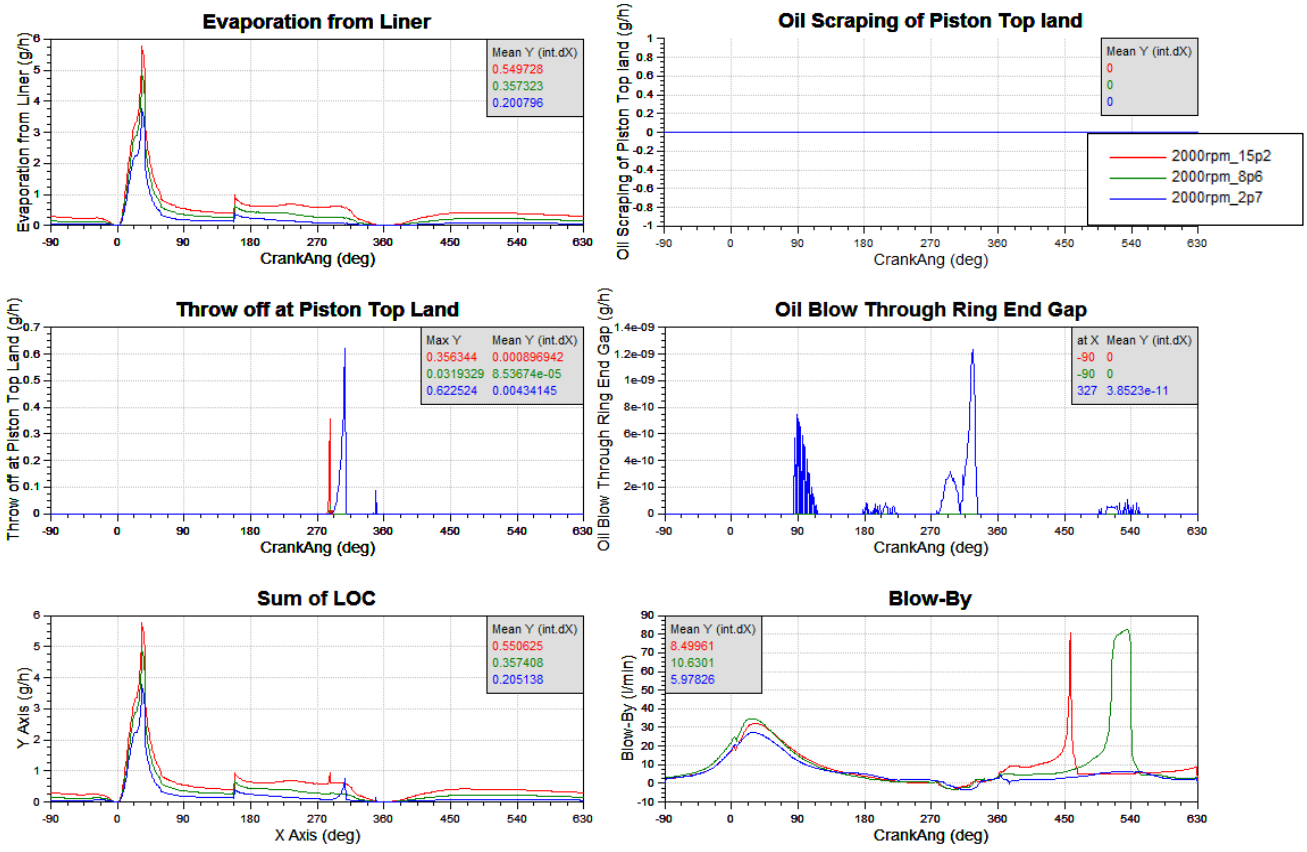

Figure A. 10. Basic ring package – Lube Oil Consumption and Blow-by overview.

Engine speed = 1500rpm

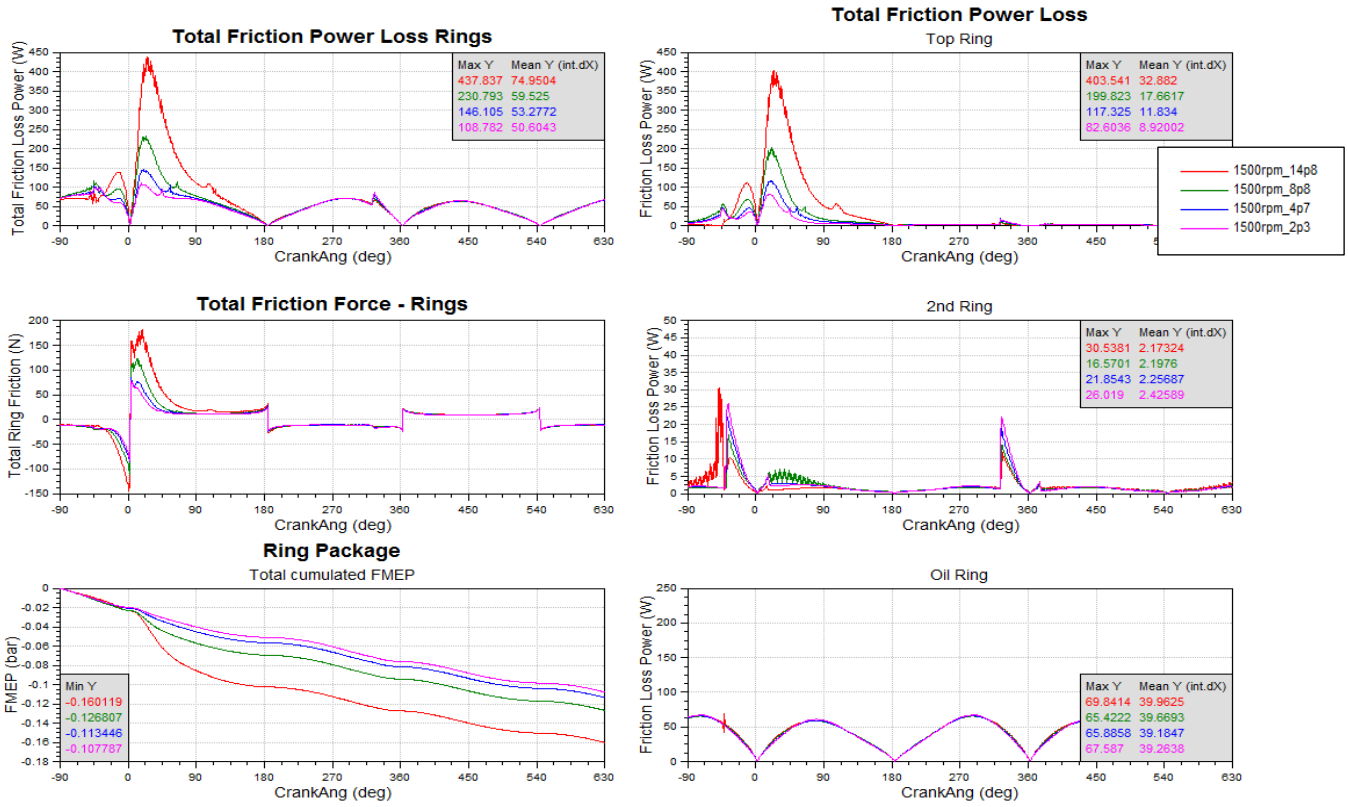

Figure A. 11. Basic ring package – Friction characteristics overview.

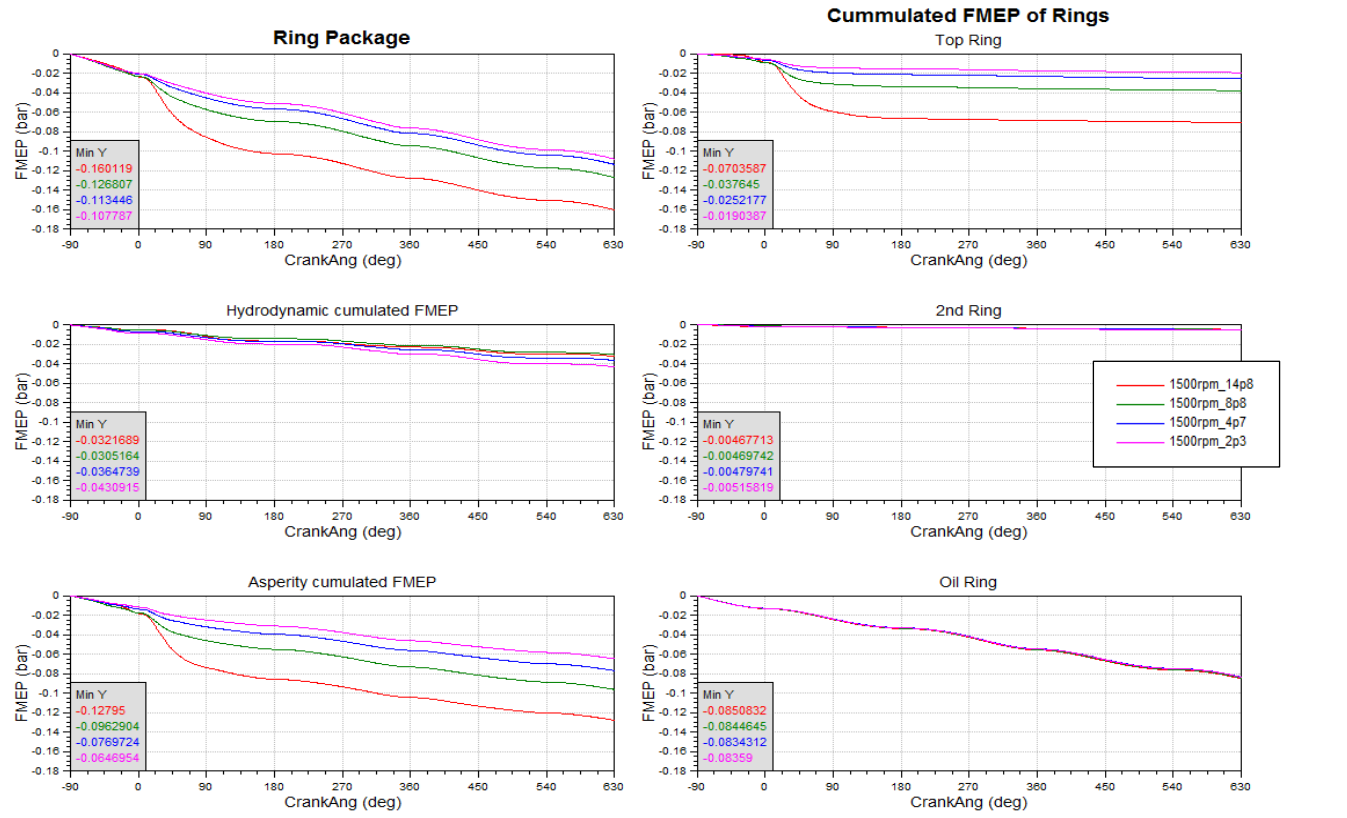

Figure A. 12. Basic ring package – FMEP overview.

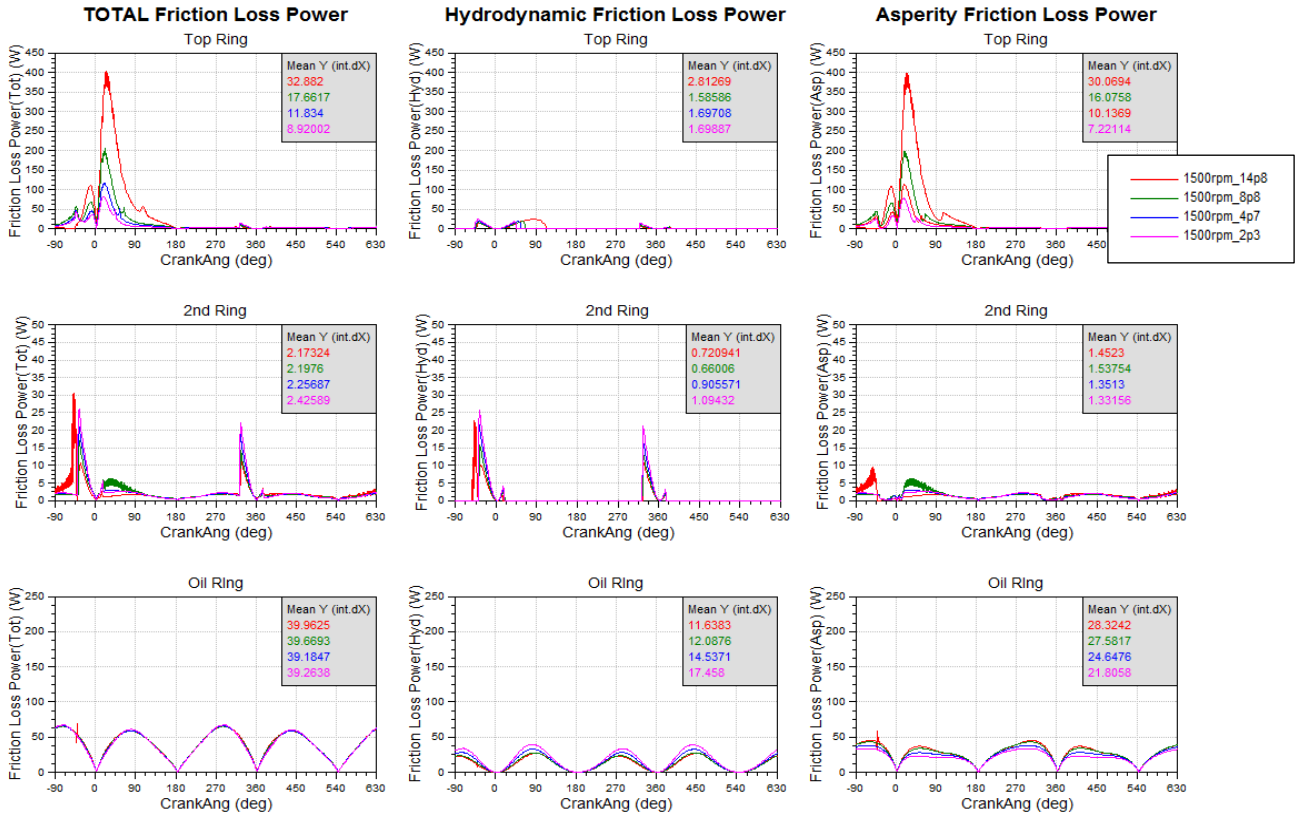

Figure A. 13. Basic ring package – Friction Power Loss overview.

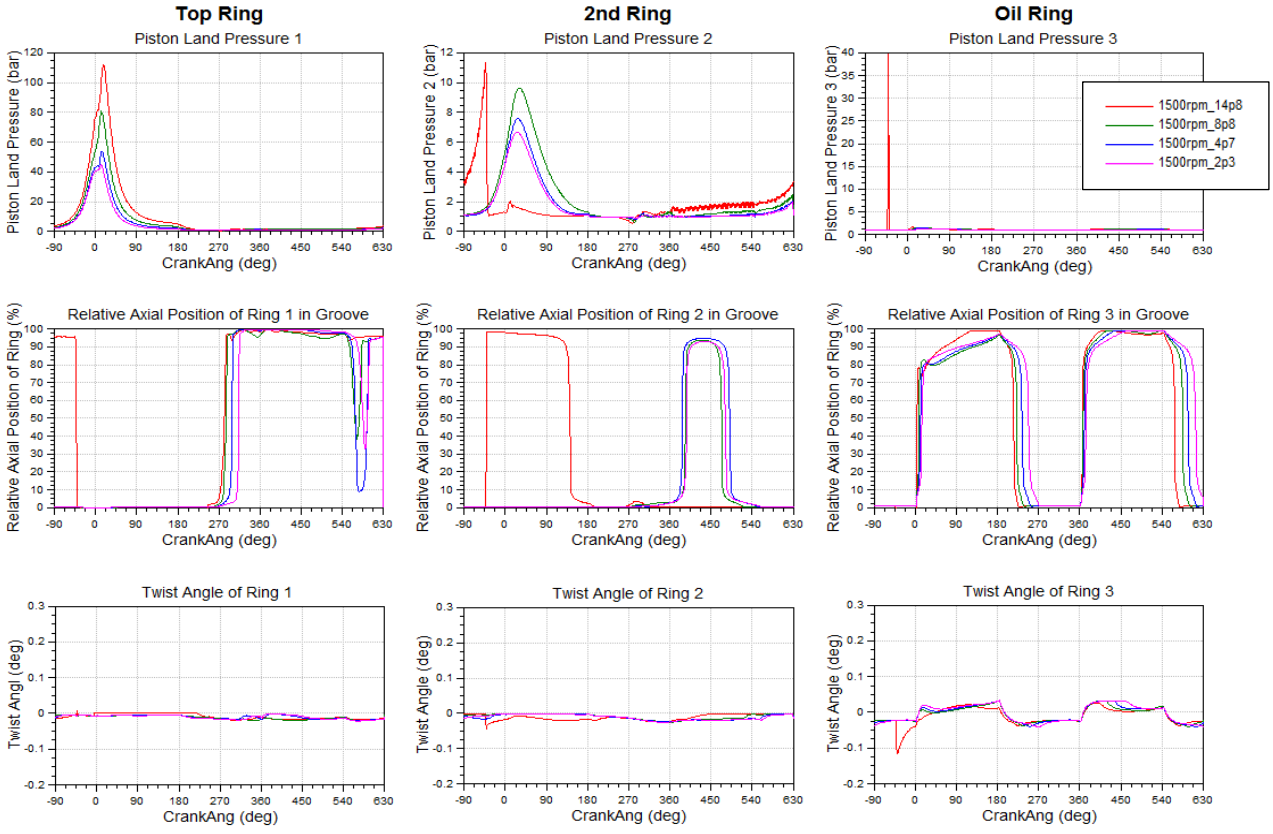

Figure A. 14. Basic ring package – Piston ring dynamics overview.

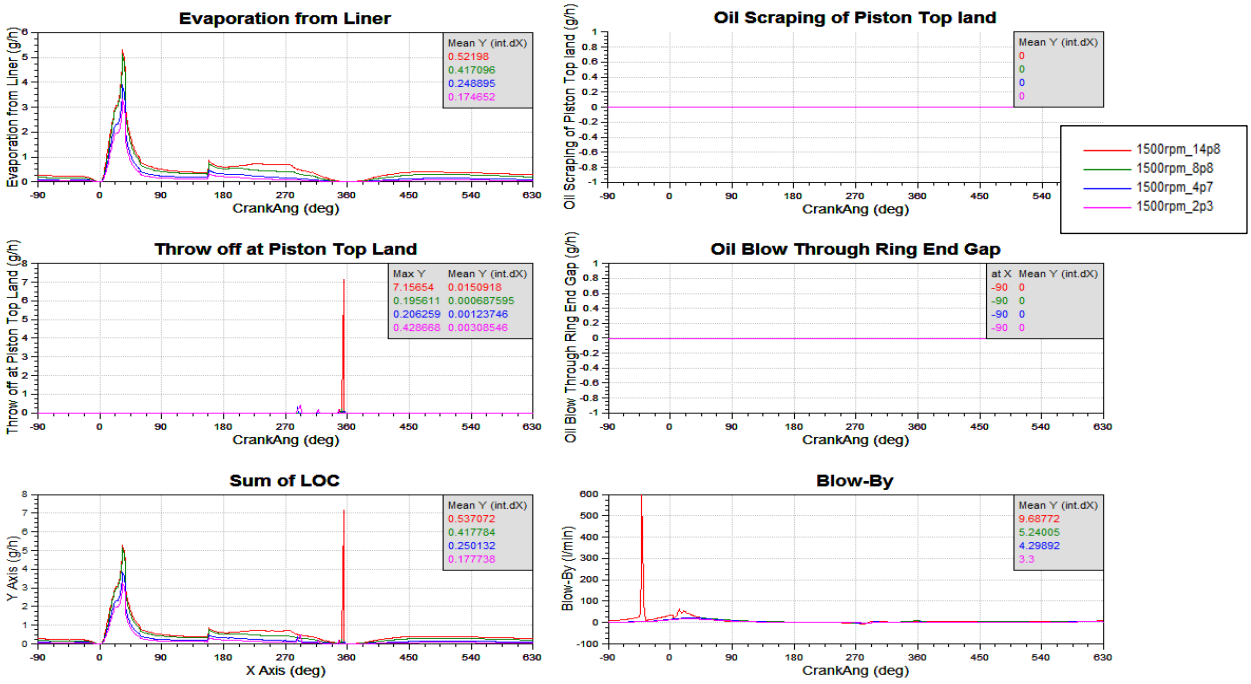

Figure A. 15. Basic ring package – Lube Oil Consumption and Blow-by overview.

Appendix B

In this appendix EXCITE™ Piston&Rings results between basic and low FT ring package for engine speed 3000 rpm are performed.

Operating point = 3000rpm_9.3

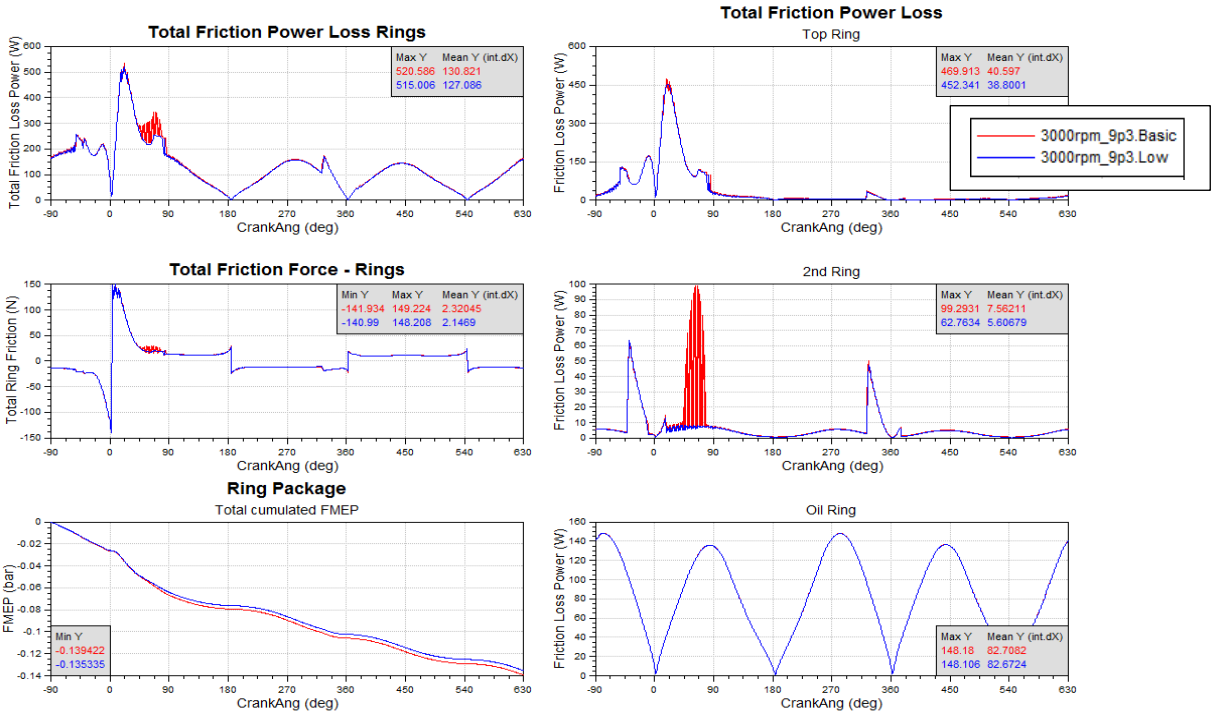

Figure B. 1. Comparison between BASIC and LOW FT ring package - Friction characteristics overview.

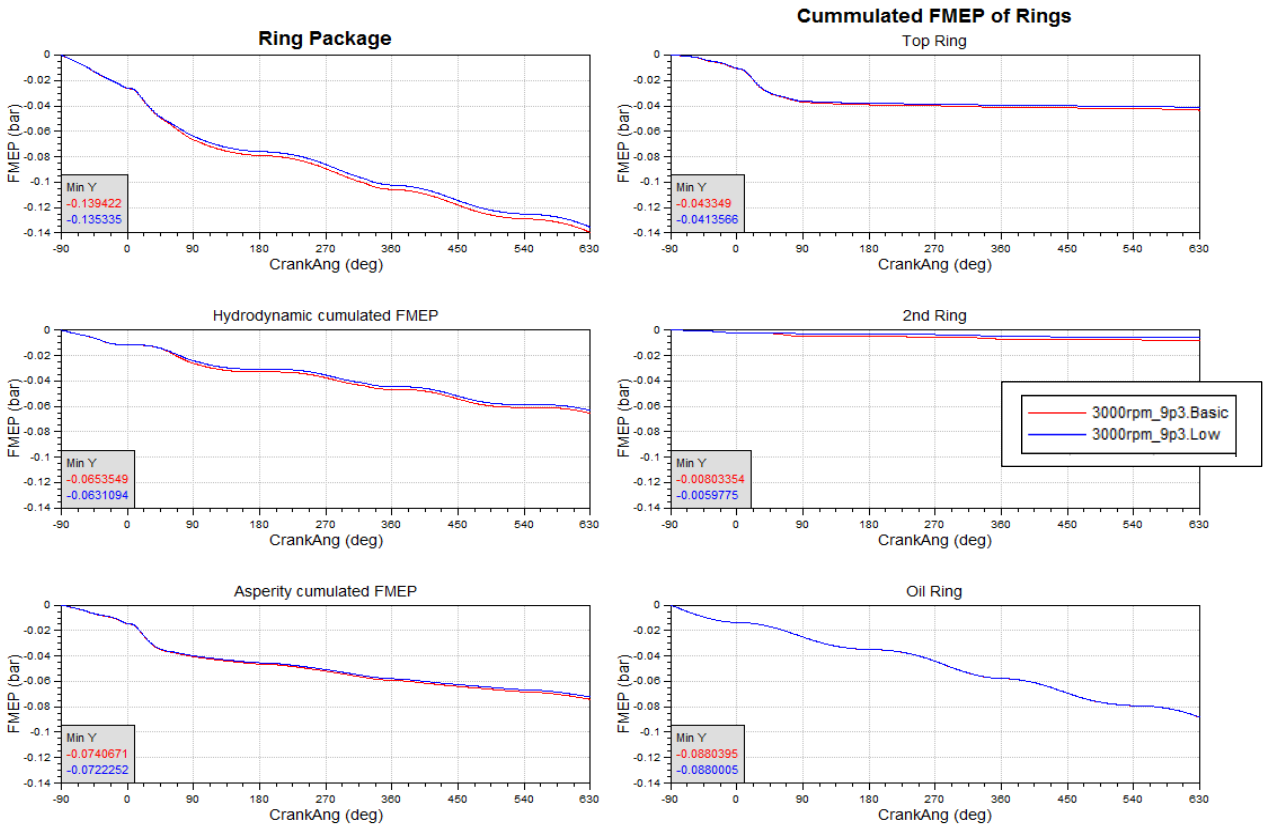

Figure B. 2. Comparison between BASIC and LOW FT ring package – FMEP overview.

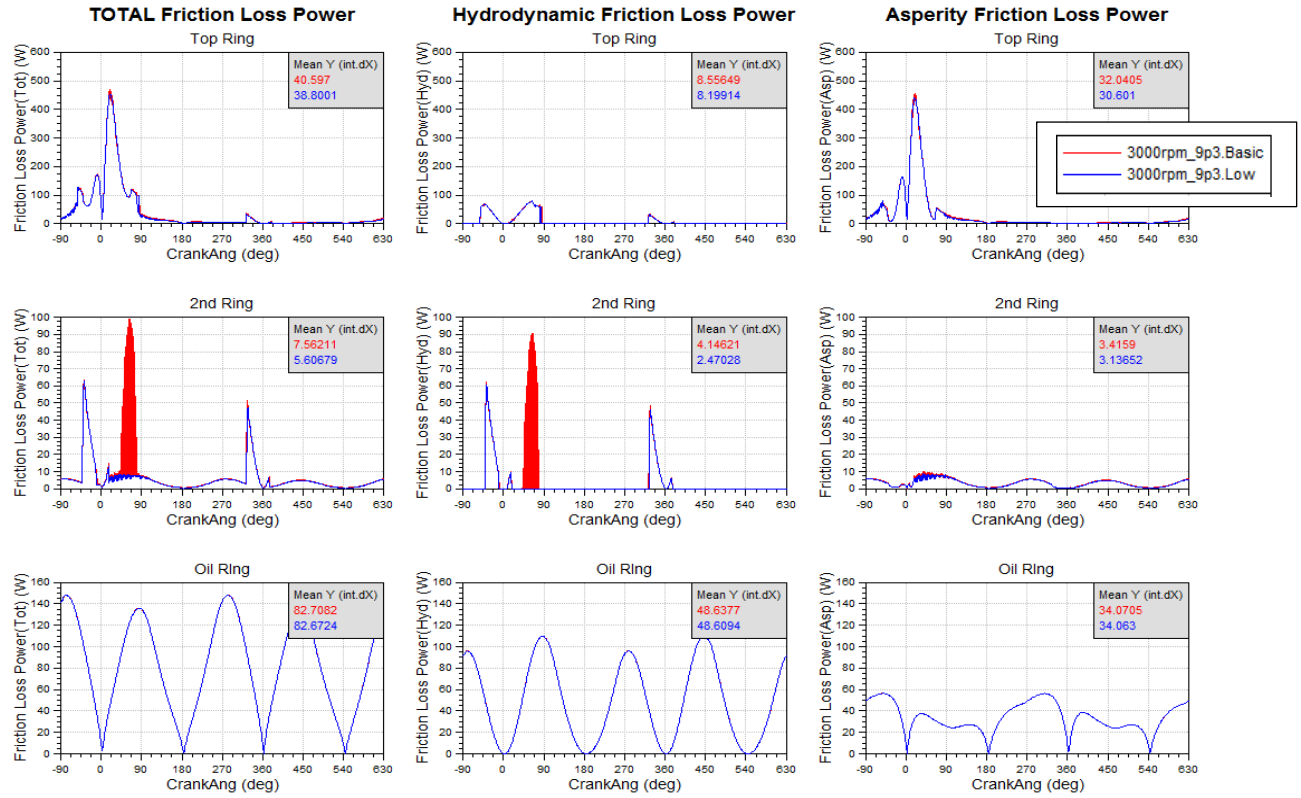

Figure B. 3. Comparison between BASIC and LOW FT ring package - Friction Power Loss overview.

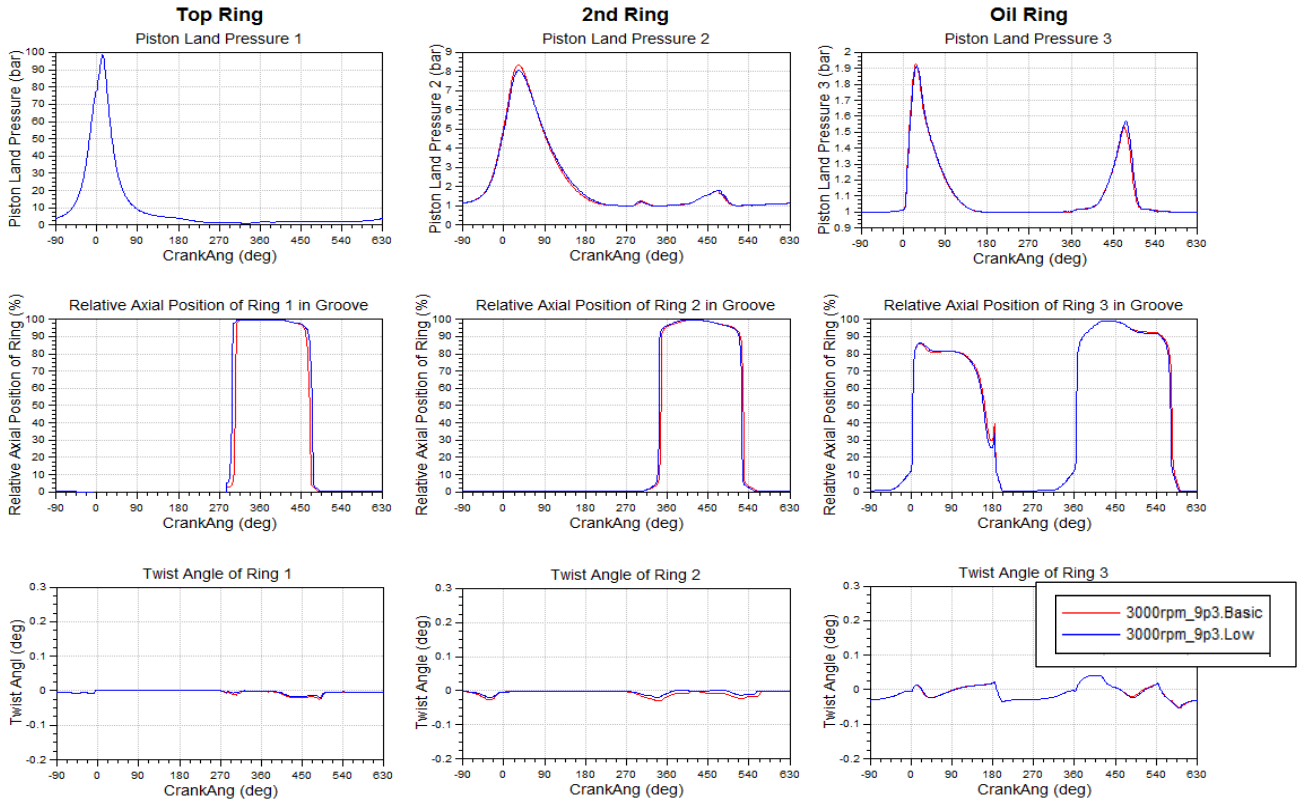

Figure B. 4. Comparison between BASIC and LOW FT ring package - Piston ring dynamics overview.

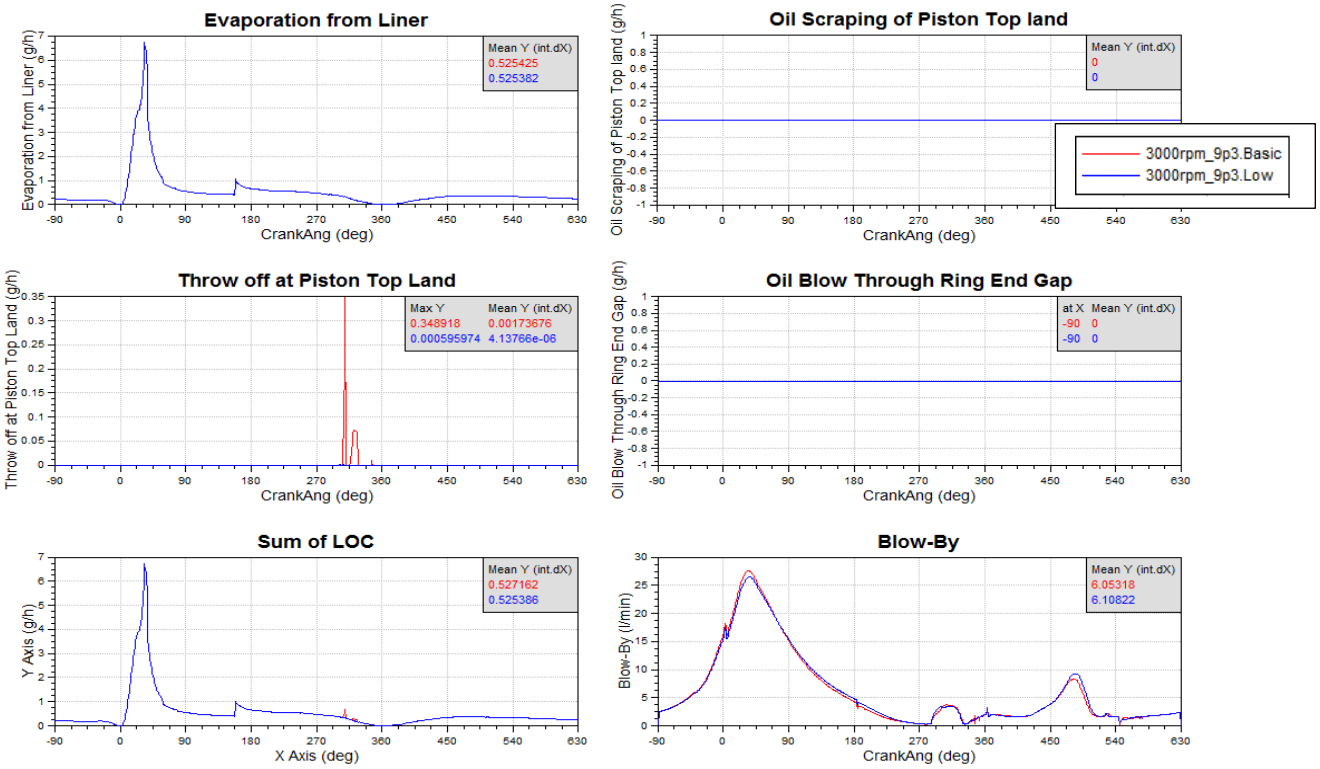

Figure B. 5. Comparison between BASIC and LOW FT ring package – Lube Oil Consumption and Blow-by overview.

Operating point = 3000rpm_5.3

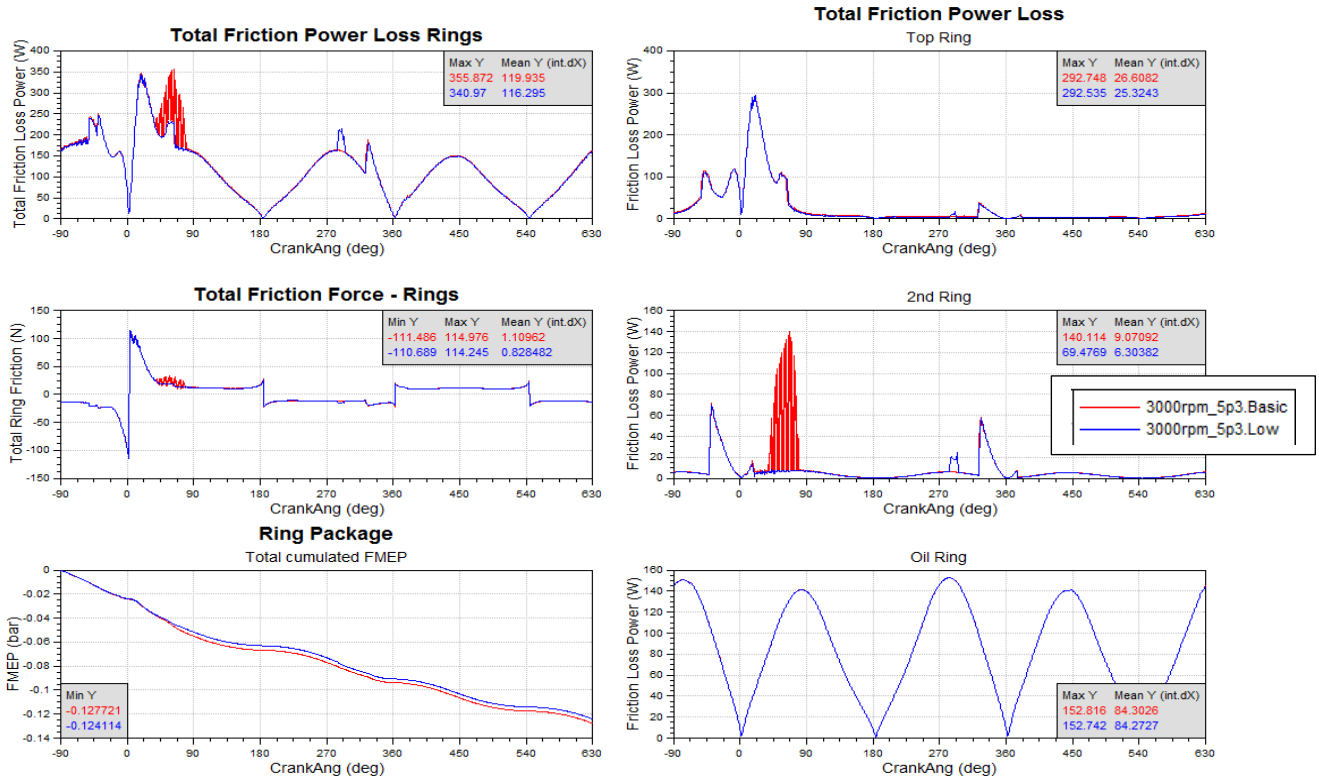

Figure B. 6. Comparison between BASIC and LOW FT ring package - Friction characteristics overview.

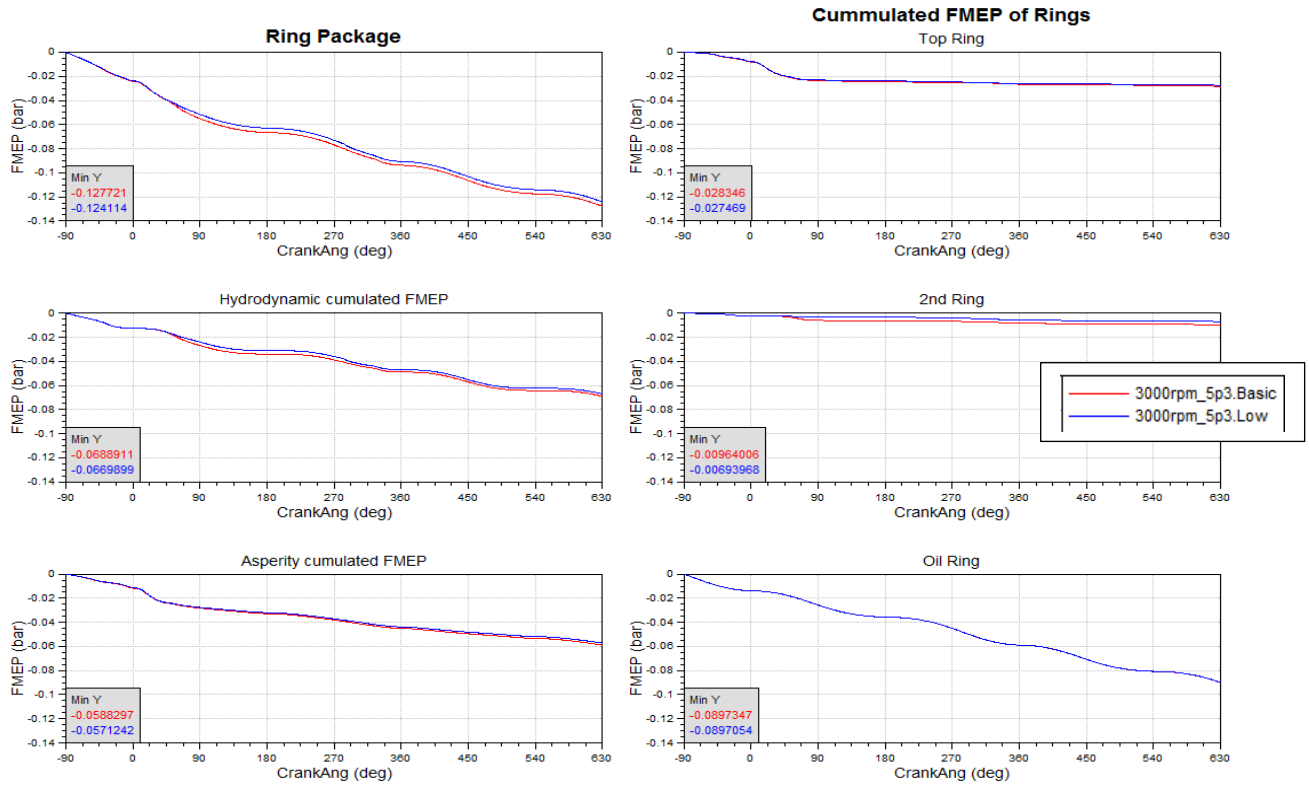

Figure B. 7. Comparison between BASIC and LOW FT ring package – FMEP overview.

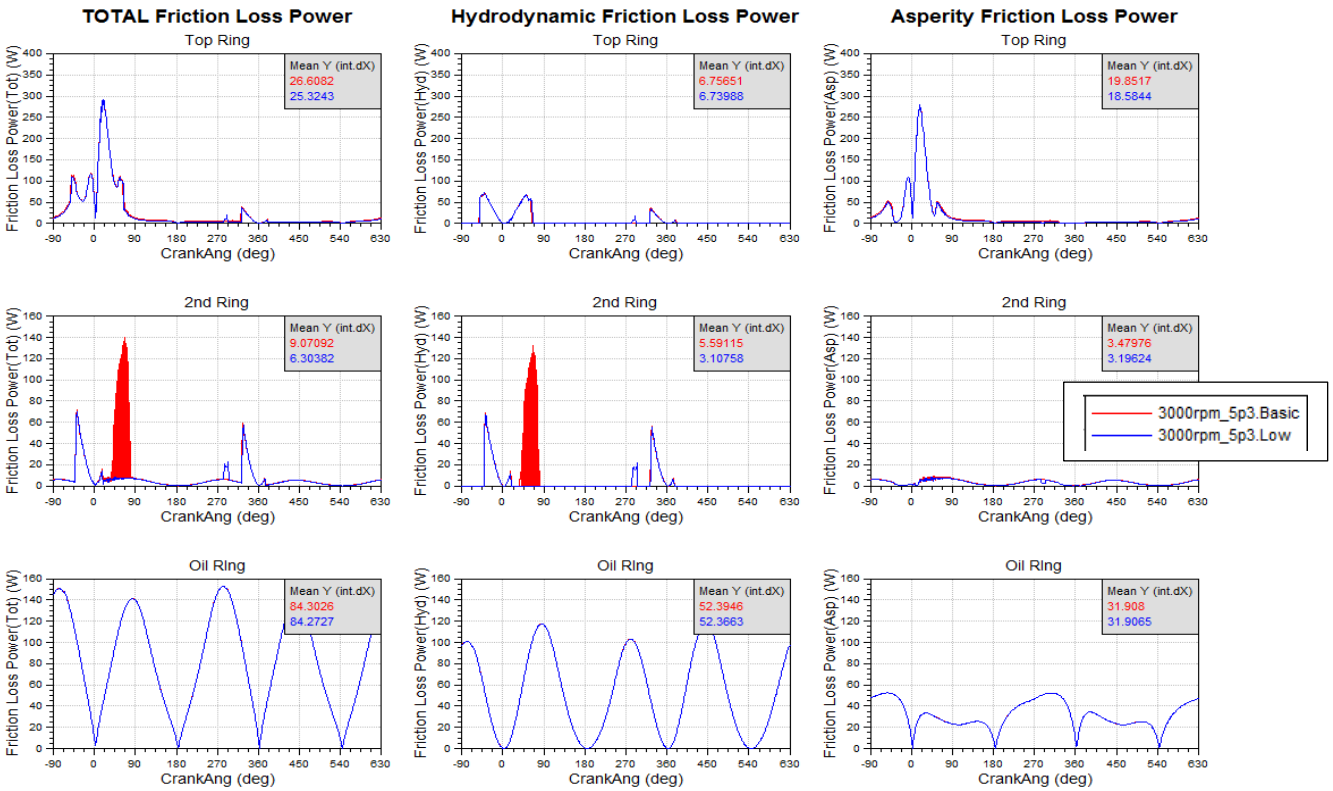

Figure B. 8. Comparison between BASIC and LOW FT ring package - Friction Power Loss overview.

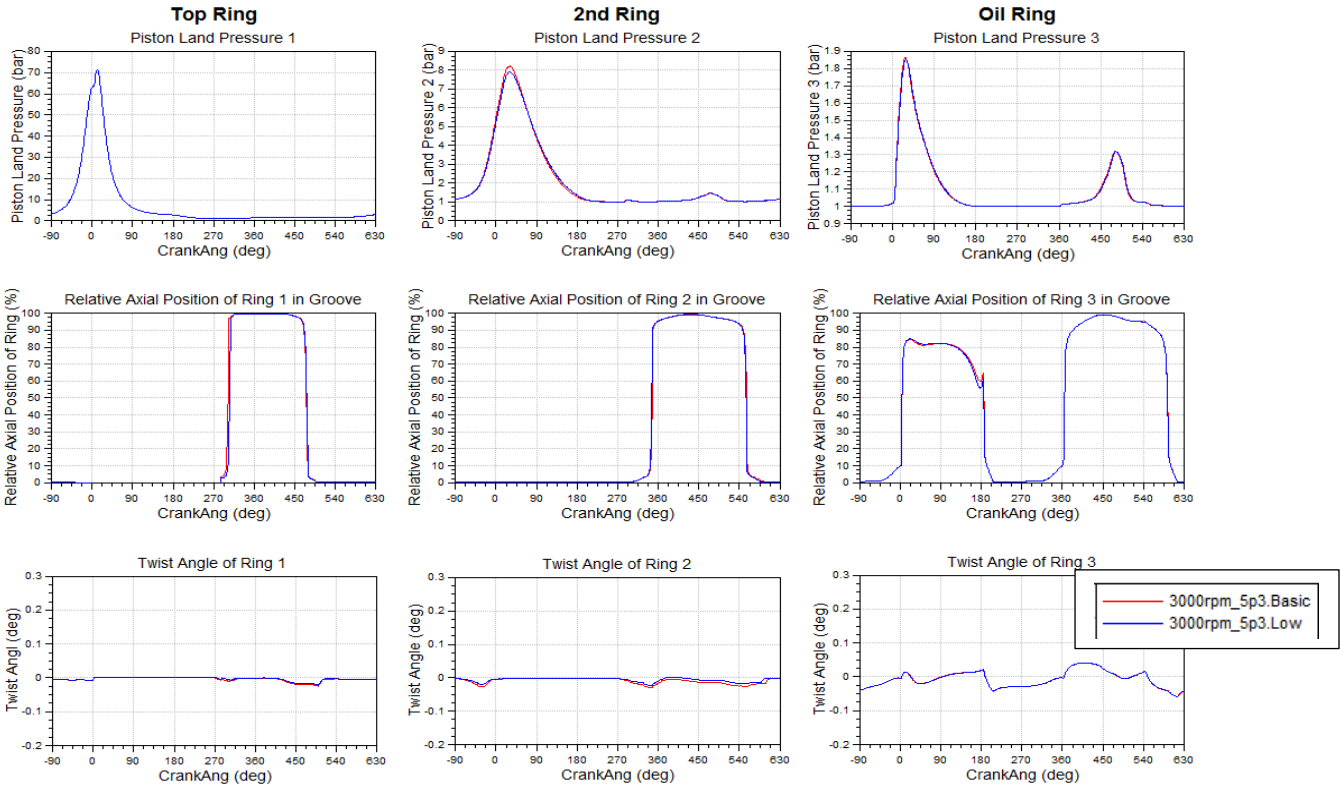

Figure B. 9. Comparison between BASIC and LOW FT ring package - Piston ring dynamics overview.

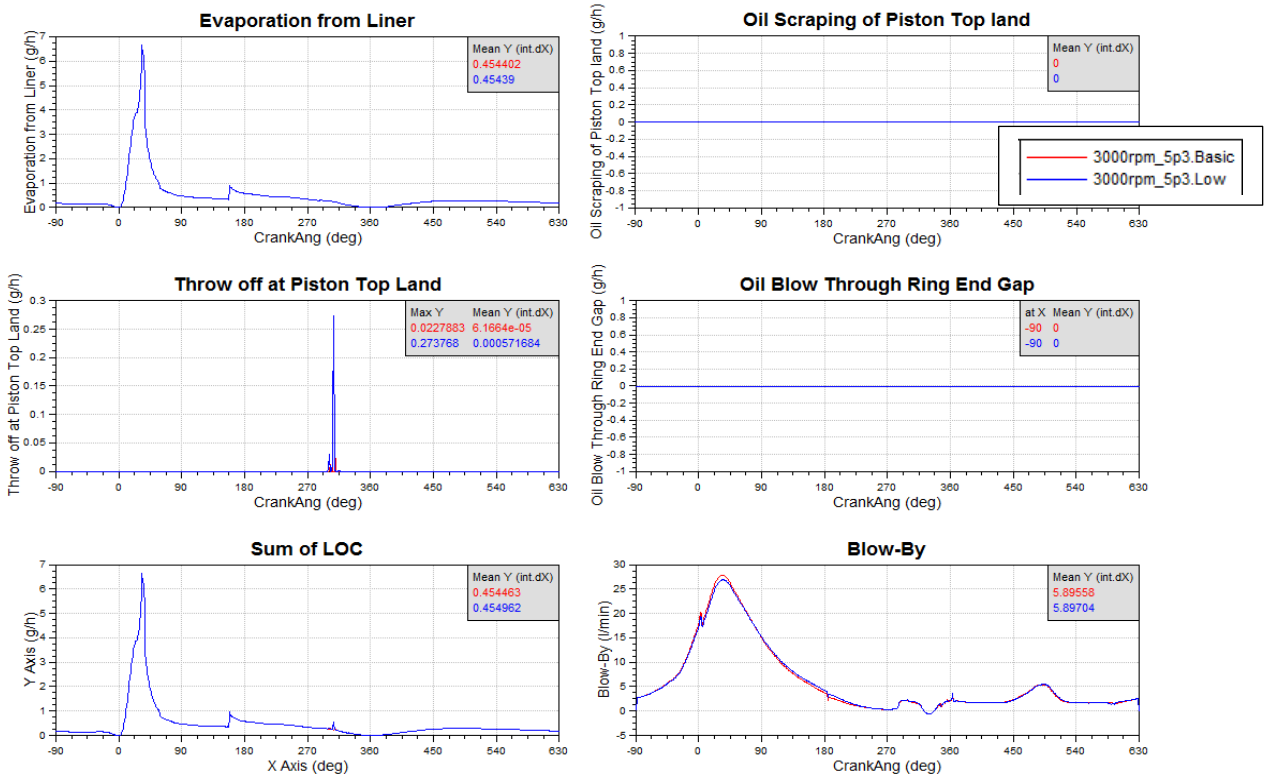

Figure B. 10. Comparison between BASIC and LOW FT ring package – Lube Oil Consumption and Blow-by overview.

Operating point = 3000rpm_2.9

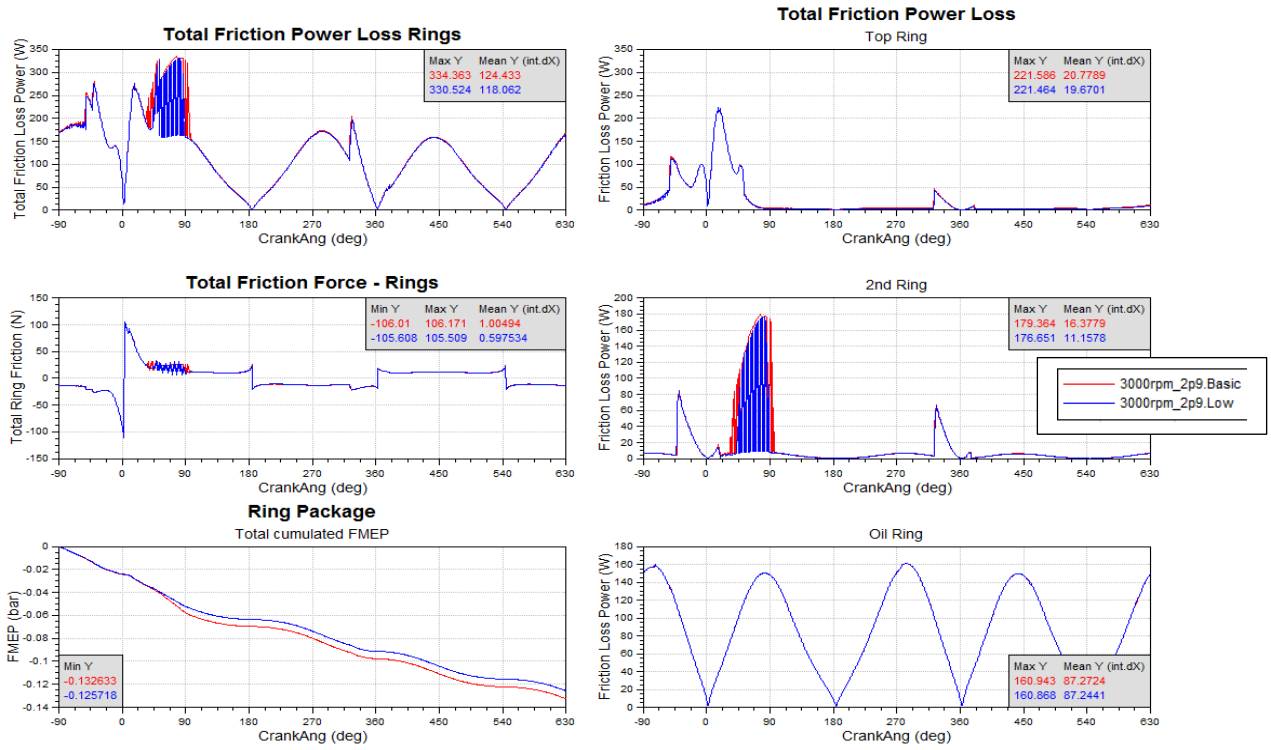

Figure B. 11. Comparison between BASIC and LOW FT ring package - Friction characteristics overview.

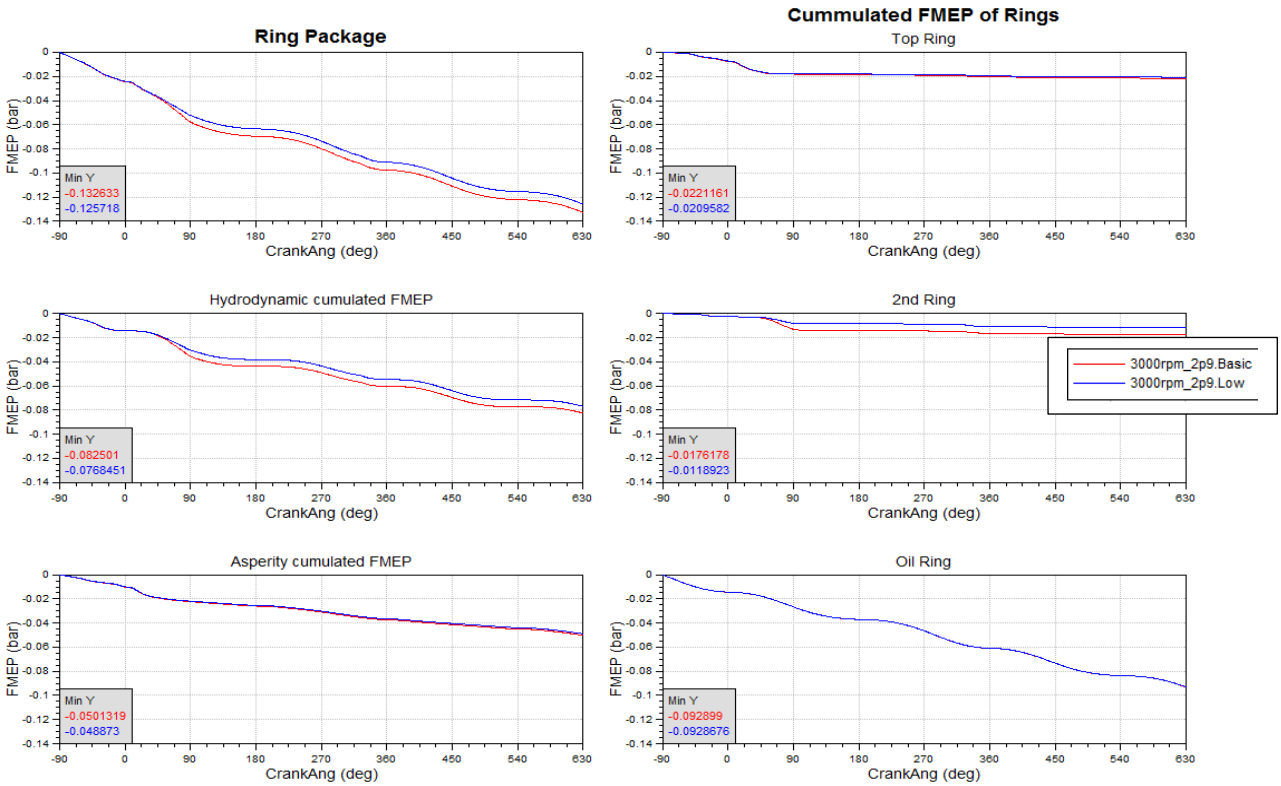

Figure B. 12. Comparison between BASIC and LOW FT ring package – FMEP overview.

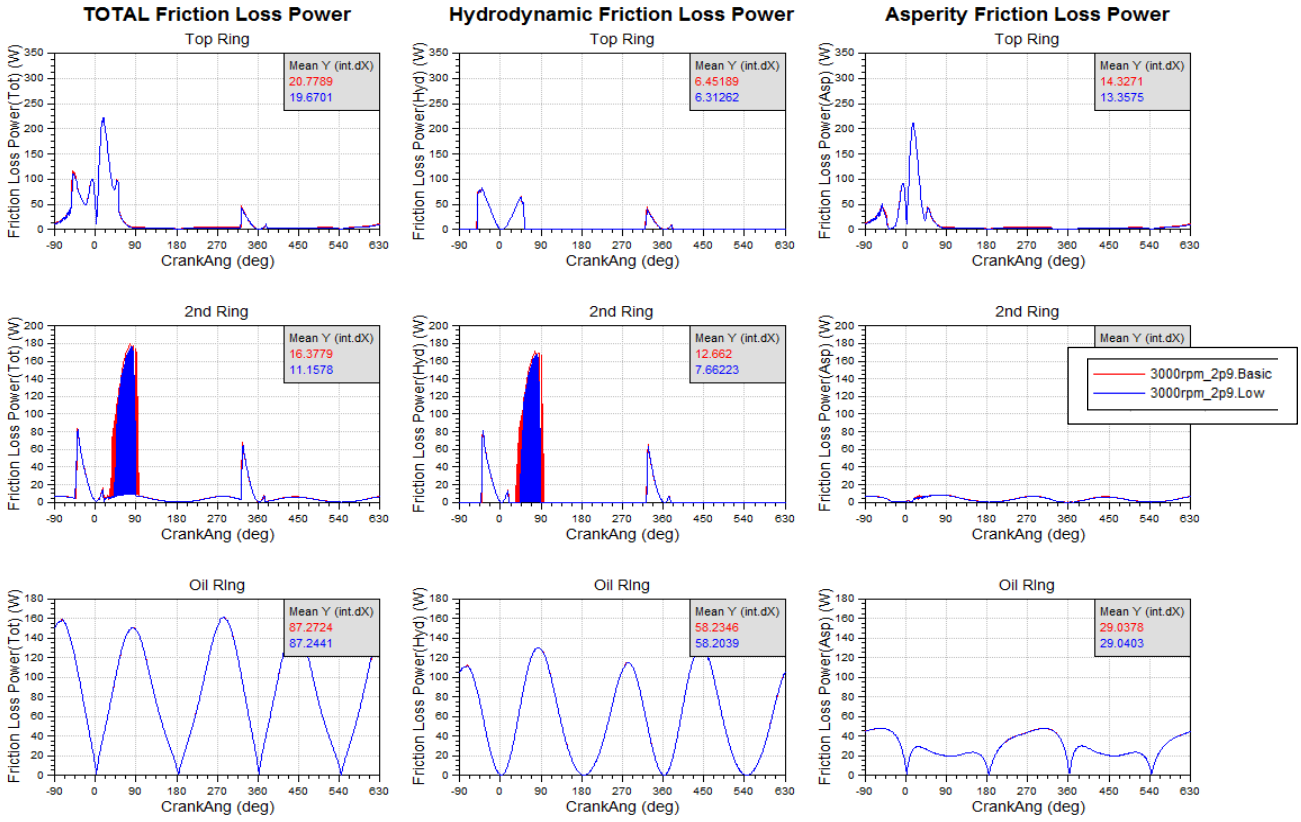

Figure B. 13. Comparison between BASIC and LOW FT ring package - Friction Power Loss overview.

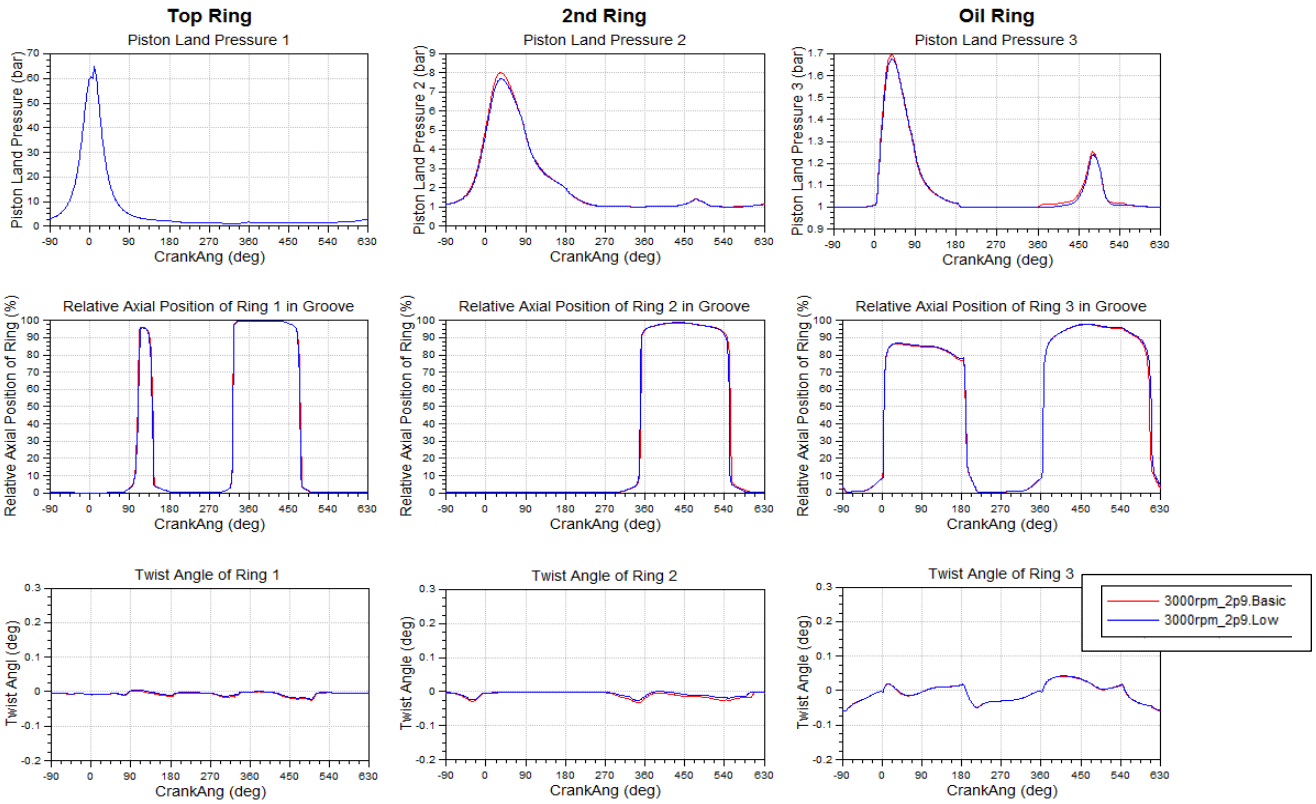

Figure B. 14. Comparison between BASIC and LOW FT ring package - Piston ring dynamics overview.

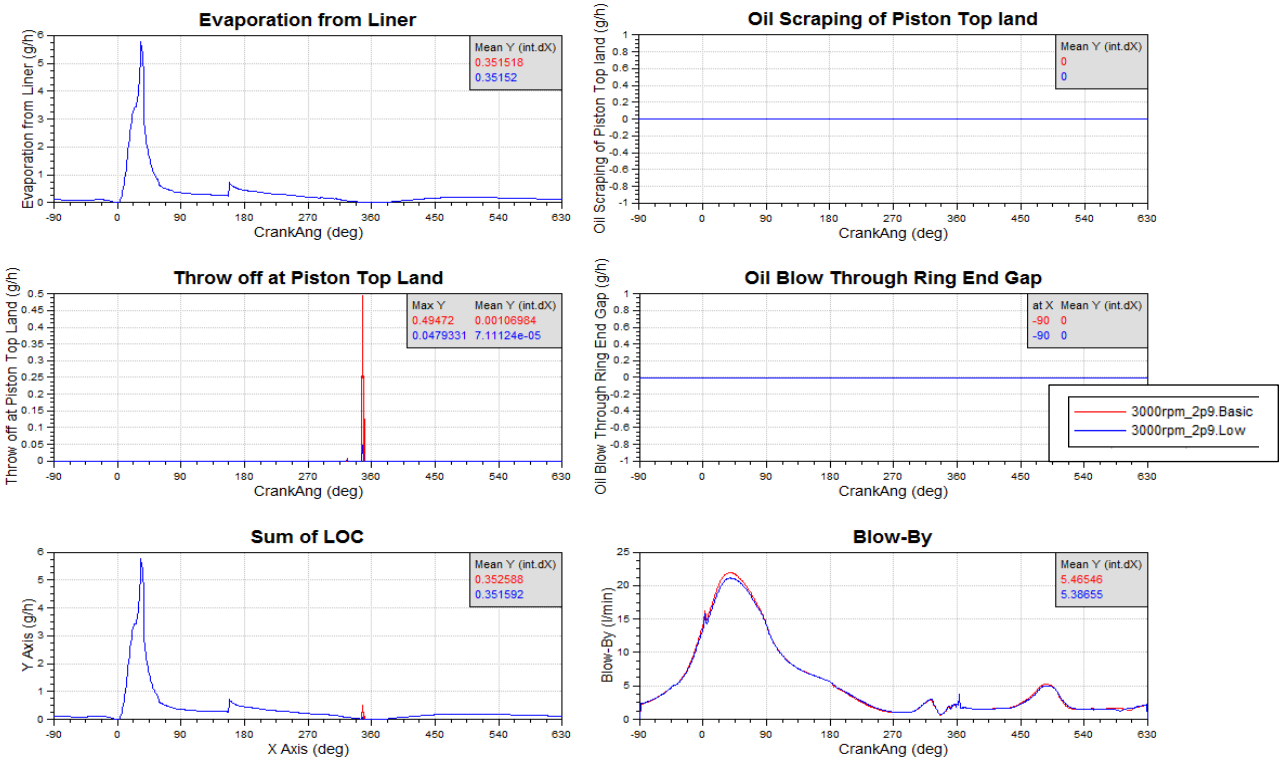

Figure B. 15. Comparison between BASIC and LOW FT ring package – Lube Oil Consumption and Blow-by overview.

Appendix C

In this appendix EXCITE™ Piston&Rings results between 2D and 3D basic ring package for engine speed 3000 rpm are performed.

Operating point = 3000rpm_9.3

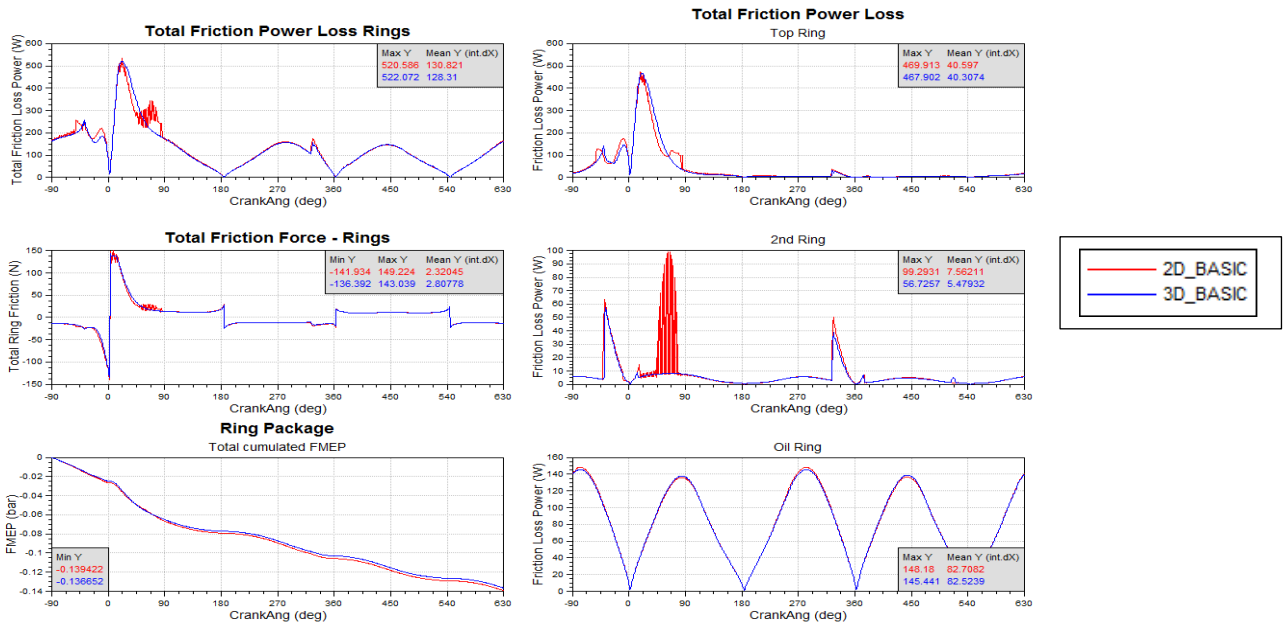

Figure C. 1. Comparison between BASIC and LOW FT ring package – Friction characteristics overview.

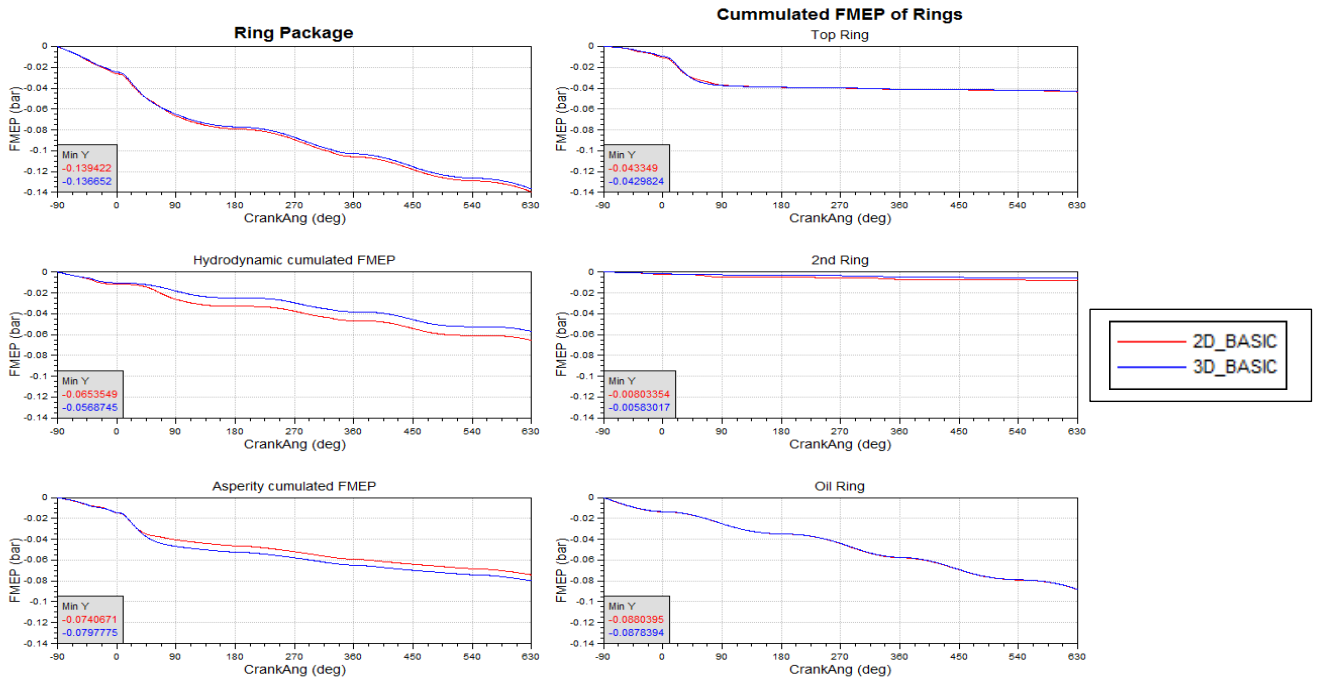

Figure C. 2. Comparison between 2D and 3D basic ring package – FMEP overview.

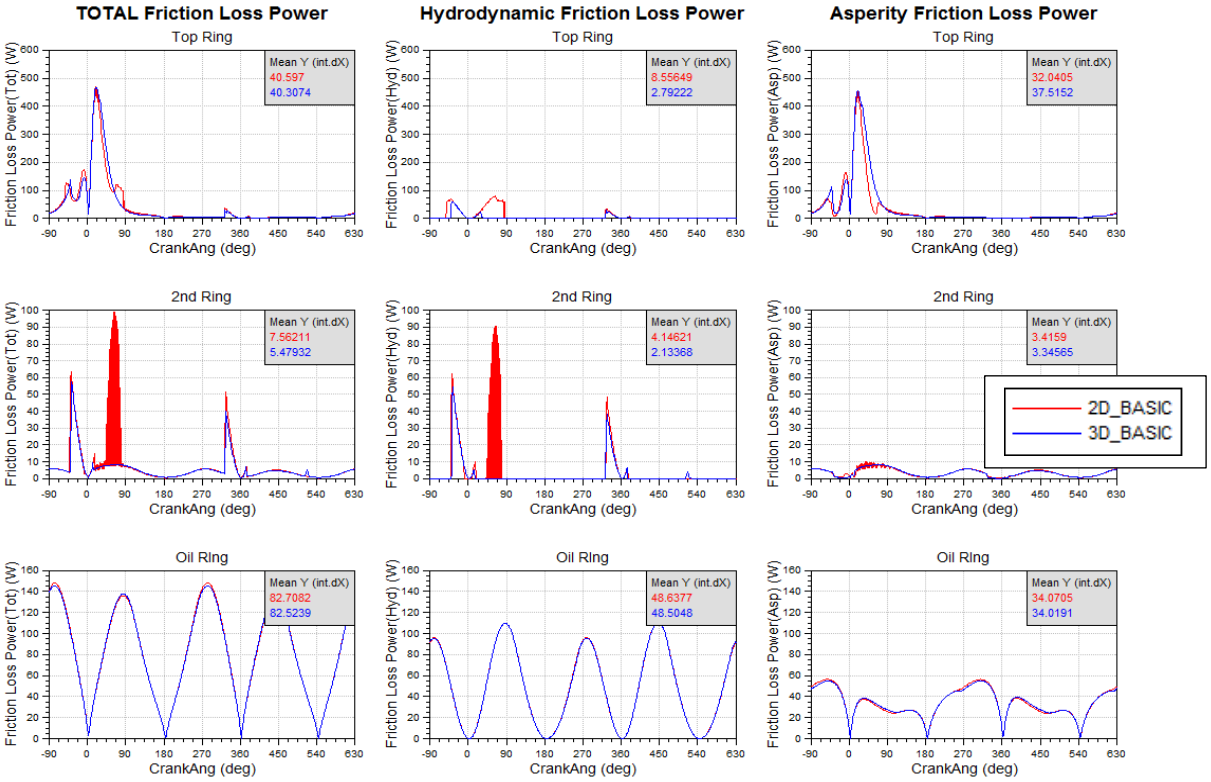

Figure C. 3. Comparison between 2D and 3D basic ring package - Friction Power Loss overview.

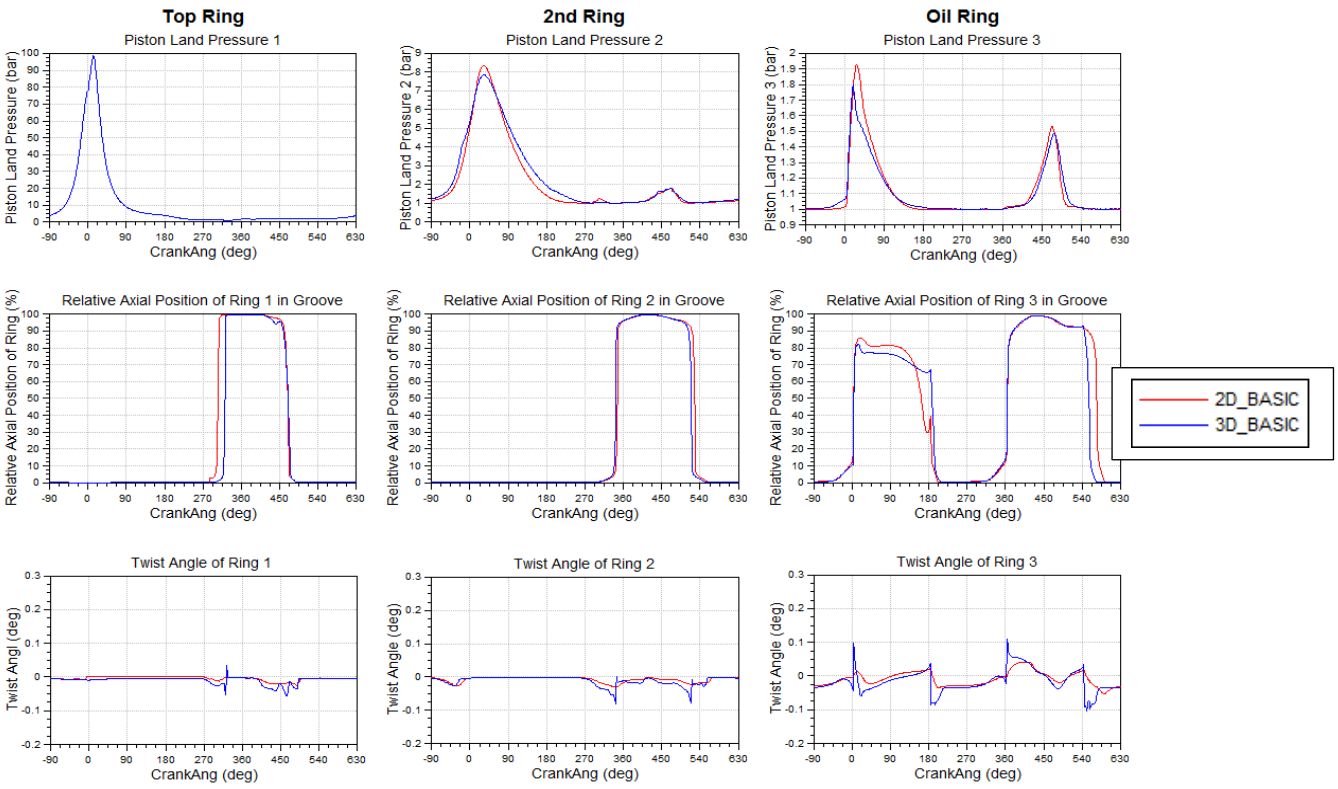

Figure C. 4. Comparison between 2D and 3D basic ring package - Piston ring dynamics overview.

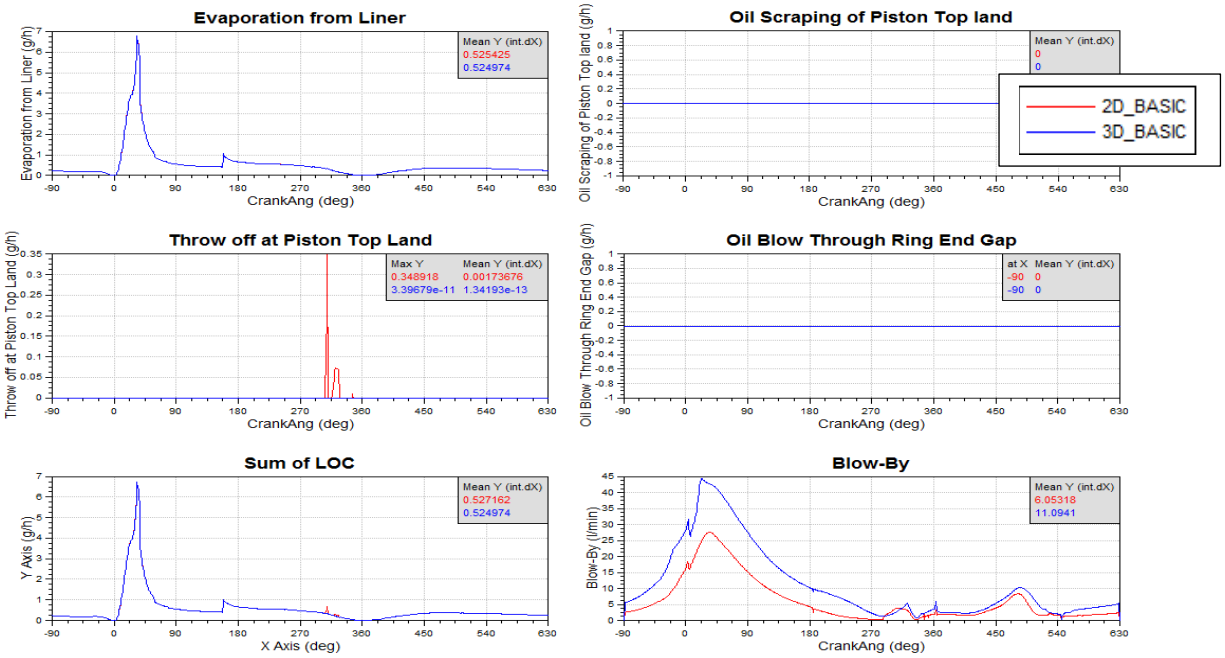

Figure C. 5. Comparison between 2D and 3D basic ring package – Lube Oil Consumption and Blow-by overview.

Operating point = 3000rpm_5.3

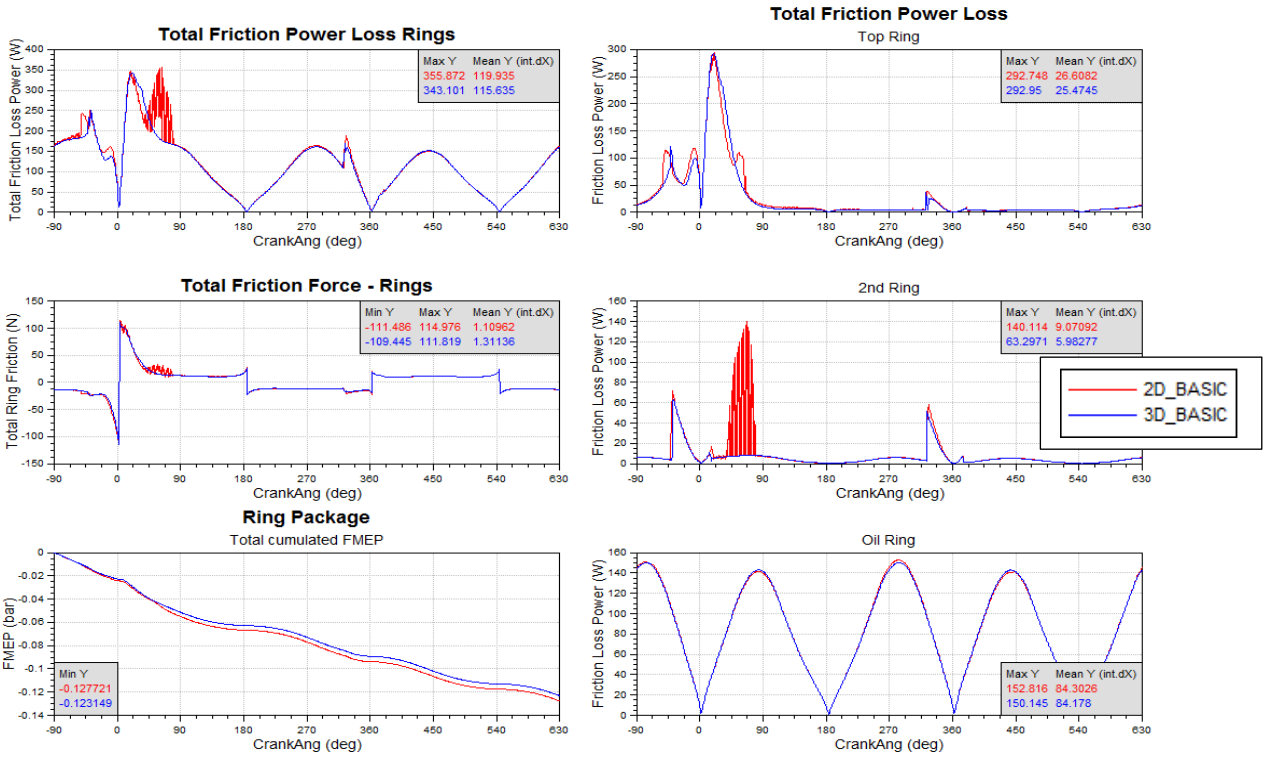

Figure C. 6. Comparison between 2D and 3D basic ring package - Friction characteristics overview.

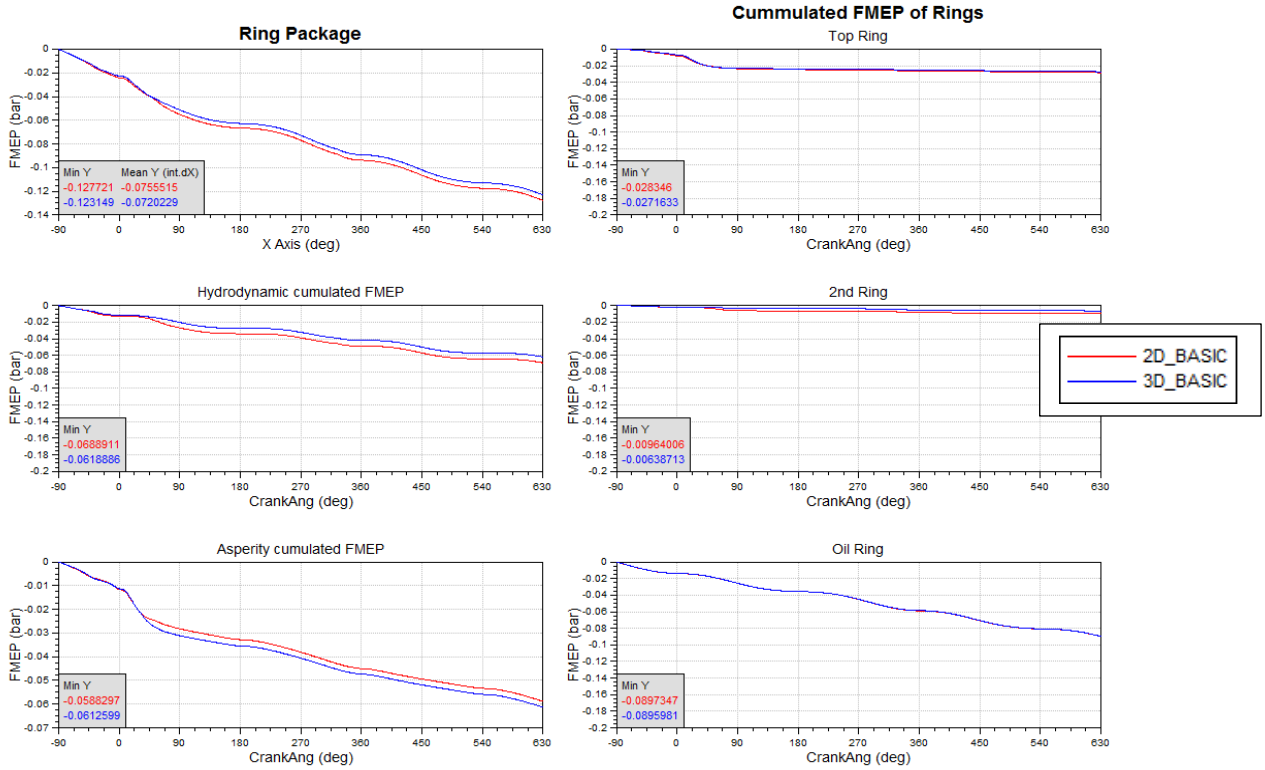

Figure C. 7. Comparison between 2D and 3D basic ring package – FMEP overview.

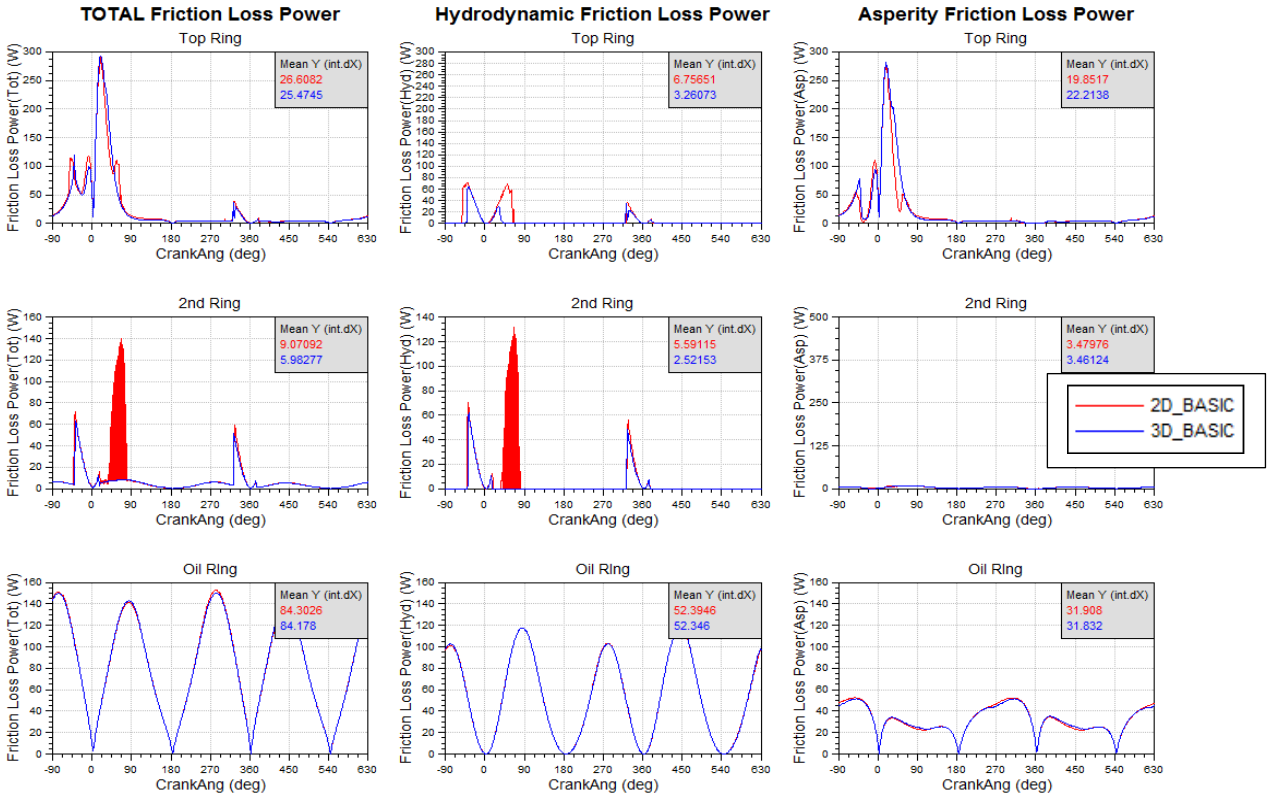

Figure C. 8. Comparison between 2D and 3D basic ring package - Friction Power Loss overview.

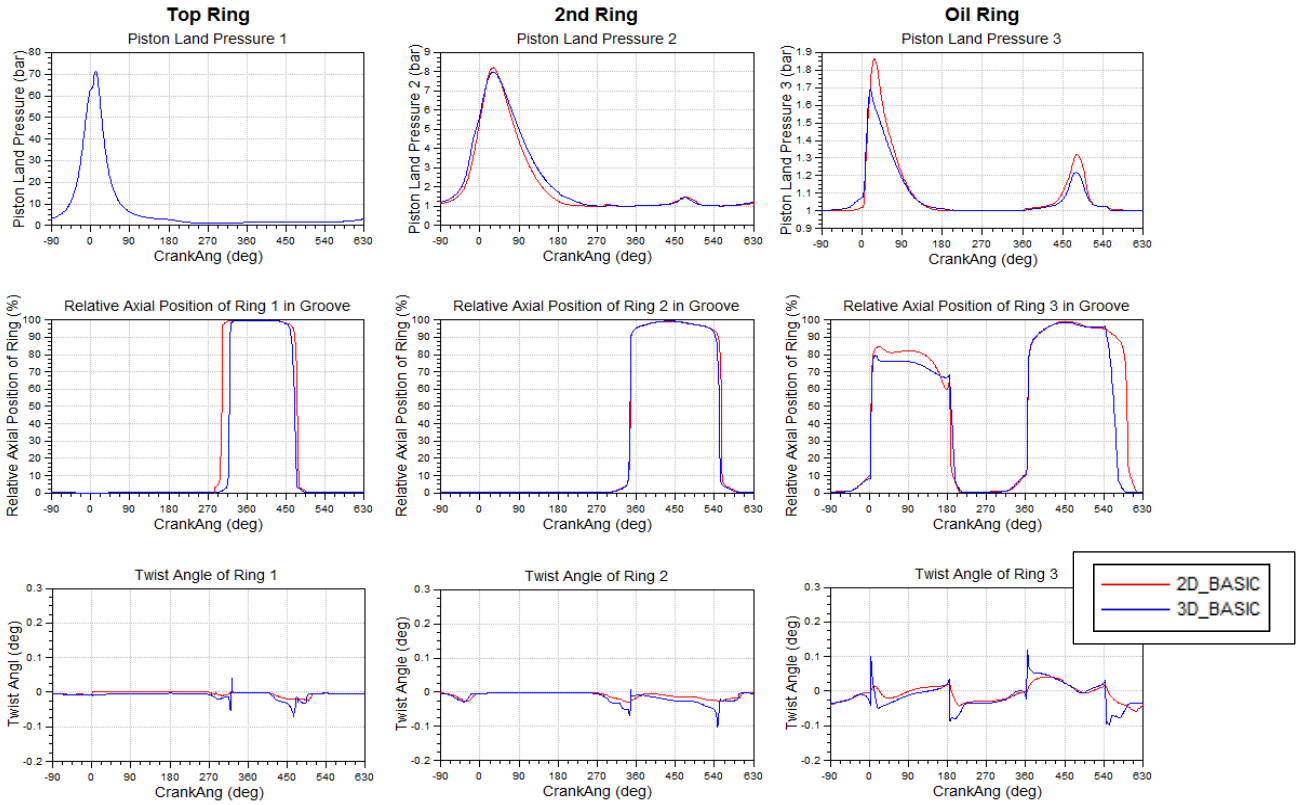

Figure C. 9. Comparison between 2D and 3D basic ring package - Piston ring dynamics overview.

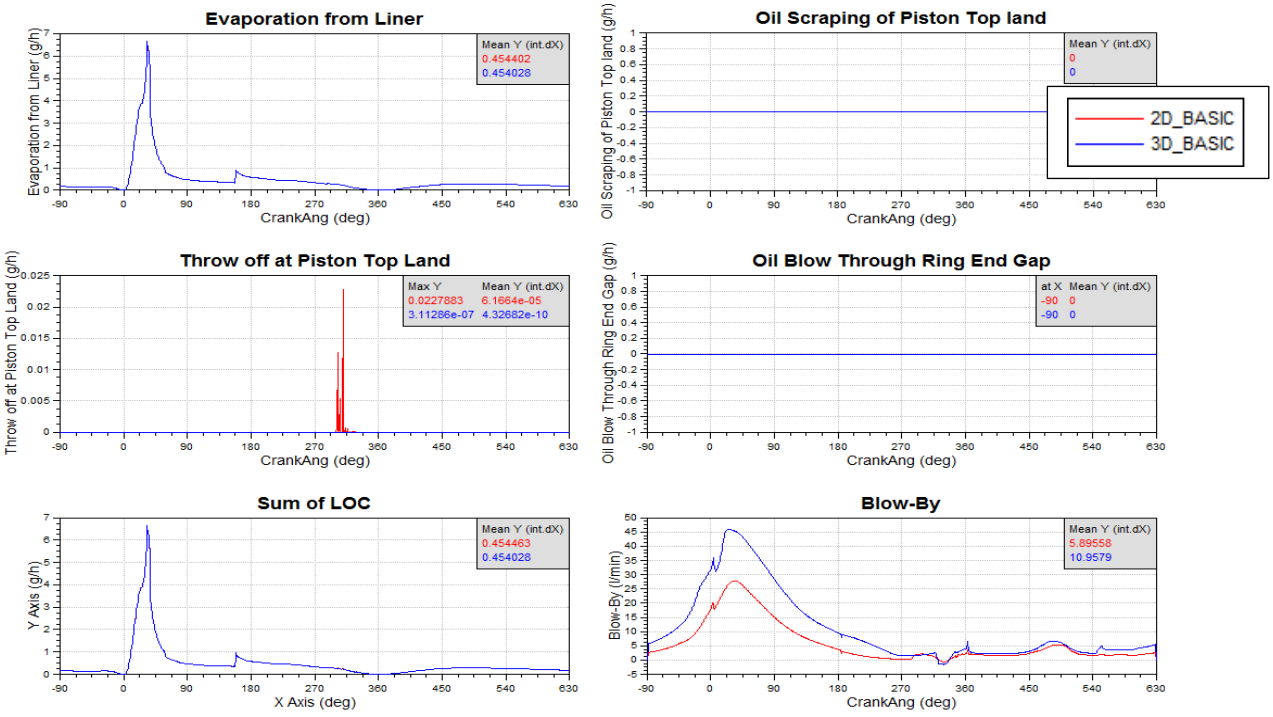

Figure C. 10. Comparison between 2D and 3D basic ring package – Lube Oil Consumption and Blow-by overview.

Operating point = 3000rpm_2.9

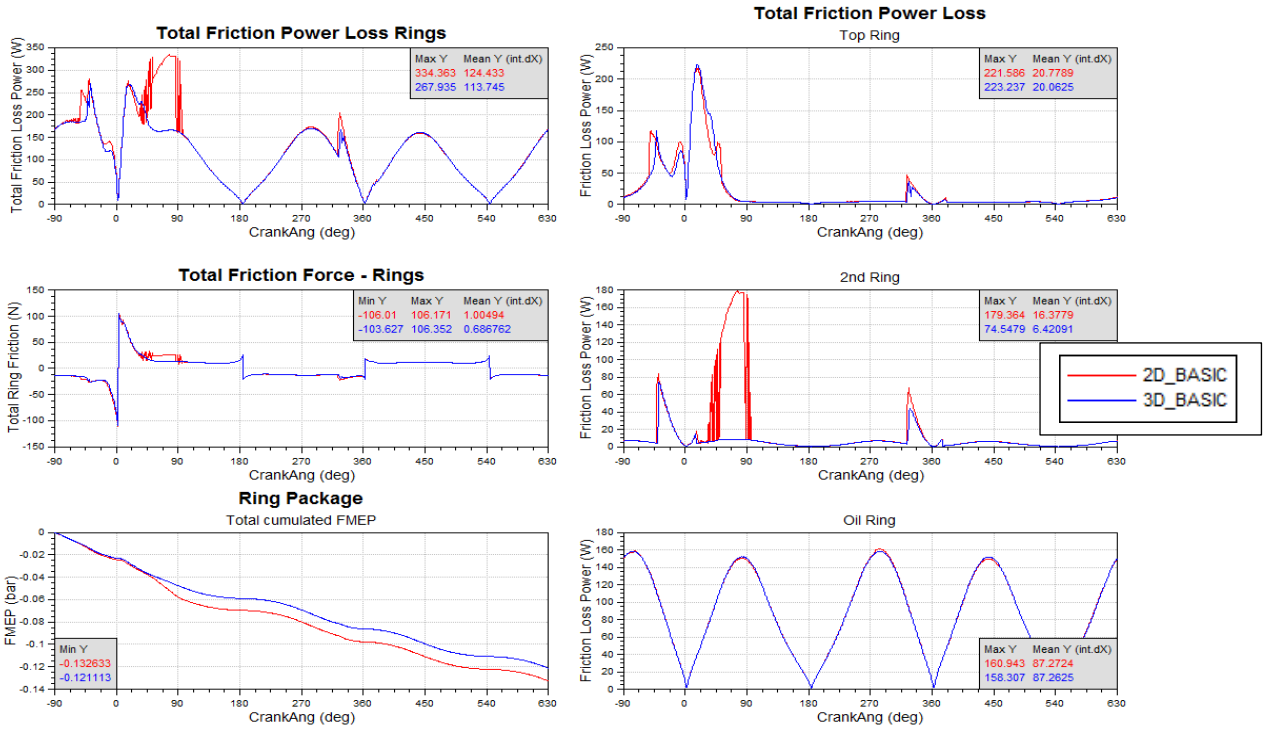

Figure C. 11. Comparison between 2D and 3D basic ring package - Friction characteristics overview.

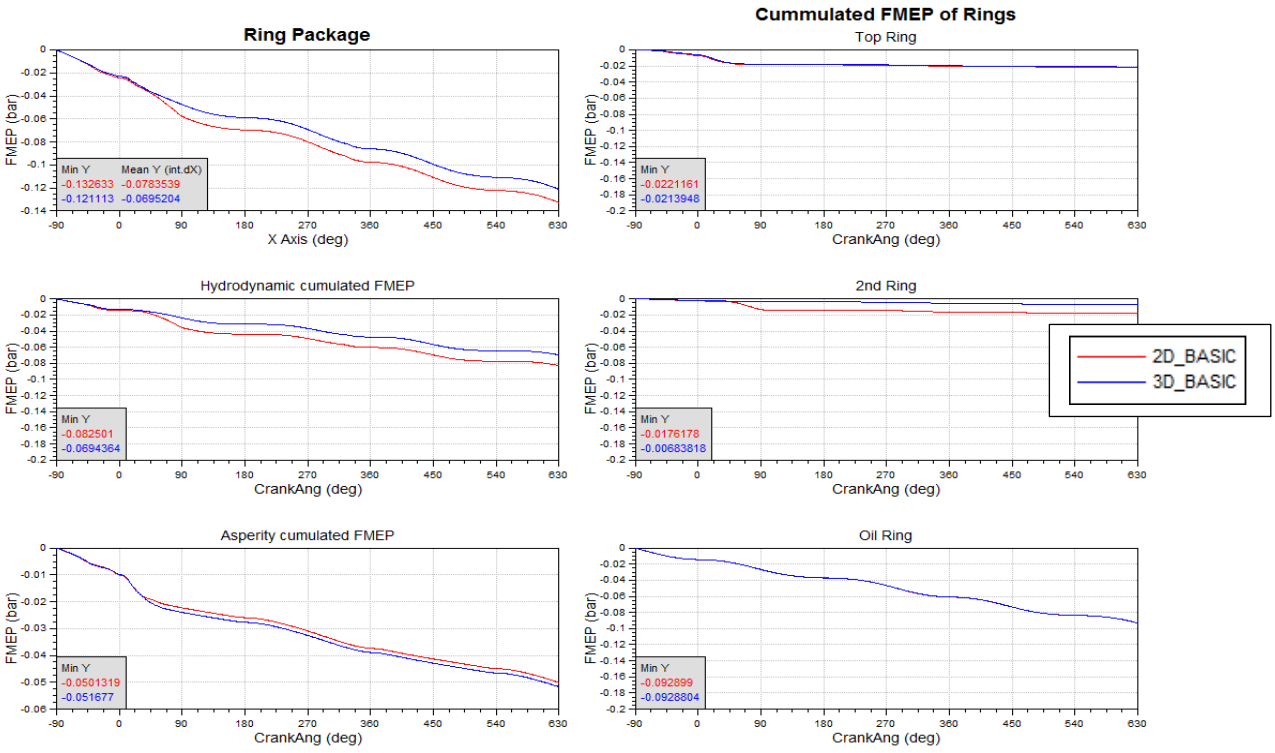

Figure C. 12. Comparison between 2D and 3D basic ring package – FMEP overview.

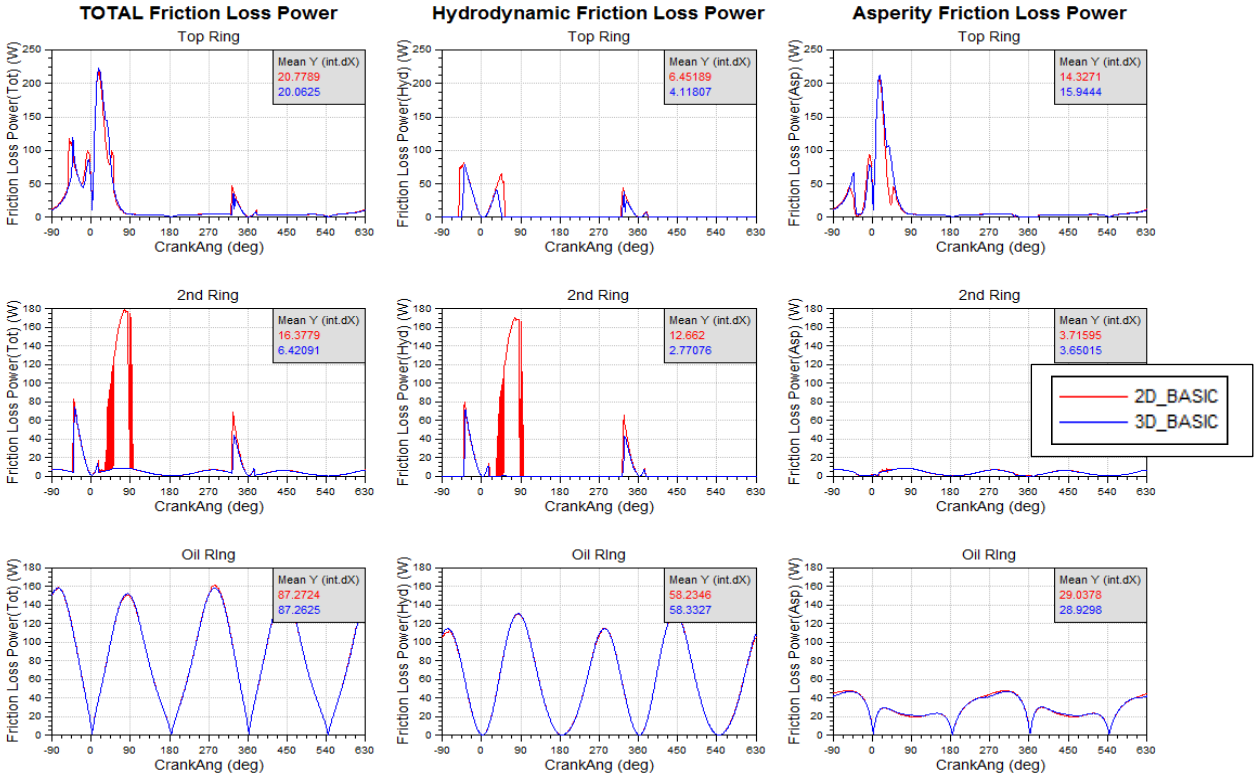

Figure C. 13. Comparison between 2D and 3D basic ring package - Friction Power Loss overview.

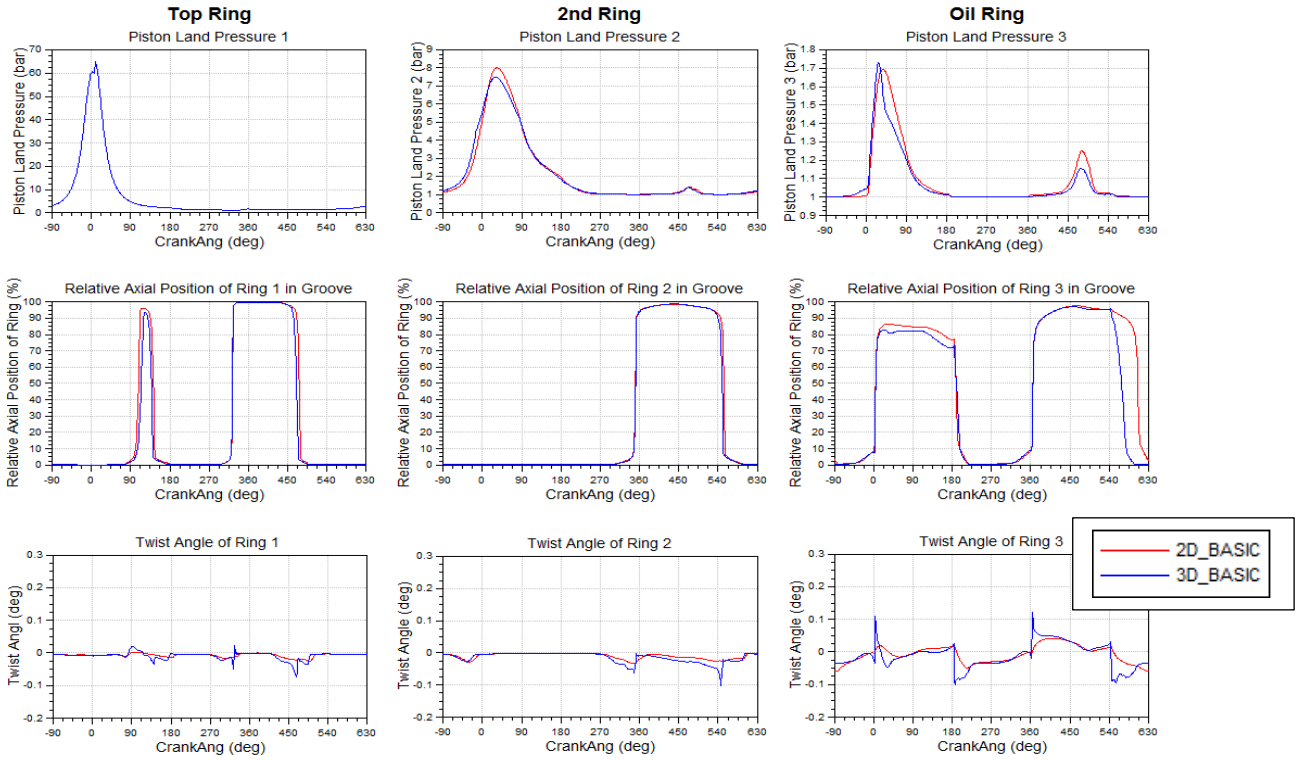

Figure C. 14. Comparison between 2D and 3D basic ring package - Piston ring dynamics overview.

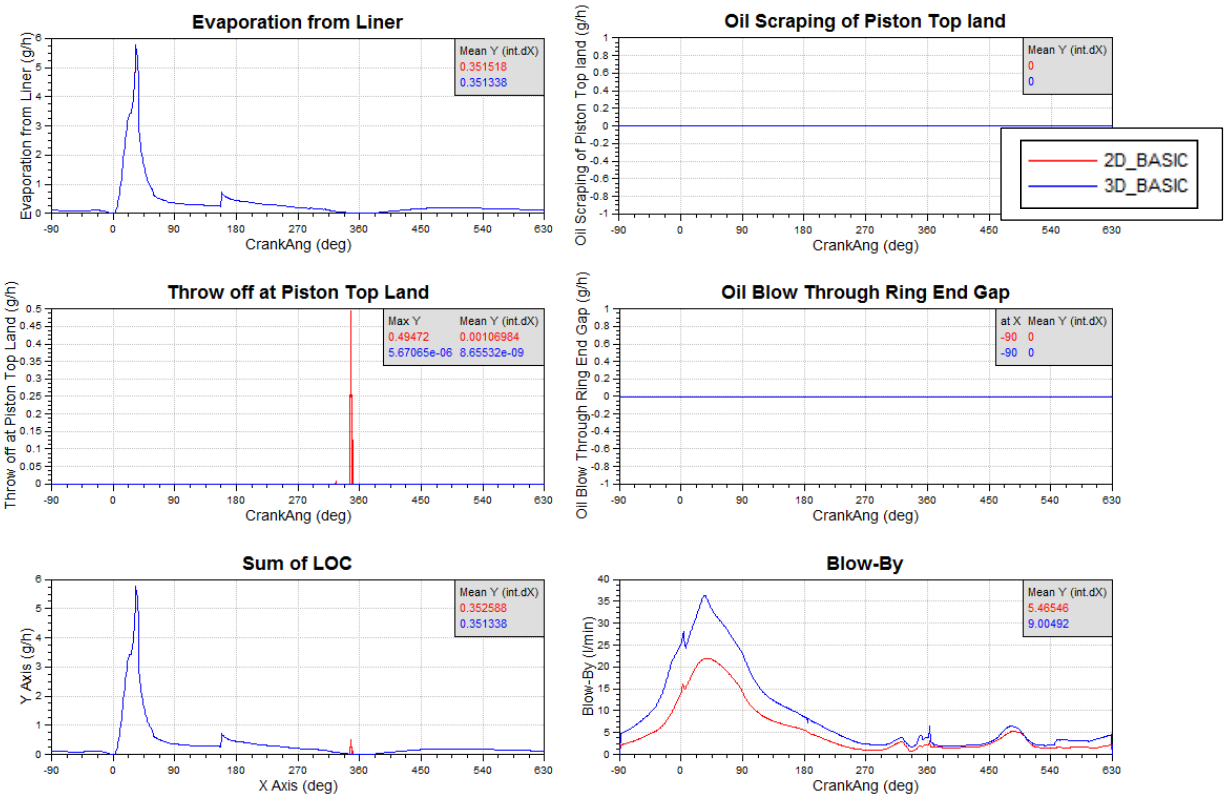

Figure C. 15. Comparison between 2D and 3D basic ring package – Lube Oil Consumption and Blow-by overview.

Appendix D

In this appendix EXCITE™ Power Unit results for other operating point at engine speed 3000 rpm with basic ring package are performed.

Operating point = 3000rpm_9.3

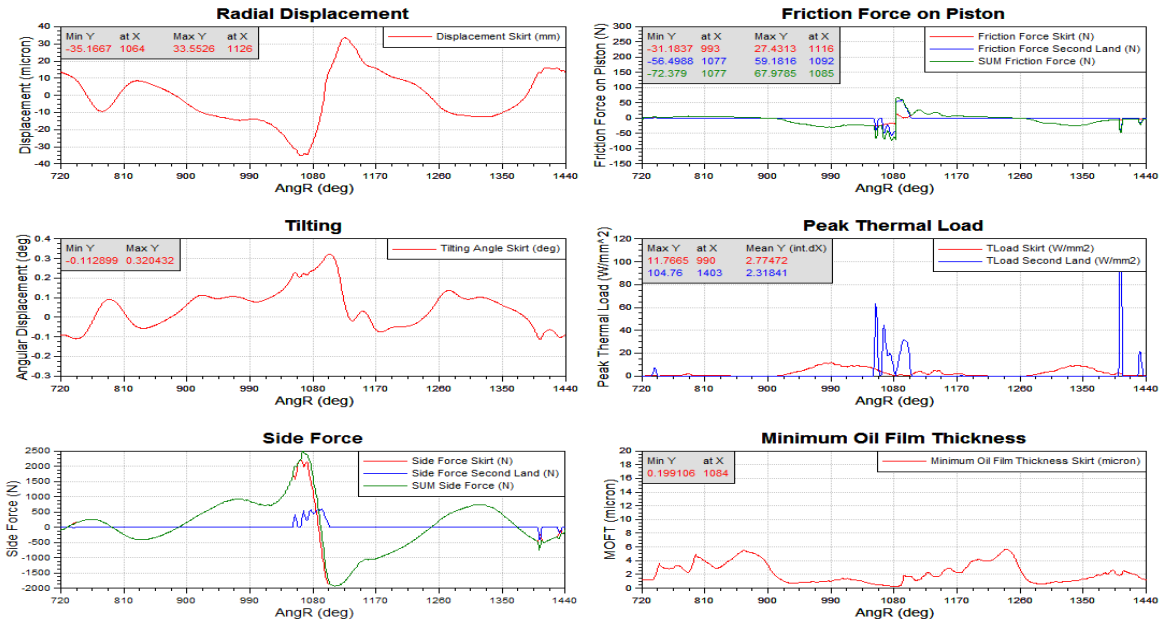

Figure D. 1. Piston results overview – 3000_9.3.

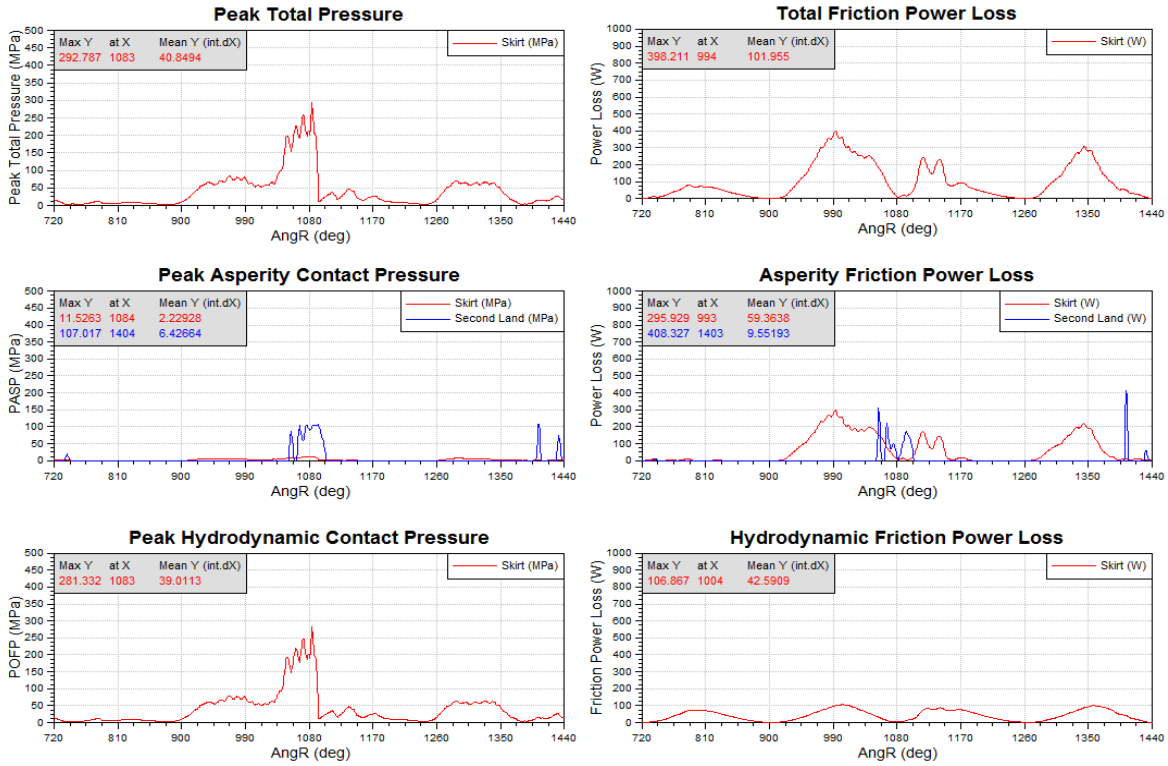

Figure D. 2. Pressure and friction results – 3000_9.3.

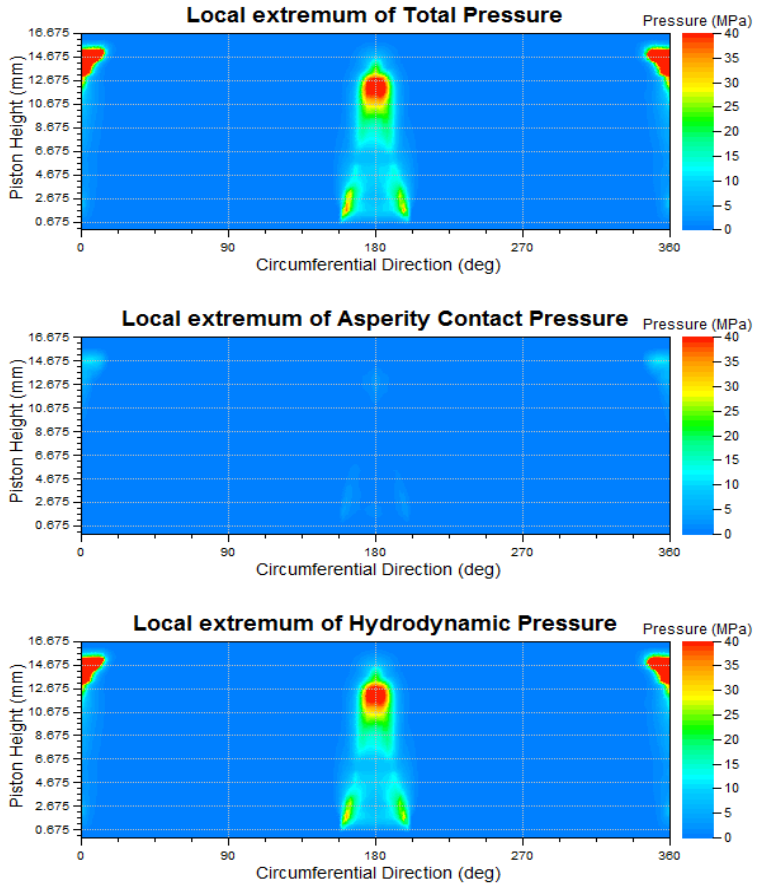

Figure D. 3. Campbell pressure distribution– 3000_9.3.

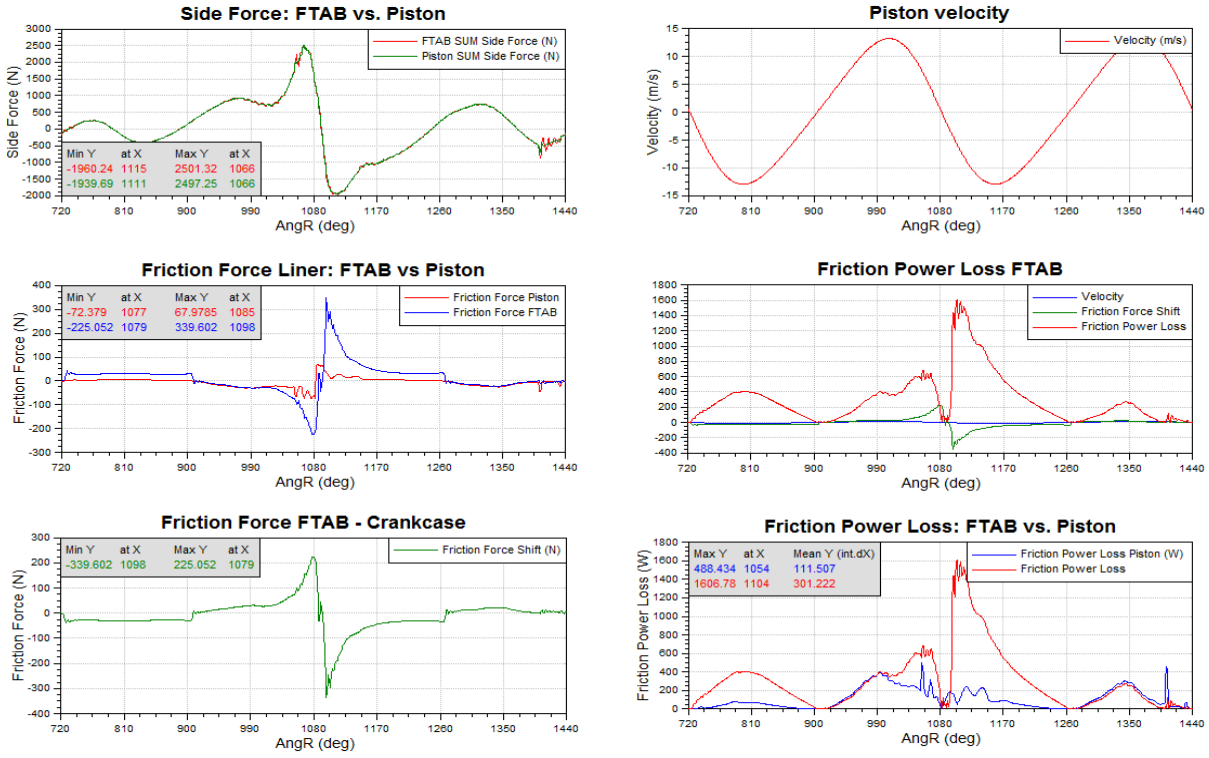

Figure D. 4. FTAB forces and friction power loss – 3000_9.3.

Operating point = 3000rpm_5.3

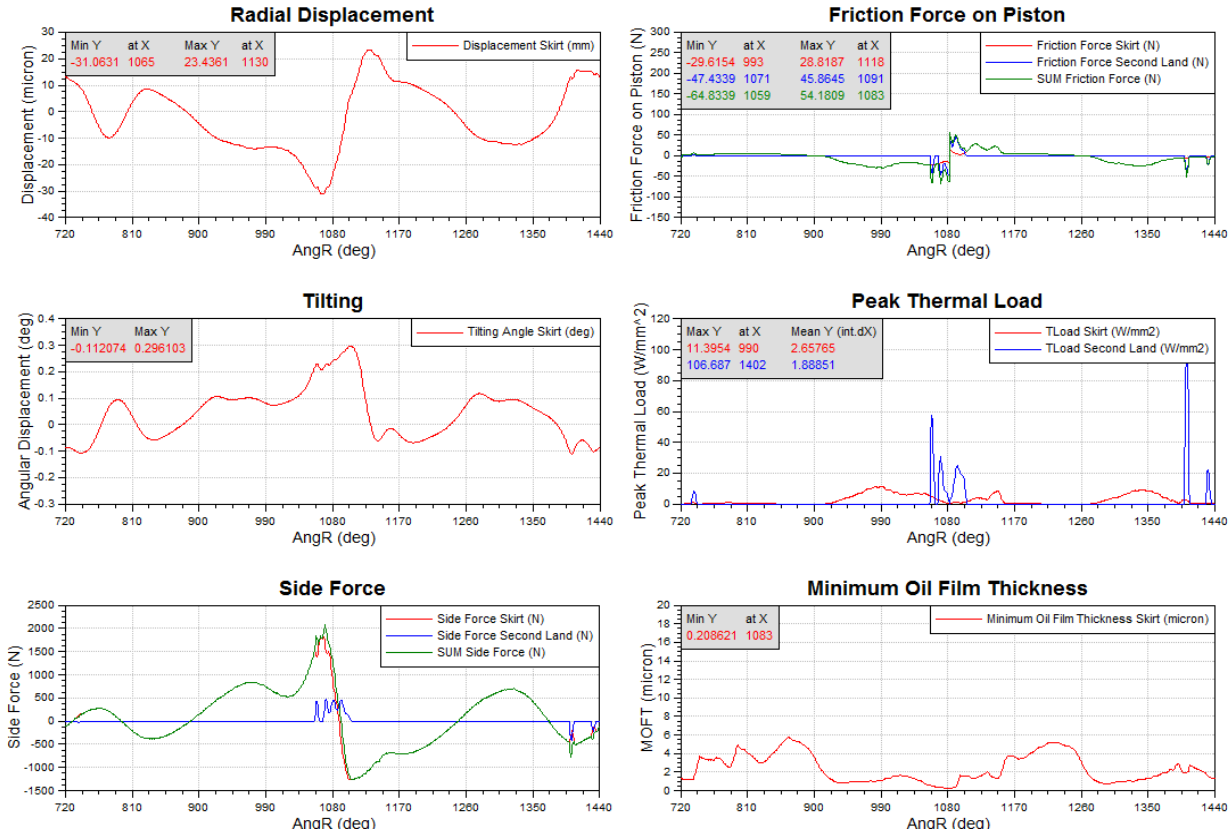

Figure D. 5. Piston results overview – 3000_5.3.

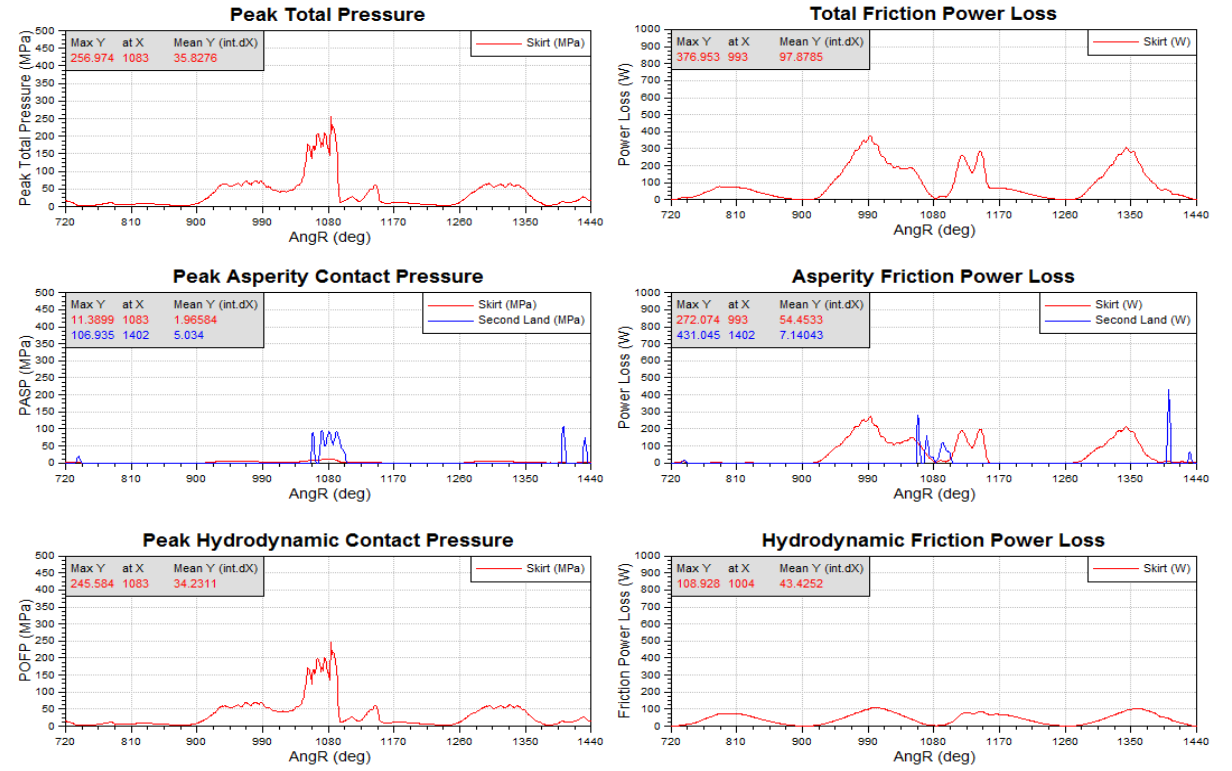

Figure D. 6. Pressure and friction results – 3000_5.3.

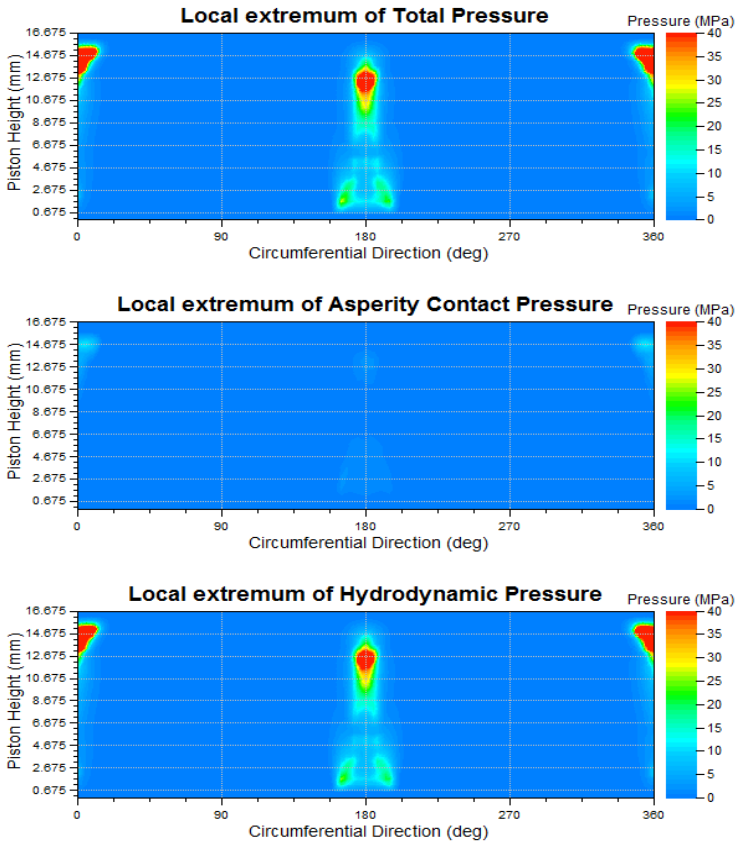

Figure D. 7. Campbell pressure distribution– 3000_5.3.

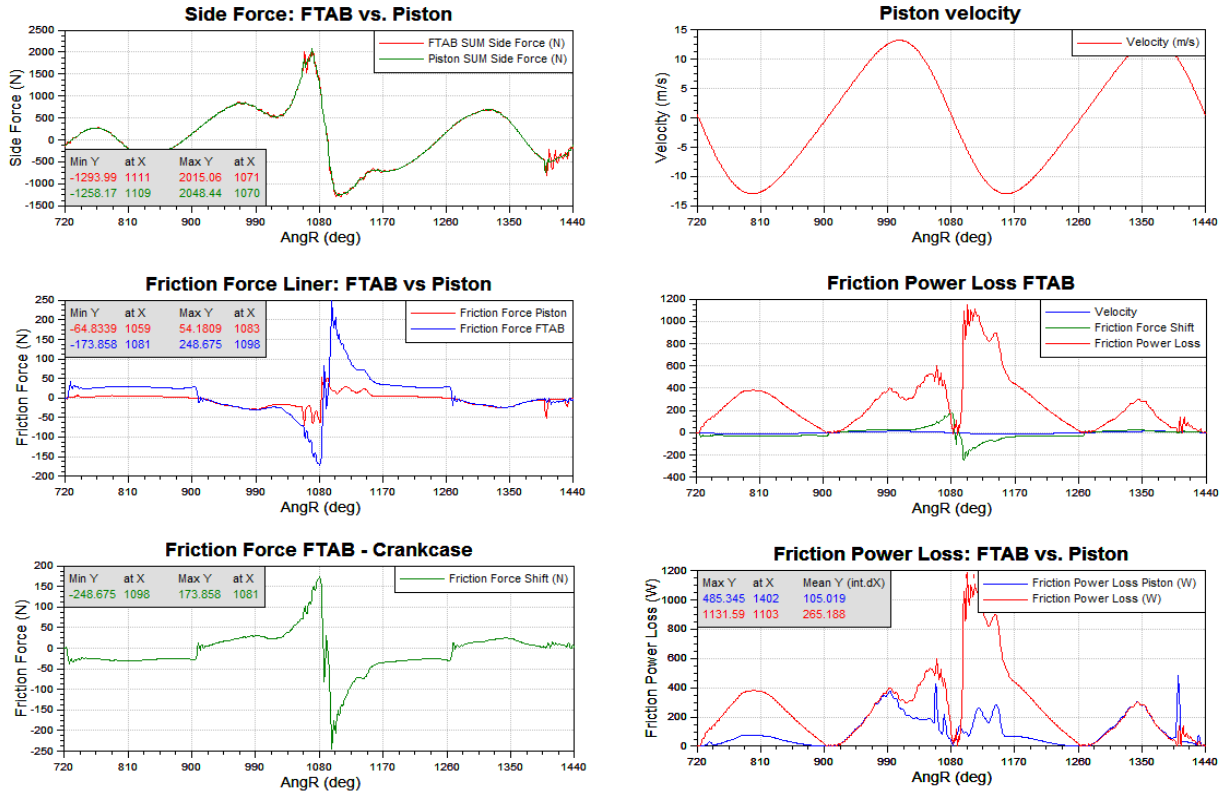

Figure D. 8. FTAB forces and friction power loss – 3000_5.3.

Operating point = 3000rpm_2.9

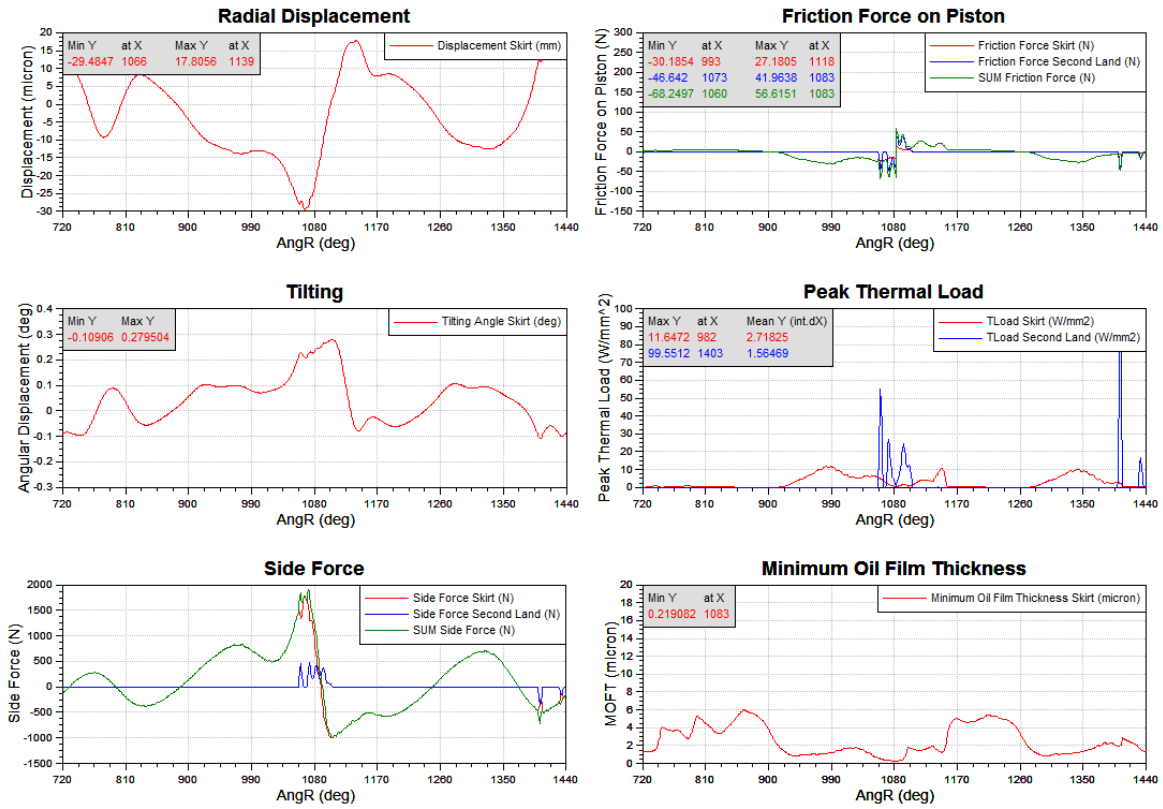

Figure D. 9. Piston results overview – 3000_2.9.

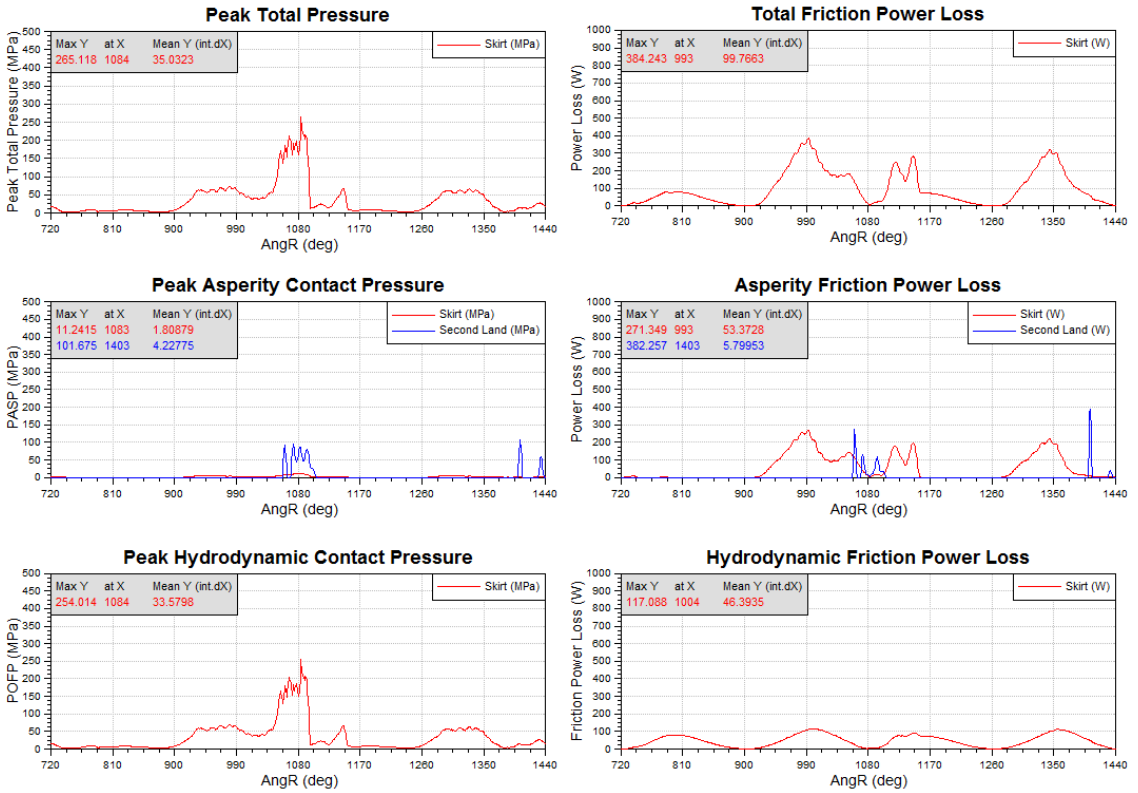

Figure D. 10. Pressure and friction results – 3000_2.9.

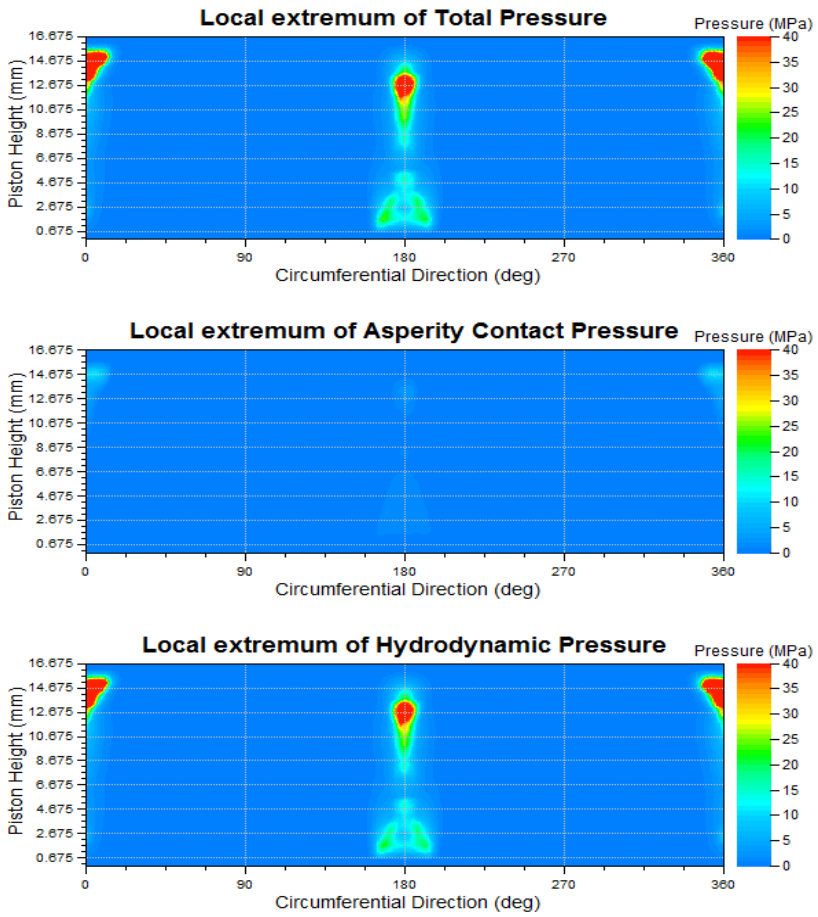

Figure D. 11. Campbell pressure distribution– 3000_2.9.

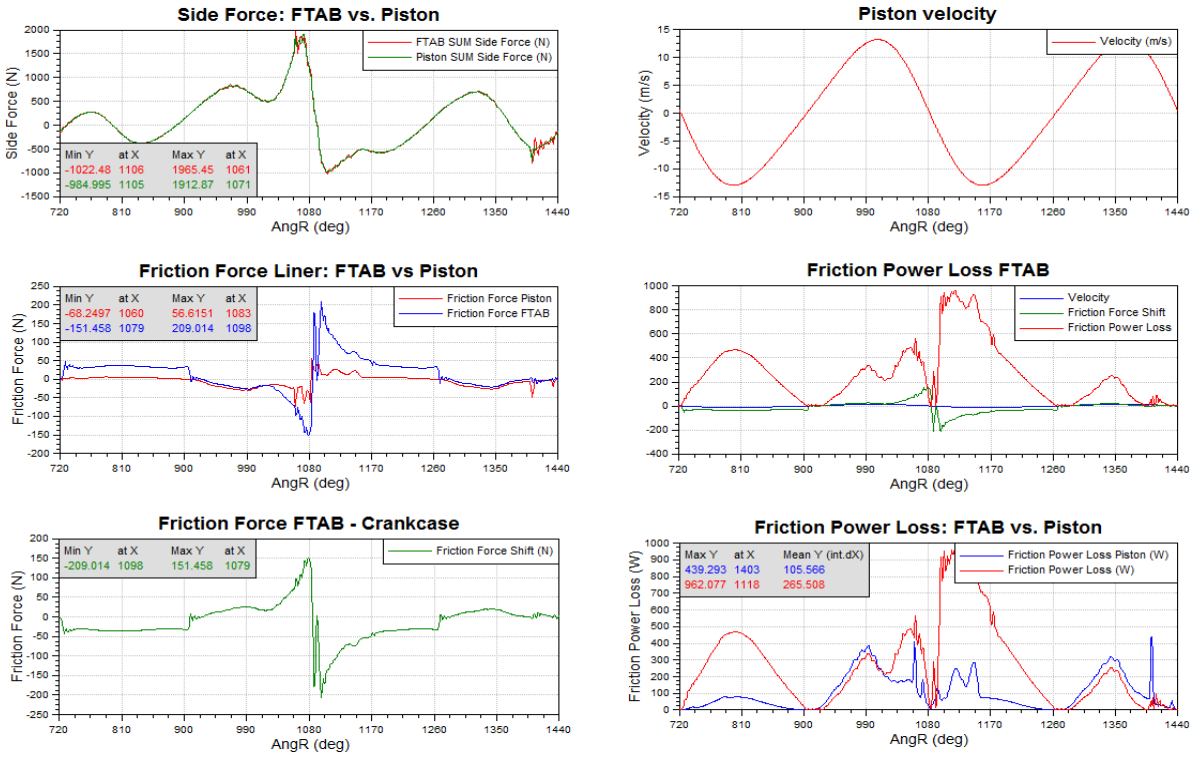

Figure D. 12. FTAB forces and friction power loss – 3000_2.9.

Appendix E

In this appendix EXCITE™ Power Unit results between basic and low FT ring package for engine speed 3000 rpm are performed.

Operating point = 3000rpm_9.3

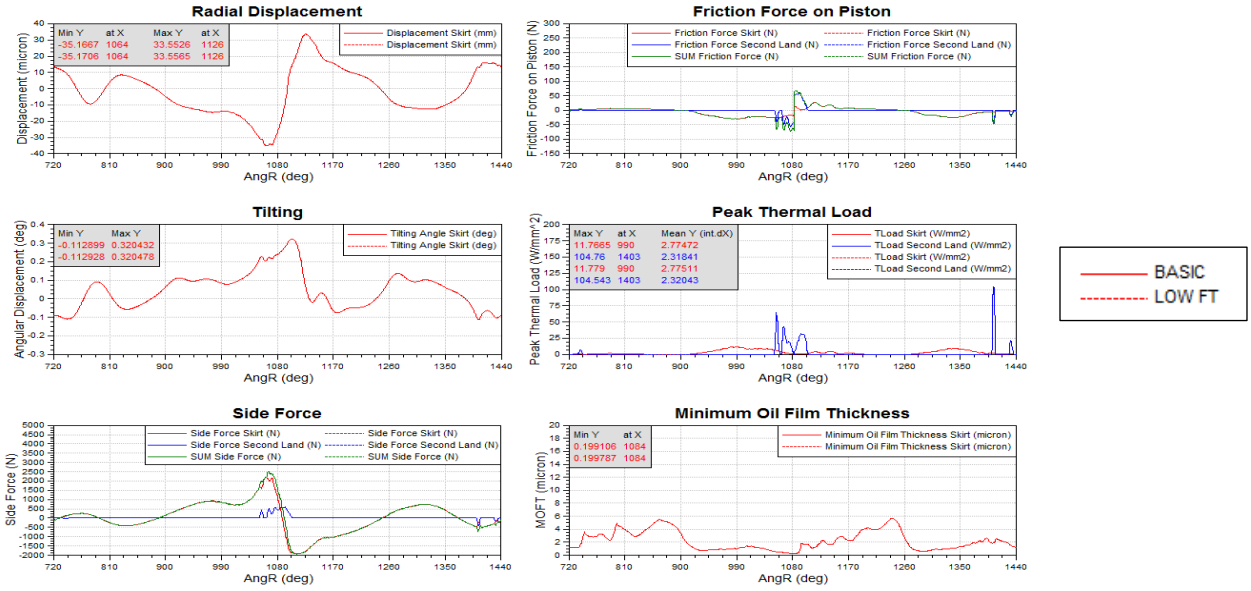

Figure E. 1. Comparison between basic and low friction ring package, REVO model, piston results overview – 3000_9.3.

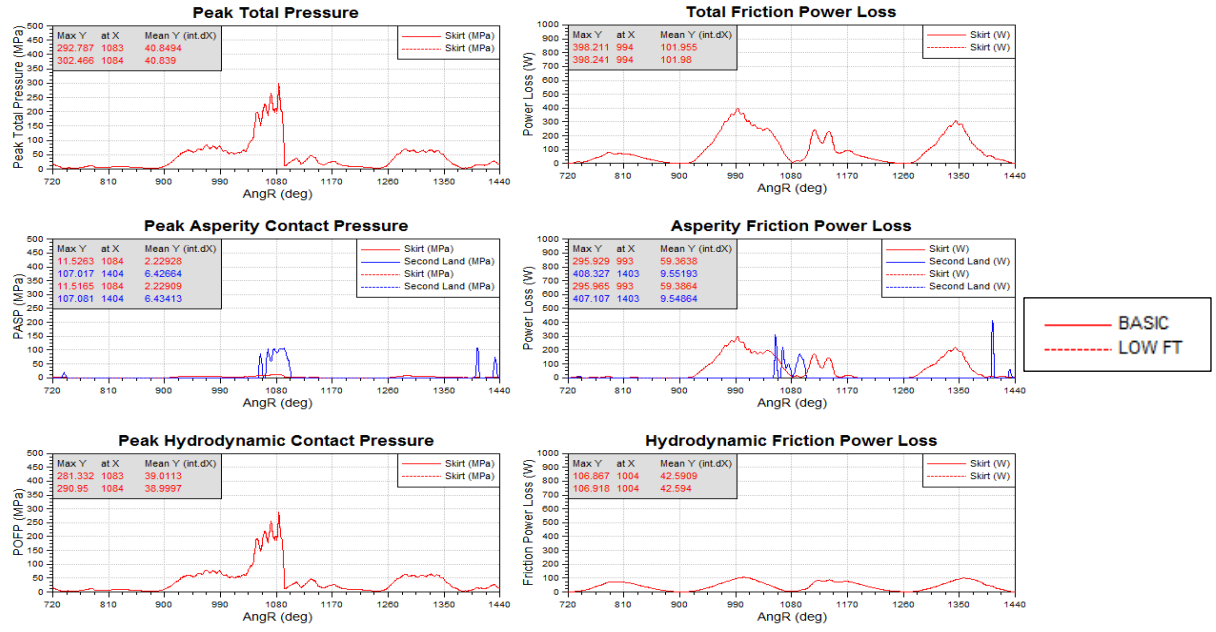

Figure E. 2. Comparison between basic and low friction ring package, REVO model, Pressure and friction results – 3000_9.3.

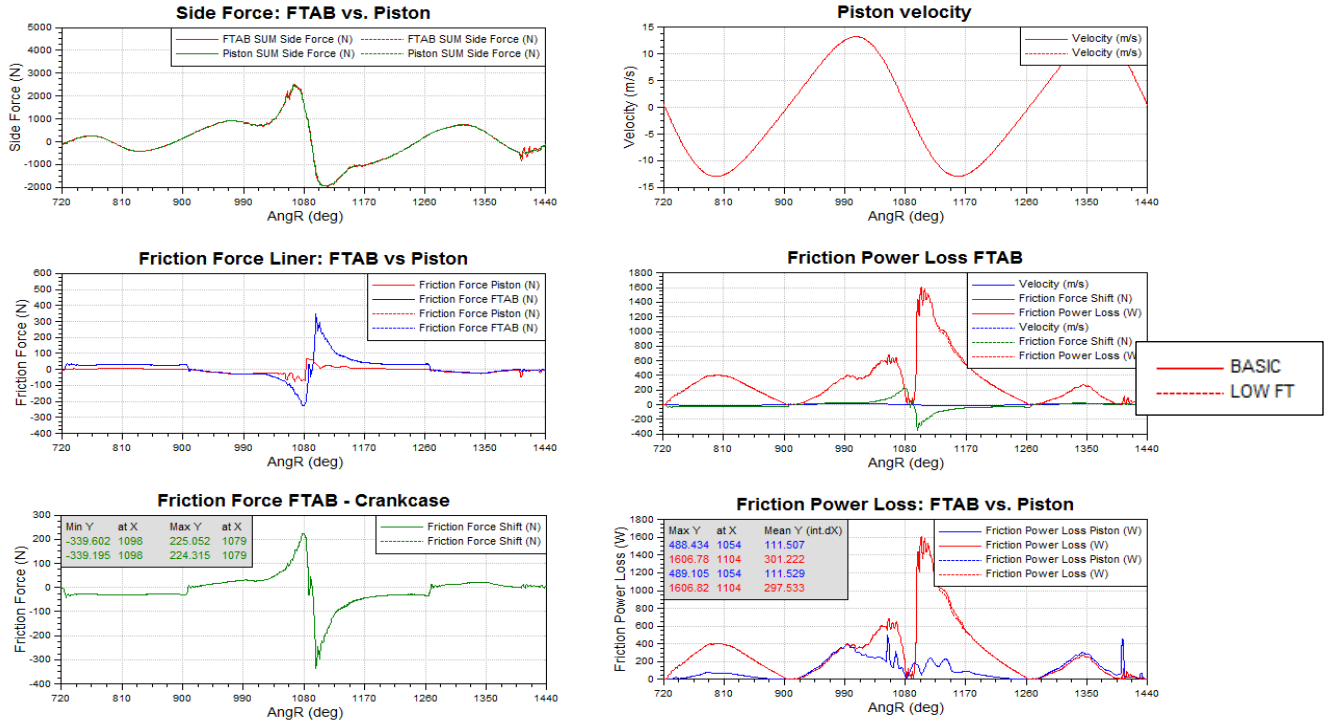

Figure E. 3. Comparison between basic and low friction ring package, REVO model, FTAB forces and friction power loss – 3000_9.3.

Operating point = 3000rpm_5.3

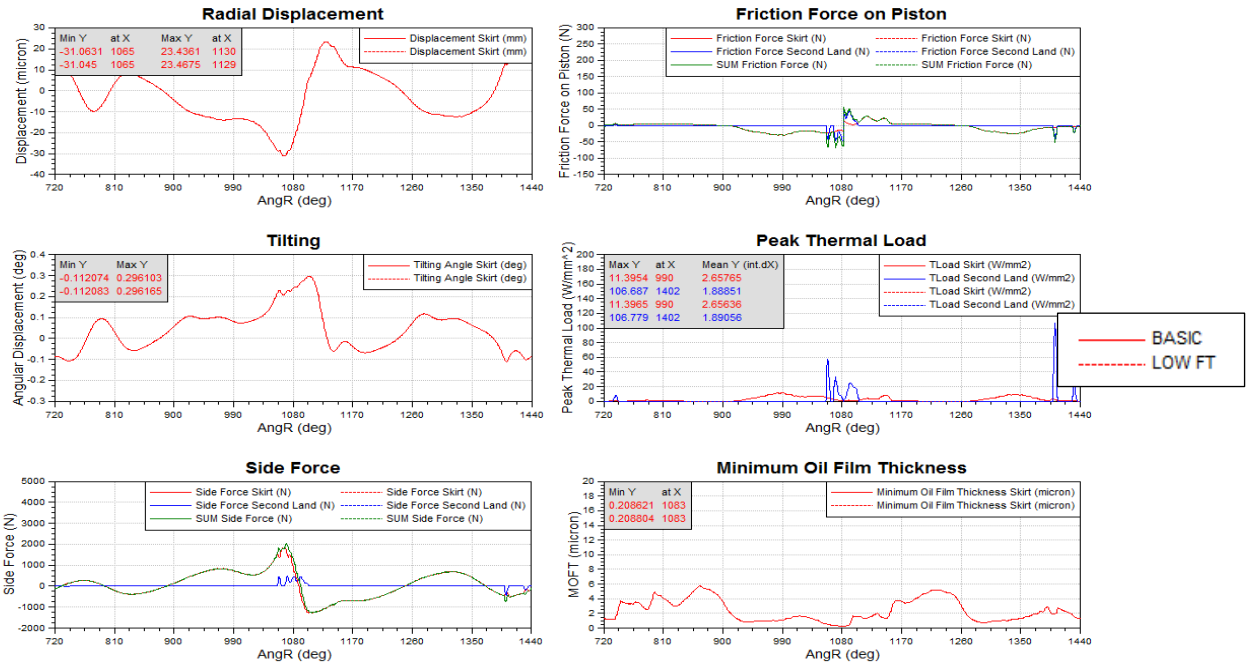

Figure E. 4. Comparison between basic and low friction ring package, REVO model, piston results overview – 3000_5.3.

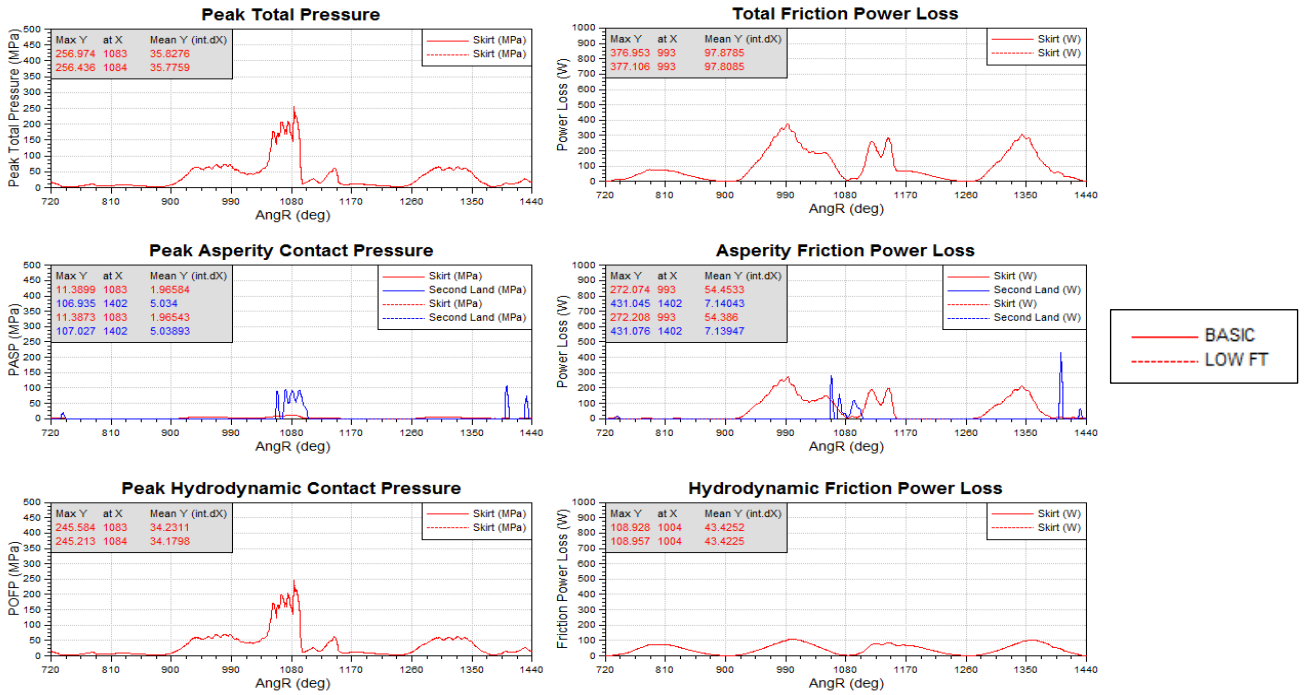

Figure E. 5. Comparison between basic and low friction ring package, REVO model, Pressure and friction results – 3000_5.3.

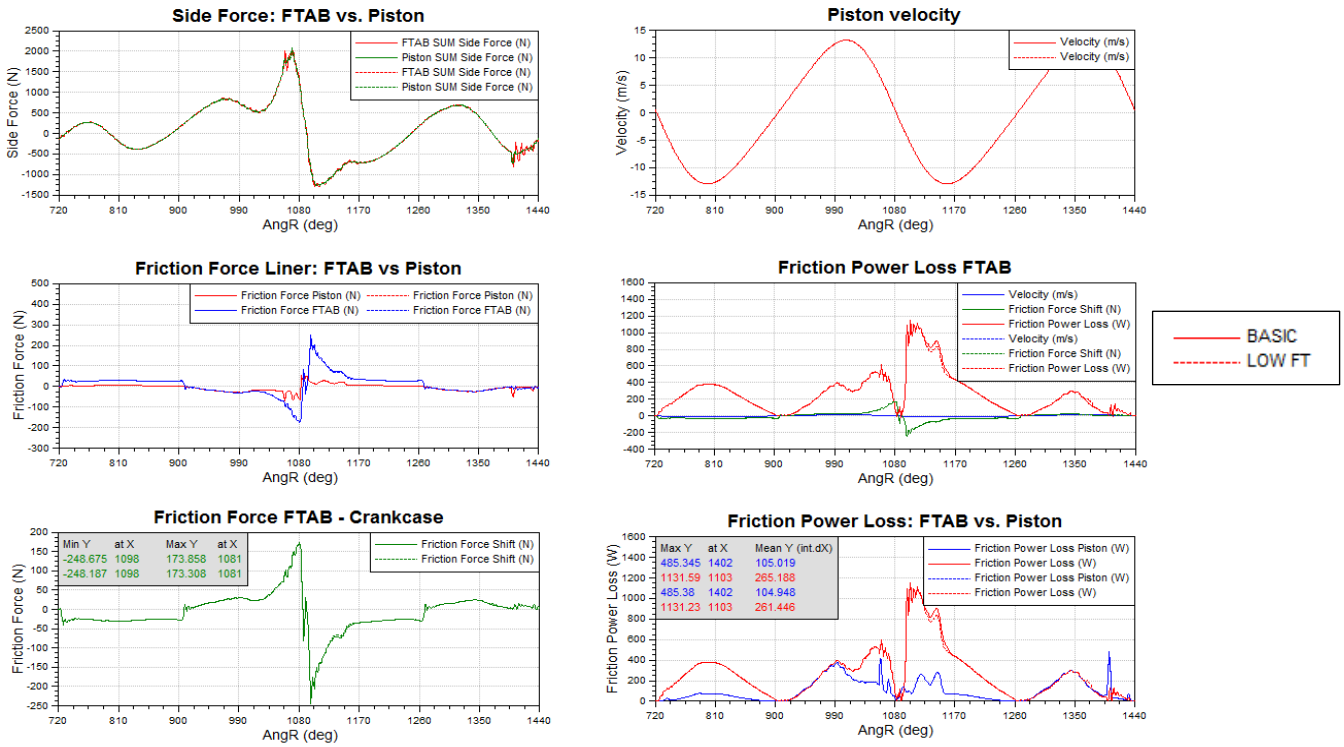

Figure E. 6. Comparison between basic and low friction ring package, REVO model, FTAB forces and friction power loss – 3000_5.3.

Operating point = 3000rpm_2.9

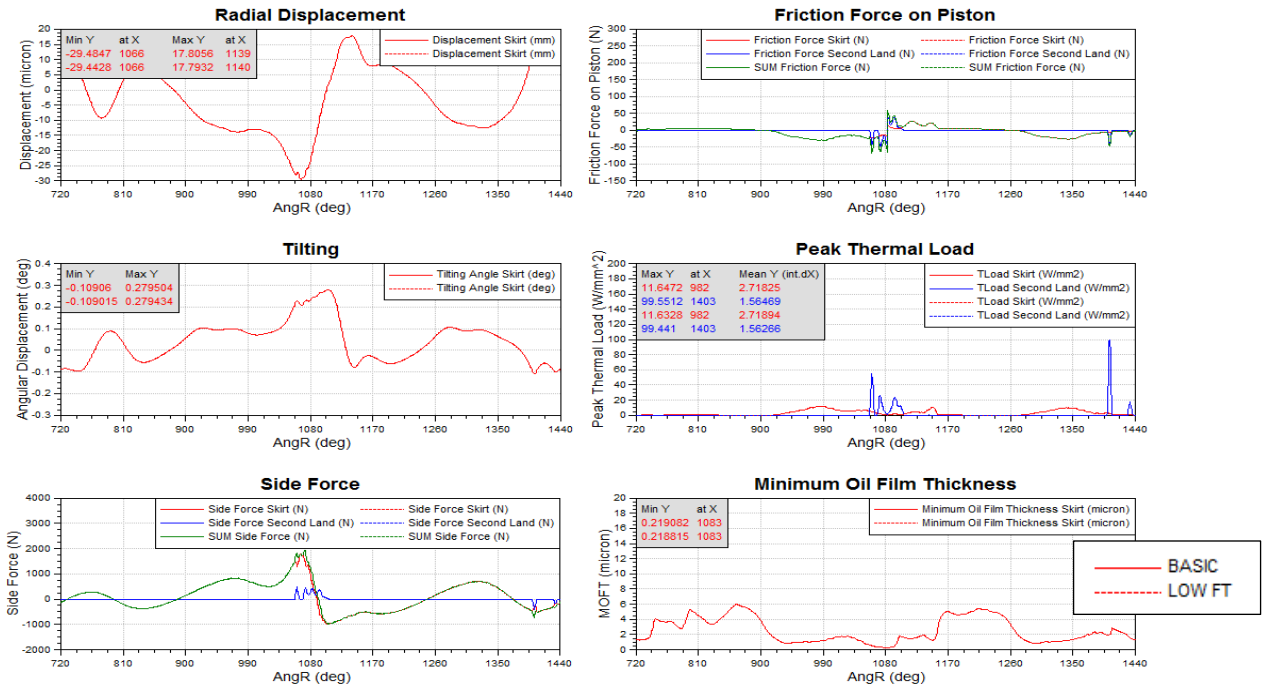

Figure E. 7. Comparison between basic and low friction ring package, REVO model, piston results overview – 3000_2.9.

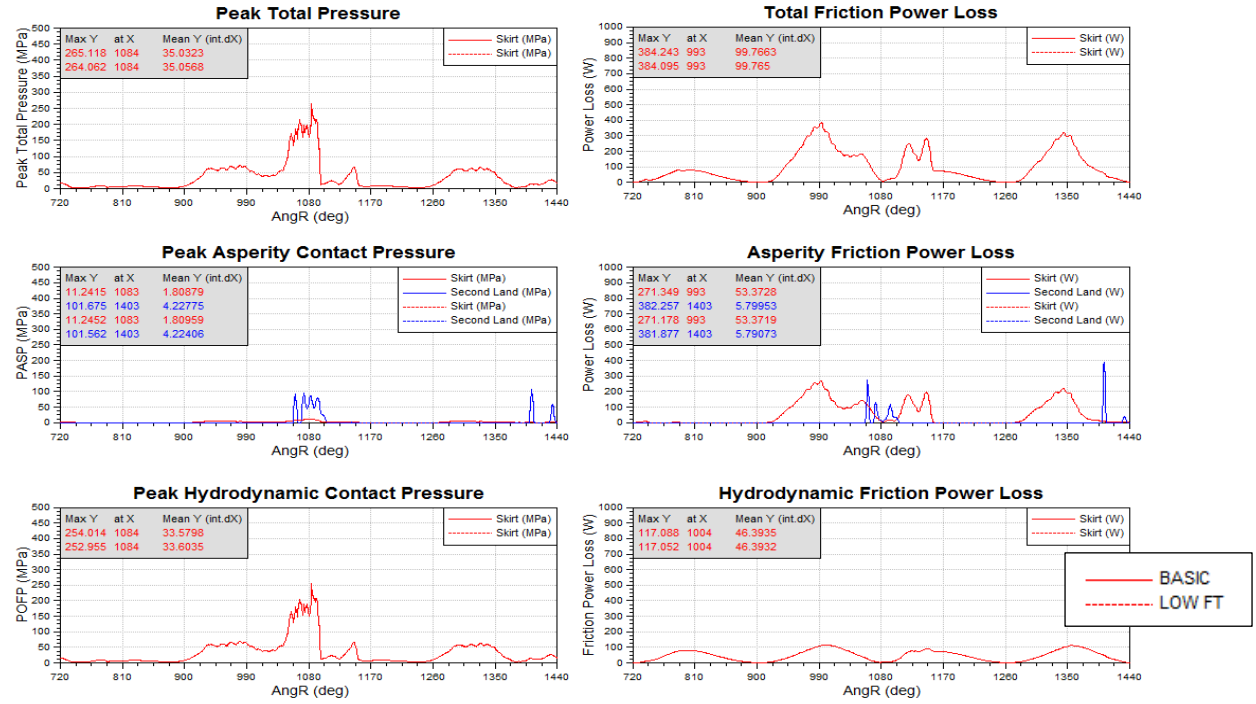

Figure E. 8. Comparison between basic and low friction ring package, REVO model, Pressure and friction results – 3000_2.9.

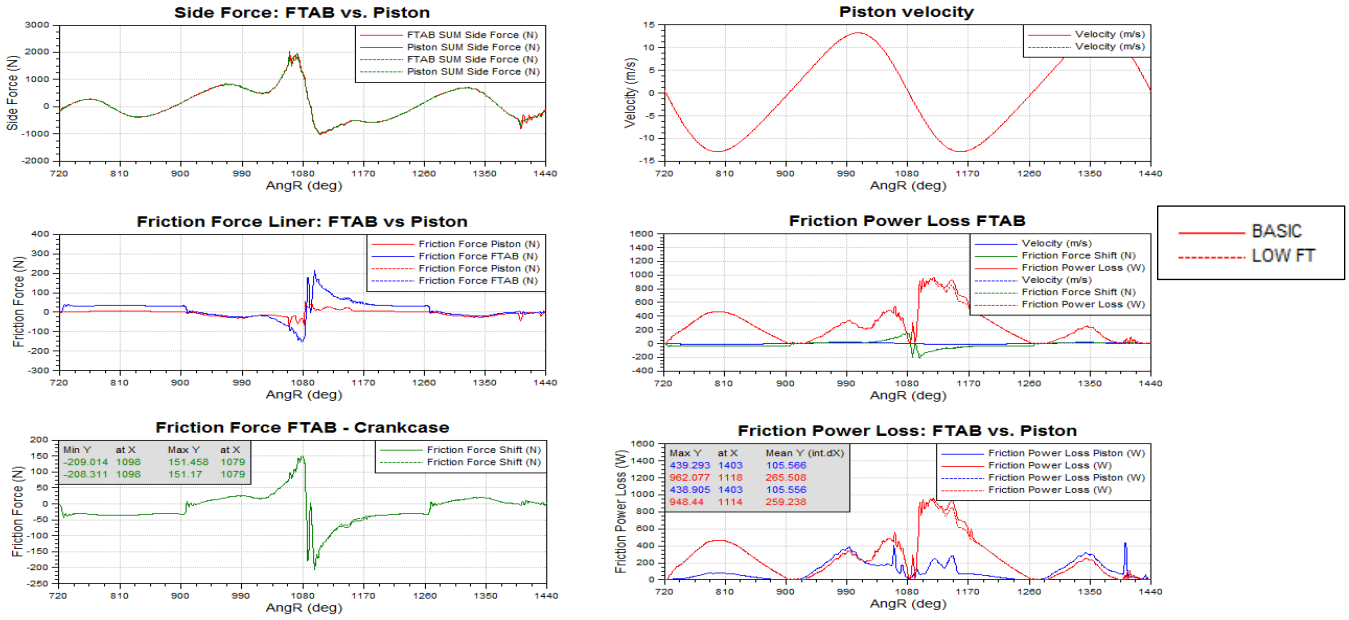

Figure E. 9. Comparison between basic and low friction ring package, REVO model, FTAB forces and friction power loss – 3000_2.9.

Appendix F

In this appendix EXCITE™ Power Unit results between REVO and EHD basic ring package for engine speed 3000 rpm are performed.

Operating point = 3000rpm_9.3

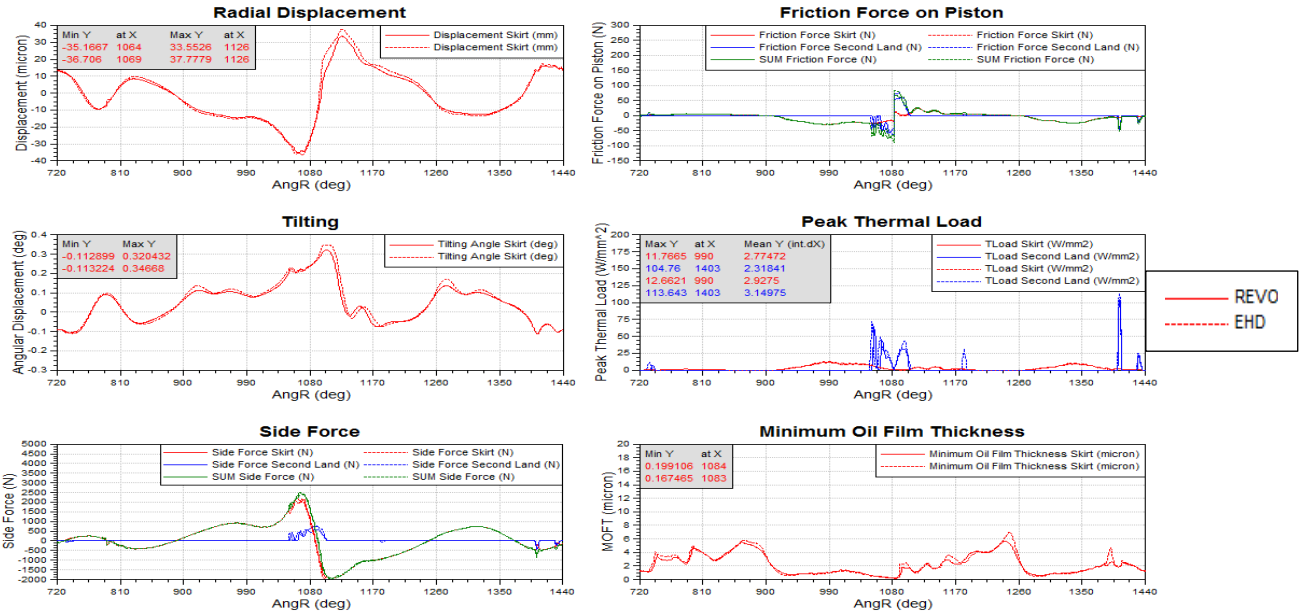

Figure F. 1. Comparison between REVO and EHD model, basic ring package, piston results overview – 3000_15.5.

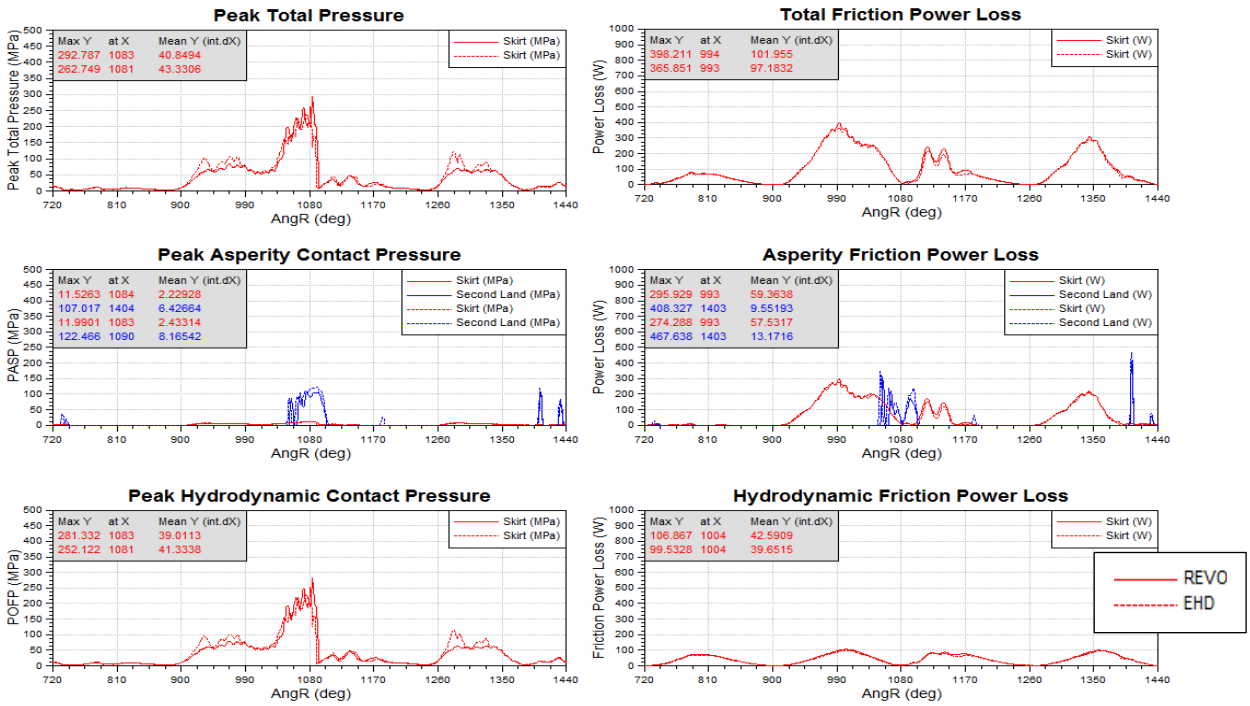

Figure F. 2. Comparison between REVO and EHD model, basic ring package, pressure and friction results – 3000_15.5.

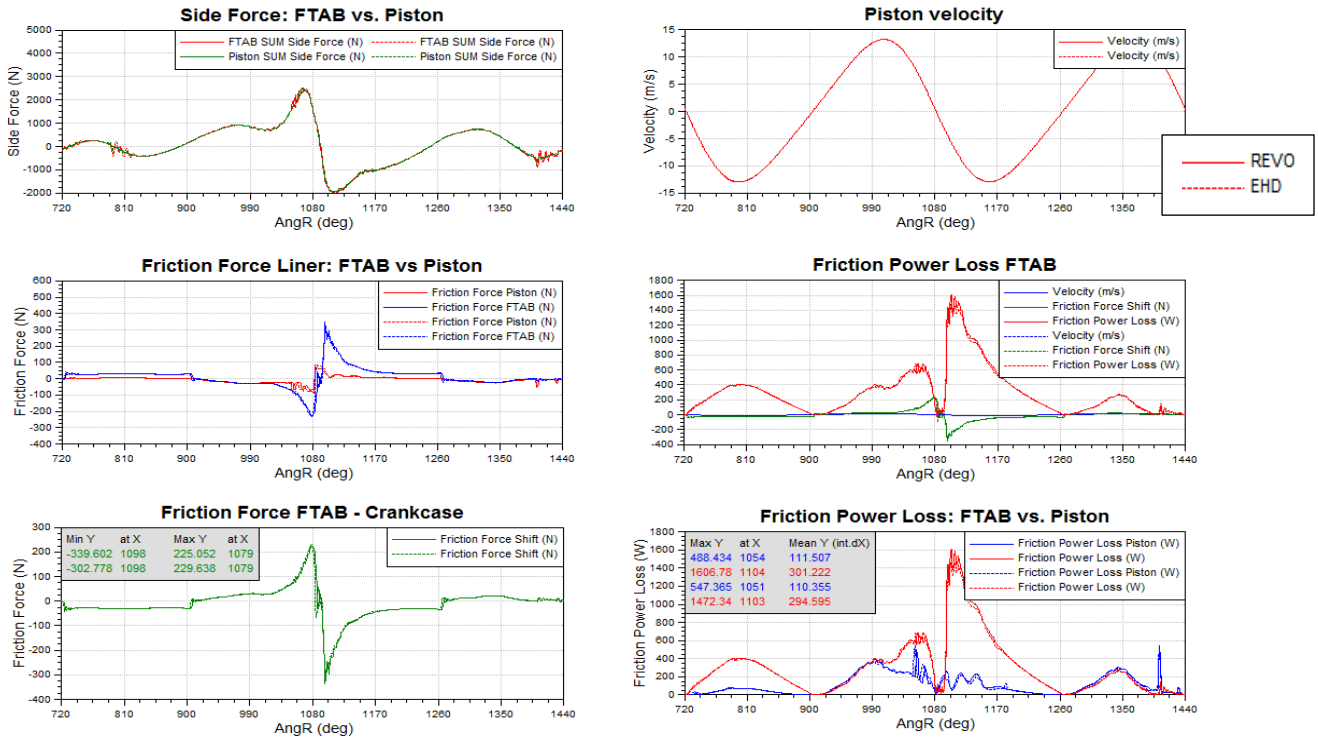

Figure F. 3. Comparison between REVO and EHD model, basic ring package, FTAB forces and friction power loss – 3000_15.5.

Operating point = 3000rpm_5.3

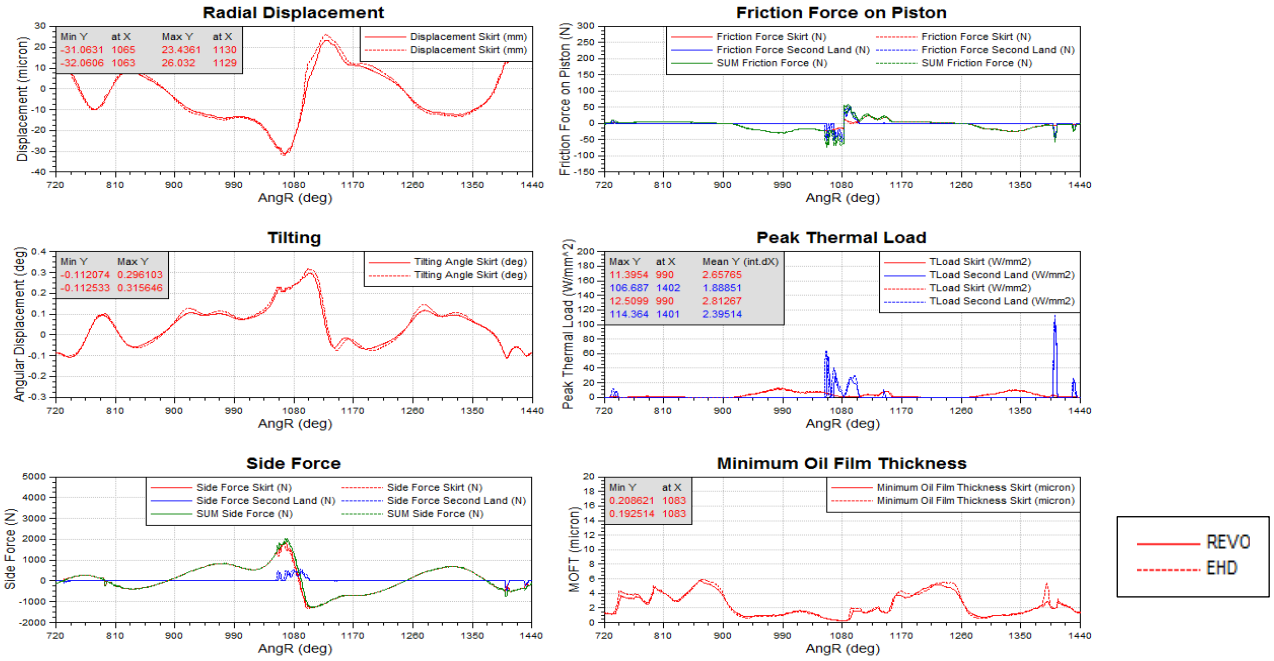

Figure F. 4. Comparison between REVO and EHD model, basic ring package, piston results overview – 3000_15.5.

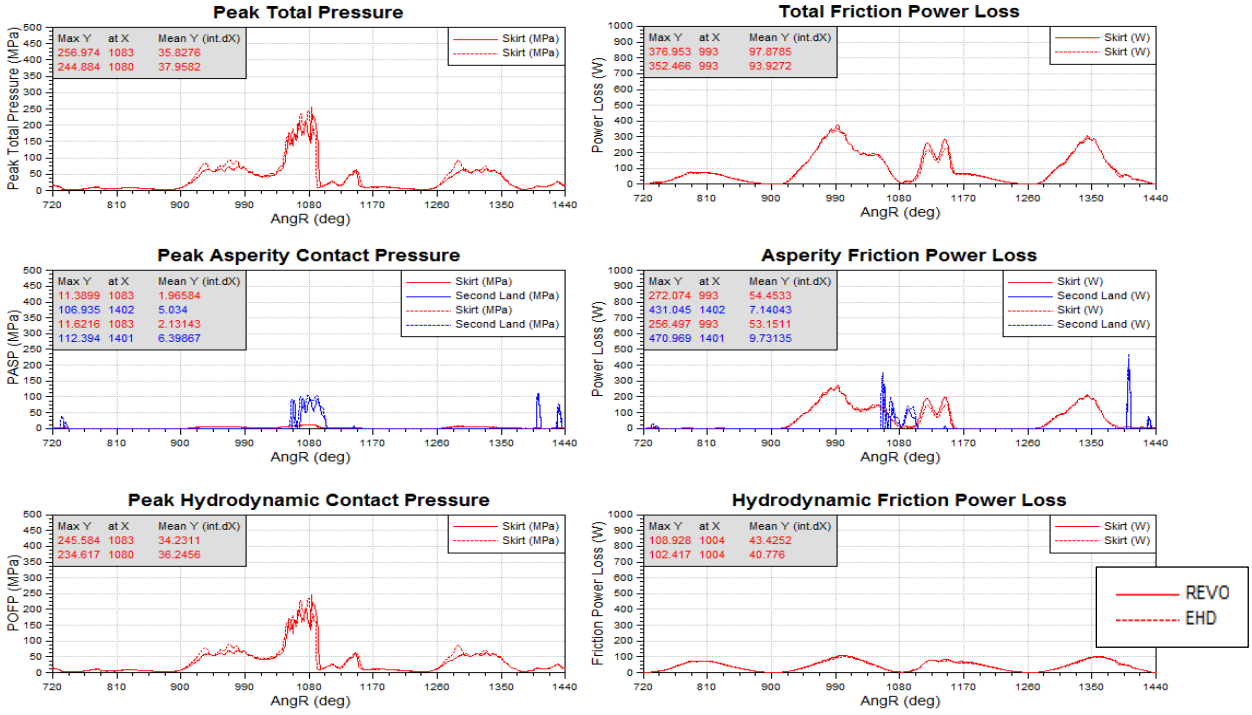

Figure F. 5. Comparison between REVO and EHD model, basic ring package, pressure and friction results – 3000_15.5.

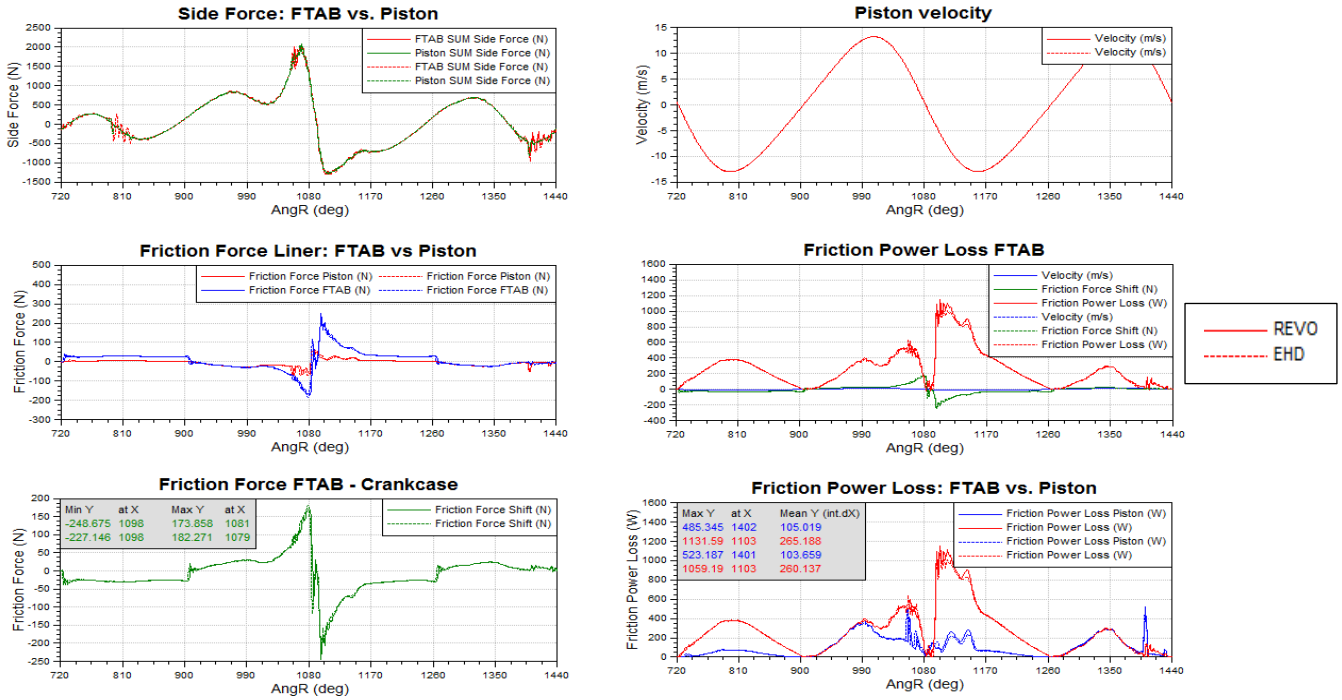

Figure F. 6. Comparison between REVO and EHD model, basic ring package, FTAB forces and friction power loss – 3000_15.5.

Operating point = 3000rpm_2.9

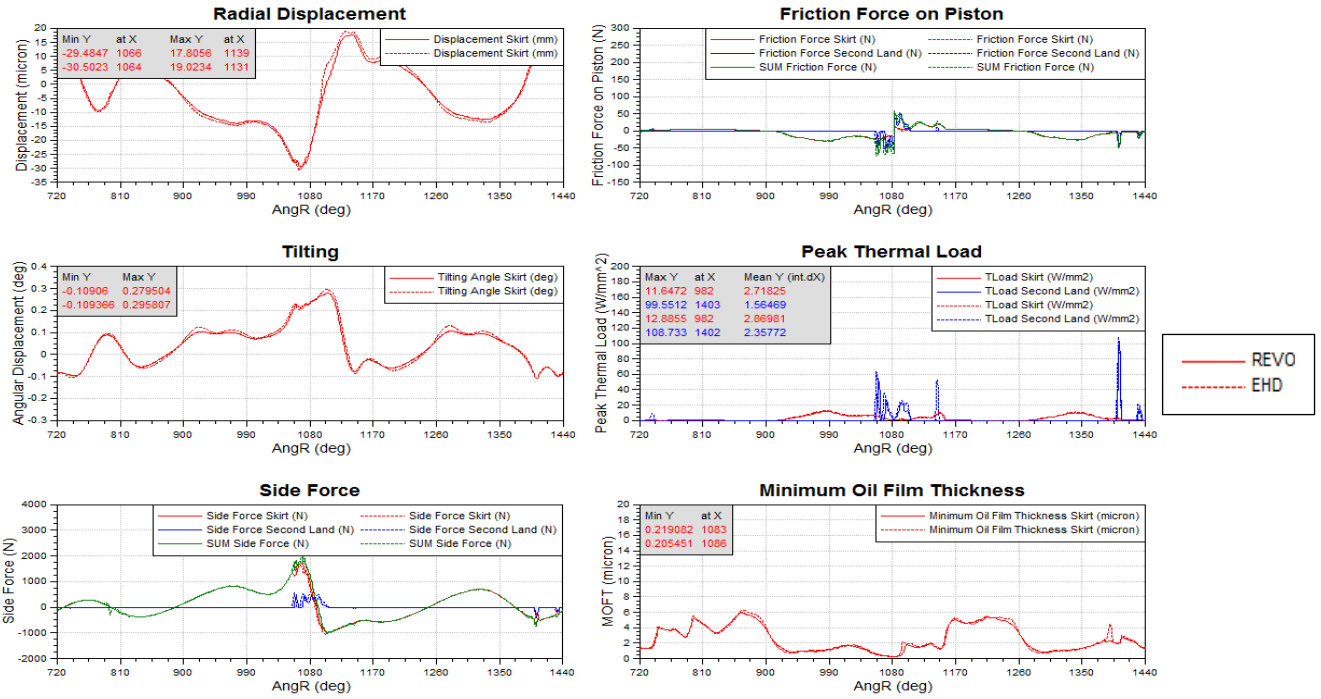

Figure F. 7. Comparison between REVO and EHD model, basic ring package, piston results overview – 3000_15.5.

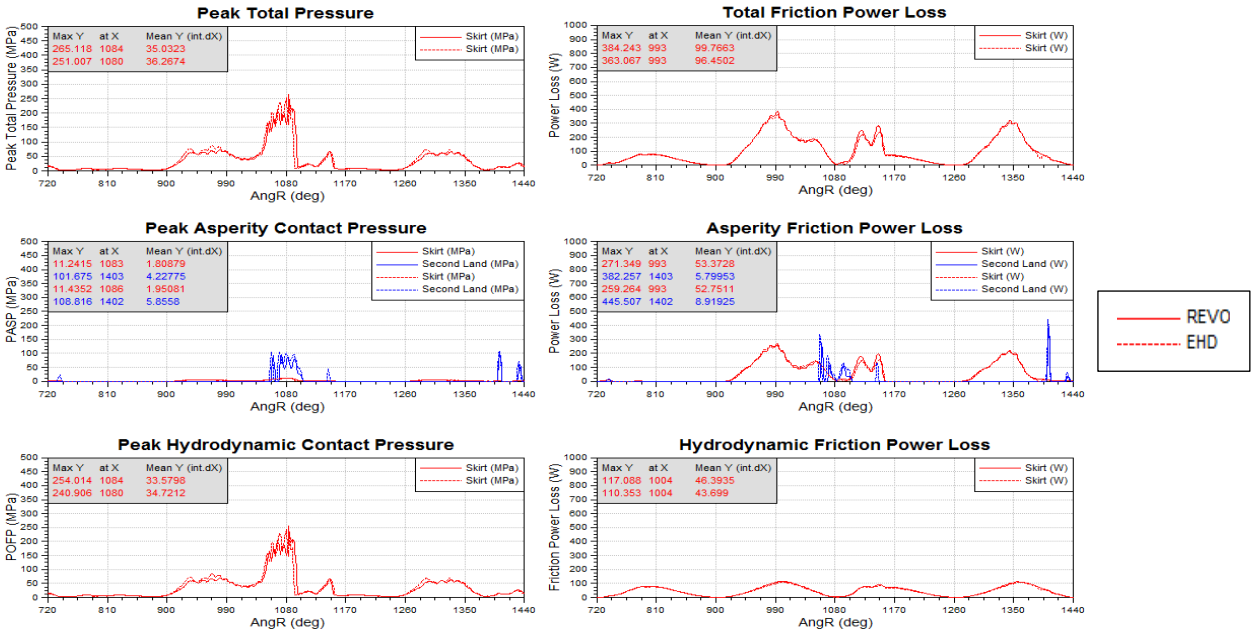

Figure F. 8. Comparison between REVO and EHD model, basic ring package, pressure and friction results – 3000_15.5.

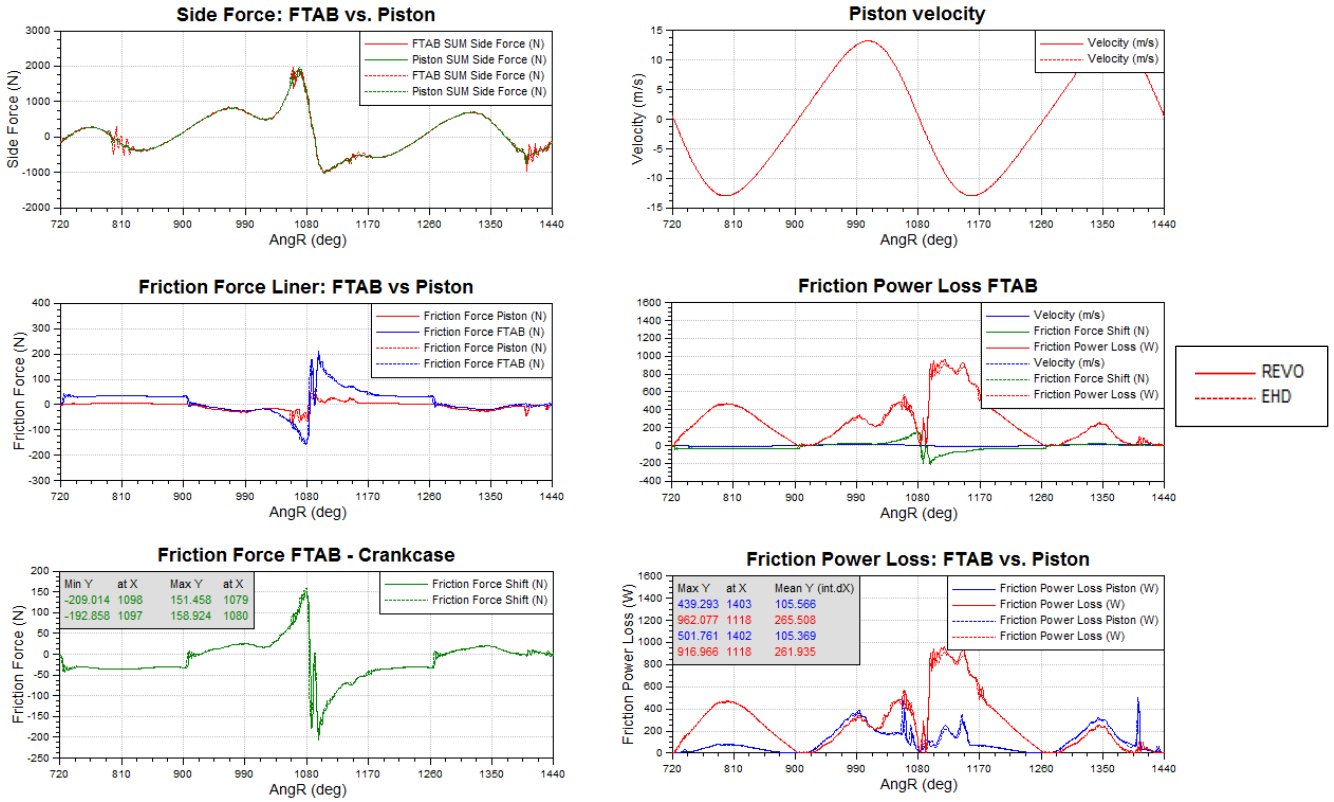

Figure F. 9. Comparison between REVO and EHD model, basic ring package, FTAB forces and friction power loss – 3000_15.5.

Appendix G

In this appendix comparison od friction forces between simulation and measurement for other operating point of engine with basic ring package are performed.

Engine speed = 2500rpm

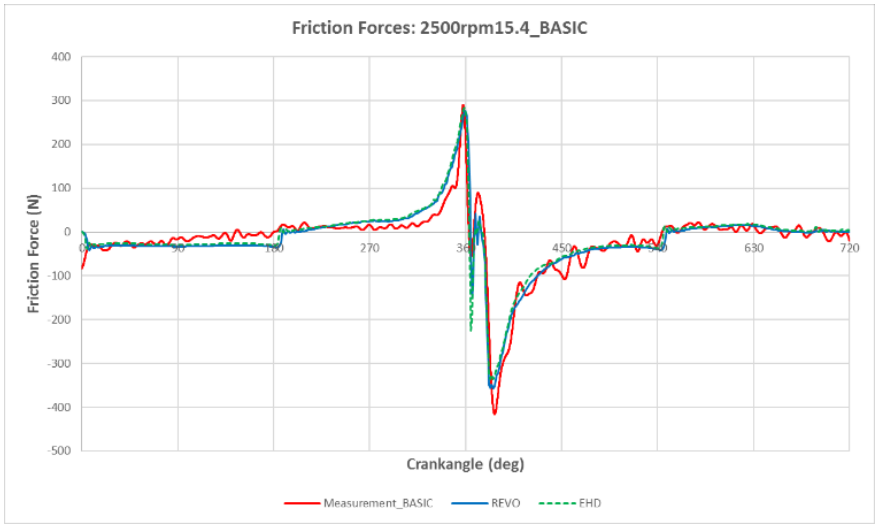

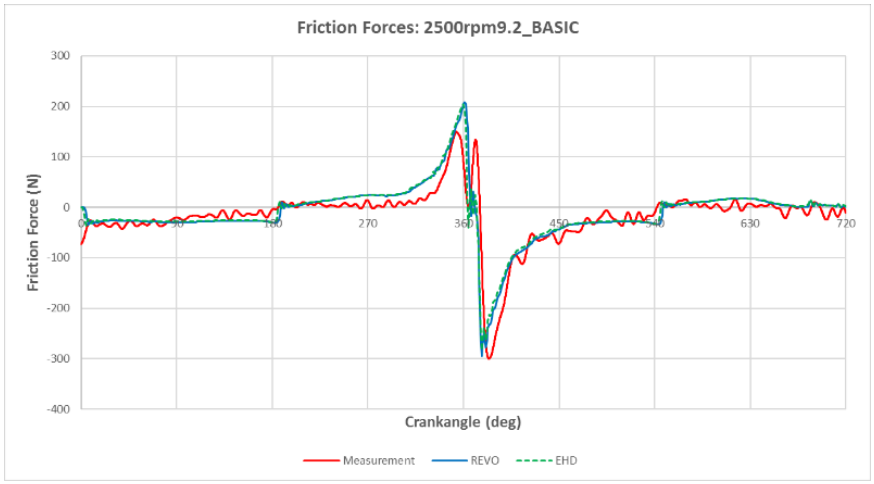

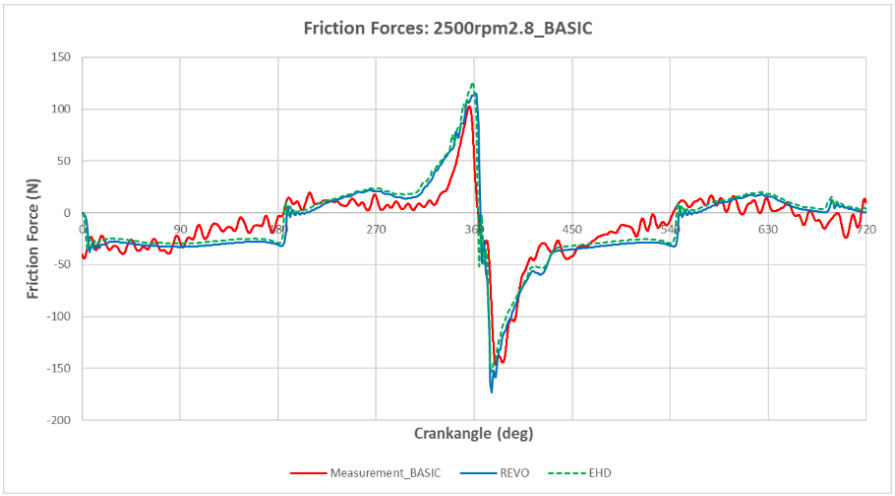

Figure G. 1. Comparison of friction forces, basic ring package, 2500rpm.

Engine speed = 2000rpm

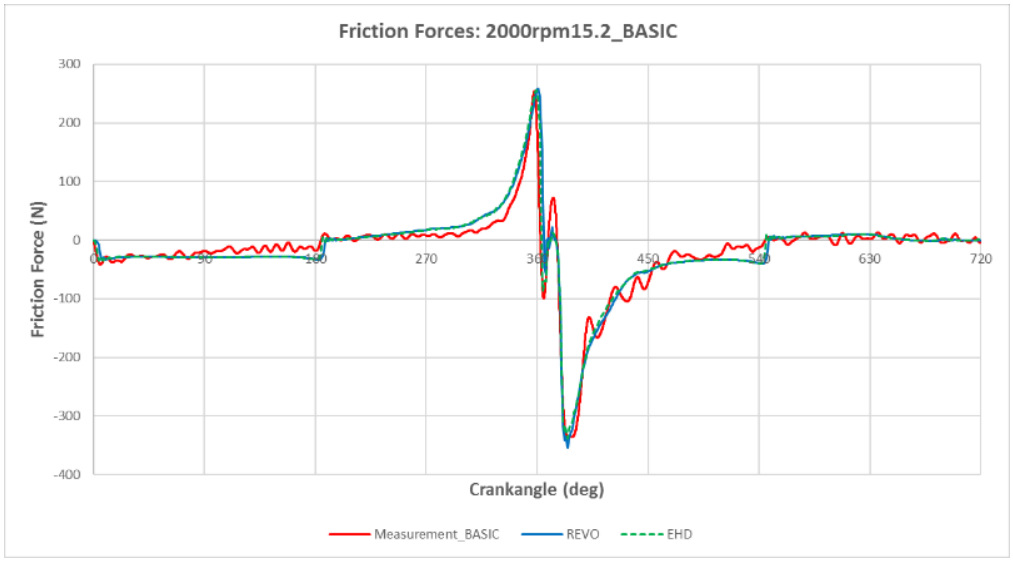

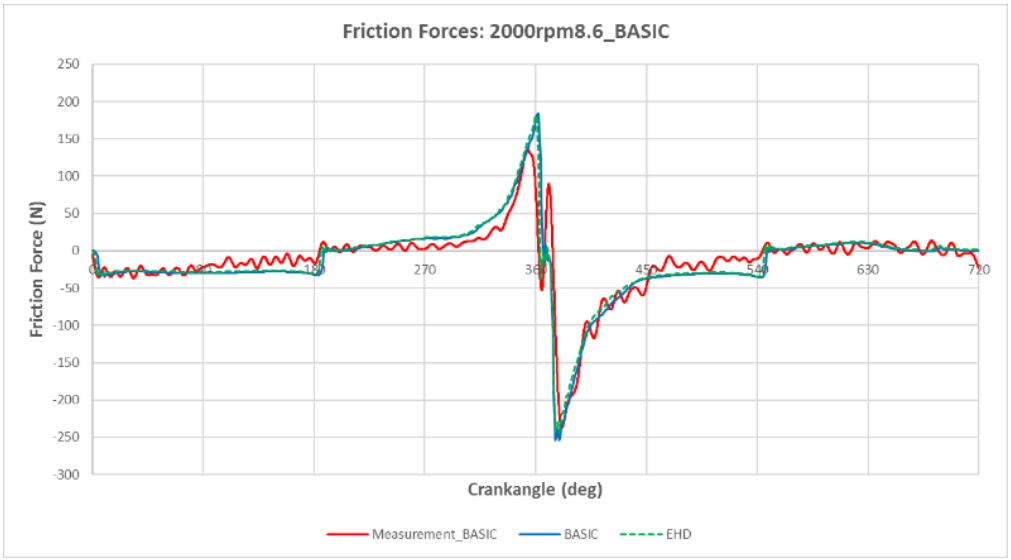

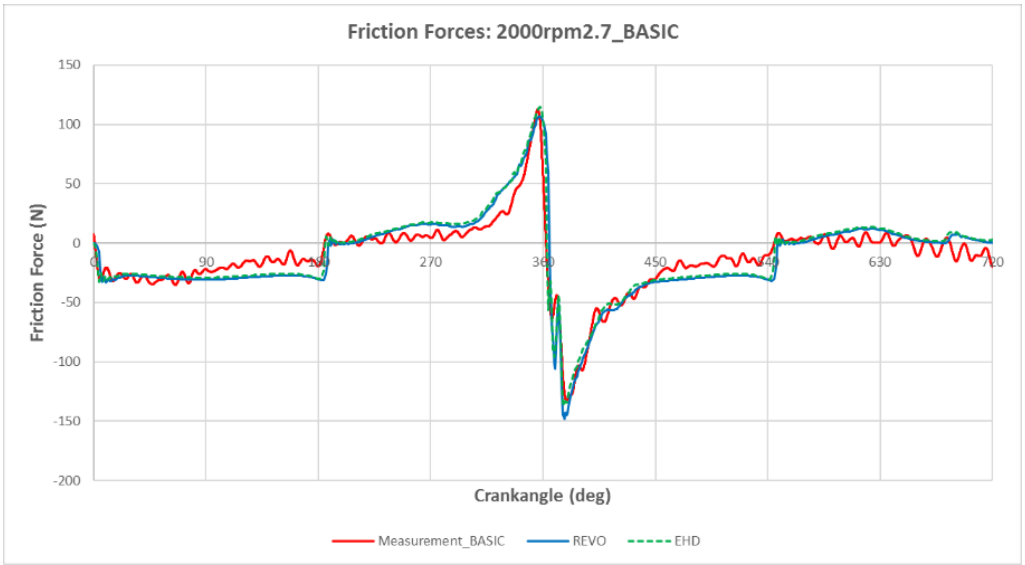

Figure G. 2. Comparison of friction forces, basic ring package, 2000rpm.

Engine speed = 1500rpm

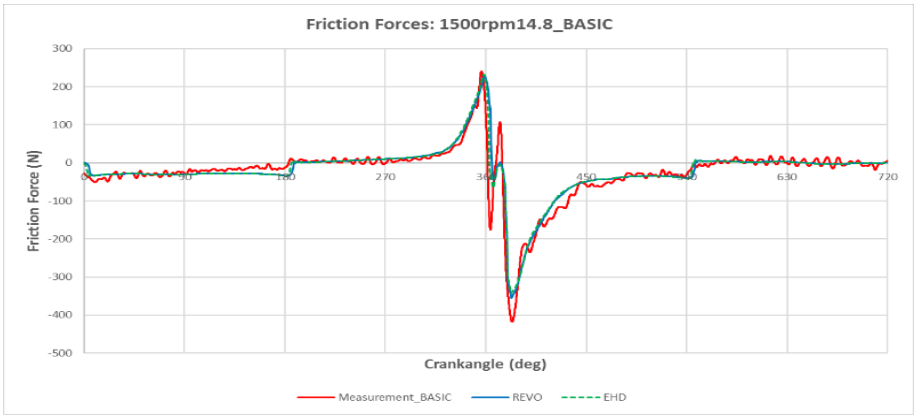

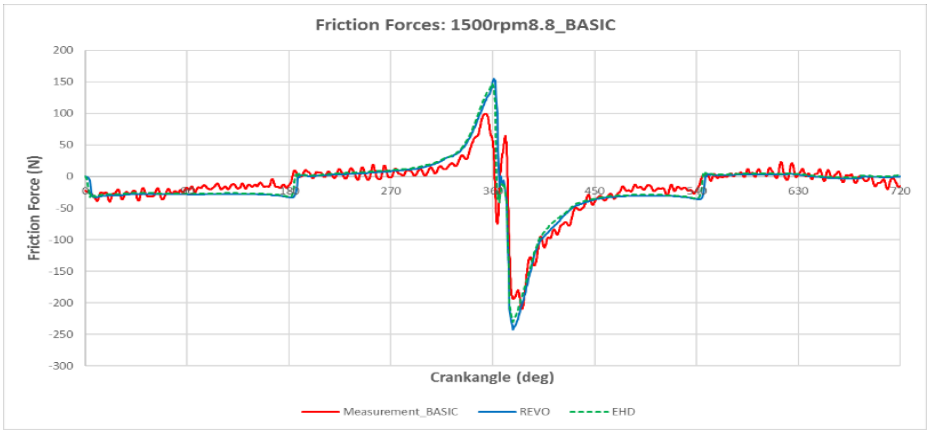

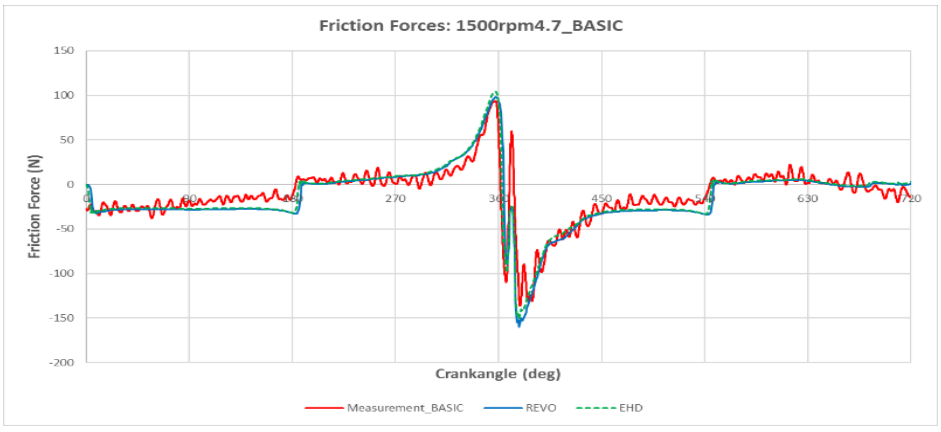

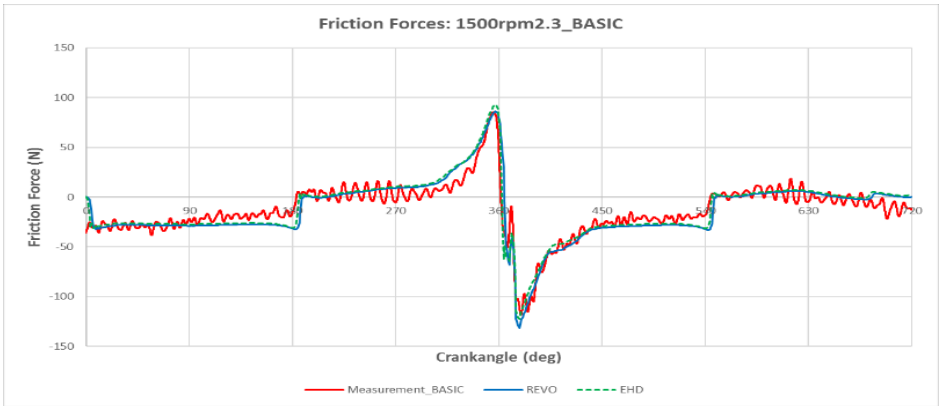

Figure G. 3 Comparison of friction forces, basic ring package, 1500rpm.

Appendix H

In this appendix comparison od friction forces between simulation and measurement for other operating point of engine with low friction ring package are performed.

Engine speed = 2500rpm

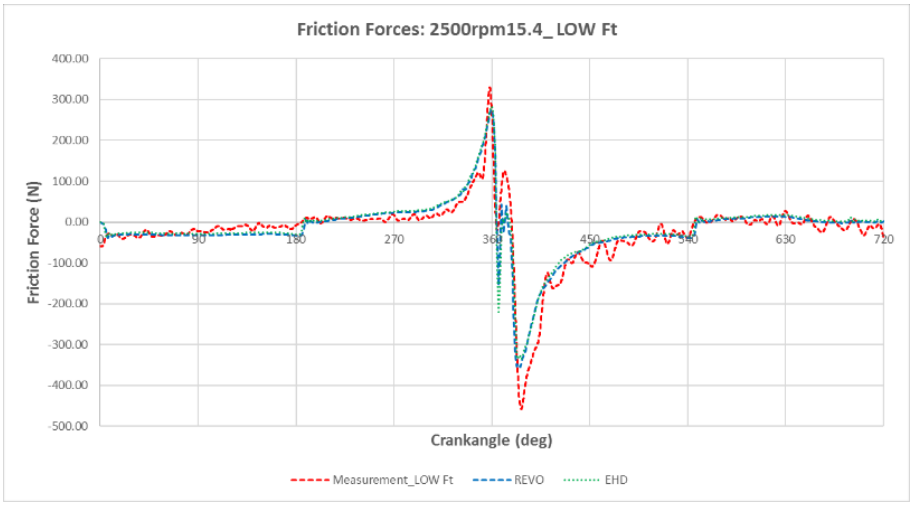

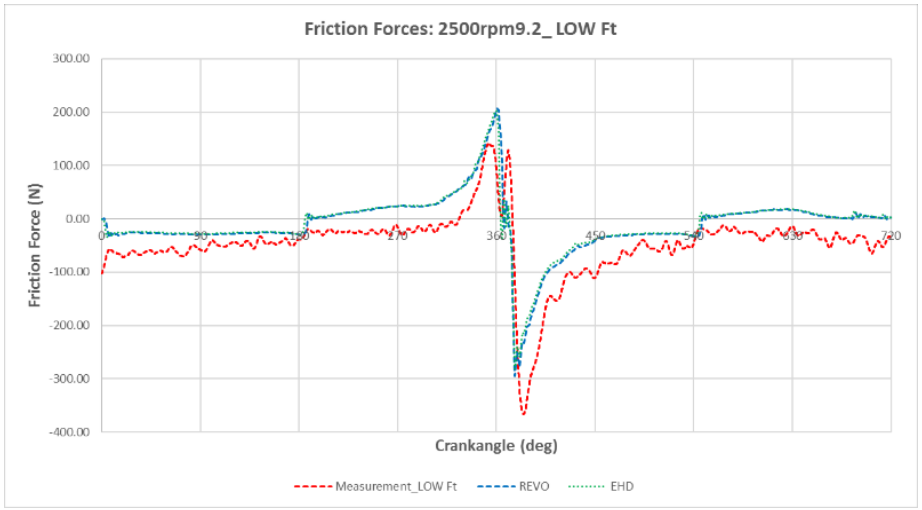

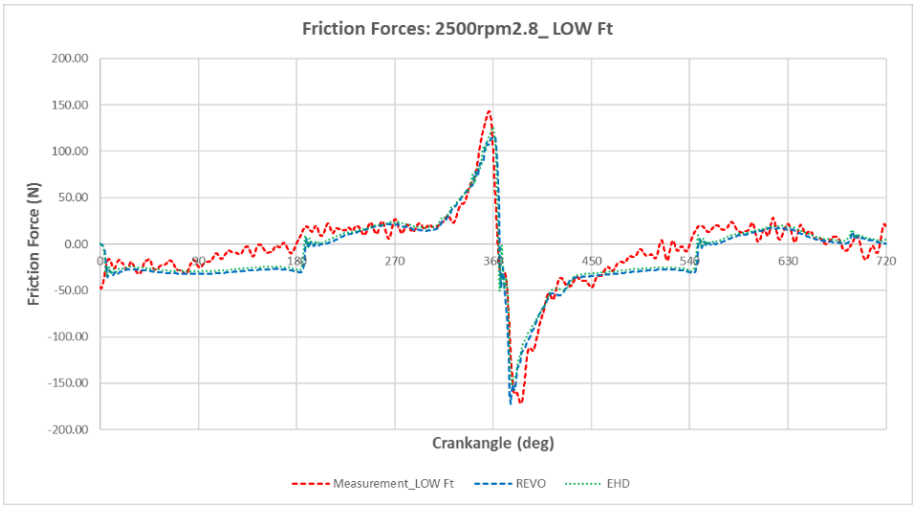

Figure H. 1 Comparison of friction forces, low friction ring package, 2500rpm.

Engine speed = 2000rpm

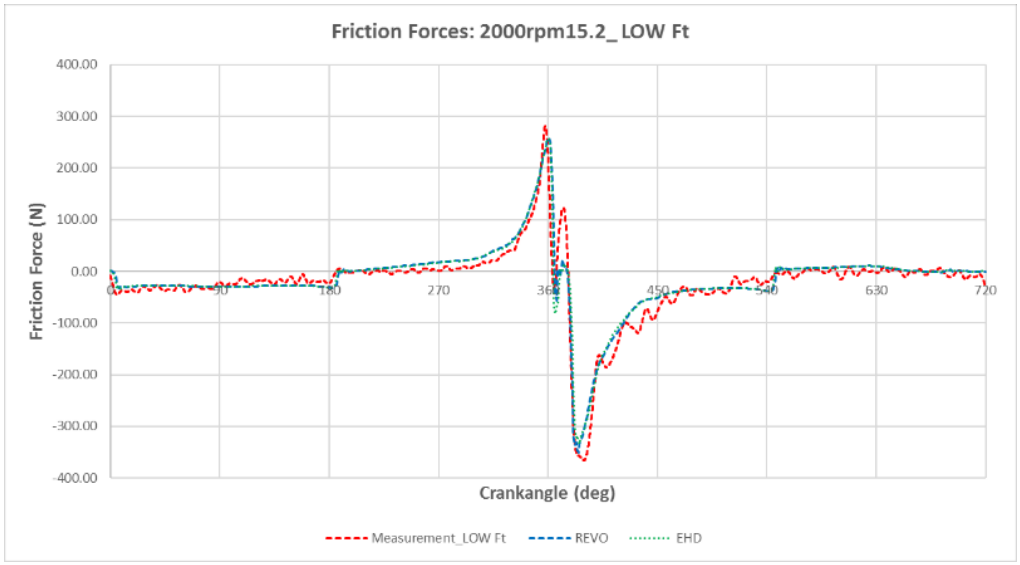

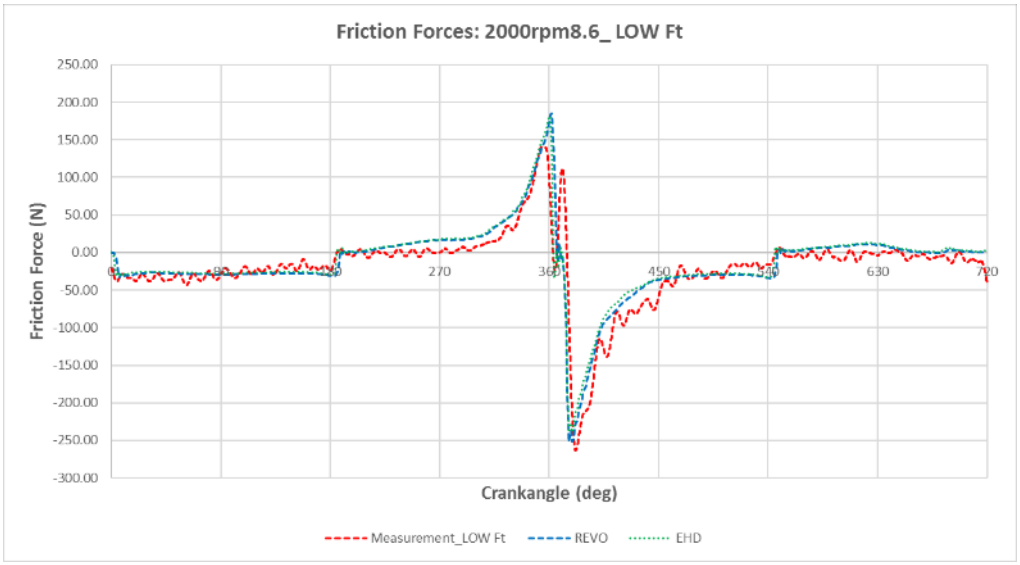

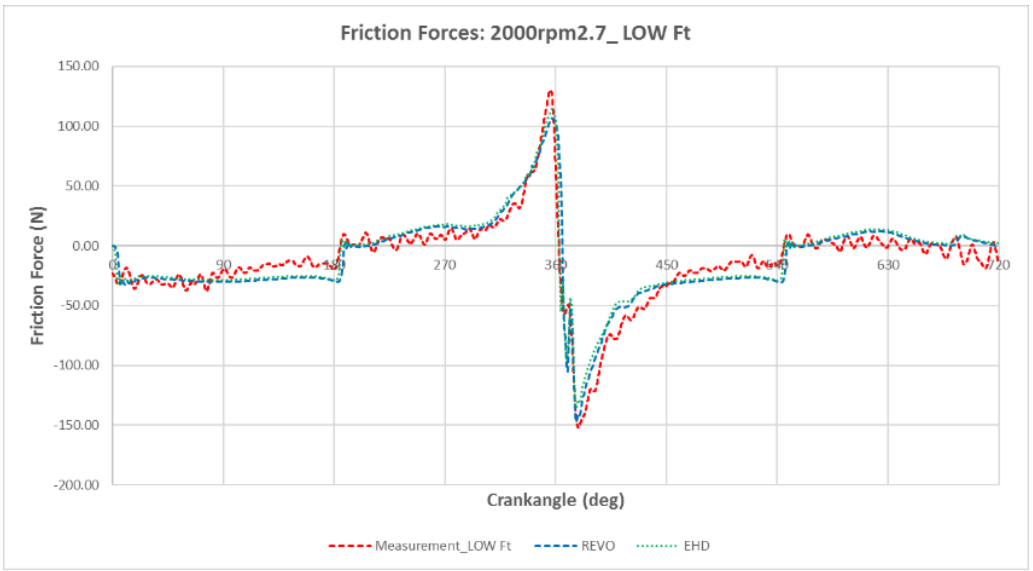

Figure H. 2. Comparison of friction forces, low friction ring package, 2000rpm.

Engine speed = 1500rpm

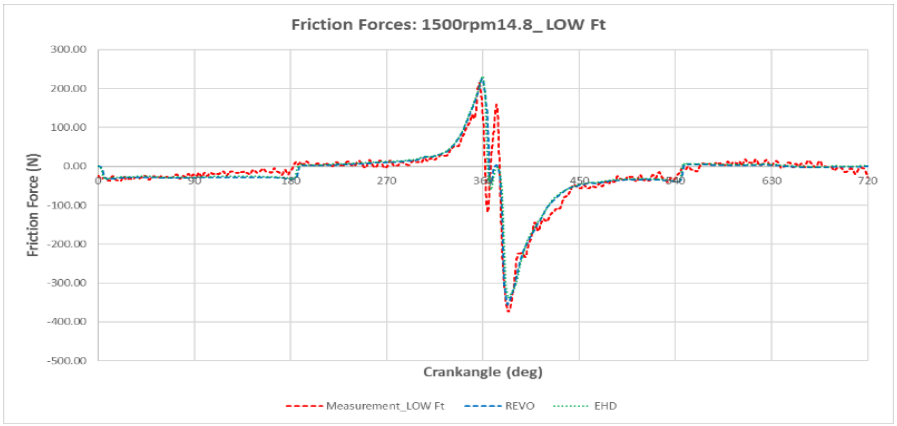

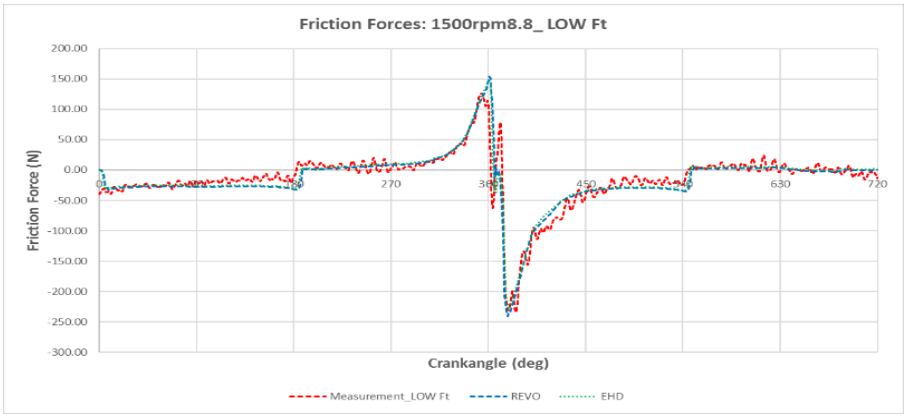

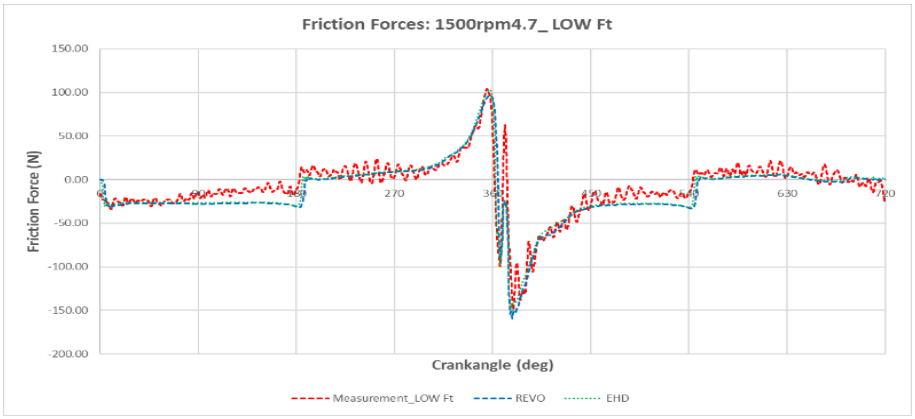

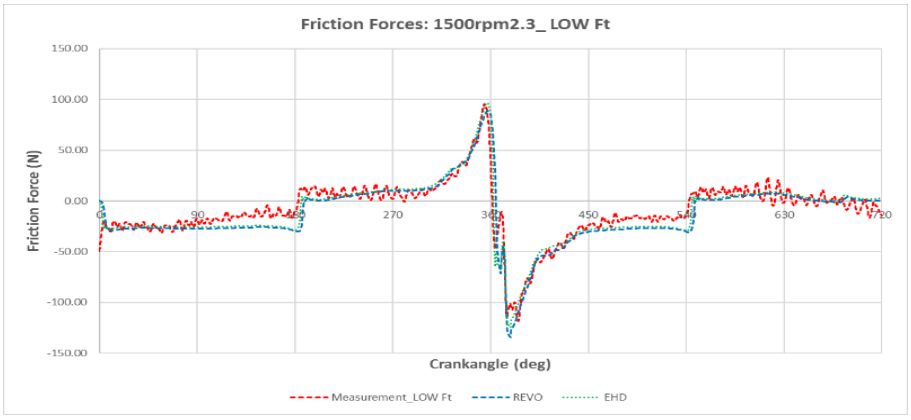

Figure H. 3. Comparison of friction forces, basic ring package, 1500rpm.

Appendix I

In this appendix comparison od side forces between simulation, measurement and analytics for other operating point of engine with basic ring package are performed.

Engine speed = 2500rpm

Figure I. 1. Comparison of side forces, basic ring package, 2500rpm.

Engine speed = 2000rpm

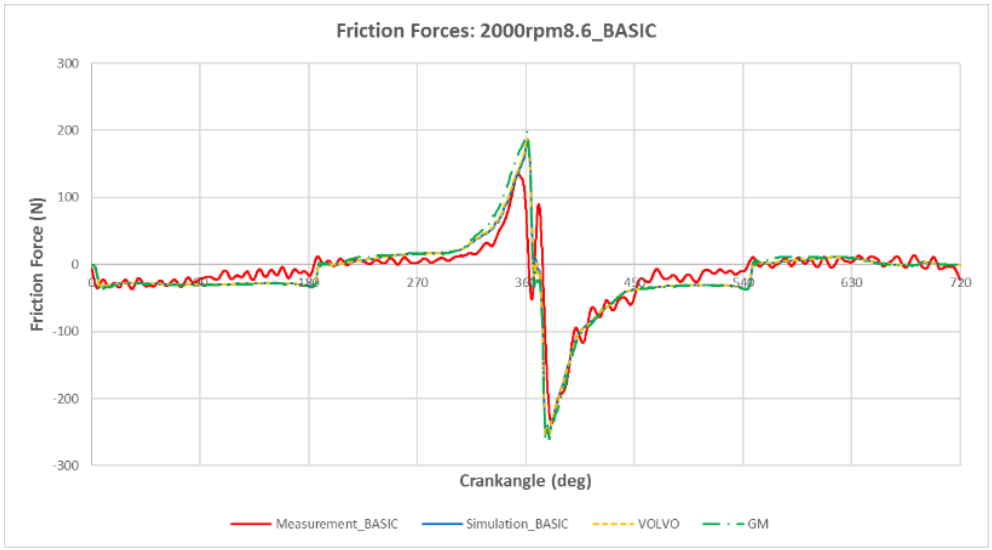

Figure I. 2. Comparison of side forces, basic ring package, 2000rpm.

Engine speed = 1500rpm

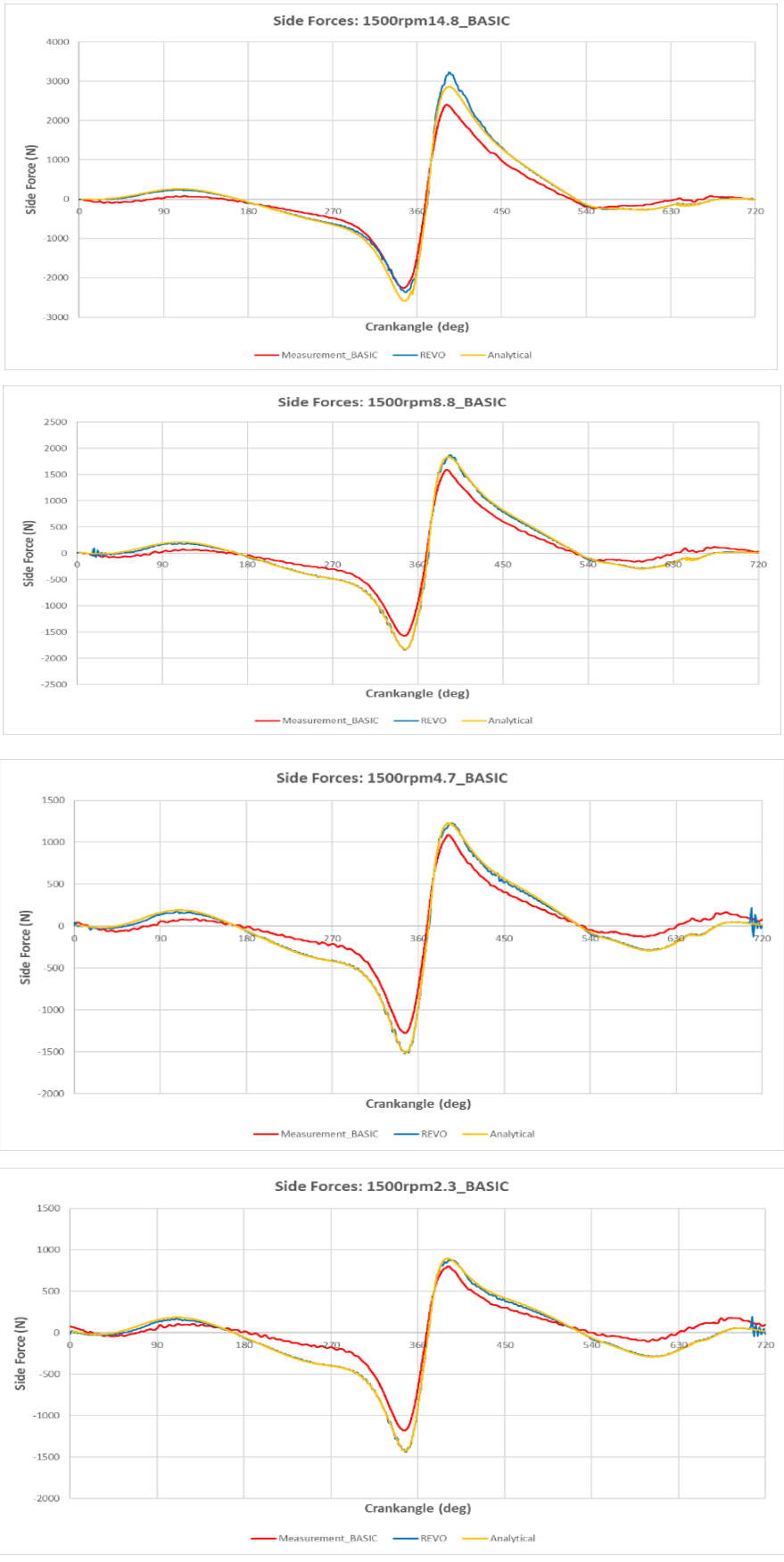

Figure I. 3. Comparison of side forces, basic ring package, 1500rpm.